Second Series *December 15, 1932* *Vol. 42, No. 6*

THE

PHYSICAL REVIEW

The Measurement of X-Ray Emission Wave-Lengths by Means of the Ruled Grating

By R. B. WITMER AND J. M. CORK
Department of Physics, University of Michigan

(Received September 27, 1932)

With a plane ruled grating, measurements have been made of the emission wave-lengths in the *L* series for the elements Va (23) to Zn (30) and in the *K* series for the elements C (6) to Si (14). With the exception of the $K\alpha$ lines of carbon, fluorine and oxygen, the method of the ruled grating yields a longer wave-length in every case than that found for the corresponding lines by the crystal method. The Moseley diagrams representing the observed results are found to be smooth curves. The possible variation of apparent wave-length with a variation in the grazing angle of incidence has been investigated. For angles such that the diffracted lines were not too diffuse, the computed wave-lengths were independent of the incident angle.

INTRODUCTION

SEVERAL investigations have now been carried out to determine the wave-lengths of x-ray spectral lines by means of ruled gratings. In certain of these investigations measurements have been made relative to some particular emission line whose wave-length assumed as a standard has been measured by the Bragg method with a crystal. In other experiments[1,2,3,4] the wave-lengths have been determined directly from the measurable constants of the apparatus. The results for the wave-lengths so far obtained by this latter method are found in every case to be greater than the corresponding values found by means of the usual crystal method. Disagreement exists only in the magnitude of the discrepancy.

The apparent existence of this difference raises a very important question. If the measurements by means of crystals are correct then there is some defect in applying to the ruled grating in the case of x-rays the same theory that is found satisfactory in the visible and the ultraviolet spectral regions. If the measurements by means of the ruled grating are correct then there is something in error in calculations involving the Bragg law, other than the effect due to the ordinary refraction of x-rays in the crystal, which can be accounted for. If this error exists in the lattice constant d then it reflects upon our knowledge of certain other more fundamental constants, namely

[1] E. Bäcklin, *Dissertation*, Upsala, 1928.
[2] J. A. Bearden, Proc. Nat. Acad. Sci. **15,** 528 (1929); Phys. Rev. **37,** 1210 (1931).
[3] J. M. Cork, Phys. Rev. **35,** 1456 (1930).
[4] C. E. Howe, Phys. Rev. **35,** 717 (1930).

the number of particles per gram molecule N or the charge of the electron e from which N is derived.

The answer to this question can be given only after the accumulation of extensive data obtained with the utmost care. This must include measurements of the indices of refraction of certain crystals for various wave-lengths as well as the determination of the wave-lengths themselves by the different methods. Toward this end the present investigation was undertaken to determine as accurately as possible the wave-lengths of the emission lines in the K series for elements Si(14) to C(6) and in the L series for elements Zn(30) to Va(23).

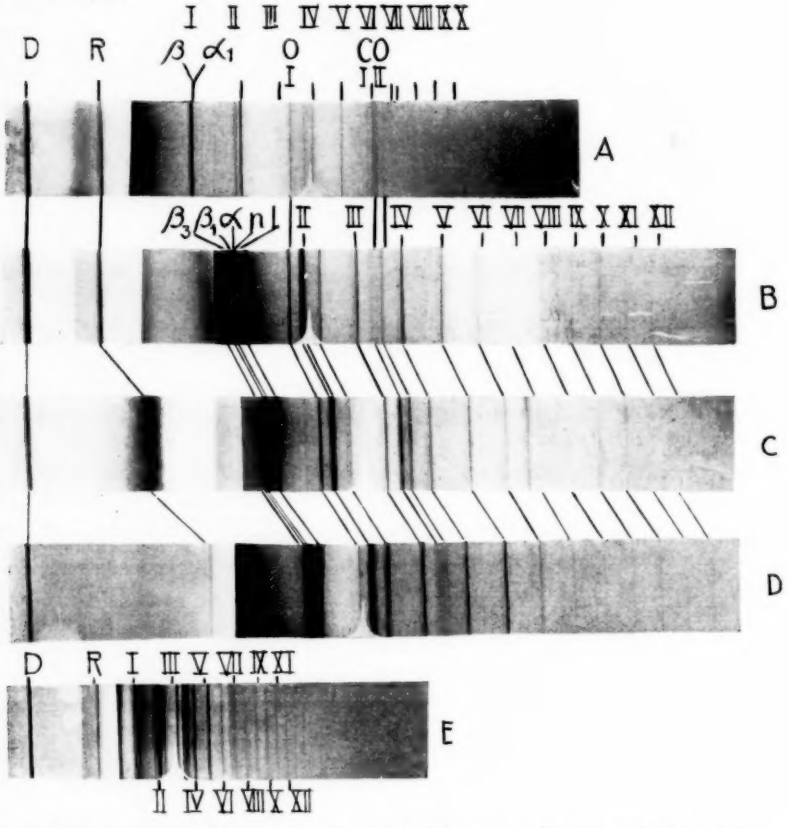

Fig. 1. Spectrograms with ruled grating. (A) K lines of silicon, $\theta = 30'\ 26''$; (B, C and D) L lines of copper for $\theta = 30'\ 26''$, $\theta = 51'\ 20''$ and $\theta = 1^\circ\ 16'\ 5''$, respectively; (E) same as (D) with photographic plate close to grating.

Apparatus

The apparatus employed is similar to that used previously by one of us[3] in the determination of the wave-lengths of the L series lines of molybdenum. It is believed that this arrangement which makes use of outside spectral orders and employs a grating which when once properly adjusted is left absolutely fixed during a series of exposures is least subject to errors of manipulation.

The following changes in the apparatus were made. The glass grating employed in this investigation was ruled in the laboratory of Professor M. Siegbahn and obtained through his kindness. The active surface was 3 mm wide and the lines were 2 cm long. Nominally having 600 lines per mm a calibration with known wave-lengths in the arc spectrum of mercury gave for the distance d between lines ($d = 0.00166309$ mm). The glass surface between the rulings and the outside of the plate was etched down on one side so that the direct beam going to the photographic plate was limited on one side by the edge of the ruled surface. The collimating system consisted of parallel slits 0.05 mm wide spaced 20 cm apart. A water-cooled x-ray tube of metal was used in place of the glass tube. A very fine knife edge was placed parallel and close to the rulings of the grating at the center. This reduced materially the stray radiation and general blackening on the photographic plate.

The procedure in taking exposures with the photographic plate at different distances from the grating was followed as previously described. For any particular substance on the target at least five exposures were taken with the photographic plate in a position a close to the grating and then in the position d at a maximum distance from the grating. Reproductions of some typical spectrograms are given in Fig. 1. At least six and sometimes as many as twelve measurable orders were obtained on each photogram.

RESULTS

A summary of the results obtained for the wave-lengths in the K series for the elements investigated is given in Table I. Similarly in Table II are given the values obtained for the wave-lengths in the L series. Along with the results of this investigation are shown the corresponding values from experiments using the crystal method as well as those of other experimenters

TABLE I. *Summary of wave-lengths in the K series.*

Element		Crystal	Söderman[5]	Thibaud[6]	Witmer and Cork
Si	β	6.754	—	—	6.764
	α	7.110	—	—	7.121
Al	β	7.965	—	—	7.967
	α	8.320	—	—	8.334
Mg	β	9.539	—	—	9.558
	α	9.869	—	—	9.898
Na	α	11.885	11.88	—	11.910
F	α	18.37	18.275	—	18.354
O	α	23.73	23.567	23.80	23.644
C	α	45.50	44.54	44.90	44.448

with the ruled grating. In the L series for the elements mentioned here, measurements by the crystal method have been carried out by Siegbahn and Thoraeus[7,8] and by Karlsson.[9] The values from these investigations are

[5] M. Söderman, Phil. Mag. **10**, 600 (1930).

[6] J. Thibaud, J. Opt. Soc. Am. **17**, 145 (1928).

[7] M. Siegbahn and R. Thoraeus, Ark. Mat. Astr. O. Fys. **18**, 24 (1924).

[8] R. Thoraeus, Phil. Mag. **1**, 312 (1926); **2**, 1007 (1926).

TABLE II. *Summary of wave-lengths of emission lines in the L series.*

Element	$\beta_{3,4}$	β_1	$\alpha_{1,2}$	η	l	Investigation
Zn 30	11.163	11.96	12.23	13.61	13.97	Ka Crystal
	11.16	11.96	12.23	13.61	13.95	S Crystal
	—	11.96	12.25	—	14.02	Ho
	11.202	11.974	12.252	13.670	14.038	Present
Cu 29	12.07	13.027	13.306	14.87	15.26	Ka Crystal
	12.10	13.03	13.316	14.83	15.19	S Crystal
	—	—	13.60	—	—	Hu
	—	—	13.32	—	15.26	K
	—	—	13.37	14.95	15.33	Ho
	12.091	13.048	13.339	14.910	15.266	Present
Ni 28	13.14	14.25	14.53	16.28	16.66	Ka Crystal
	13.12	14.24	14.53	16.17	16.55	S Crystal
	—	—	14.51	—	—	K
	—	14.28	14.62	16.36	16.73	Ho
	—	14.255	14.556	16.271	16.660	Present
Co 27	14.24	15.63	15.94	17.86	18.25	Ka Crystal
	—	15.62	15.94	17.77	18.20	S Crystal
	—	—	15.94	—	18.28	K
	—	15.64	15.99	—	18.34	Ho
	—	15.690	15.990	—	18.321	Present
Fe 26	15.71	17.23	17.58	19.76	20.09	Ka Crystal
	15.61	17.22	17.58	19.65	20.12	S Crystal
	—	—	17.70	19.60	20.10	Th
	—	—	18.00	—	—	Hu
	—	—	17.61	—	--	B
	—	—	17.54	—	20.15	K
	—	17.29	17.66	—	20.25	Ho
	—	17.281	17.602	—	20.161	Present
Mn 25	—	19.04	19.40	—	—	Ka Crystal
	—	19.04	19.39	—	—	S Crystal
	—	19.17	19.55	—	22.34	Ho
	—	19.136	19.454	—	22.296	Present
Cr 24	—	21.19	21.53	23.28	23.84	Ka Crystal
	—	21.19	21.53	—	—	S Crystal
	—	—	21.74	—	24.73	K
	—	—	21.73	—	—	Ho
	—	21.279	21.670	—	24.788	Present
Va 23	—	—	24.20	—	—	Ka Crystal
	—	—	24.31	—	27.70	Ho
	—	—	24.215	—	27.78	Present

Ka, Karlsson, reference 9; S, Siegbahn and Thoraeus, references 7 and 8; Ho, Howe, reference 4; Hu, E. L. Hunt, Phys. Rev. **30**, 227 (1927); K, G. Kellstrom, Zeits. f. Physik **58**, 511 (1929); Th, Thibaud, reference 6.

recorded in Table II. For the wave-lengths of certain η and l lines the agreement between the two crystal determinations is rather unsatisfactory. It is, however, apparent that in every case with the exception of the $K\alpha$ lines for fluorine, oxygen and carbon the value of a particular wave-length by the grating method is greater than the corresponding value found by the crystal method. The discrepancy for the lines in the L series is with few exceptions found to be not as great as was observed by Howe.[4]

[9] A. Karlsson, Ark. Mat. Ast. O. Fys. **22**, 9 (1930).

The Moseley diagrams for the various spectral lines observed, in which the square root of the frequency $(\nu/R)^{1/2}$ is plotted against the atomic number, are remarkably smooth curves. No positions are observed at which the slope of a line changes abruptly as might have been expected from the consideration of the origin of the spectral lines.

Hanawalt and Prins[10] have reported an apparent variation in the wave-length of a particular line with a change in the incident angle θ. The existence of such an effect would render uncertain any measurements made by the grating method and this effect was therefore investigated with considerable care. A complete series of spectrograms (i.e., five plates in each of the a and d positions) were obtained for the copper L lines with each of the following values for the grazing angle of incidence θ:—26′33″, 30′26″, 39′36″, 51′20″ and 1°16′15″. Reproductions of three of these spectrograms are shown in Fig. 1. For any particular wave-length the smaller the value of the grazing angle of incidence θ, the greater is the angular dispersion. This variation is not great. One very apparent effect of using a large incident angle is a broadening of any diffracted line.

TABLE III. *The wave-length of the Cu $K\alpha_{1,2}$ line for different incident angles.*

Grazing angle θ	λ in angstrom units
26′33″	13.339
30′26″	13.339
39′36″	13.335
51′20″	13.342
1°16′ 5″	13.368

The wave-length of the $L\alpha_{1,2}$ spectral line of copper as computed for the various values of θ is shown in Table III. For the first four angles the agreement is well within the experimental error. It is believed that the discordant value for the maximum θ is due to an inaccuracy in the calculation caused by the increased width of the diffracted lines.

Measurements by the crystal method of long wave-lengths are necessarily subject to inaccuracies due to the refraction of x-rays in the crystal. In the region of an absorption frequency characteristic of the atoms of the crystal there is an anomalous refractive effect which influences substantially results obtained from the Bragg law. Thus in crystals of gypsum, lauric acid or palmitic acid as used in investigating wave-lengths mentioned in this paper the calculation is complicated by the K absorption frequencies for carbon, oxygen, sulphur and calcium. Failure to consider this effect for the longer wave-length K series lines together with the uncertainty in the lattice constant of crystals of the fatty acids may account for the unsystematic discrepancy between measurements by the ruled grating and the crystal.

Influenced by calculations of wave-lengths from measurements of the index of refraction of a quartz crystal, Bearden[11] has indicated a lack of faith

[10] J. D. Hanawalt and J. A. Prins, Physica **12**, 1 (1932).
[11] J. A. Bearden, Phys. Rev. **39**, 1 (1932); **40**, 471 (1932).

in measurements made by the ruled grating. These calculations with the index of refraction demand a knowledge of: (a) the density of the crystal; (b) the absolute value of e/m for the electron; (c) a factor characteristic of the refracting crystal which is constant for a particular wave-length but which itself demands a knowledge of the wave-length in its determination and (d) an exact evaluation of the index of refraction exhibited by the crystal for the particular wave-length being investigated. If the evident uncertainties in (b) and (c) be overlooked it would still seem that the very short distances to be measured between the relatively diffuse lines on the photographic plates in the experimental procedure of (d) must render this method impotent in expressing a preference between the other two methods.

Laue Patterns from Thick Crystals at Rest and Oscillating Piezoelectrically

By J. M. Cork
University of Michigan

(Received October 26, 1932)

Laue patterns have been observed for thick crystals of quartz and Rochelle salt oscillating piezoelectrically and for the same crystals as well as for calcite, rock-salt and other materials at rest. Patterns have been obtained when the crystalline faces were the natural cleavage surfaces and when they were polished and when etched by suitable solvents. Regular Bragg reflections have been observed and compared for a quartz crystal with polished face and for the same crystal with the face etched with hydrofluoric acid. In the Laue patterns, the individual spots show a multiple structure in every case. The inner spots are double in nature. For the crystal oscillating piezoelectrically or at rest with polished faces the doubling of each spot is radially symmetrical. For the crystal with etched faces and at rest the inner component of the double spot is the stronger particularly for those spots near the center. The Bragg reflection from a quartz crystal with etched face shows the absence of any layer with reduced extinction at the surface. Further elaboration of the Laue diffraction theory seems necessary to account for the multiple structure of the spots formed by an ideally perfect crystal.

THE reflection of x-rays from quartz crystals oscillating piezoelectrically and at rest have been observed by means of the Bragg method and the Laue method in many investigations.[1,2,3,4] In the transmission method the piezoelectric oscillation leads to an intensity of the reflected x-ray beams much greater than that found for the crystals at rest. Moreover Barrett and Howe have observed that each Laue spot for the oscillating crystal appears to have a fine structure. To observe this fine structure the present investigation employing a more finely collimated beam of x-rays and crystals of greater thickness was undertaken.

Apparatus and Results

Two Laue cameras were constructed. In one the distance from the crystal to the photographic plate was 20 cm while in the other the corresponding distance was only 7 cm. It was thus possible to observe the complete pattern or only the central spots in greater detail. In both cases the x-ray beam was collimated by a fine slit system formed by two pinholes each 0.05 cm in diameter and spaced 12 cm apart. The first pinhole was 30 cms from the focal spot of the x-ray tube. A standard 200 kv Coolidge tube with a target of tungsten was employed. It was operated continuously at only 110 kv with a current of 2 milliamperes.

[1] Y. Sakisaka, Jap. Jour. Phys. **4,** 171 (1927).
[2] G. W. Fox and P. H. Carr, Phys. Rev. **37,** 1622 (1931).
[3] G. W. Fox and J. M. Cork, Phys. Rev. **38,** 1420 (1931).
[4] C. S. Barrett and C. E. Howe, Phys. Rev. **38,** 2290 (1931); **39,** 889 (1932).

Exposures were first taken with crystals of quartz ranging in thickness from 4 mm to 7 mm. In the beginning considerable difficulty was experienced in maintaining these thick crystals in the vibrating state continuously. A vacuum tube oscillator with two tubes having capacitative feed-back was arranged which accomplished this result satisfactorily.

Typical patterns obtained with the longer camera are shown in Fig. 1, A, B and C. For the quartz crystal with polished faces the spots were symmetrically double as were also the spots for the oscillating crystal regardless of the nature of the faces. When the crystal with polished faces was etched by immersion in hydrofluoric acid so that the thickness was reduced by not over 0.005 mm a pattern as shown in C, Fig. 1 was obtained. It is apparent that although the spots are now double the component parts are not of equal intensity. The inner part (i.e., that portion usually associated with reflection

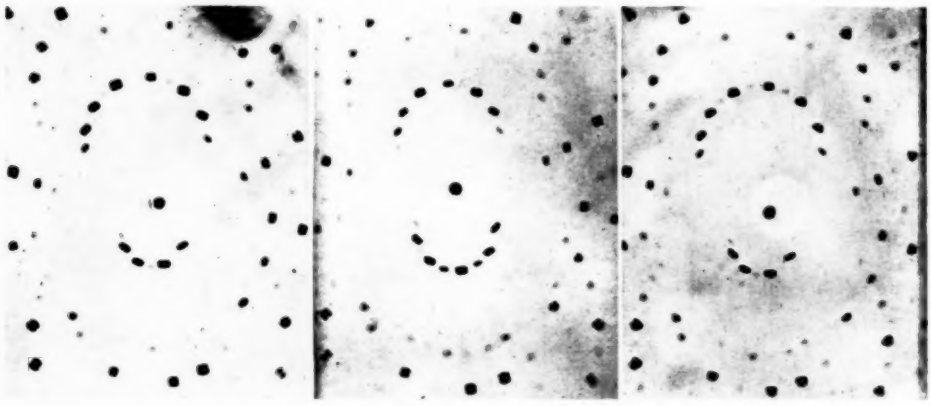

A B C

Fig. 1. Laue patterns obtained with quartz. A, etched faces oscillating 12 hr. exposure; B, polished faces non-oscillating 20 hr. exposure; C, etched faces non-oscillating 20 hr. exposure.

from the side of the crystal nearest the photographic plate) is much blacker than the outer component. This dissymmetry is not so apparent in the outer spots of the pattern as shown in the photograms obtained with the shorter camera.

To observe the effect of this etching upon the surface of the crystal the following test was carried out. The quartz crystal was mounted in a Siegbahn vacuum spectrograph and employed to measure the wave-length of the $K\alpha_1$ line of molybdenum ($\lambda = 5.41$A). The crystal was adjusted so that the desired radiation fell on the photographic plate in one position and then both crystal and plate were rotated through predetermined angles so that the same line was reflected to the photographic plate on the opposite side of the direct beam. One should obtain therefore upon the plate the segments of two inverted circles overlapping exactly at the center if the angle of displacement were chosen correctly. With the use of the quartz crystal with polished faces these lines are very diffuse so that the two segments are indistinguish-

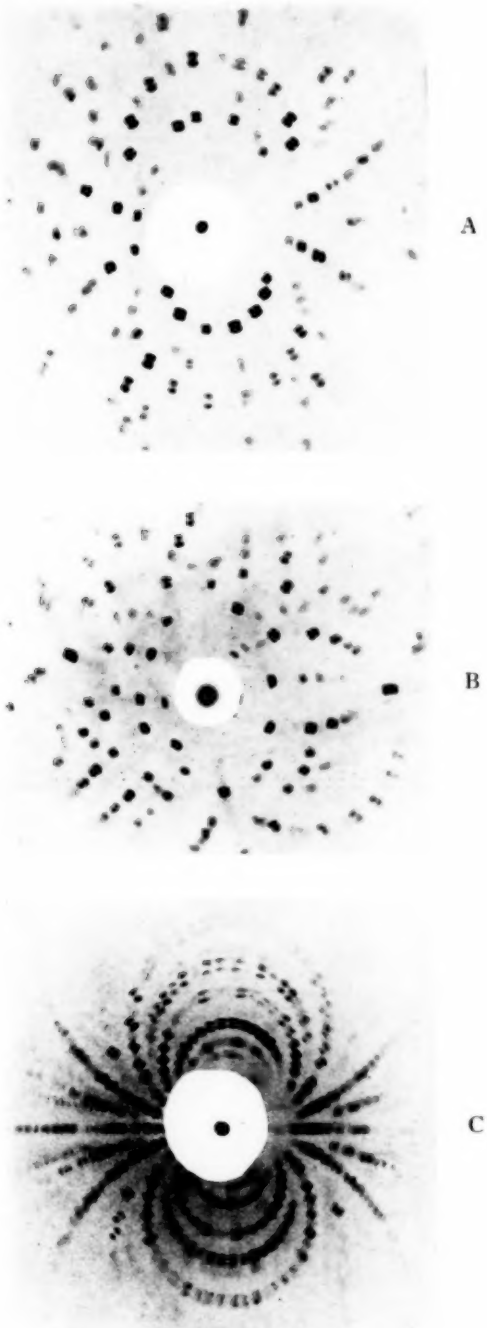

Fig. 3. Laue patterns from thick crystals at rest, A, quartz, B, calcite, C, Rochelle salt.

able as shown in Fig. 2A. Upon lightly etching the face of the quartz crystal with hydrofluoric acid these two lines become very sharp and are clearly distinguishable in Fig. 2B. For radiation of this wave-length the penetration into the crystal is exceedingly small and the sharpness of the photographic lines might safely be interpreted as indicating the almost complete absence of any disarranged particles on the surface.

It would appear therefore that the doubling of the spots was not due to a lack of extinction at the surfaces as has been generally assumed. To investigate this phenomenon further, Laue patterns were obtained with freshly cleaved slabs of several other materials. For some exposures the faces were etched by appropriate solvents while for others the specimen was left with its natural cleavage faces. Only in the case of a very bad specimen of rocksalt was a pattern obtained in which the Laue spots were not clearly multiple in structure. The spots toward the center of the pattern were double while those farthest removed from the central position were often triple in nature. Typical photograms of this sort are shown in Fig. 3 A, B and C which are for quartz, calcite and Rochelle salt, respectively.

A B

Fig. 2. Double exposures of molybdenum $L\alpha_1$ line, A, polished face, B, etched face.

This doubling or tripling of the Laue spots was undoubtedly first observed by M. de Broglie[5] when he passed a beam of x-rays through thin slips of crystal (rocksalt and fluorite) at an angle of incidence of 80° or a grazing angle of 10°. In this way he had effectively a thick crystal. The result was explained by assuming that the crystal traversed by the x-ray beam was composed of as many granules separated by accidental parallel cleavage planes as there were components in the spots. This would of course not account for the regularity and radial symmetry always observed in the reflected beams.

Freshly cleaved surfaces of calcite have been found[6] to give by Bragg surface reflection, spectral lines of width approximating that to be expected for an ideally perfect crystal. From photograms such as Fig. 2B it may be concluded that at least certain specimens of quartz are also very regular. Yet these same crystals give Laue patterns in which the spots have a multiple structure. It would appear that further elaboration of the usual Laue theory introducing interference between non-parallel radiation and perhaps with reference to a secondary structure as proposed by Zwicky,[7] is necessary.

[5] M. de Broglie, Comptes Rendus **156,** 1153, also 1461 (1913).
[6] B. Davis and W. Stempel, Phys. Rev. **17,** 608 (1921).
[7] F. Zwicky, Phys. Rev. **41,** 400 (1932).

Neutralization and Ionization of High-Velocity Ions of Neon, Argon and Krypton by Collision with Similar Atoms

By HAROLD F. BATHO
Ryerson Physical Laboratory, University of Chicago

(Received October 19, 1932)

Rudnick's work on the measurement of the free path L_0 for the ionization of a helium atom and the free path L_1 for neutralization of a helium ion in helium, has been extended to the gases neon, argon, and krypton for the velocity range corresponding to accelerating potentials of 10,000 to 22,000 volts. With neon, the work has covered the pressure range from 0.75×10^{-2} mm to 4×10^{-2} mm; with argon, from 0.30×10^{-2} mm to 1.6×10^{-2} mm; and with krypton, from 0.30×10^{-2} mm to 1.4×10^{-2} mm. In all cases, the free path for ionization, reduced to 760 mm pressure, is found to be approximately 6.5×10^{-4} cm. For neon, the free path for neutralization is 0.95×10^{-4} cm; for argon, 0.45×10^{-4} cm; and for krypton, 0.35×10^{-4} cm. Both free paths decrease with increasing velocity. The fraction F_∞ of neutral atoms in the beam when the equilibrium condition is reached is approximately 0.86 for neon, 0.93 for argon, and 0.95 for krypton. This fraction decreases with increasing velocity for neon and argon but appears to increase slightly for krypton. The observed dependence of the free paths on pressure is compared with the theoretical dependence. The results obtained are compared with the low-velocity measurements of other workers and the differences discussed. The relationship of this work to Doppler effect experiments with neon and argon is considered.

THE free paths of the positive ions of hydrogen,[1] helium,[1,2] neon,[1] and argon[1,3,4] have been measured by several investigators for velocities corresponding to accelerating potentials of less than 1000 volts. In the cases of hydrogen[5,6,7,8,9,10] and helium[11] the measurements have been extended to the voltage range from 5000 to 25,000 volts. The high-velocity work has included measurements of the free paths of the neutral atoms and determination of the fraction of neutral particles in the total beam when an equilibrium is established between the neutral and charged particles. Similar measurements with neon, argon, and krypton for high velocities (10,000 to 22,000 volts) have seemed of interest for comparison with the low-voltage measurements, and of importance in view of the unexpected absence of displaced arc lines in Doppler effect observations of the positive rays of neon[12,13] and argon[13,14].

[1] H. Kallmann and B. Rosen, Zeits. f. Physik **61**, 61 (1930).
[2] A. J. Dempster, Phil. Mag. **3**, 115 (1927).
[3] Penning and Veenemans, Zeits. f. Physik **62**, 746 (1930).
[4] F. Wolf, Phys. Zeits. **32**, 897 (1931).
[5] W. Wien, Sitz. d. K. P. Akad. d. Wiss., July, 1911, p. 773.
[6] J. Koenigsberger and J. Kutschewski, Ann. d. Physik **37** 161 (1912).
[7] A. Rüttenauer, Zeits. f. Physik **4**, 267 (1921).
[8] E. Rüchardt, Ann. d. Physik **71**, 377 (1923).
[9] H. Bartels, Ann. d. Physik **6**, 957 (1930).
[10] F. Goldmann, Ann. d. Physik **10**, 460 (1931).
[11] P. Rudnick, Phys. Rev. **38**, 1342 (1931).

Wien[5] and Rüchardt[15] have shown that if F represents the fraction of neutral particles in the total beam, assuming a simple exchange of electrons between moving and rest particles without appreciable change of velocity or direction of the moving particles, the value of F at a distance x from the point of origin of the beam is

$$F = F_\infty + (F_0 - F_\infty)e^{-(1/L_0+1/L_1)xp} \tag{1}$$

where F_0 is the neutral fraction at the point of origin, F_∞ the neutral fraction when an equilibrium is established between neutral and charged particles, $p\,dx/L_0$ the probability of ionization of a neutral atom in a distance dx, and $p\,dx/L_1$ the probability of neutralization of an ion in the same distance. L_0 may be interpreted as the mean free path for ionization of an atom and L_1 the free path for neutralization of an ion for unit pressure. Since the ratio

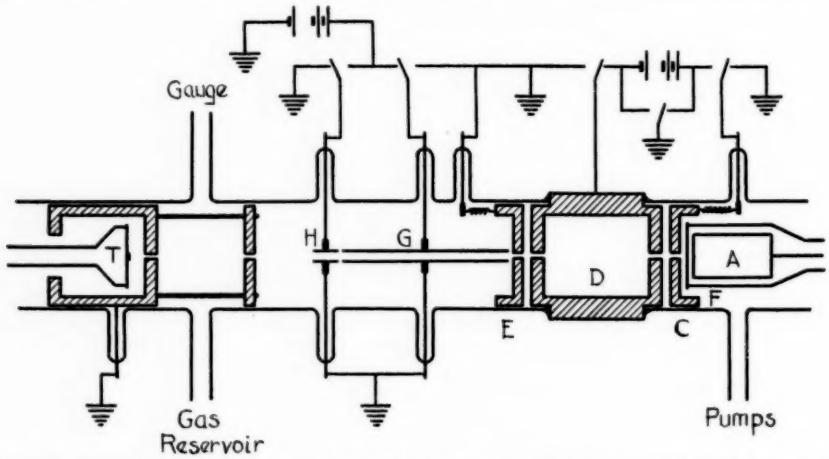

Fig. 1. Diagram of apparatus. A, anode; C, D, and E, accelerating electrodes; F, hot cathode; G, and H, deflecting condensers. T, thermocouple.

of the number of neutral to the number of charged particles in the equilibrium condition of the beam is inversely proportional to the probability of change,

$$F_\infty = L_0/(L_0 + L_1). \tag{2}$$

From Eqs. (1) and (2) it is seen that, provided F_0, p, and x are known, two measurements of F are sufficient for the determination of L_0, L_1, and F_∞. In practice, to observe F, the total intensity of the beam is measured; then, a transverse electric field is applied at the point x to remove the positive ions, allowing a measurement of the intensity of the remaining neutral atoms. In order to obtain the true value of F, the ratio of neutral intensity to total intensity thus obtained must be corrected for the finite length of the field since the field not only removes all ions already present at the point chosen

[12] W. Romig, Phys. Rev. **38**, 1709 (1931).
[13] A. I. McPherson, Phys. Rev. **41**, 686 (1932).
[14] K. Friedersdorff, Ann. d. Physik **47**, 737 (1915).
[15] R. Rüchardt, Handb. d. Physik **XXIV**, p. 90.

but also removes all ions formed along its length before they have time to return to the neutral state. If the field is applied along a length y of the path of the beam, there will be a simple exponential decay of intensity due to neutrals becoming positive given by

$$I = I_0 e^{-py/L_0} \tag{3}$$

where I_0 is the intensity of the neutrals at the beginning of the field, and I the intensity of the neutrals actually observed. Therefore, the measured ratio must be corrected by the factor e^{py/L_0} to give the true value of F at the beginning of the field.

Experimental Arrangement

The experimental arrangement used, shown in Fig. 1, was almost identical with that used by Rudnick.[11] Ions of the desired gas were formed in a low-voltage arc, by maintaining a small potential difference between the hot filament F and the hollow anode A. The heating current for the filament and the arc potential were supplied by storage batteries. For reasons to be mentioned shortly these batteries were insulated from ground. The filament F and electrode C were maintained at the same potential so that some of the ions formed were drawn through the circular opening in C where they were accelerated by the desired potential difference between C and D. Thus, a beam of high velocity particles proceeded to the thermocouple T. In Doppler effect experiments using this method of producing positive rays, it has been found that very sharp, displaced lines are obtained,[13,16] indicating that the ions are quite homogeneous in velocity.

For some of the measurements, a beam of particles, which were initially all positive, was required. In this case A, F, and C were raised to a high positive potential with D and E grounded. For other measurements a beam initially neutral was obtained by grounding F, C, and E, and raising D to a high negative potential. With this arrangement the ions were accelerated between C and D. In D they changed charge by collision with gas atoms. All ions remaining in the beam at the end of D were stopped by the retarding field between D and E, allowing only neutral atoms to proceed beyond E. In either case, deflecting fields could be applied along either G or H to remove all ions formed, allowing the measurement of the ratio (uncorrected) of the neutral intensity to the total intensity of the beam.

All cross-hatched parts in Fig. 1 were turned from rolled brass; the anode A was made of nickel; the plates of the condensers G and H of nickel gauze. The electrode D was 5.7 cm in length; G, 7.4 cm; and H, 1.1 cm. The total distance from C to the thermocouple was 24 cm. The thermocouple and the filament and anode were carried on ground joints to facilitate the alignment of the couple and the replacement of the filament. Wax joints were used between the two glass ends of the tube and the center electrode D to permit the easy adjustment and replacement of the electrodes C, D and E.

In all cases it was desirable to have only singly charged ions present. In order to ensure this the arc potential used to form the ions was always less

[16] H. F. Batho and A. J. Dempster, Astrophys. J. **75**, 34 (1932).

than the second ionizing potential of the gas in which the measurements were being taken. Doubly charged ions might be formed by collision in passage through the gas but the absence of any displaced lines due to doubly charged particles in Doppler effect experiments with neon and argon,[13] even though no precautions are taken regarding the arc voltage, seems to indicate that the number of doubly charged ions present in the beam is negligible for the pressures and velocities used.

The retarding field used to stop the positive ions, in measurements with an initially neutral beam, accelerated electrons toward the thermocouple. To avoid rather large errors due to this cause, it was necessary to use a transverse magnetic field of sufficient intensity to deflect the electrons, but small enough not to deflect the positive ions appreciably.

It was found that, above 1600 volts, increasing the potential difference across the deflecting condenser did not change appreciably the intensity as measured by the thermocouple; accordingly, this deflecting potential was used to remove all ions from the beam.

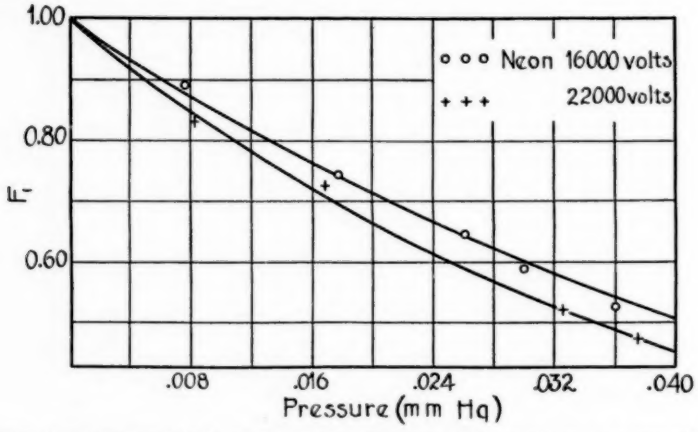

Fig. 2. Relationship between F_1 and pressure. Points shown are experimental values, curves are values plotted from Eq. (4).

The thermocouple was a junction formed by spot-welding 3 mil platinum wire and 10 mil extruded bismuth wire to a platinum foil target 1 mm^2 in area. The other ends of the wires were joined to nickel lead wires, also by means of platinum foil. The thermoelectric current was indicated by a low-resistance galvanometer of sensitivity 168 megohms. To avoid errors in the measurement of intensity it was found necessary to shield the thermocouple rather carefully. The hot filament was placed slightly off the axis of the tube and the anode was made hollow, thus reducing the amount of radiation reaching the thermocouple directly from the arc in which the ions were formed. The considerable thickness of brass between filament and thermocouple also served the same purpose. Fluctuations in room temperature caused irregular changes in the zero reading of the galvanometer, i.e., in the reading of the galvanometer when no particles were striking the target of the thermocouple. This difficulty was eliminated by enclosing the entire thermocouple end of

the tube in a large asbestos cylinder. After this precaution had been taken, it was found that the zero reading shifted only very slowly.

On account of the wax seals it was not possible to bake out the tube before admitting the gas to be used. However, the exhausting pumps were run at intervals over a period of two or three days before gas was admitted in an attempt to eliminate occluded vapors and gases. With the gases used it was not considered feasible to maintain a steady flow of gas. The neon was admitted to the tube through an adjustable lavite valve,[17] and, after entering the tube, was circulated over charcoal immersed in liquid air. The circulating pump was shut off while readings were being taken to avoid pressure differences along the path of the beam but the gas was circulated at frequent intervals between runs. This appeared sufficient to maintain the purity of the gas. The argon and krypton were purified in the reservoir before entering the tube, by evaporating magnesium in a side tube by means of a high-frequency induction heater. In all cases, a liquid air trap was placed in close connection

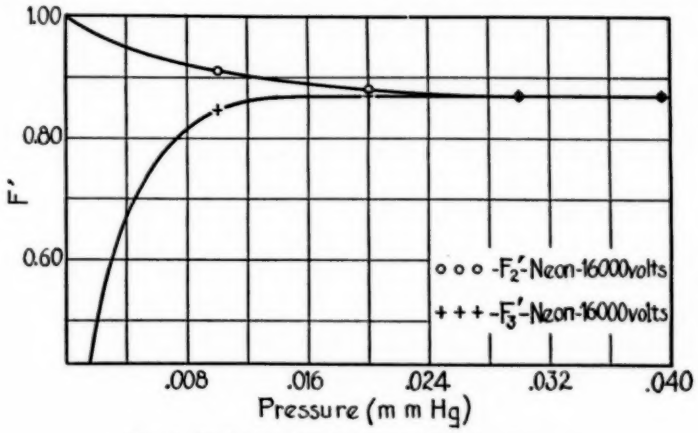

Fig. 3. Relationship between F' and pressure.

with the main tube to eliminate, if possible, vapors of mercury, stopcock grease, and wax. The leads from the reservoir, to the McLeod gauge on which pressures were read, and to the exhausting pump, passed through liquid air traps. During the period in which readings were taken, liquid air was kept on these traps continuously to prevent diffusion of mercury vapor into the tube. These precautions having been taken, the spectrum of the gas in the tube, as examined with a small hand spectroscope, failed to show any mercury lines. As will be seen later, however, there is reason to doubt that these precautions were sufficient to eliminate vapors entirely.

Measurements and Results

For each pressure and voltage three ratios were determined. The first two measurements were made with an initially neutral beam (C and E grounded,

[17] This valve consisted of a lavite cone partially covered with mercury so arranged that the rate of leak could be controlled by changing the mercury level by means of a magnetically operated soft iron plunger. The valve worked very satisfactorily for the purpose for which it was used. The lavite cone was very kindly furnished by the American Lava Corporation.

D at a high negative potential). The first, F_1, was the ratio of the number of particles reaching the thermocouple, when a deflecting field was applied to the long condenser G only, to the number of particles reaching T with no field applied; the second, F_2, was a similar ratio with the deflecting field applied to the short condenser H instead of G. The third measurement, F_3, differed from the second only in the fact that an initially positive beam was used. For each voltage the three ratios were measured at a series of pressures so that curves could be plotted showing the dependence of each ratio on pressure. With all three gases, the measurements covered the voltage range from 7000 to 22,000 volts. With neon, the pressure range was from 0.75×10^{-2} to 4.0×10^{-2} mm of mercury; with argon, from 0.30×10^{-2} to 1.6×10^{-2} mm; with krypton, from 0.30×10^{-2} to 1.4×10^{-2} mm. The lower limits for both velocity

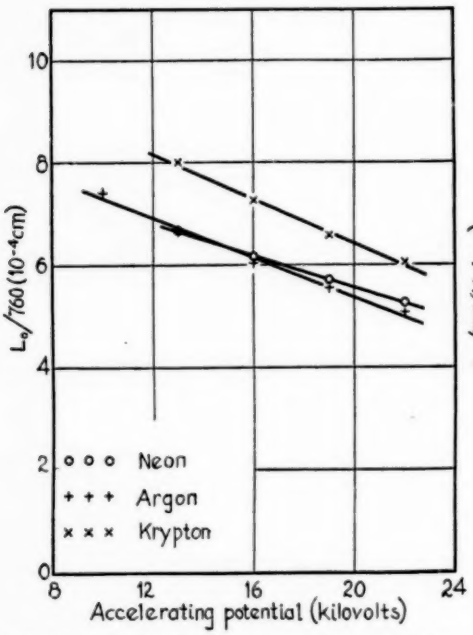

Fig. 4. Relationship between free path for ionization corrected to atmospheric pressure and accelerating potential for neon, argon, and krypton.

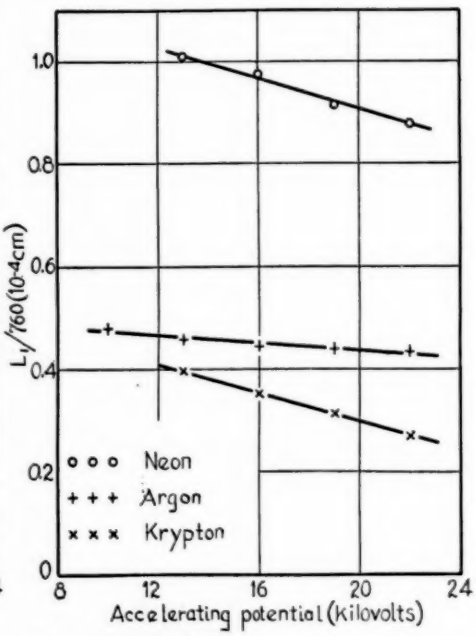

Fig. 5. Relationship between free path for neutralization corrected to atmospheric pressure and accelerating potential for neon, argon, and krypton.

and pressure were set by diminishing intensity; the upper limit of pressure was also set by diminishing intensity, apparently due to scattering; the upper velocity limit was determined by the voltage at which sparking began to occur inside the tube.

From Eqs. (1) and (3) it is seen that the equations expressing the dependence of the various measured quantities on pressure are

$$F_1 \text{ or } F_2 = e^{-py/L_0}\left[F_\infty + (1 - F_\infty)e^{-(1/L_0+1/L_1)px}\right], \tag{4}$$

$$F_3 = F_\infty e^{-py/L_0}\left[1 - e^{-(1/L_0+1/L_1)px}\right] \tag{5}$$

where x is the distance from the point of origin of the beam to the beginning of the deflecting field and y the length of the field. The expressions for F_1 and F_2 differ only in the values of x and y. For F_1, $y=y_1=7.4$ cm, $x=x_1=0.75$ cm; for F_2, $y=y_2=1.1$ cm, $x=x_2=8.25$ cm; for F_3, $y=y_3=y_2=1.1$ cm, $x=x_3=14.55$ cm.

Since x_1 is small (0.75 cm) and y_1 relatively large (7.4 cm), the value of F_1 is almost completely independent of L_1 and F_∞. Therefore, a single measurement of F_1 is sufficient for the determination of L_0. In Fig. 2, the experimental points obtained in neon for two different voltages, 16,000 and 22,000 volts, are plotted. The curves shown are plotted from Eq. (4) with $L_0=0.470$ cm for 1 mm pressure for 16,000 volts, and $L_0=0.400$ cm for 22,000 volts. These curves show good agreement with the experimental points for all pressures. They show, also, the dependence of F_1 on voltage, the curve falling as the voltage was increased in all cases.

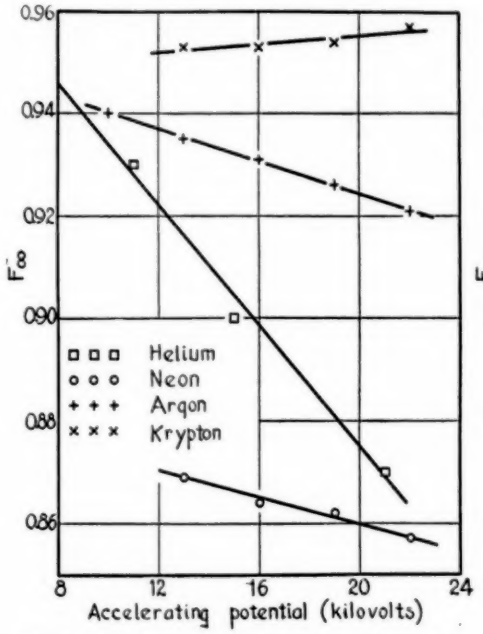

Fig. 6. Relationship between F_∞ and accelerating potential for helium, neon, argon, and krypton.

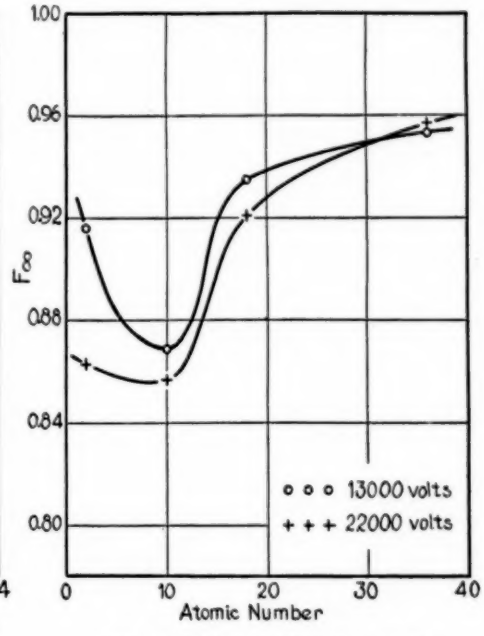

Fig. 7. Relationship between F_∞ and atomic number.

Having obtained the value of L_0 for a particular voltage, we find it possible to calculate the coefficient in front of the brackets in Eqs. (4) and (5) which arises from the decay of intensity in the short condenser. If we multiply the experimentally observed values F_2 and F_3 by e^{py_2/L_0} and denote the result by F_2', F_3', then the corrected experimental values should be connected with the free paths by the relations

$$F_2' = F_\infty + (1 - F_\infty)e^{-(1/L_0+1/L_1)px} \tag{6}$$

$$F_3' = F_\infty\left[1 - e^{-(1/L_0+1/L_1)px}\right]. \tag{7}$$

From these equations, it is seen that both F_2' and F_3' become equal to F_∞ for large pressures. In Fig. 3, the corrected experimental values at different pressures for 16,000 volts for neon have been plotted against pressure. The graph shows that F_2' and F_3' do approach the same constant value at high pressures as indicated by the equations. Thus, the value of F_∞ is obtained. L_1 may be determined from Eq. (2) with the values of L_0 and F_∞ already found.

This process was repeated to find the values of L_0, L_1, and F_∞ for each voltage used. The results are given in Table I. Column 3 gives the velocity corresponding to the accelerating potential given in column 2. Columns 4 and 5 show the mean free paths in centimeters corrected to atmospheric pressure of the neutral atoms and positive ions respectively. Column 6 contains the values of F_∞. The results of other observers and the kinetic theory values of the free paths are included for purposes of comparison. Figs. 4, 5, and 6

TABLE I.

1 Gas	2 Accelerating potential in volts	3 Velocity in cm per sec.	4 $L_0/760$ in cm	5 $L_1/760$ in cm	6 F_∞	7 Observer
Neon	22,000	4.58×10^7	5.3×10^{-4}	0.88×10^{-4}	0.86	
	19,000	4.16	5.7	0.91	0.86	
	16,000	3.91	6.2	0.98	0.86	
	13,000	3.52	6.7	1.01	0.87	
	400	0.62		0.34		Kallmann and Rosen[1]
			0.21			Kinetic theory value for 20°C and 760 mm
Argon	22,000	3.24×10^7	5.1×10^{-4}	0.44×10^{-4}	0.92	
	19,000	3.03	5.6	0.44	0.93	
	16,000	2.78	6.0	0.44	0.93	
	13,000	2.51	6.7	0.46	0.94	
	10,000	2.20	7.4	0.48	0.94	
	400	0.44		0.15		Kallmann and Rosen[1]
	200	0.31		0.13		Penning and Vennemans[3]
	837	0.64		0.067		Wolf[4]
	20 to 520	0.38		0.11		Wolf[4]
			0.11			Kinetic theory value for 20°C and 760 mm
Krypton	22,000	2.26×10^7	6.0×10^{-4}	0.27×10^{-4}	0.96	
	19,000	2.10	6.6	0.32	0.95	
	16,000	1.93	7.3	0.35	0.95	
	13,000	1.74	8.0	0.40	0.95	
			0.10			Kinetic theory value for 20°C and 760 mm

show the dependence of L_0, L_1, and F_∞, respectively, on accelerating potential. In Fig. 7, F_∞ is plotted as a function of atomic number for 13,000 and for 22,000 volts. The values for helium are taken from Rudnick's data.[11] The measurements at lowest voltages have been omitted from the table and graphs, since all measurements below 13,000 volts were difficult on account of small intensity. Particularly was this true at high pressures as scattering also decreased the intensity. Since the determination of F_∞ and L_1 depends on high-pressure measurements no reliable values could be obtained for low velocities. However, the readings made at lower pressures indicated no large changes in L_0, L_1, or F_∞ at these velocities.

Discussion of Results

The results of the preceding paragraph have been deduced from the observation of F_1 which gives L_0, the free path for ionization, and of F_∞, the equilibrium condition reached by the beam. L_1 has been deduced from the equilibrium value and not observed directly. The observations, however,

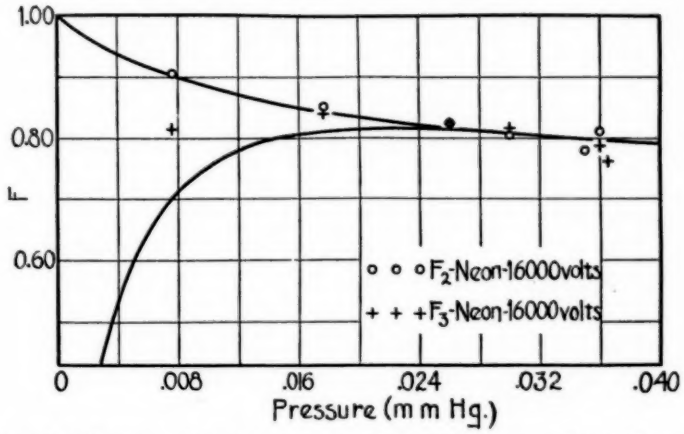

Fig. 8. Relationships between F_2 and pressure, and F_3 and pressure. Points shown are experimental values, curved are values plotted from Eqs. (4) and (5), respectively.

including the dependence of F_2 and F_3 on pressure, contain more data than are required to deduce L_0 and L_1, and may be used to check the adequacy of the theory to account for the dependence on pressure observed in the case of F_2 and F_3.

Having determined L_0, L_1, and F_∞ for any particular velocity, it is possible to plot complete curves for F_1, F_2, and F_3 from Eqs. (4) and (5) for comparison with the experimentally determined points. This has been done already for F_1 in Fig. 2. Fig. 8 is a similar comparison for F_2 and F_3. As in Fig. 2, the points shown are the observed values, the curves the theoretical values. Since L_0, L_1, and F_∞ were determined from the high-pressure data the agreement is necessarily good for these values of the pressure. It is seen that the agreement is good for F_1 and F_2 for all pressures, but that for F_3, for pressures less than 2×10^{-2} mm, the experimental points lie considerably above the curve plotted from Eq. (5). For argon and krypton the experimental

points for F_1 and F_2 also lie above the curves, but in no case is the deviation as great as for F_3. With increasing velocity the deviation decreases, being small for the highest velocities.

This deviation from the theoretical curves may be shown in another way. Given a set of values of F_1, F_2, and F_3 for a particular pressure and velocity, it is possible to solve Eqs. (4) and (5) for L_0, L_1, and F_∞, i.e., for each velocity it is possible to determine the required constants for a series of pressures. This has been done; the results are shown in Figs. 9 and 10. In Fig. 9, p/L_0 and in Fig. 10, p/L_1 are plotted against pressure. The graphs for neon for accelerating potentials of 16,000 and 22,000 volts are shown in each case. Since L_0 and L_1 are constants,—the free paths for 1 mm pressure—as expressed in the equations, p/L_0 *vs.* p and p/L_1 *vs.* p should both give straight lines through the origin. Actually the graphs are approximately straight lines but

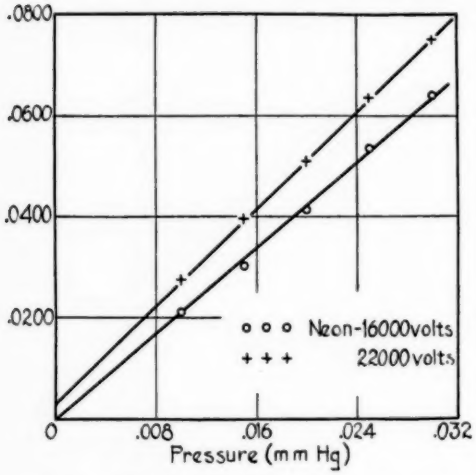

Fig. 9. Relationship between free path for ionization and pressure. Abscissa, p/L_0.

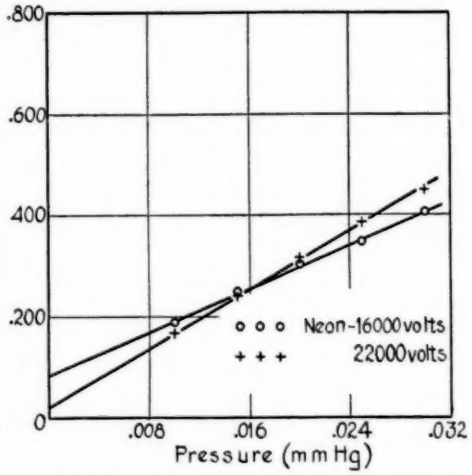

Fig. 10. Relationship between free path for neutralization and pressure. Abscissa, p/L_1.

do not pass through the origin. In Fig. 9 the displacement is small in both cases—probably less than experimental error. In Fig. 10, however, the displacement is much greater. The fact that it is smaller for 22,000 volts than for 16,000 volts corresponds to the fact that the agreement between experimental and theoretical values, shown in Fig. 8, is much better for the higher velocities. For argon and krypton, the straight lines of Fig. 9 are also displaced from the origin, since for these gases, the experimental values of F_1 and F_2 do not fall on the theoretical curves as they do in the case of neon, but here again the displacement decreases with increasing velocity.

Two arguments may be advanced to justify the calculation of the desired constants from the high-pressure data. First, the corrected curves for F_2 and F_3, shown in Fig. 3, do exhibit the properties expected at high pressures. Also, it is possible to obtain much better agreement between experimental and theoretical values by using the values of L_0 and L_1 determined for high rather than low pressures. The second is found in Rüchardt's work[8] with

hydrogen. His data also gave displaced straight lines like those shown in Figs. 9 and 10 when the reciprocals of the free paths were plotted against pressure. However, when the work was repeated, taking great precautions to eliminate all vapors, he obtained straight lines through the origin. He found that the lines obtained in the first case, were displaced considerably from the lines in the second case for low pressures, but that the displacement decreased with increasing pressure, i.e., the values for the free paths, as determined at high pressures, were the same in the two cases. In view of this work, it seems probable that the errors in the values given in Table I are not great.

Several explanations may be suggested for the disagreement between experimental and theoretical curves at low pressures. The fact that the discrepancy increases with decreasing velocity, and is greater for argon and krypton than for neon, suggests that scattering may have influenced the results since a comparison of total beam intensities at different velocities indicated that scattering increases with decreasing velocity and with increasing atomic number. This explanation is further supported by the fact that in some cases the corrected curves F_2' and F_3' of Fig. 3, do not reach a constant value, but appear to continue to decrease with increasing pressure. This can be explained by assuming that the neutral particles were scattered more than the ions. This decrease, however, is scarcely greater than experimental error in any case. An investigation of the effect of scattering shows that the results would depend only on the difference between the scattering coefficients of the atoms and ions, i.e., if they were scattered equally the results would be unaffected. Assuming a difference in scattering, we find that good agreement can be obtained between experimental and theoretical curves, but only when an unreasonably large difference in scattering coefficients is assumed—a difference so large that the intensity of the beam reaching the thermocouple would have been so small as to be quite undetectable. For this reason the scattering explanation seems to be ruled out. However, it should be pointed out that, while a small difference in the scattering of atoms and ions would not change appreciably the measured values of F_1, F_2, and F_3, the values of L_0, L_1, and F_∞, as calculated, might be very considerably in error if such a phenomenon were present.

It has been suggested that three rather than two types of particles may have been present in the beam, e.g., normal atoms, metastable atoms, and positive ions. An investigation of this possibility, with the necessary introduction of rather arbitrary assumptions about the processes involved, gives only slightly better agreement than the simple theory with the experimental values. This better agreement may, perhaps, be explained merely by the fact that another parameter is introduced into the equations; at least, the agreement obtained does not warrant any conclusions as to the correctness of the assumptions made.

In his work on hydrogen, Rüchardt[8] concluded that the observed discrepancies could be accounted for completely by the presence of vapors in the tube. In the present work, it does not seem unlikely that vapors were

present, despite the precautions taken, since a continuous flow of gas was not used. Further, Bartels[18] found that the fraction of neutral particles increased when the beam passed through a slit. This may be accounted for, probably, by the evolution of vapors due to bombardment of the edges of the slit. In the present work, vapors might be expected to be present for this reason also, since the beam passed through several circular diaphragms. The pressure of such vapors would be independent of the gas pressure in the tube. However, the number of collisions with vapor molecules relative to the number of collisions with gas atoms, would be greater at low pressures; therefore, the discrepancies introduced would be greater at these pressures. The observed deviations would be accounted for if the ions in the beam were more readily neutralized by collisions with the vapor molecules than with the gas atoms, since, in all cases, the fraction of neutral atoms in the beam at low pressures is greater than that expected from high-pressure measurements. On the whole, the presence of vapors seems to be the most reasonable explanation of the observed discrepancies, although it is quite probable that all the suggested phenomena and other more complex ones influence the measurements in some degree. If the discrepancies are accounted for by the presence of vapors, it seems likely that the values given in Table I, determined from the high-pressure measurements, are reasonably accurate. It may seem that the measurements for argon and krypton are much less reliable than for neon since the pressure range investigated was considerably lower, but in this connection, it should be noted that F_2 and F_3 became equal at much lower pressures with these gases than with neon and that the discrepancies observed were only slightly greater than with neon.

It will be seen from Figs. 4 and 5 that, for all the gases investigated in the present work, both free paths decrease slowly with increasing velocity. The behavior of helium differs in two respects; first, the rate of decrease of L_0 with increasing accelerating potential is much greater than for neon, argon, or krypton; secondly, for helium, L_1 increases rather than decreases as the velocity becomes greater. Fig. 7 shows a minimum value of F_∞ as a function of atomic number for both 13,000 and 22,000 volts, although it appears that for higher velocities this minimum would disappear. With reference to the dependence of F_∞ on atomic number, it may be noted further from Fig. 6 that the rate of change of F_∞ with velocity increases with atomic number from a relatively large negative value for helium to a small positive value for krypton. The increase of F_∞ with velocity for krypton, however, is small enough to be rather uncertain.

It is interesting to compare the measured values of the free paths with the kinetic theory values. A comparison shows that for neon the kinetic theory free path is about one-thirtieth of the free path for ionization of a high-velocity atom and about one-fifth of the free path for the neutralization of a fast ion, i.e., a moving atom is ionized at about every thirtieth collision with a rest atom and a moving ion is neutralized at about every fifth collision.

[18] H. Bartels, reference 9, p. 969.

In argon, the probability of ionization is less, occurring for approximately one collision in sixty, but the probability of neutralization is about the same. With krypton, ionization takes place at every seventieth collision, approximately, while neutralization occurs for one collision in four.

A comparison of the free paths of the ions in the present work, with those obtained from the low-velocity measurements of Kallmann and Rosen[1] and others[3,4] shows that the values for high velocities are approximately three times those for the slow ions in all cases. Since Fig. 5 shows a decrease of L_1 with increasing velocity, for neon, argon, and krypton, the comparison might suggest that the free path for neutralization for these gases, has a maximum for some accelerating potential intermediate between 800 and 7000 volts. This is not a necessary conclusion, however, as the difference in the method of measurement makes the comparison doubtful. In the present work only a difference in the scattering of the atoms and ions would affect the results, whereas with the method used in the low-velocity measurements, any scattering of ions would result in a decrease of the intensity of the ionic beam, and, therefore, in a decrease of the measured free path. It seems probable that scattering would be relatively large for the slow ions, particularly in view of the conclusion of Kallmann, Lasareff, and Rosen in a recent article[19] that slow neutral atoms are scattered at every kinetic theory collision. The difference in the values obtained may, perhaps, be completely explained by the effect of scattering in the low-velocity measurements.

Doppler effect observations of positive rays of neon[12,13] and argon[13,14] of velocities similar to those used in the present work show a surprising absence of displaced arc lines. This fact might be interpreted as proof that the particles in the beam are predominantly positive, the absence of neutral atoms accounting for the absence of displaced arc lines. This suggestion is supported by the work of Rutherford[20] and Henderson[21] in which they found that neutral atoms are present in an α-ray beam only at lower velocities. The present experiments show, however, that in neon 86 percent of the particles in the beam are neutral, while in argon 93 percent and in krypton 95 percent are neutral. This seems to rule out the suggested interpretation. The alternative interpretation appears to be that, for some reason, after a collision a moving particle is seldom, if ever, left in an excited neutral state.

The writer desires to acknowledge the assistance given by Professor A. J. Dempster in suggesting the problem, and to thank him for much valuable advice and criticism which have aided in avoiding many of the difficulties of the problem and in solving others when encountered.

[19] H. Kallmann, W. Lasareff and B. Rosen, Zeits. f. Physik **76,** 213 (1932).
[20] E. Rutherford, Phil. Mag. **47,** 277 (1924).
[21] G. H. Henderson, Proc. Roy. Soc. **A109,** 157 (1925).

Extension of the First Spark Spectrum of Caesium (Cs II)

By J. OLTHOFF AND R. A. SAWYER
University of Michigan

(Received September 1, 1932)

With an electrodeless discharge in caesium vapor as a light source, the spark spectrum of caesium has been completely rephotographed in the region λ2300–λ10,000 in the first order of 21 ft. concave grating and with a Hilger E1 quartz spectrograph. The observations of Sommer in the region λ3268–λ7280 were confirmed and extended and many new lines were photographed outside Sommer's range. These data were used to extend the classifications of Laporte, Miller and Sawyer, based on Sommer's data supplemented by vacuum spectrograph measurements, in which practically only terms belonging to the $5p^5\ ^2P_{1\frac{1}{2}}$ limit were identified. In the present work most of the terms of the $5p^5$ ($^2P_{\frac{1}{2}}$) $5d$, $6d$, $6s$, $7s$, and $6p$ configurations were located as well as a few new terms belonging to the $5p^5\ ^2P_{1\frac{1}{2}}$ limit, and about 100 additional lines were classified in the Cs II spectrum.

I. INTRODUCTION

IN A recent publication Laporte, Miller[1] and Sawyer presented an interpretation of the first spark spectrum of caesium on the basis of the material of Sommer[2] who photographed the caesium spark spectrum in the region λλ3267–7280 and arranged 51 lines in a scheme involving transitions between a middle group of five terms and an upper and a lower group of eight and five terms, respectively. Sommer pointed out the similarity to the neon spectrum but was unable to correlate the two spectra unambiguously. Laporte, Miller and Sawyer photographed the caesium spectrum from a hollow cathode discharge in helium with a 1 meter vacuum spectrograph and discovered eight new lines in the region between 962A and 612A. Identification of these ultraviolet lines as transitions between the lowest term $5p^6\ ^1S_0$, and terms of the configurations $5p^5$ ($6s$, $7s$, $5d$, $6d$) having $j=1$, made possible the interpretation of Sommer's scheme since five of the eight ultraviolet lines proved to involve terms in Sommer's scheme.

It was found that Sommer's middle set of terms belonged to the $5p^5\ 6p$ configuration and his upper and lower sets, respectively, to a blend of $5p^5\ 5d$ and $6s$, and $5p^5\ 6d$ and $7s$. However, from the table of electron configurations and expected terms in a rare gas spectrum given in Table I, it may be seen that these three term groups should contain respectively 10, 16 and 16 terms, divided in each case for (jj) coupling, into two sets having as limits, one $5p^5\ ^2P_{1\frac{1}{2}}$ and the other $5p^5\ ^2P_{\frac{1}{2}}$ of the Cs II spectrum. The two sets will be completely and widely separated in Cs II as indeed they are for the preceding spectrum of Xe I. Sommer's terms were shown to belong entirely to lower series limit $^2P_{1\frac{1}{2}}$, while the remaining three resonance lines which did not fit into his scheme were believed to arise from configurations built upon $^2P_{\frac{1}{2}}$.

[1] Laporte, Miller, Sawyer, Phys. Rev. **39**, 458 (1932).
[2] Sommer, Ann. d. Physik **75**, 163 (1924).

TABLE I. *Electron configurations and theoretical terms of the Cs II spectrum.*

Electron configuration	Russell-Saunders	(*jj*)		Number of levels
$5p^5$	^2P	$^2P_{1\frac{1}{2}}$	$^2P_{\frac{1}{2}}$	(2)
$5p^6$	$^1S_0$	0		(1)
$5p^5\,6s$ $5p^5\,7s$ $5p^5\,8s$ ...	$^1P_1$ $^3P_{210}$	21	10	(4)
$5p^5\,6p$ $5p^5\,7p$ $5p^5\,8p$ ...	$^1S_0\,^1P_1\,^1D_2\,^3S_1\,^3P_{210}\,^3D_{321}$	12 0123	01 12	(10)
$5p^5\,5d$ $5p^5\,6d$ $5p^5\,7d$ ...	$^1P_1\,^1D_2\,^1F_3\,^3P_{210}\,^3D_{321}\,^3F_{432}$	0123 1234	12 23	(12)
$5p^5\,4f$ $5p^5\,5f$ $5p^5\,6f$ ...	$^1D_2\,^1F_3\,^1S_4\,^3D_{321}\,^3F_{432}\,^3G_{543}$	1234 2345	23 34	(12)

An attempt was made in the previous work to locate more terms built on the $^2P_{\frac{1}{2}}$ limit but except for a tentative group of three terms, which combined with the three terms indicated by the three resonance lines mentioned above, none were found. The data of Sommer seemed insufficient in range for the purpose. The present study has been undertaken to extend the experimental data on the spark spectrum of caesium with the hope of locating more terms and especially those based on the $^2P_{\frac{1}{2}}$ limit.

II. EXPERIMENTAL

In the work of Laporte, Miller and Sawyer, the light source used was a hollow cathode discharge in helium. Since, however, the available excitation which can be given to caesium ions by metastable helium atoms is about 163,000 cm^{-1} and the ionization potential of Cs II was determined to be about 189,000, this source is not suitable for the excitation of the complete Cs II spectrum.[3] The electrodeless discharge was chosen for the present work because of its economy of material and easily controllable conditions.

The discharge tube was a Corex bulb about 4 cm in diameter and 15 cm long, and was originally blown with a side arm in which several seal-off constrictions separated small bulbs, as well as with a side arm for evacuating. In an atmosphere of nitrogen in a manipulation box, a small fraction of a gram of caesium was washed in anhydrous ether and placed in the side arm. The bulb was evacuated by a mercury vapor pump, the first side arm sealed off and the caesium distilled by stages through the small bulbs into the main bulb and the main bulb, after thorough heating while still on the pumps to drive off adsorbed gases and vapors, was sealed off while still hot. The bulb was suspended inside the exciting coil of eight turns of hollow copper tubing wound in a solenoid about 10 cm in diameter and 8 cm long and the whole

[3] Cf. for example, Sawyer, Phys. Rev. **36**, 44 (1930).

TABLE II.

$5p^5(^2P_{1\frac{1}{2}})5d, 6s$			$5p^4$	$5p^5(^2P_{1\frac{1}{2}})6p$		
			$^1S_0$	1_1	2_2	3_3
	J		0	1	2	3
		Relative term value	00.00	*126,518.54	*128,089.83	*129,107.65
4_3^0	3	105,949.74			22,139.77 (2) 0.32	23,157.78 (0) 0.13
5_1^0	1	106,222.77		20,295.73 (1) 0.04	21,867.31 (3) −0.25	
$^3P_2^0$	2	*107,392.33		*19,126.12 (8) 0.09	*20,697.48 (6) 0.02	*21,715.33 (10) −0.01
6_2^0	2	107,563.14		18,955.52 (4) −0.08		21,544.16 (1) 0.35
$^3P_1^0$	1	*107,905.01	*107,905 (20) 0.01	*18,613.42 (6) 0.11	*20,184.84 (6) −0.02	
7_0^0	0	108,245.86				
1_1^0	1	*110,945.18	*110,946 (20) −0.72	*15,573.14 (2) 0.18	*17,144.51 (6) 0.10	
2_2^0	2	*112,795.08			*15,294.63 (4) 0.12	*16,312.38 (4) 0.19
3_3^0	3	*113,716.01			*14,373.12 (4) 0.10	*15,390.96 (3) 0.08
$5p^5(^2P_{\frac{1}{2}})5d, 6s$						
1_0^0	0	119,465.28				
2_1^0	2	119,665.41				
3_2^0	2	120,404.87				
4_1^0	1	122,866.03	*122,872 (20) −5.97			
5_1^0	1	123,636.44	*123,645 (20) −8.56			
$5p^5(^2P_{1\frac{1}{2}})6d, 7s$						
$^3P_2^0$	2	*149,212.25		*22,693.82 (7) −0.11	*21,122.47 (4) −0.05	*20,104.64 (5) −0.04
$^3P_1^0$	1	*149,605.33	*149,604 (12)	*23,086.95 (4) −0.16	*21,515.53 (5) −0.03	
1_1^0	1	*152,172.11	*152,172 (5) 0.11	*25,653.67 (7) −0.10	*24,082.27 (4) 0.01	
2_2^0	2	*152,791.49		*26,273.12 (6) −0.17	*24,701.59 (4) 0.07	*23,683.75 (3) 0.09
3_3^0	2	*153,302.27		*26,783.83 (2) −0.10	*25,212.38 (6) 0.06	*24,194.54 (2) 0.08
4_3^0	3	*153,556.54			*25,466.74 (6) −0.03	
5_3^0	3	*153,678.17			*25,588.30 (4) 0.04	*24,570.52 (6) −0.04
6_1^0	1	*156,399.31	*156,392 (12) 7.31		*28,309.51 (0) −0.03	
$5p^5(^2P_{1\frac{1}{2}})7d, 8s; 5p^5(^2P_{\frac{1}{2}})6d, 7s$						
1_2^0	2	158,717.91			30,628.61 (1) −0.53	29,610.16 (0) 0.10
2_0^0	0	162,352.92		35,834.32 (3p) 0.06		
3_3^0	3	162,388.96			34,299.37 (3) −0.24	
4_1^0	1	163,180.20	*163,180 (7) 0.20	36,662.16 (0p) −0.50	35,090.18 (1p) 0.09	
5_2^0	2	164,444.88		37,926.67 (0p) −0.33	36,355.02 (1p) 0.03	35,337.24 (2) −0.01
6_1^0	1	164,656.77	*164,655(3) 1.77		36,567.26 (2p) −0.32	
	1	165,813.70				
	2 or 1	165,899.95		39,371.06 (2p) 0.35		
9^0	2 or 1	166,131.11			38,041.11 (2p) 0.17	
10_3^0	3	166,600.74			38,510.97 (1p) −0.06	37,493.20 (0p) −0.11

* Terms and transitions discovered by Laporte, Miller and Sawyer.

TABLE II. (*Continued*).

$5p^5(^2P_{1\frac{1}{2}})6p$			$5p^5(^2P_{\frac{1}{2}})6p$			
4_1	5_2	6_0	1_1	2_1	3_2	4_0
1	2	0	1	1	2	0
*129,989.72	*130,766.00	*133,153.54	141,555.59	143,352.12	143,394.19	144,523.45
	24,816.59 (0) −0.33				37,444.50 (1) −0.05	
	24,542.83 (1) 0.40		35,332.52 (2p) 0.30		37,171.83 (2p) −0.41	38,300.69 (0p) −0.01
*22,597.42 (2) −0.03	*23,373.78 (9) −0.11		34,163.16 (0) −0.10	35,959.78 (1) 0.01		
22,426.92 (3) −0.34			33,992.66 (7) −0.21	35,789.21 (2) −0.23		
*22,084.85 (7) −0.14	*22,861.10 (6) −0.11	*25,248.63 (5) −0.10	33,650.61 (5) −0.03	35,447.19 (2p) −0.08	35,489.04 (4p) 0.14	36,618.32 (1p) 0.12
21,744.06 (2) −0.20			33,309.52 (2) 0.21	35,106.30 (0p) −0.04		
*19,044.61 (6) −0.11	*19,820.81 (6) −0.03	*22,208.49 (7) −0.17	30,610.40 (7) −0.01	32,406.84 (1) 0.10	32,448.92 (2) 0.09	33,578.17 (1) 0.10
*17,194.57 (3) 0.07	*17,970.87 (7) 0.05		28,760.70 (0) −0.19	30,557.09 (5) −0.05	30,599.05 (7) 0.06	
	*17,049.36 (1) 0.03				29,677.65 (7) −0.07	
			22,090.41 (0) −0.10	23,886.73 (1) 0.11		
			21,890.25 (3) −0.07	23,686.83 (0) −0.12	23,728.67 (6) 0.11	
			21,150.58 (1) 0.14	22,947.39 (0) −0.14	22,989.36 (0) −0.14	
			*18,689.34 (3) 0.22	20,486.32 (0) −0.23	*20,528.06 (6) 0.10	*21,657.19 (3) 0.23
			*17,919.29 (0) −0.14	19,715.72 (0) −0.04	*19,757.88 (3) −0.13	*20,886.87 (3) 0.14
	*18,446.14 (5) 0.11					
*19,615.46 (4) 0.15	*18,839.20 (3) 0.13	*16,451.65 (2) 0.14				
*22,182.32 (2) 0.07	*21,406.02 (4) 0.09	19,018.53 (0) 0.04				
*22,801.61 (5) 0.16	*22,025.41 (6) 0.08					
*23,312.46 (7) 0.09	*22,536.21 (0) 0.06					
	*22,790.50 (0) 0.04					
	*22,912.15 (9) 0.02					
*26,409.65 (5) −0.06	*25,633.22 (0) 0.09	*23,245.86 (6) −0.09				
	27,951.81 (0) 0.10			15,365.59 (1) 0.20		
32,363.01 (1) 0.19			20,797.53 (1) −0.20			
	31,623.10 (0p) −0.14				18,994.53 (0) 0.24	
33,190.44 (2) 0.04		30,026.58 (2) 0.08	*21,624.51 (4) 0.10	19,828.56 (1) 0.48	*19,785.91 (3) 0.10	*18,656.65 (0) 0.10
	33,678.55 (2) 0.33			21,092.66 (5) 0.10	21,050.61 (2) 0.10	
34,666.98 (2) 0.07	33,890.73 (5) 0.04	31,503.30 (1) −0.07	23,101.13 (2) 0.05	21,304.73 (1) −0.08	21,262.55 (5) 0.03	
	35,047.74 (0) −0.04	32,659.85 (1) 0.31	24,257.90 (4) 0.21	22,461.66 (1) 0.08	22,419.35 (3) 0.16	21,290.55 (1) −0.30
35,900.36 (1p) −0.13	35,124.31 (4) −0.36		24,334.53 (0) −0.17	22,538.01 (4) −0.18	22,495.94 (2) −0.18	
36,141.39 (2p) 0.00	35,365.28 (0p) −0.17		24,575.44 (6) 0.08	22,779.08 (2) −0.09	22,736.88 (3) 0.04	
					23,206.44 (1)	
					23,206.44 (1) 0.11	

* Terms and transitions discovered by Laporte, Miller and Sawyer.

placed in a transite box or oven provided with nichrome heating wires on its inner walls and with a quartz window for end-on observation of the tube. The exciting current was provided by a large commercial induction furnace of quenched gap type operating on 220-volt a.c. The exciting coil was cooled when in operation by water circulation. To attain the requisite vapor pressure of caesium it was necessary to heat the bulb by the oven to a temperature in the range 120°–200°C. Once the discharge had started, the heat from the exciting coil in the luminous vapor and especially from the dielectric losses in the glass was sufficient so that no auxiliary heating was needed. In fact the dielectric loss in the glass heated it to so great an extent that it was found safe to operate the discharge only 15 seconds in each minute. The discharge was bluish-white in color, filling the entire bulb apparently uniformly, and of tremendous brilliancy.

The discharge was photographed in the region λ2300–λ3300A with a Hilger E1 quartz spectrograph and from λ2300–λ10,000A in the first order of a 21 ft, 15,000 line grating. Exposure times, i.e., actual operation of the discharge, varied from 45 sec. with contrast plates on the quartz spectrograph in the region near λ3000 to as long as 1½ hours on some of the grating exposures in the less sensitive regions. Few lines were measured on the grating below λ2700. The longest wave-length measured was λ8194 and the shortest λ2315. The short wave-length limit was doubtless due to the absorption of the Corex glass. All wave-lengths were measured against standards from an iron arc and determinations are believed to be accurate in most cases to ±0.01 or 0.02A. Practically all the lines given by Sommer (about 380) were verified and 200 additional lines were measured in his region. The coarse hyperfine structure reported by Sommer for most of the strong lines was not observed. About 300 new lines were found below Sommer's limit in the ultraviolet and a few in the red.

III. Analysis of Data

In Table II are given the results of the classification of the spectrum of Cs II. In the first column are given the electronic configurations of the odd terms and spectroscopic notations of the levels where known. Numbers have

Table III. *Wave-length list of Cs II lines classified.*

Int.		λ in air	ν (vac)	Classification
3	vac.	607.31	164,655	$5p^6\,{}^1S_0-({}^2P_{1\frac{1}{2}}\,7d, 8s; {}^2P_{\frac{1}{2}}\,6d, 7s)6_1{}^0$
7	"	612.82	163,180	$5p^6\,{}^1S_0-({}^2P_{\frac{1}{2}}\,6d, 7s)4_1{}^0$
12	"	639.42	156,392	$5p^6\,{}^1S_0-({}^2P_{1\frac{1}{2}}\,6d)6_1{}^0$
5	"	657.15	152,172	$5p^6\,{}^1S_0-({}^2P_{1\frac{1}{2}}\,6d)1_1{}^0$
12	"	668.43	149,604	$5p^6\,{}^1S_0-({}^2P_{1\frac{1}{2}}\,7s\,{}^3P_1{}^0$
20	"	808.77	123,645	$5p^6\,{}^1S_0-({}^2P_{1\frac{1}{2}}\,5d, 6s)5_1{}^0$
20	"	813.85	122,872	$5p^6\,{}^1S_0-({}^2P_{\frac{1}{2}}\,5d, 6s)4_1{}^0$
20	"	901.34	110,946	$5p^6\,{}^1S_0-({}^2P_{1\frac{1}{2}}\,5d)1_1{}^0$
20	"	926.75	107,905	$5p^6\,{}^1S_0-({}^2P_{1\frac{1}{2}}\,6s)\,{}^3P_1{}^0$
2p		2539.174	39,371.06	$({}^2P_{1\frac{1}{2}}\,6p)1_1-({}^2P_{1\frac{1}{2}}\,7d, 8s; {}^2P_{\frac{1}{2}}\,6d, 7s)8^0$
1p		2595.886	38,510.97	$({}^2P_{1\frac{1}{2}}\,6p)2_2-({}^2P_{1\frac{1}{2}}\,7d, 8s; {}^2P_{\frac{1}{2}}\,6d, 7s)10_2{}^0$
0p		2610.140	38,300.69	$({}^2P_{\frac{1}{2}}\,6p)4_0-({}^2P_{1\frac{1}{2}}\,5d, 6s)5_1{}^0$
2p		2627.952	38,041.11	$({}^2P_{1\frac{1}{2}}\,6p)2_2-({}^2P_{1\frac{1}{2}}\,7d, 8s; {}^2P_{\frac{1}{2}}\,6d, 7s)9^0$
0p		2635.882	37,926.67	$({}^2P_{1\frac{1}{2}}\,6p)1_1-({}^2P_{1\frac{1}{2}}\,7d, 8s; {}^2P_{\frac{1}{2}}\,6d, 7s)5_2{}^0$
0p		2666.358	37,493.20	$({}^2P_{1\frac{1}{2}}\,6p)3_3-({}^2P_{1\frac{1}{2}}\,7d, 8s; {}^2P_{\frac{1}{2}}\,6d, 7s)10_3{}^0$

TABLE III. (*Continued*).

Int.	λ in air	ν (vac)	Classification
1*p*	2669.792	37,444.50	$(^2P_{\frac{1}{2}}\ 6p)3_2-(^2P_{1\frac{1}{2}}\ 5d,\ 6s)4_3^0$
2*p*	2689.412	37,171.83	$(^2P_{\frac{1}{2}}\ 6p)3_2-(^2P_{1\frac{1}{2}}\ 5d)5_1^0$
0*p*	2726.802	36,662.16	$(^2P_{1\frac{1}{2}}\ 6p)1_1-(^2P_{1\frac{1}{2}}\ 7d,\ 8s;\ ^2P_{\frac{1}{2}}\ 6d,\ 7s)4_1^0$
1*p*	2730.065	36,618.32	$(^2P_{\frac{1}{2}}\ 6p)4_0-(^2P_{\frac{1}{2}}\ 6s)^3P_1^0$
2*p*	2733.879	36,567.26	$(^2P_{1\frac{1}{2}}\ 6p)2_2-(^2P_{1\frac{1}{2}}\ 7d,\ 8s;\ ^2P_{\frac{1}{2}}\ 6d,\ 7s)6_1^0$
1*p*	2749.839	36,355.02	$(^2P_{1\frac{1}{2}}\ 6p)2_2-(^2P_{1\frac{1}{2}}\ 7d,\ 8s;\ ^2P_{\frac{1}{2}}\ 6d,\ 7s)5_2^0$
2*p*	2766.095	36,141.39	$(^2P_{1\frac{1}{2}}\ 6p)4_1-(^2P_{1\frac{1}{2}}\ 7d,\ 8s;\ ^2P_{\frac{1}{2}}\ 6d,\ 7s)9^0$
1*p*	2780.065	35,959.78	$(^2P_{\frac{1}{2}}\ 6p)2_1-(^2P_{1\frac{1}{2}}\ 6s)^2P_2^0$
1*p*	2784.666	35,900.36	$(^2P_{1\frac{1}{2}}\ 6p)4_1-(^2P_{1\frac{1}{2}}\ 7d,\ 8s;\ (^2P_{\frac{1}{2}}\ 6d,\ 7s)8^0$
3*p*	2789.797	35,834.32	$(^2P_{1\frac{1}{2}}\ 6p)1_1-(^2P_{1\frac{1}{2}}\ 7d,\ 8s;\ ^2P_{\frac{1}{2}}\ 6d,\ 7s)2_0^0$
2*p*	2793.316	35,789.21	$(^2P_{\frac{1}{2}}\ 6p)2_1-(^2P_{1\frac{1}{2}}\ 5d,\ 6s)6_2^0$
4*p*	2816.943	35,489.04	$(^2P_{\frac{1}{2}}\ 6p)3_2-(^2P_{1\frac{1}{2}}\ 6s)^3P_1^0$
2*p*	2820.268	35,447.19	$(^2P_{\frac{1}{2}}\ 6p)2_1-(^2P_{1\frac{1}{2}}\ 6s)^3P_1^0$
0*p*	2826.802	35,365.28	$(^2P_{1\frac{1}{2}}\ 6p)5_2-(^2P_{1\frac{1}{2}}\ 7d,\ 8s;\ (^2P_{\frac{1}{2}}\ 6d,\ 7s)9^0$
2	2829.045	35,337.24	$(^2P_{1\frac{1}{2}}\ 6p)3_3-(^2P_{1\frac{1}{2}}\ 7d,\ 8s;\ ^2P_{\frac{1}{2}}\ 6d,\ 7s)5_2^0$
2*p*	2829.423	35,332.52	$(^2P_{\frac{1}{2}}\ 6p)1_1-(^2P_{1\frac{1}{2}}\ 5d)5_1^0$
5	2846.193	35,124.31	$(^2P_{1\frac{1}{2}}\ 6p)5_3-(^2P_{1\frac{1}{2}}\ 7d,\ 8s;\ ^2P_{\frac{1}{2}}\ 6d,\ 7s)8^0$
0*p*	2847.655	35,106.30	$(^2P_{\frac{1}{2}}\ 6p)2_1-(^2P_{1\frac{1}{2}}\ 5d)7_0^0$
1*p*	2848.955	35,090.18	$(^2P_{1\frac{1}{2}}\ 6p)2_2-(^2P_{1\frac{1}{2}}\ 7d,\ 8s;\ ^2P_{\frac{1}{2}}\ 6d,\ 7s)4_1^0$
0	2852.415	35,047.74	$(^2P_{1\frac{1}{2}}\ 6p)5_2-(^2P_{1\frac{1}{2}}\ 7d,\ 8s;\ ^2P_{\frac{1}{2}}\ 6d,\ 7s)7_1^0$
2	2883.745	34,666.98	$(^2P_{1\frac{1}{2}}\ 6p)4_1-(^2P_{1\frac{1}{2}}\ 7d,\ 8s;\ ^2P_{\frac{1}{2}}\ 6d,\ 7s)6_1^0$
3	2914.652	34,299.37	$(^2P_{1\frac{1}{2}}\ 6p)2_3-(^2P_{1\frac{1}{2}}\ 7d,\ 8s;\ (^2P_{\frac{1}{2}}\ 6d,\ 7s)3_2^0$
0	2926.274	34,163.16	$(^2P_{\frac{1}{2}}\ 6p)1_1-(^2P_{1\frac{1}{2}}\ 6s)^3P_2^0$
7	2940.953	33,992.66	$(^2P_{\frac{1}{2}}\ 6p)1_1-(^2P_{1\frac{1}{2}}\ 5d)\ 6_2^0$
5	2949.800	33,890.73	$(^2P_{1\frac{1}{2}}\ 6p)5_2-(^2P_{1\frac{1}{2}}\ 7d,\ 8s;\ ^2P_{\frac{1}{2}}\ 6d,\ 7s)6_1^0$
2	2968.383	33,678.55	$(^2P_{1\frac{1}{2}}\ 6p)5_3-(^2P_{1\frac{1}{2}}\ 7d,\ 8s;\ ^2P_{\frac{1}{2}}\ 6d,\ 7s)5_2^0$
5	2970.851	33,650.61	$(^2P_{\frac{1}{2}}\ 6p)1_1-(^2P_{1\frac{1}{2}}\ 6s)^3P_1^0$
1	2977.258	33,578.17	$(^2P_{\frac{1}{2}}\ 6p)4_0-(^2P_{1\frac{1}{2}}\ 5d)1_1^0$
2	3001.271	33,309.52	$(^2P_{\frac{1}{2}}\ 6p)1_1-(^2P_{1\frac{1}{2}}\ 5d)7_0^0$
2*p*	3012.041	33,190.44	$(^2P_{1\frac{1}{2}}\ 6p)4_1-(^2P_{1\frac{1}{2}}\ 7d,\ 8s;\ ^2P_{\frac{1}{2}}\ 6d,\ 7s)4_1^0$
1	3060.976	32,659.85	$(^2P_{1\frac{1}{2}}\ 6p)6_0-(^2P_{1\frac{1}{2}}\ 7d,\ 8s;\ ^2P_{\frac{1}{2}}\ 6d,\ 7s)7_1^0$
2	3080.874	32,448.92	$(^2P_{\frac{1}{2}}\ 6p)3_2-(^2P_{1\frac{1}{2}}\ 5d)1_1^0$
1	3084.875	32,406.84	$(^2P_{\frac{1}{2}}\ 6p)2_1-(^2P_{1\frac{1}{2}}\ 5d)1_1^0$
1*p*	3089.053	32,363.01	$(^2P_{1\frac{1}{2}}\ 6p)4_1-(^2P_{1\frac{1}{2}}\ 7d,\ 8s;\ ^2P_{\frac{1}{2}}\ 6d,\ 7s)2_0^0$
0*p*	3161.333	31,623.10	$(^2P_{1\frac{1}{2}}\ 6p)5_2-(^2P_{1\frac{1}{2}}\ 7d,\ 8s;\ ^2P_{\frac{1}{2}}\ 6d,\ 7s)3_2^0$
1	3173.355	31,503.30	$(^2P_{1\frac{1}{2}}\ 6p)6_0-(^2P_{1\frac{1}{2}}\ 7d,\ 8s;\ ^2P_{\frac{1}{2}}\ 6d,\ 7s)6_1^0$
1	3263.982	30,628.61	$(^2P_{1\frac{1}{2}}\ 6p)2_2-(^2P_{1\frac{1}{2}}\ 7d,\ 8s;\ ^2P_{\frac{1}{2}}\ 6d,\ 7s)1_2^0$
7	3265.924	30,610.40	$(^2P_{\frac{1}{2}}\ 6p)1_1-(^2P_{1\frac{1}{2}}\ 5d)1_1^0$
7	3267.135	30,599.05	$(^2P_{\frac{1}{2}}\ 6p)3_2-(^2P_{1\frac{1}{2}}\ 5d)2_2^0$
5	3271.626	30,557.09	$(^2P_{\frac{1}{2}}\ 6p)2_1-(^2P_{1\frac{1}{2}}\ 5d)2_2^0$
2	3329.428	30,026.58	$(^2P_{1\frac{1}{2}}\ 6p)6_0-(^2P_{1\frac{1}{2}}\ 7d,\ 8s;\ (^2P_{\frac{1}{2}}\ 6d,\ 7s)4_1^0$
7	3368.575	29,677.65	$(^2P_{\frac{1}{2}}\ 6p)3_2-(^2P_{1\frac{1}{2}}\ 5d)3_2^0$
0	3376.261	29,610.16	$(^2P_{1\frac{1}{2}}\ 6p)3_3-(^2P_{1\frac{1}{2}}\ 7d,\ 8s;\ ^2P_{\frac{1}{2}}\ 6d,\ 7s)1_2^0$
0	3475.973	28,760.70	$(^2P_{\frac{1}{2}}\ 6p)1_1-(^2P_{1\frac{1}{2}}\ 5d)2_2^0$
0	3531.376	28,309.51	$(^2P_{1\frac{1}{2}}\ 6p)2_2-(^2P_{1\frac{1}{2}}\ 6d)6_1^0$
0	3576.570	27,951.81	$(^2P_{1\frac{1}{2}}\ 6p)5_2-(^2P_{1\frac{1}{2}}\ 7d,\ 8s;\ ^2P_{\frac{1}{2}}\ 6d,\ 7s)1_2^0$
2	3732.539	26,783.83	$(^2P_{1\frac{1}{2}}\ 6p)1_1-(^2P_{1\frac{1}{2}}\ 6d)\ 3_2^0$
5	3785.424	26,409.65	$(^2P_{1\frac{1}{2}}\ 6p)4_1-(^2P_{1\frac{1}{2}}\ 6d)6_1^0$
6	3805.096	26,273.12	$(^2P_{1\frac{1}{2}}\ 6p)1_1-(^2P_{1\frac{1}{2}}\ 6d)2_2^0$
7	3896.978	25,653.67	$(^2P_{1\frac{1}{2}}\ 6p)1_1-(^2P_{1\frac{1}{2}}\ 6d)1_1^0$
0	3900.09	25,633.22	$(^2P_{1\frac{1}{2}}\ 6p)5_2-(^2P_{1\frac{1}{2}}\ 6d)6_1^0$
4	3906.939	25,588.30	$(^2P_{1\frac{1}{2}}\ 6p)2_2-(^2P_{1\frac{1}{2}}\ 6d)5_2^0$
6	3925.583	25,466.74	$(^2P_{1\frac{1}{2}}\ 6p)2_3-(^2P_{1\frac{1}{2}}\ 6d)4_2^0$
5	3959.495	25,248.63	$(^2P_{1\frac{1}{2}}\ 6p)6_0-(^2P_{1\frac{1}{2}}\ 6s)^3P_1^0$
6	3965.187	25,212.38	$(^2P_{1\frac{1}{2}}\ 6p)2_2-(^2P_{1\frac{1}{2}}\ 6d)3_2^0$
0	4028.43	24,816.59	$(^2P_{1\frac{1}{2}}\ 6p)5_2-(^2P_{1\frac{1}{2}}\ 5d)4_2^0$
4	4047.184	24,701.59	$(^2P_{1\frac{1}{2}}\ 6p)2_2-(^2P_{1\frac{1}{2}}\ 6d)2_2^0$
6	4067.958	24,575.44	$(^2P_{\frac{1}{2}}\ 6p)1_1-(^2P_{1\frac{1}{2}}\ 7d,\ 8s;\ ^2P_{\frac{1}{2}}\ 6d,\ 7s)9^0$
6	4068.773	24,570.52	$(^2P_{1\frac{1}{2}}\ 6p)3_3-(^2P_{1\frac{1}{2}}\ 6d)5_3^0$
1	4073.364	24,542.83	$(^2P_{1\frac{1}{2}}6p)5_2-(^2P_{1\frac{1}{2}}\ 5d)5_1^0$
0	4108.232	24,334.53	$(^2P_{\frac{1}{2}}\ 6p)1_1-(^2P_{1\frac{1}{2}}\ 7d,\ 8s;\ ^2P_{\frac{1}{2}}\ 6d,\ 7s)8^0$
4	4121.210	24,257.90	$(^2P_{\frac{1}{2}}\ 6p)1_1-(^2P_{1\frac{1}{2}}\ 7d,\ 8s;\ ^2P_{\frac{1}{2}}\ 6d,\ 7s)7_1^0$
2	4132.003	24,194.54	$(^2P_{1\frac{1}{2}}\ 6p)3_3-(^2P_{1\frac{1}{2}}\ 6d)3_2^0$
4	4151.267	24,082.27	$(^2P_{1\frac{1}{2}}\ 6p)2_2-(^2P_{1\frac{1}{2}}\ 6d)1_1^0$

TABLE III. (*Continued*).

Int.	λ in air	ν (vac)	Classification
1	4186.249	23,886.73	$(^2P_{\frac{1}{2}}\ 6p)2_1-(^2P_{\frac{1}{2}}\ 5d,\ 6s)1_0^0$
6	4213.129	23,728.67	$(^2P_{\frac{1}{2}}\ 6p)3_2-(^2P_{\frac{1}{2}}\ 5d,\ 6s)2_2^0$
0	4220.571	23,686.83	$(^2P_{\frac{1}{2}}\ 6p)2_1-(^2P_{\frac{1}{2}}\ 5d,\ 6s)2_2^0$
3	4221.119	23,683.75	$(^2P_{1\frac{1}{2}}\ 6p)3_3-(^2P_{1\frac{1}{2}}\ 6d)2_2^0$
9	4227.100	23,373.78	$(^2P_{1\frac{1}{2}}\ 6p)5_2-(^2P_{1\frac{1}{2}}\ 6s)^3P_2^0$
7	4228.350	23,312.46	$(^2P_{1\frac{1}{2}}\ 6p)4_1-(^2P_{1\frac{1}{2}}\ 6d)3_2^0$
1	4307.942	23,206.44	$(^2P_{\frac{1}{2}}\ 6p)3_2-(^2P_{1\frac{1}{2}}\ 7d,\ 8s;\ ^2P_{\frac{1}{2}}\ 6d,\ 7s)10_3^0$
6	4330.636	23,245.86	$(^2P_{1\frac{1}{2}}\ 6p)6_0-(^2P_{1\frac{1}{2}}\ 6d)6_1^0$
0	4316.992	23,157.78	$(^2P_{1\frac{1}{2}}\ 6p)3_3-(^2P_{1\frac{1}{2}}\ 5d)4_3^0$
2	4327.580	23,101.13	$(^2P_{1\frac{1}{2}}\ 6p)1_1-(^2P_{1\frac{1}{2}}\ 7d,\ 8s;\ ^2P_{\frac{1}{2}}\ 6d,\ 7s)6_1^0$
4	4330.239	23,086.95	$(^2P_{1\frac{1}{2}}\ 6p)1_1-(^2P_{1\frac{1}{2}}\ 7s)^3P_1^0$
0	4348.620	22,989.36	$(^2P_{\frac{1}{2}}\ 6p)3_2-(^2P_{\frac{1}{2}}5d,\ 6s)3_2^0$
0	4356.575	22,947.39	$(^2P_{\frac{1}{2}}\ 6p)2_1-(^2P_{\frac{1}{2}}\ 5d,\ 6s)3_2^0$
9	4363.375	22,912.15	$(^2P_{1\frac{1}{2}}\ 6p)5_2-(^2P_{1\frac{1}{2}}\ 6d)5_2^0$
6	4373.018	22,861.10	$(^2P_{1\frac{1}{2}}\ 6p)5_2-(^2P_{1\frac{1}{2}}\ 6s)^3P_1^0$
5	4384.428	22,801.61	$(^2P_{1\frac{1}{2}}\ 6p)4_1-(^2P_{1\frac{1}{2}}\ 6d)2_2^0$
0	4386.566	22,790.50	$(^2P_{1\frac{1}{2}}\ 6p)5_2-(^2P_{1\frac{1}{2}}\ 6d)4_3^0$
2	4388.764	22,779.08	$(^2P_{\frac{1}{2}}\ 6p)2_1-(^2P_{1\frac{1}{2}}\ 7d,\ 8s;\ ^2P_{\frac{1}{2}}\ 6d,\ 7s)9^0$
3	4396.909	22,736.88	$(^2P_{\frac{1}{2}}\ 6p)3_2-(^2P_{1\frac{1}{2}}\ 7d,\ 8s;\ ^2P_{\frac{1}{2}}\ 6d,\ 7s)9^0$
7	4405.253	22,693.82	$(^2P_{1\frac{1}{2}}\ 6p)1_1-(^2P_{1\frac{1}{2}}\ 7s)^3P_2^0$
2	4424.046	22,597.42	$(^2P_{1\frac{1}{2}}\ 6p)4_1-(^2P_{1\frac{1}{2}}\ 6s)^3P_2^0$
4	4435.708	22,538.01	$(^2P_{\frac{1}{2}}\ 6p)2_1-(^2P_{1\frac{1}{2}}\ 7d,\ 8s;\ ^2P_{\frac{1}{2}}\ 6d,\ 7s)8^0$
0	4436.06	22,536.21	$(^2P_{1\frac{1}{2}}\ 6p)5_2-(^2P_{1\frac{1}{2}}\ 6d)3_2^0$
2	4444.004	22,495.94	$(^2P_{\frac{1}{2}}\ 6p)3_2-(^2P_{1\frac{1}{2}}\ 7d,\ 8s;\ ^2P_{\frac{1}{2}}\ 6d,\ 7s)8^0$
1	4450.785	22,461.66	$(^2P_{\frac{1}{2}}\ 6p)2_1-(^2P_{1\frac{1}{2}}\ 7d,\ 8s;\ (^2P_{\frac{1}{2}}\ 6d,\ 7s)7_1^0$
3	4457.680	22,426.92	$(^2P_{1\frac{1}{2}}\ 6p)4_1-(^2P_{1\frac{1}{2}}\ 5d)6_2^0$
3	3459.185	22,419.35	$(^2P_{\frac{1}{2}}\ 6p)3_2-(^2P_{1\frac{1}{2}}\ 7d,\ 8s;\ ^2P_{\frac{1}{2}}6d,\ 7s)7_1^0$
7	4501.525	22,208.49	$(^2P_{1\frac{1}{2}}\ 6p)6_0-(^2P_{1\frac{1}{2}}\ 5d)1_1^0$
2	4506.834	22,182.32	$(^2P_{1\frac{1}{2}}\ 6p)4_1-(^2P_{1\frac{1}{2}}\ 6d)1_1^0$
2	4515.495	22,139.77	$(^2P_{1\frac{1}{2}}\ 6p)2_2-(^2P_{1\frac{1}{2}}\ 5d)4_2^0$
0	4525.59	22,090.41	$(^2P_{\frac{1}{2}}\ 6p)1_1-(^2P_{\frac{1}{2}}\ 5d,\ 6s)\ 1_0^0$
7	4526.725	22,084.85	$(^2P_{1\frac{1}{2}}\ 6p)4_1-(^2P_{1\frac{1}{2}}\ 6s)^3P_1^0$
6	4538.942	22,025.41	$(^2P_{1\frac{1}{2}}\ 6p)5_2-(^2P_{1\frac{1}{2}}\ 6d)2_2^0$
3	4566.983	21,890.25	$(^2P_{\frac{1}{2}}\ 6p)1_1-(^2P_{\frac{1}{2}}\ 5d,\ 6s)2_2^0$
3	4571.786	21,867.31	$(^2P_{1\frac{1}{2}}\ 6p)2_2-(^2P_{1\frac{1}{2}}\ 5d)5_1^0$
2	4497.673	21,744.06	$(^2P_{1\frac{1}{2}}\ 6p)4_1-(^2P_{1\frac{1}{2}}\ 6d)7_0^0$
10	4603.755	21,715.33	$(^2P_{\frac{1}{2}}\ 6p)3_2-(^2P_{1\frac{1}{2}}\ 6s)^3P_2^0$
3	4616.13	21,657.19	$(^2P_{\frac{1}{2}}\ 6p)4_0-(^2P_{\frac{1}{2}}\ 5d,\ 6s)4_1^0$
4	4623.091	21,624.51	$(^2P_{\frac{1}{2}}\ 6p)1_1-(^2P_{1\frac{1}{2}}\ 7d,\ 8s;\ (^2P_{\frac{1}{2}}\ 5d,\ 7s)4_1^0$
1	4640.333	21,544.16	$(^2P_{1\frac{1}{2}}\ 6p)3_3-(^2P_{1\frac{1}{2}}\ 5d)6_2^0$
5	4646.508	21,515.53	$(^2P_{1\frac{1}{2}}\ 6p)2_2-(^2P_{1\frac{1}{2}}\ 7s)^3P_1^0$
4	4670.280	21,406.02	$(^2P_{1\frac{1}{2}}\ 6p)5_2-(^2P_{1\frac{1}{2}}\ 6d)1_1^0$
1	4692.482	21,304.73	$(^2P_{\frac{1}{2}}\ 6p)2_1-(^2P_{1\frac{1}{2}}\ 7d,\ 8s\ ^2P_{\frac{1}{2}}\ 6d,\ 7s)6_1^0$
1	4695.610	21,290.55	$(^2P_{\frac{1}{2}}\ 6p)4_0-(^2P_{1\frac{1}{2}}\ 7d,\ 8s;\ (^2P_{\frac{1}{2}}\ 6d,\ 7s)7_1^0$
5	4701.793	21,262.55	$(^2P_{\frac{1}{2}}\ 6p)3_2-(^2P_{\frac{1}{2}}\ 7d,\ 8s;\ (^2P_{\frac{1}{2}}\ 6d,\ 7s)6_1^0$
1	4726.684	21,150.58	$(^2P_{\frac{1}{2}}\ 6p)1_1-(^2P_{\frac{1}{2}}\ 6d,\ 6s)3_2^0$
4	4732.975	21,122.47	$(^2P_{1\frac{1}{2}}\ 6p)2_2-(^2P_{1\frac{1}{2}}\ 7s)^3P_2^0$
5	4739.665	21,092.66	$(^2P_{\frac{1}{2}}\ 6p)2_1-(^2P_{1\frac{1}{2}}\ 7d,\ 8s;\ ^2P_{\frac{1}{2}}\ 6d,\ 7s)5_2^0$
2	4749.132	21,050.61	$(^2P_{\frac{1}{2}}\ 6p)3_2-(^2P_{1\frac{1}{2}}\ 7d,\ 8s;\ ^2P_{\frac{1}{2}}\ 6d,\ 7s)5_2^0$
3	4786.363	20,886.87	$(^2P_{\frac{1}{2}}\ 6p)4_0-(^2P_{\frac{1}{2}}\ 5d,\ 6s)5_1^0$
1	4806.924	20,797.53	$(^2P_{\frac{1}{2}}\ 6p)1_1-(^2P_{1\frac{1}{2}}\ 7d,\ 8s;\ ^2P_{\frac{1}{2}}\ 6d,\ 7s)2_0^0$
6	4830.161	20,697.48	$(^2P_{1\frac{1}{2}}\ 6p)2_2-(^2P_{1\frac{1}{2}}\ 6s)^3P_2^0$
6	4870.024	20,528.06	$(^2P_{\frac{1}{2}}\ 6p)3_2-(^2P_{\frac{1}{2}}\ 5d,\ 6s)4_1^0$
0	4879.95	20,486.32	$(^2P_{\frac{1}{2}}\ 6p)2_1-(^2P_{\frac{1}{2}}\ 5d,\ 6s)4_1^0$
1	4925.744	20,295.73	$(^2P_{1\frac{1}{2}}\ 6p)1_1-(^2P_{1\frac{1}{2}}\text{-}5d)5_1^0$
6	4952.835	20,184.84	$(^2P_{1\frac{1}{2}}\ 6p)2_2-(^2P_{1\frac{1}{2}}\ 6s)^3P_1^0$
5	4972.593	20,104.64	$(^2P_{1\frac{1}{2}}\ 6p)3_3-(^2P_{1\frac{1}{2}}\ 7s)^3P_2^0$
1	5041.828	19,828.56	$(^2P_{\frac{1}{2}}\ 6p)2_1-(^2P_{1\frac{1}{2}}\ 7d,\ 8s;\ ^2P_{\frac{1}{2}}\ 6d,\ 7s)4_1^0$
6	5043.800	19,820.81	$(^2P_{1\frac{1}{2}}\ 6p)5_2-(^2P_{1\frac{1}{2}}\ 5d)1_1^0$
3	5052.696	19,785.91	$(^2P_{\frac{1}{2}}\ 6p)3_2-(^2P_{1\frac{1}{2}}\ 7d,\ 8s;\ ^2P_{\frac{1}{2}}\ 6d,\ 7s)4_1^0$
3	5059.866	19,757.88	$(^2P_{\frac{1}{2}}\ 6p)3_2-(^2P_{\frac{1}{2}}\ 5d,\ 6s)5_1^0$
0	5070.684	19,715.72	$(^2P_{\frac{1}{2}}\ 6p)2_1-(^2P_{\frac{1}{2}}\ 5d,\ 6s)5_1^0$
4	5096.604	19,615.46	$(^2P_{1\frac{1}{2}}\ 6p)4_1-(^2P_{1\frac{1}{2}}\ 7s)^3P_1^0$
8	5227.002	19,126.12	$(^2P_{1\frac{1}{2}}\ 6p)1_1-(^2P_{1\frac{1}{2}}\ 6s)^3P_2^0$

TABLE III. (*Continued*).

Int.	λ in air	ν (vac.)	Classification
6	5249.373	19,044.61	$(^2P_{1\frac{1}{2}}\ 6p)4_1-(^2P_{1\frac{1}{2}}\ 5d)1_1^0$
0	5256.572	19,018.53	$(^2P_{1\frac{1}{2}}\ 6p)6_0-(^2P_{1\frac{1}{2}}\ 6d)1_1^0$
0	5263.21	18,994.53	$(^2P_{\frac{1}{2}}\ 6p)3_2-(^2P_{1\frac{1}{2}}\ 7d, 8s; {}^2P_{\frac{1}{2}}\ 6d, 7s)3_3^0$
4	5274.044	18,955.52	$(^2P_{1\frac{1}{2}}\ 6p)1_1-(^2P_{1\frac{1}{2}}\ 5d)6_2^0$
3	5306.609	18,839.20	$(^2P_{1\frac{1}{2}}\ 6p)5_2-(^2P_{1\frac{1}{2}}\ 7s)^3P_1^0$
3	5349.10	18,689.34	$(^2P_{\frac{1}{2}}\ 6p)1_1-(^2P_{\frac{1}{2}}\ 5d, 6s)4_1^0$
10	5358.53	18,656.65	$(^2P_{\frac{1}{2}}\ 6p)4_0-(^2P_{1\frac{1}{2}}\ 7d, 8s; {}^2P_{\frac{1}{2}}\ 6d, 7s)4_1^0$
6	5370.979	18,613.42	$(^2P_{1\frac{1}{2}}\ 6p)1_1-(^2P_{1\frac{1}{2}}\ 6s)^3P_1^0$
5	5419.687	18,446.14	$(^2P_{1\frac{1}{2}}\ 6p)5_2-(^2P_{1\frac{1}{2}}\ 7s)^3P_2^0$
7	5563.019	17,970.87	$(^2P_{1\frac{1}{2}}\ 6p)5_2-(^2P_{1\frac{1}{2}}\ 5d)2_2^0$
0	5579.033	17,919.29	$(^2P_{\frac{1}{2}}\ 6p)1_1-(^2P_{\frac{1}{2}}\ 5d, 6s)5_1^0$
3	5814.181	17,194.57	$(^2P_{1\frac{1}{2}}\ 6p)4_1-(^2P_{1\frac{1}{2}}\ 5d)2_2^0$
5	5831.159	17,144.51	$(^2P_{1\frac{1}{2}}\ 6p)2_2-(^2P_{1\frac{1}{2}}\ 5d)1_1^0$
1	5863.701	17,049.36	$(^2P_{1\frac{1}{2}}\ 6p)5_2-(^2P_{1\frac{1}{2}}\ 5d)3_3^0$
2	6076.738	16,451.65	$(^2P_{1\frac{1}{2}}\ 6p)6_0-(^2P_{1\frac{1}{2}}\ 7s)^3P_1^0$
4	6128.619	16,312.38	$(^2P_{1\frac{1}{2}}\ 6p)3_3-(^2P_{1\frac{1}{2}}\ 5d)2_2^0$
2	6419.541	15,573.14	$(^2P_{1\frac{1}{2}}\ 6p)1_1-(^2P_{1\frac{1}{2}}\ 5d)1_1^0$
3	6495.528	15,390.96	$(^2P_{1\frac{1}{2}}\ 6p)3_3-(^2P_{\frac{1}{2}}\ 5d, 6s)3_3^0$
1	6506.254	15,365.59	$(^2P_{\frac{1}{2}}\ 6p)2_1-(^2P_{1\frac{1}{2}}\ 7d, 8s; {}^2P_{\frac{1}{2}}\ 6d, 7s)1_2^0$
3	6536.440	15,294.63	$(^2P_{1\frac{1}{2}}\ 6p)2_2-(^2P_{1\frac{1}{2}}\ 5d)2_2^0$
4	6955.519	14,373.12	$(^2P_{1\frac{1}{2}}\ 6p)2_2-(^2P_{1\frac{1}{2}}\ 5d)3_3^0$

been assigned to those levels whose L and S values are not fixed. The second column contains the J values of the odd levels, and the third the relative term values referred to $5p^6\ {}^1S_0$. The headings of the remaining columns give the electron configurations, spectroscopic notations, J values, and relative term values of the even terms to which are assigned numbers in order of their magnitude in lieu of their undetermined L and S values. In the body of the table are the wave numbers of the classified lines, followed in the parenthesis by their intensities. Except in the case of intensities followed by p (prism) these intensities are from grating measurements. Below each wave number is the discrepancy (calculated value minus observed value) between the observed wave numbers and the wave number calculated from the values assigned to the terms. The terms and transitions established in the previous paper are preceded by asterisks. It will be observed that the only transitions in that work involving terms of the $^2P_{\frac{1}{2}}$ limit were fixed in relation to the rest of the system only by the three resonance lines $\nu\nu$122,872, 123,645 and 163,180 and were thus uncertain by as much as ± 5 cm^{-1} because of the limited accuracy of the extreme ultraviolet measures. In the present work the first attempt was to remove this uncertainty by finding intercombinations between the $5p^5\ (^2P_{\frac{1}{2}})\ 6p$ terms thus established and the terms of the $^2P_{1\frac{1}{2}}$ limit. The lack of precision in the values of the $^2P_{\frac{1}{2}}$ terms, however, made it more feasible to approach the task by searching in the region indicated by these approximate terms for lines having the accurately known differences of the established terms of the $5p^5\ (^2P_{1\frac{1}{2}})5d$, $6s$ configuration. This procedure in fact not only located the three known terms of $5p^5(^2P_{\frac{1}{2}})\ 6p$ with precision as 141,555.59, 143,394.19 and 144,523.45 cm^{-1}, but located also one new term of this configuration as 143,352.12 cm^{-1}. The ν differences thus established were used in looking for new odd terms. Sixteen such terms were definitely established, and in addition the three terms involving the three resonance

lines discussed above were accurately fixed as $\nu\nu$122,866.03, 123,636.44 and 163,180.20. It will be noted that in the case of most of the new terms one or two expected transitions are missing. However, each terms seems established beyond doubt by several close coincidences and by expected positions. A few less definitely established terms have been omitted.

Table III contains a list of the Cs II lines classified both in this and in the preceding investigation. In the first column are the intensities from the present grating measurements or in a few cases, where the intensity is followed by p, from the prism measurement; in the second and third columns are the λ's in air, and the wave numbers in vacuum; the last column contains the classification, with $5p^5$ omitted from all configurations above the ground state.

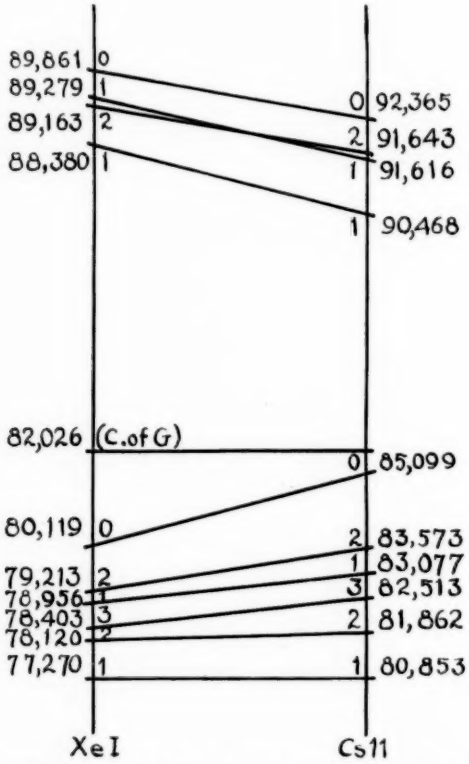

Fig. 1. The $5p^5\,6p$ terms of Xe I and Cs II referred to their centers of gravity and reduced in the case of Cs II by multiplying with 9,120/14,270, the ratio of the relativistic doublets $5p^5$.

It is now of interest to compare the terms as found with those expected as shown in Table I and to consider them in relation to the terms of Xe I.[4] In Fig. 1 the relative term values of the ten p ($5p^5\,6p$) terms of Xe I are drawn referred to their center of gravity, and beside them the ten p terms of Cs II likewise referred to their center of gravity but reduced by multiplication with 9,120/14,270, the ratio of the relativistic doublets in the two cases. The correspondence is very good. The only crossing over is in two levels which

[4] Meggers, deBruin and Humphreys, Bureau Standards J. Research **3**, 731 (1929).

are very close together. The same crossing occurred in the Kr I–Rb II sequence.[5] The close correlation of the Xe I terms with those of Cs II is a convincing argument for the correctness of the Cs II analysis.

We may next consider the odd terms. Of the low group around 110,000 cm^{-1}, five terms come from Sommer's work. Four more terms were added in this work. The group was ascribed by Laporte, Miller and Sawyer to a mixture of $5p^5$ $(^2P_{1\frac{1}{2}})$ $5d$ and $6s$. Inspection of Table I shows that $6s$ should contribute two terms of $J=1, 2$; and $5d$, eight terms of $J=0, 1, 1, 2, 2, 3, 3, 4$. The group is then completely identified with the exception of the term with $J=4$, which it is impossible to locate since only one even term with $J=3$ is known with which this term could combine. In the previous work *vv*107,392, 107,905 were identified as $6s\ ^3P_2$ and $^3P_1$. The present work adds a new term with $J=2$ between these terms but the much greater intensities of the transitions to 107,392 make it almost certain that this assignment is correct. The remaining terms should arise from $5d$ and may be compared with the corresponding Xe I terms. Since two of the $5d$ terms in Xe I, and one ($J=3$) in Cs II are unknown, a graphical representation as made for the p-terms in Fig. 1 is not useful. The most interesting anomaly is the term with $J=0$. In Xe I as in Ne I this term is the lowest of the $^2P_{1\frac{1}{2}}$ d group. In Rb II, however, it is the highest while in Cs II it is in the middle of the group. The remaining $5d$ and $6s$ terms, having $^2P_{\frac{1}{2}}$ as limit form a group of five terms near 120,000 cm^{-1}. As mentioned above two of these terms were located approximately in the work of Laporte, Miller and Sawyer by two extreme ultraviolet lines. They are now definitely fixed in position through the intercombinations of the $(^2P_{\frac{1}{2}})$ $6p$ group, with which they combine, with $(^2P_{1\frac{1}{2}})$ $6d$, $7s$. Except for the $J=0$ term which must belong to $6s$ it is not possible to assign these terms definitely to $6s$ or $5d$.

The remaining ten odd terms form a group near 160,000 cm^{-1}. These terms are probably a mixture of terms arising from $5p^5$ $(^2P_{\frac{1}{2}})$, $6d$, $7s$ and $5p^5(^2P_{1\frac{1}{2}})$ $7d$, $8s$. Laporte, Miller and Sawyer estimated $5p^6\ ^1S_0$ to be about 189,000 cm^{-1}. On this basis the assumption of a simple Rydberg formula would predict $5p^5(^2P_{1\frac{1}{2}})$ $7d$, $8s$, from the known positions of $5p^5(^2P_{1\frac{1}{2}})$ $5d$, $6s$ and $5p^5(^2P_{1\frac{1}{2}})$ $6d$, $7s$, as a group centered about approximately 165,000 cm^{-1}. Also, on the assumption that the group $5p^5(^2P_{\frac{1}{2}})$ $5d$, $6s$ centered about 120,000 cm^{-1} is the first member of a sequence which approaches a limit about 150,000 cm^{-1} (estimated from the relativistic doublet) higher than 189,000 cm^{-1}, the second member would center around approximately 162,000 cm^{-1}. The only basis upon which these terms could be assigned to one group or the other would be a careful determination of the relative intensities of transitions of each term with the $(^2P_{1\frac{1}{2}})$ $6p$ group and with the $(^2P_{\frac{1}{2}})$ $6p$ group. Transitions between terms having the same series limit should of course be stronger than between terms having different limits. On the basis of the present eye estimates of lines, which also for the two p-groups lie in quite different spectral regions, little can be said on this basis.

[5] Laporte, Miller and Sawyer, Phys. Rev. **38**, 843 (1931).

All the terms in this group around 160,000 cm^{-1} are new with the exception of 163,180.20 cm^{-1} which was fixed by a resonance line and three other transitions in the earlier paper. One of the new terms, 164,656.77 cm^{-1} is also confirmed by a vacuum spectrograph line, λ607.31, ν164,655, intensity 3, which was not previously reported.

Transitions involving terms arising from $5p^5nf$ configurations and also from higher members of the s, p, and d configurations might be expected in our data. Although the position of such terms can be predicted with a fair degree of approximation, no certain evidence of transitions involving them has as yet been obtained. The present extension of the Cs II spectrum, however, completes the essential outlines of a scheme analogous in all essentials to the Xe I spectrum, with the terms of each electron configuration divided into two completely separated groups having as series limits in the Cs II spectrum, $5p^5\ {}^2P_{1\frac{1}{2}}$ and $5p^5\ {}^2P_{\frac{1}{2}}$.

Infrared Absorption Spectrum of Hydrogen Cyanide

By KYU NAM CHOI AND E. F. BARKER
University of Michigan

(Received October 24, 1932)

The absorption spectrum of HCN in the gas phase has been investigated by a grating spectrometer with high resolution in the region $3\mu-15\mu$. Five of the infrared bands were studied, and of these the very intense fundamental at 14μ has been resolved into individual lines forming P, R and Q branches. The first harmonic of the band at 7μ has two maxima, very nearly symmetrical and equal in intensity, and no Q branch. Although fine structure is indicated, it is not possible to determine the position of successive individual lines. Three other maxima, less intense and unsymmetrical are found at 4.728μ, 4.760μ, and 4.794μ forming the second harmonic of the same vibration. There is a sharp single maximum at 3.57μ with another very strong double band at 3.04μ.

Form of the HCN molecule. The HCN molecule is linear with fundamental frequencies $\nu_2=712$ cm^{-1}, $\nu_3=3289$ cm^{-1} and ν_1 approximately 2100 cm^{-1}. The latter has not been observed directly since the band associated with it is of extremely low intensity, but the combination $\nu_1+\nu_2$ explains the band at 3.57μ. The moment of inertia determined from the fine structure of the 14μ band is 18.68×10^{-40} g cm^2.

INTRODUCTION

RECENT improvements in the apparatus available for measuring infrared absorption have made possible the detailed study of spectra of much greater complexity than could be observed only a few years ago. As a consequence, the infrared absorption spectra have furnished decisive information for determining the molecular configurations of a number of molecules, especially when the fine structure of the bands is observable. The purpose of the present investigation is to examine both the fundamental and harmonic bands of HCN; especially to determine the fine structure of the low-frequency bands which have never been studied before with high resolution.

In 1912, Burmeister[1] investigated the absorption spectrum of gaseous HCN in the region from 3μ to 14μ, finding four bands. Of these, the one having the shortest wave-length 3.04μ is very narrow and intense, apparently corresponding to the fundamental of one of the characteristic vibrations of the molecule. The two bands of greatest wave-length near 7μ and 14μ, are also intense, but appear as broad double maxima. The absorption at the two intermediate-maxima, 4.77μ and 3.57μ, is relatively weak and Burmeister was in doubt as to whether these bands should be attributed to HCN.

In 1923, Barker[2] investigated some of the absorption bands of HCN with special gratings ruled by himself, giving higher dispersion than was previously employed. He found two maxima, very nearly symmetrical and of equal

[1] Burmeister, D. Ges. Verh. **15,** 589 (1913).
[2] Barker, Phys. Rev. **23,** 200 (1924).

intensity, appearing at 6.94μ and 7.32μ. Three others, less intense and unsymmetrical, were observed at 4.756μ, 4.723μ and 4.79μ. Observation at that time did not extend beyond 12μ. From the envelope of the 7μ band he estimated the moment of inertia to be about 13.2×10^{-40}g cm^2.

In 1930, Badger and Binder[3] investigated photographically the absorption spectrum in the region $\lambda\lambda$7000–9200 using HCN gas in a 280 cm absorption cell. They observed two weak bands of very simple structure occurring at λ8563 and λ7912 which are interpreted as $3\nu_3+\nu_1$ and $4\nu_3$ respectively. In these bands they have been able to resolve the rotational structure, and compute the moment of inertia as 18.79×10^{-40} g cm^2.

Very recently, Brackett and Liddel[4] examined the absorption spectrum of HCN both in liquid and vapor phase mostly in the region from 1μ to 2μ. The instrument used in their investigation was an automatic recording apparatus yielding high resolution. Three bands were observed at 1.5μ, 1.1μ and 1.0μ in the gas absorption. They were interpreted as second and third harmonics of 3.04μ (ν_3) and the combination $2\nu_3+\nu_1$. All these bands are doublets but the rotational structure was not resolved. The moment of inertia as computed from the envelope of the third harmonic band was $18\pm2\times10^{-40}$ g cm^2.

Apparatus

The grating spectrometer used in this work is of a type similar to that employed by Barker and Meyer[5] and therefore will not be described here in detail. Modifications of an important nature, however, lead to a high degree of sensitivity of the recording apparatus and hence allow investigation with a grating to a greater wave-length than has been previously reached. As a further consequence of the increased sensitivity, it has been possible to reduce the slit widths considerably and thus obtain improved definition. A grating ruled with 1200 lines per inch was found to be most effective for the region between 7μ and 15μ. From 3μ to the neighborhood of 5μ, the best results were obtained with a grating having 4800 lines per inch. The detecting system consists of a vacuum thermocouple, a Moll thermal relay with a Kipp and Sons high-sensitivity galvanometer of the D'Arsonval type. The calibration is in terms of the mercury line at 1.014μ.

The absorption cells have potassium bromide (K Br) windows and can be used effectively throughout the entire spectral region from 3μ to 15μ. Two absorption cells were used whose lengths are 25 cm and 2.5 cm respectively.

The HCN gas was generated by introducing below the surface of H_2SO_4 a nearly saturated solution of NaCN in water. The gas was frozen in a liquid air trap provided with two stopcocks, and each sample to be examined was distilled over to the absorption cell by warming the trap to 30°C. In order to eliminate the water vapor in the gas, two U tubes were used, the first containing $CaCl_2$ and the second P_2O_5.

[3] Badger and Binder, Phys. Rev. **37**, 800 (1931).
[4] Brackett and Liddel, Smithsonian Institute **85**, No. 5 (1931).
[5] Barker and Meyer, Trans. Faraday Soc. **25**, 12 (1929).

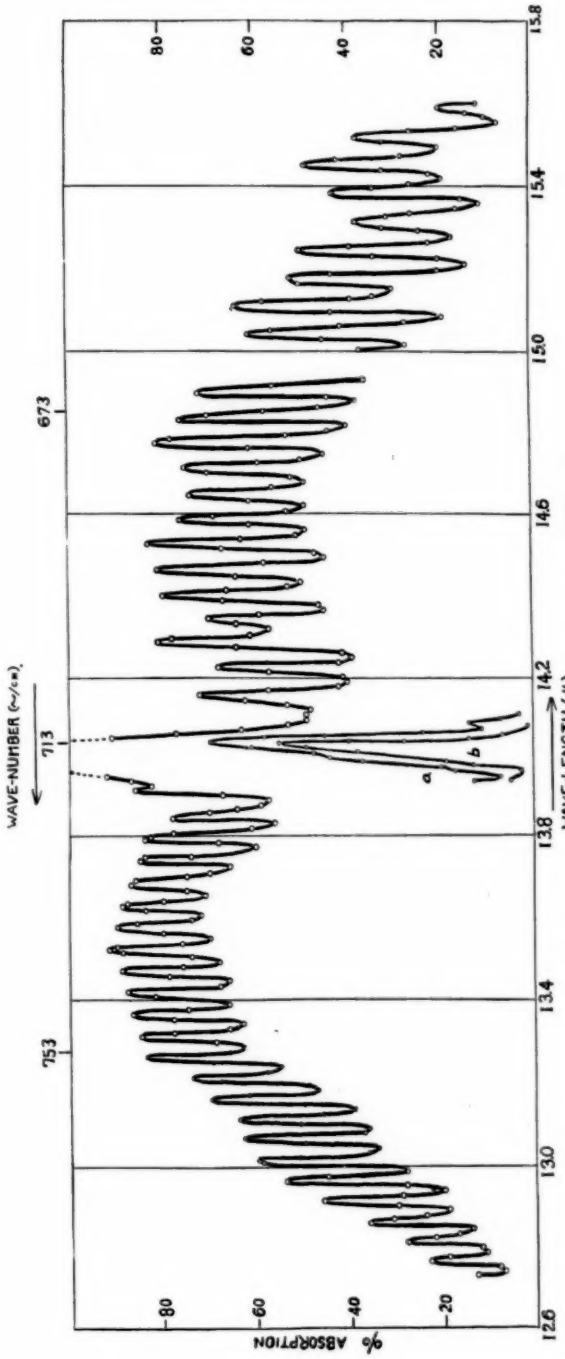

Fig. 1. Fine structure of the 14μ band of HCN.

Discussion of Results

Region of 14μ

The wide and intense absorption previously observed with two maxima, was resolved into a band consisting of R, Q and P branches as shown in Fig. 1. Repeated observations were taken over this region, using the point by point method, with different pressures of gas and different slits. An extremely small cell, 2.5 cm long with KBr windows, was used, and the figure represents observations made with 35 cm pressure and 0.5 mm slit width. The Q branch is so strong that it was impossible to observe it satisfactorily even with 4 or 5 cm of pressure. In order to locate its maximum, the pressure was considerably reduced. The detached portion of curves a and b shown in Fig. 1 represent observations taken with pressures of 3 mm and 1 mm respectively. The irregularities of the lines which are apparent at the right end of the P branch may be attributed to the CO_2 band at 14.8μ. The energy falls off very rapidly in this region due to absorption by the carbon dioxide of the atmosphere. As shown in Fig. 1 there is a small gap near 14.8μ region where the Q branch of CO_2 falls and observations could not be made. No convergence is apparent in either the R or the P branch, the average spacing

Table I. *Rotation lines in the 14 μ band. Q branch at 14.0392 μ or 712.28 cm^{-1}.*

R branch: $\Delta J=+1$			Initial J	P branch: $\Delta J=-1$		
λ	ν	$\Delta\nu$		λ	ν	$\Delta\nu$
13.9780	715.40	3.12	0	—	—	—
13.9200	718.40	3.00	1	—	—	—
13.8544	721.68	3.28	2	14.1554	706.44	—
13.8016	724.55	2.87	3	14.2256	702.95	3.49
13.7489	727.33	2.78	4	14.2841	700.00	2.95
13.6962	730.11	2.78	5	14.3426	697.21	2.79
13.6477	732.72	2.61	6	14.4011	694.39	2.82
13.5909	735.80	3.08	7	14.4654	691.30	3.09
13.5340	738.87	3.07	8	14.5298	688.24	3.06
13.4798	741.85	2.98	9	14.5853	685.62	2.74
13.4299	744.60	2.75	10	14.6438	682.88	2.74
13.3780	747.49	2.89	11	14.7140	679.62	3.26
13.3240	750.72	3.03	12	14.7725	676.92	2.70
13.2711	753.52	3.00	13	14.8310	674.26	2.66
13.2181	756.52	3.00	14	14.8953	671.42	2.84
13.1653	759.57	3.05	15	—	—	—
13.1183	762.27	2.70	16	15.0320	665.24	—
13.0693	765.15	2.88	17	15.1010	662.20	3.04
13.0166	768.24	3.04	18	15.1720	659.10	3.10
12.9640	771.36	3.08	19	15.2410	656.12	2.98
12.9113	774.51	3.15	20	15.3100	653.16	2.96
12.8593	777.65	3.14	21	15.3790	650.23	2.93
12.8203	780.50	1.85	22	15.4480	647.33	2.91
12.7650	783.38	2.88	23	15.5170	644.45	2.88
—	—	—	24	15.5860	641.40	2.85

of the lines being 2.98 cm^{-1}. The small deviations from this value shown in the Table I are partly due to experimental error but also indicate the effect of superposition of bands due to absorption by excited molecules and disturbances from the CO_2 bands. If the above value of the average spacing is applied to the central portion of the band, it is apparent that there are just

3 intervals between the innermost lines as would be expected for a linear molecule. The positions of maximum absorption of the R, Q and P branches fall, approximately, at 737.89, 712.29 and 688.00 cm^{-1} respectively. The most probable frequency of rotation $\bar{\nu}_r$ is thus found to be about 24.9 cm^{-1}.

Region of 7μ

This band is unquestionably the first harmonic of the 14μ band, although it has no Q branch since ΔL is even. It was examined with the 2.5 cm cell

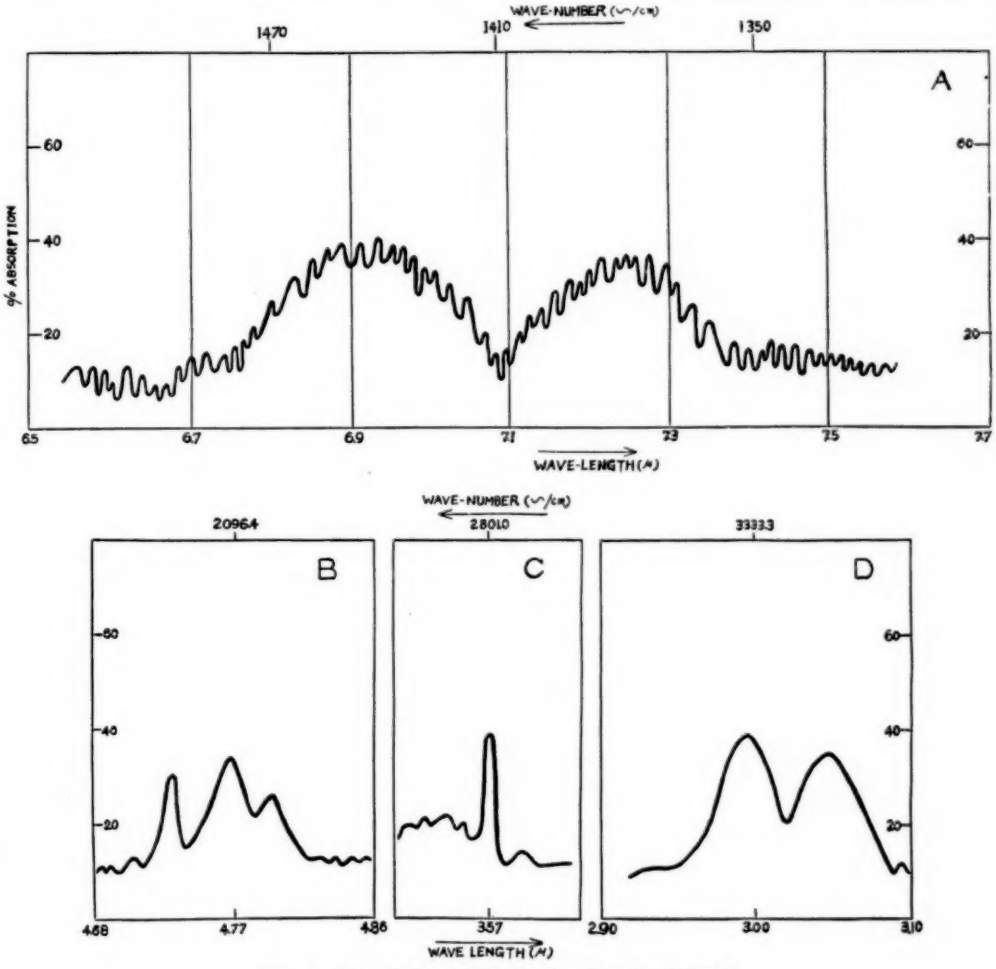

Fig. 2. Near infrared absorption bands of HCN.
$A: 2\nu_2$. $B: 3\nu_2$. $C: \nu_1+\nu_2$. $D: \nu_3$.

and 35 cm pressure, and with a grating having 1200 lines per inch, using the second order. Observations in this region are rendered difficult by the absorption of atmospheric water vapor which presents many sharp maxima where deflections taken either with or without the absorbing cell are reduced below the limit permissible for precise measurement. Several efforts have been made to resolve the individual lines of this band, but the curve shown

in the Fig. 2A represents the best definition obtained. The irregularities of the rotational lines are to a great extent attributable to the water vapor in the atmosphere but there may also be appreciable absorption here by molecules already excited to the level 1. There are two maxima, very nearly symmetrical, with almost equal intensities, separated by a sharp minimum. The position of the missing line is about 1412.4 cm^{-1}. Measurements have been extended in either direction to the region of very low absorption, with some loss in precision, because on the long wave-length side, the energy of the beam falls off rapidly and on the short wave-length side, the intensity of the water vapor absorption increases. Although fine structure is indicated, it is not possible to determine the positions of successive individual lines.

Region of 4.7μ

This region was examined with a grating having 4800 lines per inch and with 0.3 of mm slit. The absorption was very much less intense and could scarcely be located with the 2.5 cm cell. The third curve Fig. 2B represents the absorption, using the 25 cm cell of saturated vapor at about 25°C and atmospheric pressure. The cell was moved alternately in and out of the beam as before. The principle maximum appears at 4.760μ with a second narrow one at 4.728μ and with a third at 4.794μ. These peaks have the appearance of Q branches. From this curve it would be difficult to make an estimate of the value of the moment of inertia in the usual way, but obviously the wave-number differences are not of the same magnitude as those exhibited at 14μ.

Region of 3.6μ

The absorption band near 3.6μ Fig. 2C is also weak, although it was observed with 2.5 cm cell and with the pressure of 65 cm. A single narrow and fairly intense maximum was found at 3.57μ, with a low background on either side. Some indications of fine structure appear in the R branch but further resolution could not be obtained.

Region of 3μ

The single intense absorption band shown by Burmeister was resolved into a doublet Fig. 2D. It was examined with the 2.5 cm cell and with almost atmospheric pressure. The maxima appear at 2.996μ and 3.045μ. Several unsuccessful efforts have been made to resolve the individual lines with the 7200 line grating and different amounts of absorbing gas. The spacing of the maxima is about 53.7 cm^{-1} which is much greater than that observed at 14μ, but nearly the same as at 7μ. This fact combined with the difficulty in resolving the rotation lines, indicates that the absorption by excited molecules must be appreciable.

Mechanical Interpretation of the Vibration-Rotation Band

Assuming that the rotation of this molecule may be represented by the equation for the symmetrical top rotator, the total energy in any stationary state is

$$E = E_p + \frac{h^2}{8\pi^2}\left\{\frac{J(J+1)}{A} + l^2\left(\frac{1}{C} - \frac{1}{A}\right)\right\},$$

where E_p is the potential energy of deformation and C and A are the moments of inertia about the axis of figure and any axis normal to it.

If $C=0$, as in the unexcited molecule, then E will be finite only if $l=0$, and E_p will also vanish, so that the equation passes over into the expression for the energy of a simple rotator,

$$E_r = J(J+1)h^2/8\pi^2 A$$

or $E_r/h = BJ(J+1)$ where $B=h/8\pi^2 A$ and J may assume all integral values.

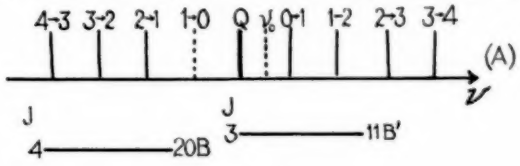

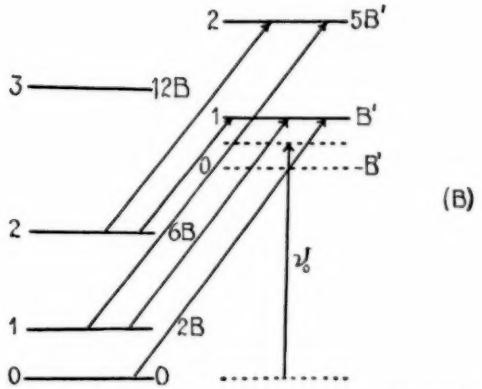

Fig. 3. Band pattern and scheme of energy levels for the transition 0→1 in l.

For the special case of an excited molecule in which $l=1$ the equation becomes

$$E' = E_p' + \frac{h^2}{8\pi^2}\left\{\frac{J(J+1)}{A'} + \left(\frac{1}{C'} - \frac{1}{A'}\right)\right\}$$

or $E'/h = B'\ (J^2+J-1)+\nu_0$ where $\nu_0 = E_p'h + h/8\pi^2 C'$ and $B' = h/8\pi^2 A'$. J may assume all values except 0, since $J \geqq l$.

Fig. 3 shows the energy diagrams for both normal and excited states, with permitted transitions indicated by arrows. Those lines in a band which are due to $\Delta J=0$ belong to the Q branch, those with $\Delta J = \pm 1$ lead to P and R branches respectively. In other words, the absorption 0→1 corresponds to the first line of the R branch and the absorption 2→1 to the first line of the P branch. There is no transition 1→0 since in the excited state, J cannot be

zero. For levels in which $l=0$, J will of course assume all values including 0, while for a level in which $l=2$, J cannot be either 0 or 1.

Fig. 3A represents a system of lines corresponding to a change in l from 0 to 1. ν_0 lies between the Q branch and the first line of the P branch.

The Scheme of Vibration Levels and Interpretation of the Observed Bands

Fig. 4 represents the energy levels for the deformation vibration ν_2 following Dennison's analysis. The principal quantum number is the value of v_2 while the subscript is the value of l associated with it. When Δv is odd,

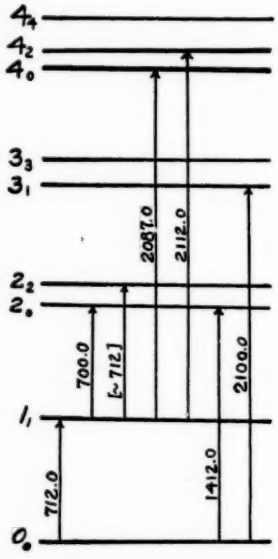

Fig. 4. Vibrational levels for ν_2.

Δl is restricted to ± 1 and the change in electric moment is normal to the axis of figure, giving rise to bands with Q branches. When Δv is even, $\Delta l=0$ and there are no Q branches. The most intense absorption bands originate in the level 0_0 but even at room temperature some molecules are excited to higher states. The population of any upper state is determined by the Boltzmann factor and by the statistical weight, the latter being 1 when $l=0$, and 2 when $l\neq 0$. Thus in the state 1_1 there are about 0.06 times as many, in the state 2_0 about 0.0009 times as many, and in 2_2 about 0.0018 times as many as in the state 0_0.

In addition to the three fundamental vibrations and their harmonics, all of which we should expect to be active, combination bands should appear. There is no restriction upon the values of Δv_1, Δv_2 and Δv_3 in combinations. Although ν_1 has not been observed directly, its value is apparently very close to 2100 cm^{-1}. ν_2 and ν_3 have been identified, their values being 712 cm^{-1} and 3289 cm^{-1} respectively. The rest of the observed bands may now be classified. The band at 4.7μ is apparently the second harmonic of ν_2, $\Delta\nu_2=3$, for which zero branches should appear. It cannot be ν_1 since the latter would be a doublet. The three maxima may be interpreted as indicated in the dia-

TABLE II. *Observed band centers and their assigned quantum transitions.*

ν_1	ν_2	ν_3	Band center		Approximate relative intensity
			Wave No. ($cm.^{-1}$)	Wave-length (μ)	
0–$1(\nu_1)$			(2100)	(4.76)	?
	0_0–$1_1(\nu_2)$		712	14.00	1000
	1_1–2_0		700	14.30	12.0
	1_1–2_2		712	14.00	
	0_0–3_1		2100	4.76	0.12
	1_1–4_0		2087	4.79	0.095
	1_1–4_2		2112	4.73	0.105
	0_0–2_0		1412.0	7.00	1.33
		0–$1(\nu_3)$	3289	3.04	4.4
0–1	0_0–1_1		2801	3.57	1.30

gram, $0_0 \rightarrow 3_1$ being the most intense peak at 4.76μ, $1_1 \rightarrow 4_0$, the weakest one at 4.79μ and $1_1 \rightarrow 4_2$ the intermediate one at 4.73μ. Table II shows the observed band centers and their assigned quantum transitions.

The fact that ν_1 has not been observed is somewhat surprising, and must indicate that for this motion the electric moment has a very small amplitude. The resulting weak band might have been observed if the three components of $3\nu_2$ had not been so intense. That ν_1 actually lies in this region is indicated by the Raman spectrum in which it appears as the most intense line. Kastler[6] finds the Raman displacement to be 2089 in the gas and 2098 in the liquid. Bhagavantam[7] gives measurements for liquid HCN only. He finds ν_1 at 2094 for normal molecules, with a weaker line at 2062 doubtless corresponding to absorption by molecules in the excited state 1_1, the intensity ratio being estimated as 24:1. The frequency ν_3 as indicated by his measurements is 3213.

ON THE SHAPE OF THE MOLECULE

All of the bands observed, as well as those reported by Badger and by Brackett are consistent with the hypothesis that the molecule is linear. Only for the linear configuration can the simple structure of the 14μ band be understood. From the frequencies given in Table I a value of the moment of inertia may be obtained, since

$$\nu(J' \rightarrow J'') - \nu(J' + 2 \rightarrow J'') = 2B'(2J' + 1)$$

the primes referring to the normal state. Computing in this fashion for each pair of lines, we find an average value $I' = 18.68 \times 10^{-40}$ g cm^2, which compares very well with Badger's value, 18.79×10^{-40} g cm^2. The same order of magnitude is indicated by the frequency interval between the maxima of the P and R branches in the 14μ band, but not in the bands at 7μ and 3μ. For the former with $\Delta\nu = 24.9$ cm^{-1}, the classical formula gives $I = 18.32 \times 10^{-40}$ g cm^2.

It is not possible at present to determine the interatomic distances from the moment of inertia, nor to decide between the two possible configurations designated as hydrogen cyanide HCN or iso-cyanide HNC. However, the simplicity of the rotational structure suggests that probably only one type of molecule is present.

[6] C. R. Kastler, Comptes Rendus **194,** 858 (1932).

[7] Bhagavantam, Nature **126,** 995 (1930).

The Positive Ion Current at the Cathode in the Glow Discharge

By A. KEITH BREWER AND R. R. MILLER
Fertilizer and Fixed Nitrogen Investigations, U. S. Bureau of Chemistry and Soils, Washington, D. C.

(Received August 29, 1932)

The positive ion current passing through a perforation in the cathode of a glow discharge tube has been measured with various types of collectors and the factors influencing the ratio of positive ions to total current studied. At pressures above 0.5 mm the positive ion current constitutes but a small fraction of the total current, while at lower pressures it increases inversely with the pressure, reaching approximately half the total current below 0.01 mm. The fraction of the current carried by positive ions is independent of the size and shape of the perforation, of the current passing through the discharge, and of the position of the anode provided it is not within a certain critical distance from the edge of the Crookes dark space; it does, however, vary with the gas, increasing for decreasing molecular weight.

The possible sources of current to the collector are discussed. The method by which the current due to positive ions is separated from that due to metastable molecules is described. The energy of the positive ions passing through the cathode is shown to correspond to an appreciable fraction of the cathode fall of potential.

IN A series of recent experiments on chemical action in the glow discharge (I–X)[1] it has been shown that the rate of reaction in the discharge can be expressed by a simple electrochemical equivalence law somewhat analogous to Faraday's law for electrolytes and also that the molecules formed in the negative glow are carried to the walls largely as positive ions; little or no reaction occurs in the dark spaces. An estimation of the M/N ratio for the positive ions formed in the discharge necessitates a knowledge of the rate of positive ion formation. Two separate methods used for evaluating the rate of ion formation yield M/N ratios similar to those found by Lind[2] for α-particles, provided the positive ion current to the cathode is small compared to the electron current.[3] The present research was undertaken, therefore, to measure the fraction of the current carried to the cathode by positive ions.

Many attempts have been made to analyze the current at the cathode. Aston[4] using a perforated cathode measured the current received by a collector immediately behind the performation. He concluded that as much as half the current might be carried by positive ions, but felt that this conclusion must be accepted with considerable caution, since a negative ion rather than a positive ion current was received by the collector when an appreciable positive charge was applied to it. Guntherschulze[5] from measurements of the power appearing as heat at the cathode infers that the positive ion cur-

[1] A. Keith Brewer, et al., J. Phys. Chem. **33,** 883 (1929) to **36,** 2133 (1932).
[2] S. C. Lind, *Chemical Effect of α-Rays*, A.C.S. Monograph.
[3] A. K. Brewer and P. D. Kueck, J. Phys. Chem. (1932).
[4] F. W. Aston, Proc. Roy. Soc. **A96,** 200 (1919).
[5] Guntherschulze, Zeits. f. Physik **37,** 828 (1926).

rent may exceed the electron current by a factor of ten. Uyterhoeven and Harrington[6] have shown that metastable molecules formed in the discharge exert a prepondering effect over positive ions in the emission of electrons from the cathode. It is now felt that these metastable molecules have largely been responsible for the difficulties involved in measuring the current carried to the cathode by positive ions.

Method

The method adopted for this study was a modification of that used by Aston; it consisted of measuring the current passing through a hole pierced in the cathode. There are many difficulties involved in using this method of measurement, most of which can be overcome by a current collector of the proper design. These difficulties are: (1) the discharge is not distributed uniformly over the cathode; (2) the cathode field may be distorted at the perforation; (3) metastable molecules and atoms as well as positive ions will

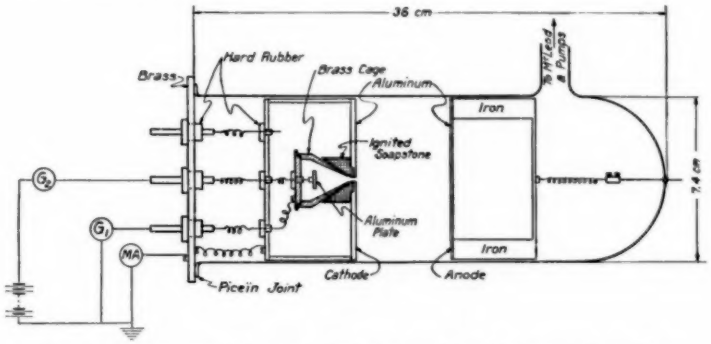

Fig. 1. Apparatus for measuring the positive ion current passing through a perforation in the cathode.

pass through the opening; all are capable of giving off electrons from the collector; (4) the high positive space charge at the opening causes an appreciable electron current to flow from the collecting plate to the cathode even in the absence of applied fields. It is believed that the apparatus as designed overcomes most of these difficulties and that the results give a fair estimation of the positive ion current.

The Apparatus

Many types of collectors were tried, including flat plates and a duplicate of that used by Aston. The currents received at the collector varied considerably, depending on the design and dimensions. The apparatus illustrated in Fig. 1 was finally chosen as giving the most reliable results.

The dimensions of the tube are given in the illustrations. The anode was an aluminum plate backed by iron, so its position could be changed by a magnet. The cathode was an aluminum disk covering one end of an enclosed aluminum cylinder 5 cm long and 7.3 cm in diameter. The perforation was a hole 2 mm in diameter placed in the center of the cathode, the cathode wall

[6] Uyterhoeven and Harrington, Phys. Rev. **36**, 709 (1930).

being about 0.5 mm in thickness at this point. The collecting cage was insulated from the cathode by an ignited soapstone block. It was found necessary to have a 5 mm opening in the cage with the soapstone shadowing the cage from the perforation to minimize space charge induced currents between the cage and the cathode. All parts were made tightly fitting to prevent metastable molecules from drifting between the cathode and the cage, thus giving rise to abnormal currents between these points.

The cone shaped cage was superior to the cylindrical type in practice, since it tended to screen the cathode perforation from fields applied to the collecting plate. This prevented a spurious discharge current between the collecting plate and the cathode when a potential was applied to the plate, and also it prevented the number of positive ions entering the cage from being influenced by the plate field.

Results

The effect of pressure

The effect of the pressure in the discharge tube on the positive ion current entering the cage is shown for various gases in Fig. 2.

These data were obtained with no potential applied to either the cage or the plate. In the case of nitrogen the currents to both the cage and the plate are shown. The measured positive ion current in every instance is the sum of these two currents. The corrected positive ion current is the measured current corrected for the fraction of the cathode covered by the discharge at the various pressures. The voltage is the difference in potential between the anode and the cathode; the electrodes were so placed that the positive column was absent.

The currents to the cage and plate are similar for all gases, the only appreciable difference being in magnitude. The cage current, which is larger than the plate current for the higher pressures passes through a maximum and reaches a comparatively small value at low pressures; the current to the plate, however, increased rapidly at the point where the cage current passes through a maximum.

The fraction of the total current carried by the positive ions passing through the perforation is given by the right-hand ordinates. The positive ion current appears to increase with decreasing pressures, the relation between pressure and current being very nearly hyperbolic for every gas except hydrogen. It is of interest to note that when the observed current is corrected for the fraction of the surface covered by the discharge, the positive ion current approaches 50 percent at the lowest pressures for which reliable readings can be taken, about 0.01 mm. At pressures above 0.5 mm the fraction of the total current carried by positive ions in argon, oxygen, and nitrogen is very small, being less than 5 percent. In helium and hydrogen, however, the positive ion current is materially larger.

The effect of pressure on the distribution over the cathode

The positive ion current arriving at various points on the cathode surface as affected by the gas pressure is shown in Fig. 3a. These values given are

for nitrogen and are typical of all gases. The currents passing through holes 2 mm in diameter were measured with plane plate collectors at the cathode center and at 1, 2 and 3 cm from the center. It will be observed that at

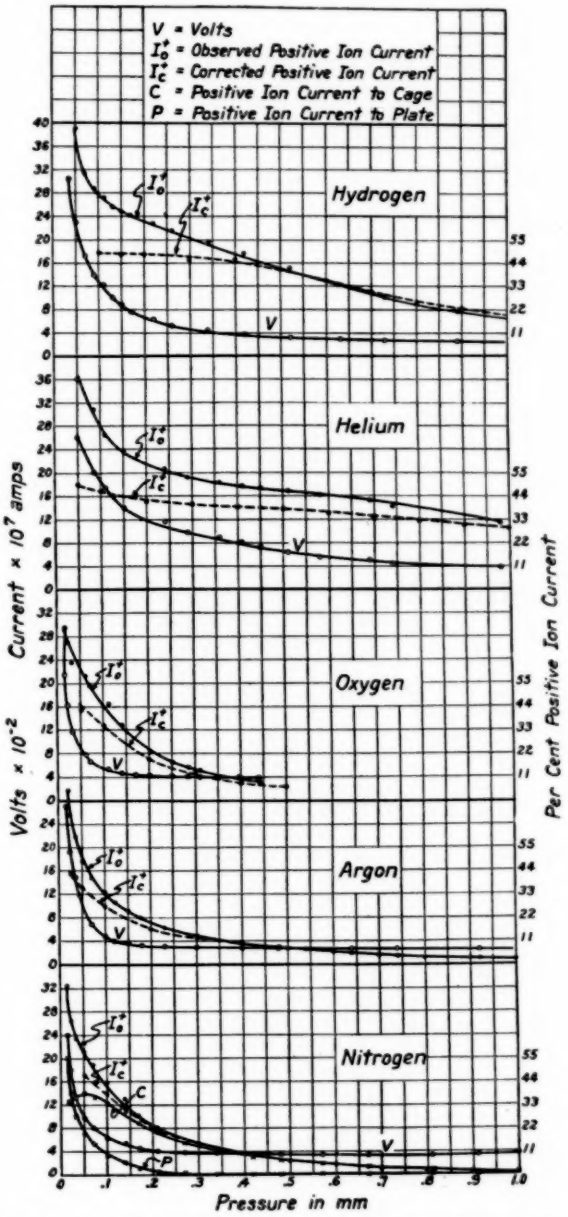

Fig. 2. Curves showing the positive ion current through the cathode perforation and the fraction of the total current carried to the cathode by positive ions.

pressures above 0.3 mm the discharge is quite uniformly distributed over the surface, while at pressures below this point the discharge creeps away from the edge of the cathode and tends to concentrate in two bright sections, one

at the center and the other in the form of a ring at the outer edge of the glowing area.

The effect of the discharge current

The variation of the positive ion current with the current passing the discharge is shown in Fig. 3b. These data are for the current passing through the center perforation in the cathode used in Fig. 3a. The results show the positive ion current to be proportional to the discharge current.

The effect of the cathode potential drop

The correlation between the cathode fall of potential and the positive ion current is illustrated in Fig. 2. In the region where the voltage change with pressure is appreciable, the change is approximately inversely proportional

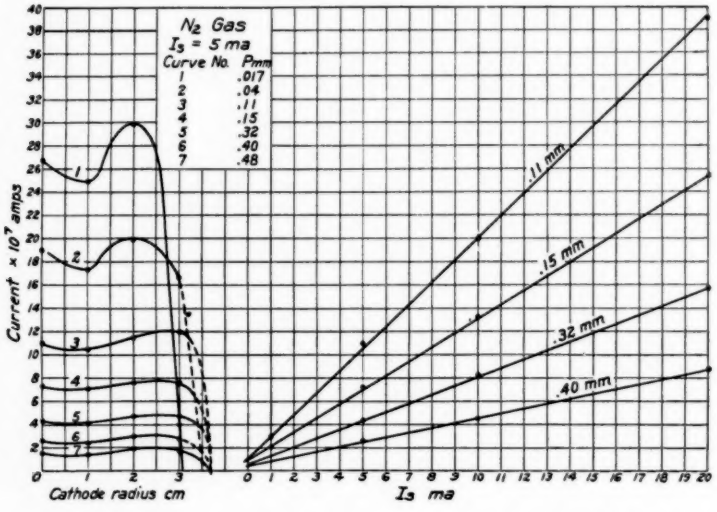

Fig. 3a. The distribution of the positive ion current over the cathode at various discharge pressures.

3b. The dependence of the positive ion current on the total current through the system.

to the pressure. With the possible exception of hydrogen, the positive ion current depends on the pressure in a similar manner.

The effect of area and shape of the perforation

A cathode with an adjustable slit passing through the center was used to test the effect of size of the opening on the positive ion current. The slit was 2.2 cm in length; the areas were varied from 0.007 sq. cm to 0.07 sq. cm, and the pressures from 0.2 mm to 0.5 mm. Over this entire range the positive ion current at each pressure was proportional to the slit area.

The shape of the perforation appears to have little effect on the positive ion current when the distribution of the discharge over the cathode was uniform. Thus round holes gave practically the same current values as did long narrow slits for equivalent areas.

The effect of the anode

The effect of the distance between the anode and cathode on the positive ion current is shown in Fig. 4.

The edge of the dark space is represented by the dotted line at 1 cm. The voltage is the difference in potential between the electrodes. The data show that the position of the anode in the negative glow has no effect on the cathode potential fall, on the current through the system, I_s, or on the positive ion current, I_p, until it approaches within a very short distance from the edge of the dark space. This effective region which determines the characteristics of the discharge is referred to as the vital segment.

The effect of collector potential

The effect of various voltages applied to the plate of the collector illustrated in Fig. 1 is given in Fig. 5.

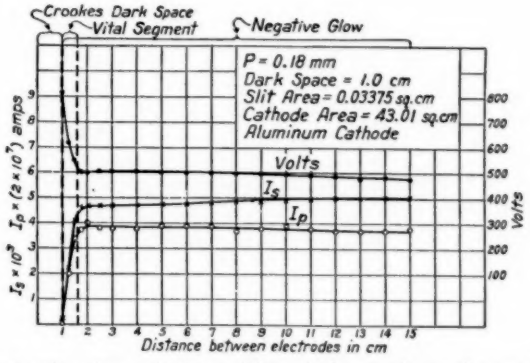

Fig. 4. The effect of the position of the anode on the positive ion current arriving at the cathode.

The results were all very similar in nature so only representative curves are shown. Line 1 shows the effect of potential on the current received by the plate, while line 2 is the current simultaneously received by the cage. Line 3 is the sum of these two currents. It will be seen that the sum of the currents received by the plate and cage is very nearly constant, irrespective of the plate potential. Lines 4, 5, and 6 represent the sums of curves similar to lines 1 and 2 for the pressures indicated.

Line 7 for hydrogen is distinct from those obtained for argon, nitrogen, and oxygen in that it shows a pronounced hump for low applied voltages. The size of the hump decreases with increasing pressure. Similar humps were obtained with helium at the lower pressures.

Line 1 for the current received by the plate is similar to that obtained with a simple plate collector or with a collector of the type used by Aston, the sudden drop for small applied potentials and the negative current for large positive potentials are characteristic of all simple collectors.

The results obtained with a collector of the same type as that shown in Fig. 1, but with a cylindrical rather than a cone shaped cage, were different from those given in Fig. 5 when various accelerating and retarding voltages

were applied to the plate. Two cylinders were used, one with an opening into the cylinder, 2 mm in diameter, the same as the cathode perforation and the other with a 6 mm opening placed symmetrically over the cathode perforation. The walls of the cylinders were machined to a knife edge at the opening in both cases and were insulated from the cathode by a thin sheet of mica. The cylinder with the smaller opening gave unsatisfactory results as the positive space charge due to the ions entering the perforation induced an appreciable electron current from the cage to the cathode. This effect was materially minimized by the 6 mm cage opening. With the larger opening the plate current corresponded exactly to line 1 of Fig. 5. The cage current, however, is illustrated by the dotted line 8, and differs materially from line 2 for the cone shaped cage in that many of the positive ions and metastable molecules that were caught by the cone now go to the cathode and also the number of

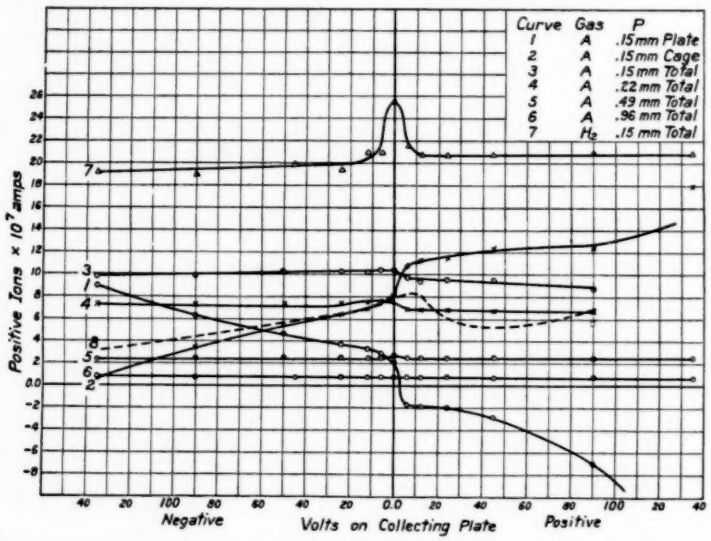

Fig. 5. The effect of plate potentials on the current to the plate and to the cage, and on the total positive ion current passing through the perforation.

positive ions passing through the cathode is doubtlessly materially reduced by the positively charged plate placed immediately over the perforation. Decreasing the distance between the plate and the perforation increased the current from the plate to the cathode, and decreased the current to the cage.

Discussion of Results

The results just presented may be better understood by a consideration of the possible sources of the currents received by the collector cage and plate. The currents received by the collector may be divided into two types; (1) the primary current entering from the discharge, and (2) secondary current arising within the collector. These types may be subdivided as follows:

(1) Primary current
   1. Positive ions from discharge (I^+)
   2. Electrons from discharge (e_c)
      (Dragged in by I^+ or by charge on plate)

(2) Secondary current
   1. Secondary electrons ejected by ions (e_{I^+})
   2. Secondary electrons ejected by metastable molecules and atoms (e_m)
   3. Photoelectrons (e_λ)
   4. Ionization by mutual impact of 2 metastables.

The components of the currents received by the plate and cage may now be analyzed as follows:

When plate is negative

Current at the plate
1. I^+
2. e_m from plate
3. e_{I^+} from plate
4. e_λ from plate

Current at cage
1. e_m from plate
2. e_{I^+} from plate
3. e_λ from plate
4. e_c from discharge

When plate is positive

Current at the plate
1. e_m from cage
2. e_λ from cage
3. c_{I^+} from cage
4. e_c from discharge

Current at cage
1. I^+
2. e_m from cage
3. e_λ from cage
4. e_{I^+} from cage

In addition to the above there are two other sources of current that might be registered by the collecting electrodes, namely, an electron current from the plate to the cathode perforation, and an electron current from the cage to the cathode. An example of the plate to cathode current is shown by line 8 in Fig. 5; this did not occur for the cone collector. A cage to cathode current is difficult to avoid but can be reduced by making the cage opening materially larger than the cathode perforation, and also by screening the cage opening from the cathode with some insulating material; a potential on the plate also decreases this current.

A survey of the various currents received by the plate and cage shows that the currents of secondary origin neutralize one another, in that what is lost by one electrode is gained by the other. The sum of the currents to the cage and plate, therefore, represents only the primary currents passing through the cathode perforation, provided no spurious discharges to the cathode occur. Thus it follows that the lines 3, 4, 5, 6, 7, of Fig. 5 represent the current due to the positive ions passing through the orifice minus that due to any electrons that might be dragged along by the inrushing positive ions.

An accurate estimation of the primary electron current passing through the cathode perforation cannot be made from the present data; nevertheless the results indicate it to be small compared with the positive ion current. Since the primary electrons necessarily enter the cage with very low initial energy they should be easily stopped by a negative plate potential; the fact that the total current passing through the perforation remains almost constant irrespective of the potential on the plate indicates a negligible electron current. It may be, however, that the small break in line 7 near zero plate voltage is due to the primary electron current.

The hump in curve 7 is characteristic of all the sum curves, although it is negligible for argon, nitrogen, and oxygen, and small for helium. The presence of the hump results from an abnormal electron current from the cage to the cathode that is apparently due to electrons liberated from the edge of the cage by metastable molecules and atoms and drawn to the cathode by the positive space charge set up by the inrushing ions. This type of discharge is readily checked by a charge on the plate and ordinarily breaks off more readily for positive than for negative potentials.

It is impossible to obtain an accurate estimation of the energy of the positive ions since the data do not distinguish between electrons liberated by the ions and by metastable molecules. The energy of the ions must be an appreciable fraction of the cathode potential drop, however, since the point of crossing of lines similar to 1 and 2 in Fig. 5 moves toward the positive voltages for decreasing pressure, as well as the positive potential at which the plate current became zero increased with a decrease in pressure. In the case of helium the plate did not register a negative current until a stopping potential of one-quarter the cathode potential was reached. This does not mean that the energy of the ions is but one-quarter of the cathode potential drop but rather that at this retarding voltage the positive ion current to the plate is just balanced by the electron current from the cage to the plate. When there is no charge on the plate the positive ions strike the plate at the lower pressures in a well-defined spot about twice the size of the cathode perforation; this is an indication of a fairly homogeneous beam of ions. It seems probable from a survey of the results as a whole that the ions striking the cathode possess an energy near that of the cathode fall. Such an interpretation is not surprising since it has been shown previously that the length of the Crookes dark space is approximately equal to one mean free path for an electron between ionizing collisions.

These results indicate that the current carried to the cathode by positive ions constitutes but a small fraction of the total current passing through the discharge for all pressures above a few millimeters of mercury. The positive ion current, however, is greater in gases of low molecular weight, the currents being roughly proportional to the relative rate of diffusion of ions in the various gases. Since the potential gradient at the junction of the Crookes dark space and the vital segment is small it is not surprising that the cathode potential drop has little or no effect on the values of the positive ion currents; diffusion is evidently the important thing in determining the movement of ions from the negative glow to the cathode. Even in this vital segment of the negative glow the natural tendency is for the ions to be driven further into the glow rather than towards the cathode, since the average electron producing the ionization has an energy component equal to the cathode potential.[7] The studies of chemical action in the discharge show clearly that a majority of the ions formed in the negative glow are neutralized on the walls of the discharge tube[8] rather than at the cathode.

[7] A. K. Brewer and P. D. Kueck, J. Phys. Chem. (1932).
[8] A. K. Brewer and P. D. Kueck, J. Phys. Chem. **35**, 1281 (1931).

On the Nature of Active Nitrogen

By J. Okubo and H. Hamada
Physical Laboratory, Tohoku Imperial University, Sendai, Japan

(Received July 15, 1932)

Since active nitrogen is essentially atomic nitrogen, the following two assumptions (without assuming the existence of the metastable atoms as Cario and Kaplan did) accounts for all the observed results as reasonable consequences of the Franck-Condon principle and the general properties of molecular spectra. The assumptions are: (1) In the vibrational states with $v''=\sim 8$ in the metastable $A^3\Sigma$ state, and also in those with $v'=\sim 6$ in the upper $B^3\Pi$ state, the near-nuclear turning points of the vibration have the same or nearly equal nuclear separations as those in the equilibrium position of nuclei in the normal molecular state; (2) With the exception of the neutral unexcited molecules and atoms in active nitrogen, the metastable $A^3\Sigma$ molecules in the vibrational state with $v''=7$ or 8 are most concentrated.

DURING the past few years, considerable progress has been made in our knowledge of the true nature of active nitrogen. From the results of the exhaustive experiments of Herzberg,[1] Kneser,[2] Wrede,[3] Bay and Steiner,[4] and others, it is at present generally accepted that active nitrogen is composed of nitrogen atoms and that its main properties are natural consequences of its atomic nature. It seems, however, that some further assumptions are required to account for the emission of the visible afterglow itself.

Assuming the existence of the metastable molecules and metastable atoms, Cario and Kaplan[5] have made good the defectiveness of Sponer's view[6] with regard to the nature of active nitrogen, and they have succeeded in explaining the emission of the visible afterglow as well as its other properties. Though their view is very helpful in explaining the special enhancements and energies of the bands emitted by the transitions from the initial levels corresponding to the vibrational quantum numbers ~ 11 and ~ 6 in the $B^3\Pi$ state, we have shown, on the one hand, that the "dark modification," does not exist,[7] (at least in the sense which they have mentioned) and that active nitrogen has an energy, content independent of its temperature ($-190°\rightarrow$ 650°C). On the other hand, we have shown that the enhanced appearance of the bands above described is not confined to the case of the afterglow bands of active nitrogen, but is also observable in the case of the first-positive bands excited by passing a very weak electrical discharge through nitrogen,[8] the only difference in the two cases being that in the latter case in comparison with the former, the relative intensities of the bands with $v'=\sim 6$ are greater

[1] G. Herzberg, Zeits. f. Physik **49,** 512 (1928).
[2] H. O. Kneser, Ann. d. Physik **87,** 717 (1928).
[3] E. Wrede, Zeits. f. Physik **54,** 53 (1929).
[4] Z. Bay and W. Steiner, Zeits. f. phys. Chemie **B3,** 149 (1929).
[5] G. Cario and J. Kaplan, Zeits. f. Physik **58,** 769 (1929).
[6] H. Sponer, Zeits. f. Physik **34,** 622 (1925).
[7,8,9] Detailed statements will be shortly published elsewhere.

than those with $v' = \sim 11$. Moreover, from the investigations of metallic spectra excited by active nitrogen, contrary to expectation, no resonance enhancements of the lines due to the metastable atoms (2:37 and 3.56 volts) and metastable molecules (8.2 volts) were found. It seems that the concentrations of these metastable entities should not be so high as Cario and Kaplan expected, even if they exist in active nitrogen.[9] To explain the observed results, *viz.*, that the maximum of the intensity distribution of the bands in the group, or that of the groups in the band system, is displaced in the direction of the longer wave-lengths by the increase of the pressure,[10] the introduction of inert gases,[11] the raising of the temperature,[7,10] and by the lapse of time directly after the exciting discharge of the active nitrogen has been cut off,[10] some further assumptions are required.

From the result that the selective enhancements of the bands with $v' = \sim 11$, $v' = \sim 6$, and $v' = \sim 2$ in the upper state $B^3\Pi$ are observable not only in the α-bands of active nitrogen, but also in the first-positive bands emitted from nitrogen, especially at the temperature of liquid air. When very weakly excited by the electrons of various velocities, it will be very natural to consider that the appearance of these bands is entirely due to the transitions between the energy levels of nitrogen molecules, and has no direct connection at all with atoms of any kind. Of course, the true nature of active nitrogen will be brought out clearly only after the results of further observations regarding its various properties have been reported, but the following consideration is a means of explaining the excitations of the bands with $v' = \sim 11$, ~ 6, and ~ 2 above described, the displacements of the maximum of intensity in the band group, or in the band system, accompanying the changes of excitational conditions, as well as other properties of active nitrogen, without assuming the existence of metastable atoms.

It seems that the main observed results of the afterglow of active nitrogen will follow very well as consequences of the following two assumptions coupled with the Franck-Condon principle. It is assumed that, (1) in the vibrational states with $v'' = \sim 8$ in the metastable $A^3\Sigma$ state, and also in those with $v' = \sim 6$ in the upper $B^3\Pi$ state, the near-nuclear turning points of the vibration have the same or nearly equal nuclear separations as those in the equilibrium position of nuclei in the normal $X^1\Sigma$ molecular state; and that (2) with the exception of the neutral unexcited molecules and atoms in active nitrogen, the metastable $A^3\Sigma$ molecules in the vibrational states corresponding to the quantum numbers $v'' = \sim 7$ or 8 are most numerous. The approximate potential energy of the molecular states $A^3\Sigma$ and $B^3\Pi$, calculated by the ordinary method with the molecular constants known from the vibrational and rotational analysis,[12] or simply by Morse's function, are plotted in Fig. 1. The equilibrium distance r_e of nuclei in the normal molecular state can be calculated, approximately, by means of the formula $r_e^2\omega_e = \text{constant}$ or $r_e^3\omega_e = \text{constant}$, and it is fairly certain that its value is in the vicinity of

[10] G. Herzberg, Zeits. f. Physik **49,** 512 (1928).
[11] Lord Rayleigh, Proc. Roy. Soc. **A102,** 453 (1923).
[12] S. M. Naudé, Phys. Rev. **38,** 372 (1931).

1.09A, and also that it is nearly equal to the values of the nuclear distance of near-nuclear turning points of the vibration in the $A^3\Sigma$ state corresponding to the vibrational quantum numbers ~ 8, and approximately to those in the $B^3\Pi$ state corresponding to the vibrational quantum numbers ~ 6. Therefore assumption (1) may be reasonably accepted. As the energy of the $v'' = 8$ level in the $A^3\Sigma$ state is in the range between 9.5 and 7.5 volts[13] the excitation of the $A^3\Sigma^{(\sim 8)}$ levels (and so the assumption (2)) is also conceivable from the observed results of the metallic spectra excited by active nitrogen, taking into consideration the Franck-Condon principle.

Certainly, the excitation of these $A^3\Sigma^{(\sim 8)}$ levels may be due to the triple collisions. Here it is only necessary that the energy of the $A^3\Sigma^{(\sim 8)}$ state be not greater than the dissociation energy of the nitrogen molecule. It is not necessary to assume that the former is equal to the latter. Therefore, no modification of this consideration is necessary even though we take the latter as 9.0 or 9.1 volts, so long as the former is not greater than the latter. It is regretted that we have now no reliable data to determine the energies of triplet levels

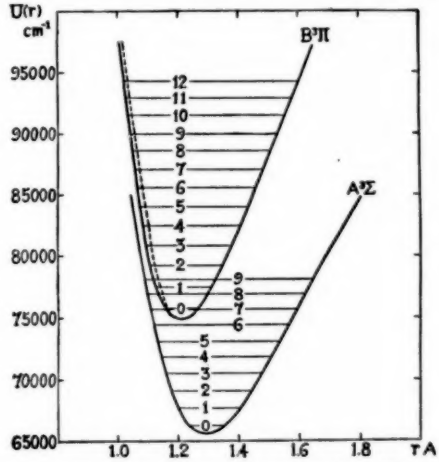

Fig. 1. Approximate potential energy curves for $A^3\Sigma$ and $B^3\Pi$ of N_2.

of a nitrogen molecule. If it were certain that the energy of the $A^3\Sigma^{(\sim 8)}$ state is greater than the energy of dissociation, a slight modification with regard to the explanation of high concentration of the metastable $A^3\Sigma^{(7 \text{ or } 8)}$ molecules will be necessary, but no alternation of the above assumptions.

From the general nature of triple collisions, i.e., that the metallic lines of the lower excitational energy are excited much more intensely than those of the higher energy in comparison with other cases of excitation, and from the already recognized fact that the only known excited state of the nitrogen molecule directly combined with the $A^3\Sigma$ state is the $B^3\Pi$ state, it is certain that, in the triple collisions between two nitrogen atoms and the metastable molecule in the $A^3\Sigma^{(7 \text{ or } 8)}$ state, the transitions to the $B^3\Pi$ state from the $A^3\Sigma$ state will be most probable in comparison with the transitions to other states. According to the general property above mentioned, the $B^3\Pi$ mole-

[13] R. S. Mulliken, Rev. Mod. Phys. **4**, 54 (1932).

cules in the vibrational level corresponding to the quantum number 11 or 12 will predominate over those corresponding to the quantum number 6 or 7. Consequently, it will be expected that, in the visible afterglow, the bands which are emitted by the transitions from the vibrational level with $v'=11$ or 12 in the $B^3\Pi$ state will appear more enhanced than those from the level with $v'=6$ or 7 in the same state. It will also be easily understood why the bands with smaller v', especially those with $v'=2$ or v' thereabout, are selectively enhanced in the α-bands of active nitrogen, (of in the spectrum of ordinary nitrogen excited by a very weak electric current at low temperature), as some little concentration of the $A^3\Sigma$ molecules with smaller v'' or $v''=0$ will result from the vibrating metastable molecules $A^3\Sigma^{(\sim 3)}$ etc. In this manner it is possible to understand the special enhancements of the bands in the α-bands of active nitrogen.

As the lifetime of the $A^3\Sigma$ metastable state is believed to be sufficiently long, in the case where a suitable quantity of the inert gas is mixed with nitrogen, or where the pressure of nitrogen is relatively high, the $A^3\Sigma^{(7 \text{ or } 8)}$ molecules will collide more frequently with other neutral unexcited molecules or atoms before the former are again excited to the $B^3\Pi$ state, and the vibrational levels of the former will descend to lower levels ($^3\Sigma^6$, $^3\Sigma^5$, $^3\Sigma^4$, $\cdots$) than those before the collisions. As a result the $B^3\Pi$ molecules having vibrational quantum numbers less than $\sim$11 or $\sim$6 will predominate. Therefore, the maximum of intensity in the band system or in each group will be displaced towards longer wave-lengths, and the greater the number of collisions, i.e., the higher the pressure of the nitrogen or the inert gas, the greater will be this effect.

At a high temperature on account of the greater relative velocities of molecules and atoms, the probability of triple collisions will naturally be reduced, and in addition there will be required two-stepped excitations for the visible afterglow (α-bands) and a one-stepped excitation for the metallic spectra. The former will appear weaker and weaker in comparison with the latter.[14] This is conceivably the reason the intensity of the visible afterglow is markedly reduced at a high temperature, independent of its energy content (9.51 volts). It is also to be expected that, at high temperature, the vibrational energies of the $A^3\Sigma^{(7 \text{ or } 8)}$ states will be reduced before they undergo the second excitation because triple collisions between molecules and other atoms take place relatively less frequently. The maximum of intensity in the group or band system of the visible afterglow will be naturally displaced towards the longer wave-lengths. On the other hand, where, owing to the smaller relative velocities of molecules and atoms at a low temperature, triple collisions take place frequently, the probability that the $A^3\Sigma^{(7 \text{ or } 8)}$ molecules will be excited again to the $B^3\Pi$ state is considerably increased. There are then observed enhanced intensities and a rapid decay of the after-

[14] In the case where the active nitrogen is flowing through the heated (or cooled) portion of the tube, the decrease (or increase) of intensity of the glow due to the local reduction (or increase) of density of normal atoms and molecules must be taken into consideration.

glow bands, while there is no displacement of the maximum of intensity towards the longer wave-lengths.[14]

The reason the intensity of the visible afterglow is considerably reduced in the case where a weak electric discharge is being passed through the active nitrogen, may be that a recombination of the atoms which take part in the triple collisions[3] is taking place.

It is probable that in the case where a very weak current is passed through ordinary nitrogen, there is a concentration of electrons which has sufficient energy to produce the $B^3\Pi$ molecules with vibrational quantum number ~ 6 by the single collision with the nonvibrating normal $X'\Sigma$ molecules, so that the molecules in that vibrational level will be more concentrated than those in the level with $v' = \sim 11$, because the latter are excited from the $A^3\Sigma^{(7 \text{ or } 8)}$ level indirectly. For this reason the bands emitted from the former, as the initial level of transition, will appear more enhanced than those from the latter, as the results of observations show.

As explained above, considering that the active nitrogen is essentially atomic nitrogen, and, making the two assumptions above stated, it seems, (without assuming the existence of the metastable atoms as Cario and Kaplan did) that all the observed results will follow as reasonable consequences of the Franck-Condon principle, as well as from the general properties of molecular spectra.

Jackson and Broadway[15] consider that they have obtained from their experiment evidence of the presence of metastable nitrogen atoms in the $^2P_{\frac{1}{2}}$ state, but not of the normal ^4S atoms. As triple collisions may possibly take place between three normal atoms, it is not unreasonable that such metastable atoms will be present in very small quantity. However, if there were only metastable molecules (8.2 volts) and metastable atoms in active nitrogen, it would be very hard to explain the main properties of it, for example, very long persistence of afterglow, the absence of resonance enhancements of the metallic lines due to these metastable molecules and metastable atoms, and the temperature effect, etc.

[15] L. C. Jackson and L. F. Broadway, Proc. Roy. Soc. **A127,** 678 (1930).

The Origin of the Mercury Bands at 2480A

By J. GIBSON WINANS
University of Wisconsin

(Received October 19, 1932)

The group of eight mercury bands near 2480A was photographed under varied excitation conditions with the purpose of determining their origin. The source was a discharge through mercury vapor produced in a quartz tube through external electrodes by a low-voltage Tesla coil. Five tubes containing distilled mercury and commercial mercury arc lamp showed this group of bands. These bands were weakened by heat along with known mercury bands. The origin is undoubtedly some form of mercury molecule. The most probable forms are Hg_2^+ and Hg_2. Five observations favor Hg_2^+ over Hg_2. (1) These bands have never been observed in fluorescence. (2) The 2476 band is more intense than the 2345 Hg_2 band under strong field excitation but weaker than 2345 under low field excitation. (3) No other bands with properties like those of the 2480 group have been observed in the mercury spectrum and Rayleigh has shown that these bands do not occur in absorption. (4) The bands in this group may be classified as sequences $v'-v''=0\pm1\pm2\pm3$, and a lower limit for D of 0.3 volts estimated. (5) In the $v'-v''=0$ sequence, emission is observed from state $v'=41$ indicating molecules with very high vibrational energy. This energy may be supplied by the electric field if the emitter is an ion but not if it is a neutral molecule.

INTRODUCTION

THE spectrum of a discharge through mercury vapor shows a group of eight bands near 2480A whose origin has been uncertain. These bands are shown in Fig. 1. The most intense band of the group with sharp limits at 2476 and 2482 and a fainter one between 2470 and 2476 were discovered

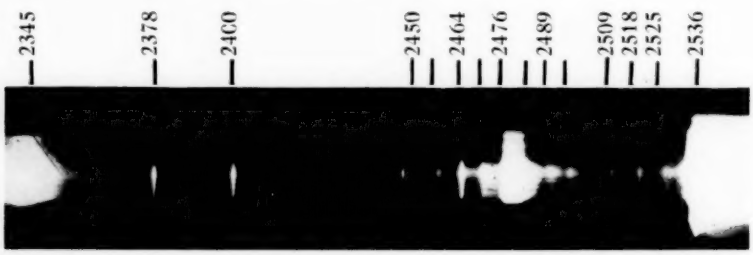

Fig. 1. Mercury bands near 2480A.

by Stark and Wendt[1] who described them as continuous. These bands were observed also by Nagaoka[2] in the light from a special type of mercury arc. Bands will be referred to by their short wave edges. Pienkowski[3] observed some flutings in the 2476 band and Rayleigh[4] showed that the flutings con-

[1] J. Stark and G. Wendt, Phys. Zeits. **14,** 562 (1913).
[2] H. Nagaoka, Japanese Jour. Phys. **1,** 1 (1922).
[3] St. Pienkowski, Bull. de. l. Acad. Pol. 171 (1928).
[4] Rayleigh, Proc. Roy. Soc. **A782,** 349 (1928).

verged toward shorter wave-lengths. Rayleigh also observed that neither 2476 nor 2470 were absorption bands and that 2470 was either continuous or had flutings much more closely spaced than 2476. Condon[5] suggested that 2476 might be a "diffraction band" of Hg_2 and showed that the frequencies of the flutings followed the law of convergence calculated for diffraction bands. The intensities, however, did not decrease exponentially as predicted. Miss Brozowska[6] obtained photographs using a spectrograph of $1A/\text{mm}$ dispersion and showed that the flutings of 2476 converged according to the equation

$$\nu = A + Cm(m+1)$$

like the lines in the Q branch of a single band. From her photometer record, reproduced in Fig. 2, it is seen that the flutings are broad in the center and double near the long wave side. Miss Brozowska observed three bands in addition to 2476 and 2470 with short wave edges at 2458, 2450, and 2464. The short wave limit for the 2464 band was hidden by a mercury arc line. She suggested HgH as a possible emitter.

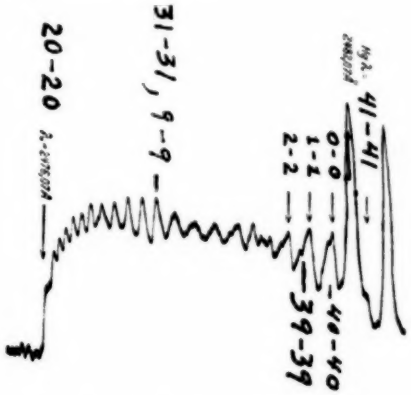

Fig. 2. Flutings of 2476.

These five bands and three new ones were observed by the writer[7] in the spectrum of an electrodeless discharge through mercury vapor. The new bands have short wave edges at 2495.6, 2489.2, and 2482. They are shown in Fig. 1. The edge of the 2482 band was covered by a mercury arc line.

The entire group of eight bands was observed independently by Hamada[8] in the spectrum emitted from the hollow cathode of a discharge tube filled with mercury vapor. He found in addition two new bands whose wave-lengths at the maxima he gives as 2504 and 2513.

In the following experiments this group of bands has been studied under varied excitation conditions with the purpose of determining their origin.

[5] E. U. Condon, Phys. Rev. **32,** 858 (1928).
[6] Miss J. Brozowska, Zeits. f. Physik **63,** 577 (1930).
[7] J. G. Winans, Phys. Rev. **38,** 583 (1931).
[8] H. Hamada, Phil. Mag. **22,** 50 (1931).

Apparatus

The apparatus for these experiments consisted simply of an evacuated quartz tube containing mercury, a low power Tesla coil, and small quartz spectrograph (Hilger E31). Wires were wrapped about each end of the quartz tube, one was grounded and the other was connected to the Tesla coil. The optimum vapor pressure for band emission was maintained by a furnace or by Bunsen burners. In all, five tubes were used, two of which had plane windows and could be viewed end on. Each tube was baked out in a vacuum, a drop of mercury was distilled into it and it was sealed off. The tubes were prepared at different times from different samples of mercury. Sufficient intensity was obtained to photograph the 2476 band in the third order of a 21 foot grating with slit width 0.03 mm and exposure of one week. Exposures with the small quartz spectrograph were made with a very small image of the discharge tube focussed for λ2480 on the slit. In this way the light from different parts of the discharge could be compared with a single exposure.

All five tubes gave the bands shown in Fig. 1 and listed in Table I. The wave-lengths agree with those given by Hamada[8] with the exception of 2518

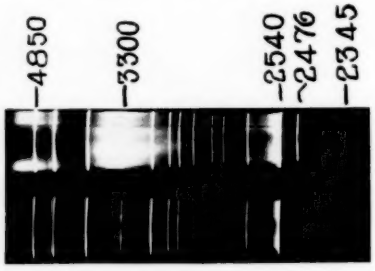

Fig. 3. Effect of heat on mercury bands.

and 2509. Hamada gives 2513 and 2504. He does not list any corresponding to 2525. The discharges also showed a continuous spectrum from 2536 to 2345 with a minimum at 2410. This may be seen in Fig. 1. Some of the tubes gave the HgH bands at 4219, 4017, and 3728 and others did not. The HgH bands when present were emitted only in the neighborhood of the electrodes.

The effect of heat without change in pressure on these bands is shown in Fig. 3 taken while a section of the discharge tube near the center was heated with a blow torch. The central part of the spectrum shows the light emitted by the heated part. Heat was found to weaken the bands at 2495, 2489, 2482, 2476, 2470, 2456 of the 2480 group in addition to the Hg_2 bands with maxima at 4850, 3300, 2650, 2540, and 2345. The others listed in Table I were too weak to be studied in this way. The effect on the 4850 and 3300 bands is the same as that observed in fluorescence.[9] This assures that the weakening is due to heat and not to a change in discharge conditions.[10]

A photometer record of the plate taken on the 21 foot grating verified the structure of 2476 observed by Miss Brozowska and shown in Fig. 2.

[9] H. Niewodniczanski, Zeits. f. Physik **49,** 59 (1928).

[10] J. G. Winans, Phys. Rev. **39,** 745 (1932).

TABLE I.

	Short wave limits A	ν cm^{-1}	$\Delta\nu$	$v'-v''$	Intensity
1	2525.4	39,586			3
			116		
2	2518.0	39,702			3
			136		
3	2509.4	39,838			2
			221		
4	2495.6	40,059		−3	3
			98		
5	2489.5	40,157		−2	4
			121		
6	2482	40,278		−1	5
			97		
7	2476.07	40,375		0	10
			107		
8	2469.5	40,482		1	5
			110		
9	2464	40,572		2	3
			99		
10	2458.0	40,671		3	3
			141		
11	2449.5	40,812			1

To observe these bands under excitation fields of different strength, one set of photographs was made with the Tesla coil disconnected from the discharge tube and operated at different distances from the tube in air. Excitation of the discharge by strong or weak fields could be obtained by changing the distance between the Tesla coil and the discharge tube. Fig. 4, No. 1 shows that for weak fields the 2345 Hg_2 band and the 2536 line are much stronger than the 2476 band. Fig. 4, No. 2 shows that for strong fields 2476 was more intense than 2345.

Fig. 4, Nos. 3 and 4 give a comparison of the spectra from an ordinary mercury arc with that from a high-frequency discharge. Fig. 4, No. 3 is the spectrum of the mercury arc. Fig. 4, No. 4 is the spectrum obtained by shutting off the arc and operating a high-frequency discharge through the arc chamber while it was cooling. No. 4 shows bands while No. 3 does not, although the vapor pressure for No. 3 was greater than that for No. 4. The exposure for No. 3 was about 0.01 that for No. 4.

DISCUSSION

The origin of the group of bands near 2480 can be definitely taken as some form of mercury molecule, since it was observed in six different tubes containing pure mercury in the present experiments and by other experimenters in previous experiments. This is indicated also by the fact that heat, which is known from the experiments of Koernicke,[11] and Kuhn and Freudenberg[12] to reduce the number of mercury molecules causes a weakening of this group of bands along with the mercury bands at 4800, 3300 and 2345. HgH is very unlikely to be the emitter since known HgH bands were found to

[11] E. Koernicke, Zeits. f. Physik **33,** 219 (1925).

[12] H. Kuhn and K. Freudenberg, Zeits f. Physik **76,** 38 (1932).

differ greatly in intensity relative to the 2476 band in different tubes and at different parts of the discharge. The most probable forms of mercury molecule are Hg_2 and ionized Hg_2 (Hg_2^+). Five observations favor Hg_2^+ over Hg_2 as the emitter.

(1) The 2476 mercury band has never been observed in fluorescence. All of the known Hg_2 bands from λ7000–2000 as well as most of the mercury arc lines have been observed in fluorescence with no trace of 2476.[13,14] This indicates that 2476 requires more energy than is available in a fluorescence tube in air, i.e., more energy than that needed for Hg_2 bands and Hg arc lines. This favors Hg_2^+ over Hg_2 as the emitter.

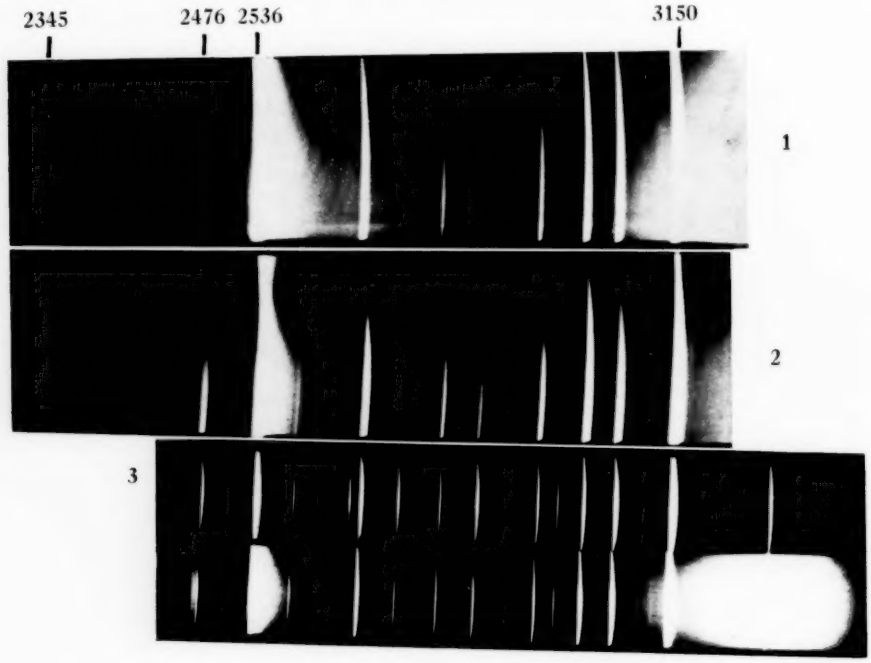

Fig. 4. No. 1 discharge under weak field, No. 2 discharge under strong field, No. 3 mercury arc, No. 4 discharge through mercury arc lamp.

(2) The comparison of intensities of the 2345 Hg_2 band and 2476 under strong and weak field excitation showed that 2476 although of longer wavelength required more energy for excitation than 2345. This also indicates Hg_2^+ instead of Hg_2 as the emitter of 2476.

(3) Rayleigh observed that 2476 is not an absorption band, and no other groups of bands similar to the 2480 group have been observed in the mercury spectrum. If 2476 were due to Hg_2 and not to Hg_2^+ it must be emitted by a transition to a final state which dissociates into one mercury atom in the normal state and one excited to 2^3P_0 or some state of greater energy. The initial molecular state for 2476 would dissociate into one 1^1S atom and an

[13] R. W. Wood and V. Voss, Proc. Roy. Soc. **A119,** 698 (1928).
[14] Rayleigh, Proc. Roy. Soc. **A137,** 101 (1932).

excited atom of 9.7 or more volts energy if D' is approximately equal to D''. The ionization potential of mercury is 10.4 volts. An atomic state of energy greater than 9.7 volts would lie near the series limit and be one of a large number of similar states. Each of these atomic states would be associated with molecular states and we should observe many bands of character like 2476 instead of only one. Since only one is observed, its origin is very unlikely to be Hg_2 or $D'' \ll D'$ for 2476.

(4) The flutings in the 2476 band are too widely spaced to be rotational lines of Hg_2 or Hg_2^+.[15] Each fluting must then represent an unresolved band and each member of the 2480 group a sequence of bands. To account for the sharp short wave edge, 2476 must be a sequence which turns back on itself forming a head of bands like those observed in sodium vapor by Loomis and Nile.[16] This point of view explains the intensity distribution, diffuseness, and doubling of flutings shown in Fig. 2. Near the head of the sequence two bands coincide to give sharp intense flutings, near the center they are separated enough to cause diffuseness, and near the long wave edge they are resolved into one strong and one weak component. If the strongest fluting is taken as band 0–0, the weakest is 41–41. If 2476 is taken as the $v'-v''=0$ sequence, the other bands in the 2480 group may be classified as the sequences $v'-v'' = \pm 1 \pm 2 \pm 3$ as shown in Table I. The narrow wave-length range of these sequences indicates that $r_e'-r_e''$ and, if Bates and Andrews relation holds,[17] $D'-D''$ are small. This strengthens the conclusion from observation (3).

Assuming this classification, a lower limit for D may be estimated. Band $v'-v''=3$–0 falls in the narrow sequence 2458 with wave number about 40670. By substracting from this, the wave number of $v'-v''=0$–0 gives the energy of the third vibration level of the excited molecule as about 380 cm^{-1}. From this $\omega_e' > 125$ cm^{-1}. If ω converges linearly with v' the average separation of vibration levels is >60 cm^{-1}. Since emission is observed from $v'=41$, D must be >2460 cm^{-1} or 0.3 volts.

(5) On the basis of the classification given above, emission by molecules in state $v'=41$ (vibration energy greater than 0.3 volts) is observed. This favors Hg_2^+ over Hg_2 as the emitter since a charged molecule may acquire high vibration energy from it's motion in the electric field. A neutral molecule will possess vibration energy more nearly corresponding to the temperature of the vapor. If $r_e'-r_e''$ is large a neutral molecule might possess high vibrational energy immediately after excitation and emit radiation from that state, but when $r_e'-r_e''$ is small as for 2476, this possibility does not exist.

Each of the five observations discussed indicates that the emitter of the 2480 group of mercury bands is Hg_2^+.

There are several other observations of interest which remain to be explained. They are (1) The 2470 band sequence has no flutings. This may mean that the flutings do not coincide sufficiently well for resolution. (2) The clas-

[15] Assume $r_e=4A$ and the energy difference between the first two rotational states is 0.005 cm^{-1}. The smallest separation between flutings is 1.5 cm^{-1}.

[16] F. W. Loomis and S. W. Nile, Phys. Rev. **32**, 873 (1928).

[17] J. R. Bates and D. H. Andrews, Proc. Nat. Acad. Sci. **14**, 124 (1928).

sification given above accounts for only seven of the eleven bands listed in Table I. Bands 1, 2, and 3 in Table I resemble somewhat bands 7, 8, and 9 and may be another group of sequences of Hg_2^+. (3) There is a continuous spectrum between 2536 and 2345 with a minimum near 2410. The regions between 2536 and 2410 and between 2400 and 2345 fall just beyond the limits for the 2^3P_2 and 2^3P_1 sharp and diffuse series of Hg. The continuous spectrum is probably the recombination spectra associated with these series. (4) The high-frequency discharge gave greater intensity of bands relative to lines than the mercury arc operated at greater pressure. A possible explanation is that collisions with high-velocity ions destroyed Hg_2 molecules in the arc more than in the discharge because of the greater concentration of ions in the arc.

The explanations suggested here for these last four observations need verification by further experiments.

The writer wishes to thank Professor R. S. Mulliken for suggesting the interpretation of the spectrum as a set of band sequences.

The Auroral Spectrum

By JOSEPH KAPLAN
University of California at Los Angeles

(Received October 24, 1932)

The first-negative bands of nitrogen, which comprise most of the nitrogen radiation in the auroral spectrum, have been excited under conditions which suggest those in the aurora very closely. Active nitrogen is produced in uncondensed discharges in concentrations sufficient to give a strong visible glow. A very strong flash is observed at the beginning of the afterglow, and this flash indicates a high concentration of active material in the exciting discharge itself. Under the best conditions for the production of the afterglow the spectrum of the exciting discharge consists almost entirely of the first-negative bands. The most important characteristic of these bands, as excited under the present conditions, is the absence of lines due to N^+. The usual excitation of the N_2^+ bands in discharges at low pressures produces these lines, whereas they are almost entirely absent in the auroral spectrum. The excitation of N_2^+ bands in the present experiments is thought to be due to the large concentration of metastable nitrogen molecules in the $A(^3\Sigma)$ state, and this experiment is presented as a proof of their presence in both the aurora and in nitrogen afterglows.

I. INTRODUCTION

RECENT discussions of the origin of the Aurora Borealis have aroused considerable interest in the problems associated with this beautiful and startling phenomenon. Of special interest is the ultraviolet light theory which was proposed by E. O. Hulburt and H. B. Maris[1] in 1929. According to that theory, the auroral displays are caused by blasts of ultraviolet light from the sun which ionize the atoms of the upper atmosphere. These ions are carried to the polar regions where they recombine and emit the auroral radiations. The earlier theories of Birkeland, Störmer and Vegard suggested that the aurora was due to charged particles from the sun which are diverted to polar regions by the earth's magnetic field, and then their energy is given to the atmosphere and converted into auroral radiation. In their paper on auroras and magnetic storms Maris and Hulburt suggested that a complete theory of auroras "will require, among other things, complete knowledge of the energy levels, metastable states and transition probabilities of the atmospheric atoms and molecules, as well as of the exact processes which give rise to the aurora light." It is the purpose of this short paper to make a contribution to that phase of the problem.

The spectrum of the aurora consists in most part of the green aurora line, due to atomic oxygen, and of the first-negative bands, due to N_2^+. Other bands have been reported in the auroral spectrum, which are members of the second-positive and the first-positive groups of N_2, but in general these radiations are very weak in comparison with the green line and the negative bands.

[1] Maris and Hulburt, Phys. Rev. **33**, 412 (1929).

The green aurora line has been studied with great success in recent years, and much has been written about it. In the present paper we will describe experiments in which the negative nitrogen bands have been studied. Because of the enormous interest shown in the green line, not much work has been done on the study of the conditions of excitation of the negative bands. We have succeeded in exciting them under conditions which suggest the actual auroral conditions so closely that it will be tempting to conclude that we have reproduced the auroral conditions.

II. Experimental Method

The experimental method used in this work was a rather unusual one. Active nitrogen was produced by passing an electrical discharge through nitrogen at pressures ranging from 5 to 10 mm, not from the condensed discharge source usually employed in active nitrogen experiments, but from an ordinary uncondensed discharge from two 1-kw, 25,000-volt Thordarssen transformers. In all other experiments of which the writer is aware active nitrogen has been produced by passing a condensed discharge through nitrogen at a pressure of about 0.5 mm or by using an electrodeless discharge at pressures around 0.01 mm. An uncondensed discharge through a tube containing nitrogen will in general not produce active nitrogen in quantities sufficient to show a visible glow. In the present experiment this was not the case. It was possible to produce a strong visible glow in nitrogen even with an uncondensed discharge.

In the present experiments the tube was filled with nitrogen, and a small amount of oxygen was added. Then the tube was run steadily for several days during which the oxygen was gradually cleaned up. At first, the afterglow was the green continuous glow which is so readily produced by an uncondensed discharge in oxygen-nitrogen mixtures. As the oxygen was cleaned up this glow disappeared, and the afterglow due to active nitrogen appeared with increasing intensity. It is interesting to note the continuous transition between the two types of glow. The long running of the tube undoubtedly conditioned the surface of the tube in such a way as to allow it to adsorb nitrogen atoms. These adsorbed atoms react with other nitrogen atoms which collide with the wall, and the production of the visible afterglow is made possible. More will be said about this in a forthcoming paper on active nitrogen. The novelty of the present experiment is in the extremely long treatment of the tube, which finally resulted in walls which were more favorable for the production of the visible glow than those in previously reported experiments. It is difficult to account for the production of the afterglow in an uncondensed discharge in any other way. The strong afterglow in uncondensed discharges has probably been missed by others because of insufficient treatment of the discharge tubes. A condensed discharge will produce a strong afterglow in tubes in which an uncondensed discharge produces a very weak glow, hence experimenters have resorted in general to condensed discharges for the production of active nitrogen. So much, however, for the preparation of the tube. We will now discuss the actual aurora experiments.

The spectra in which we are interested were photographed in the bulb part of a discharge tube consisting of a 500 cc Pyrex bulb and a short length of 1 mm capillary tubing, and the usual large internal aluminum electrodes. The afterglow in the bulb showed a peculiar behavior which the present writer has never observed before. For a very short time after the exciting discharge was interrupted, the glow consisted of an extremely intense flash, much more intense than the afterglow which followed the flash. The writer has seen this "flash glow" hundreds of times, and there is absolutely no question of its existence. The flash was followed by the usual type of steadily decaying afterglow.

It was observed that when the afterglow in the bulb showed the short-lived flash (and this occurred only at the end of a very long treatment of the tube), the spectrum of the exciting discharge consisted of the first-positive bands of nitrogen, the negative bands of N_2^+ and the second-positive bands of N_2. The more intense the afterglow became, the more thoroughly were the second-positive bands quenched. By not running the tube steadily, but by making and breaking the current about once a second, it was possible to almost completely quench the second-positive group and to weaken the first-positive bands relative to the negative bands. Under the best conditions, the spectrum of the discharge in the bulb part of the tube consisted almost entirely of the negative bands. The plate was exposed to the light from the bulb during the entire "make," and for that reason the spectrum contained more of the second-positive group than if the exposures had been limited to the later part of the make. This could readily be seen by noticing that the second-positive bands flashed up and then died down during the first part of the make. Evidently the condition, which is responsible for the presence of the negative bands, is being produced during the first part of the discharge, and hence is not as steady as it is during the rest of the discharge time.

The spectra which are reproduced will show that some very striking changes have taken place in the nature of the electric discharge as the intensity of the afterglow increases. The spectrum of a discharge in N_2 in which no afterglow is produced consists of the first-positive and the second-positive bands. There is practically no sign of the negative bands. As a rule, the negative bands are produced with high intensity in discharges at pressures of 10^{-2} to 10^{-3} mm, and then they are accompanied by lines due to N^+. The presence of a strong afterglow changes the spectrum entirely. The spectrum of N_2^+ is now produced at a relatively high pressure and it is not associated with the strong line spectrum of N^+ which is present at low pressures. The first negative bands of the auroral spectrum are also excited without the strong excitation of the N^+ line spectrum. A comparison of the results of the present experiments with actual auroral spectra will show the remarkable resemblance between the two. The absence of the line spectrum of N^+ in the present experiment and in the auroral spectra is probably the most important point of resemblance between the two. These results are shown in Fig. 1.

When the current in the tube is diminished to about one-third of the value

at which the negative bands are produced, the afterglow is of course a very weak one, the negative bands are weak, and the first-positive bands appear with definite maxima in bands arising on B_{10} and B_6. The 6323 band, corresponding to B_{10}–A_7, has been reported in auroral displays, and considerable discussion has taken place recently regarding Vegard's[2] observations of infrared bands in the aurora which are identified as transitions $B_7 \rightarrow A_6$. The B_6 maximum is quite strong in the negative glow of a discharge tube, and is often prominent in very red nitrogen discharges. The strong excitation of the B_{10} level in the same tube in which the N_2^+ bands appear is a very significant result for an understanding of the auroral spectrum.

III. Discussion

The most significant characteristic of a nitrogen afterglow, for our present discussion, is the presence in it of molecules in the metastable $A(^3\Sigma)$ state. The reader will be referred to papers on active nitrogen for evidence regard-

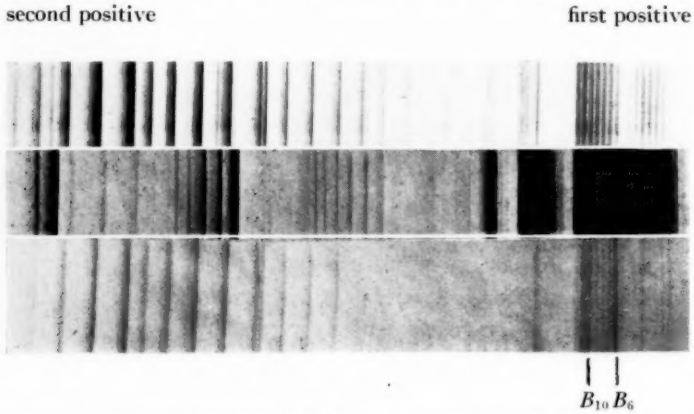

Fig. 1. Spectrum 1, normal excitation of N_2; spectrum 2, excitation in an active nitrogen producing discharge; spectrum 3, enhancement of bands which originate on B_6 and B_{10}.

ing the existence of metastable nitrogen molecules in the afterglow. In auroral displays metastable molecules will accumulate as a result of the excitation processes which are responsible for the aurora. The only mechanism for the destruction of metastable molecules in the upper atmosphere is collision with some other particle, whereas in laboratory discharges there is undoubtedly considerable destruction of metastable molecules at the walls. In a tube in which the afterglow is very strong there is a rapid production of metastable molecules, and hence a comparison between the upper atmosphere and such a tube is a reasonable one.

The excitation of the negative bands in these experiments can be explained in a very simple manner. It is only necessary to postulate that the light, emitted in a discharge in which there is a relatively high concentration of metastable molecules, is due to the direct excitation of these molecules by

[2] Vegard, Nature **129,** 468 (1932). Jevons, Nature **129,** 754 (1932).

electron impact in the discharge rather than to the excitation of normal nitrogen molecules. Thus, a process which in ordinary tubes is a secondary process, and hence very rare, now becomes quite frequent. The present experiment can be presented as a new proof of the existence of metastable molecules in active nitrogen. The metastable nitrogen molecules in the aurora are probably produced in the same way as in an active nitrogen tube; i.e., during the recombination of atomic nitrogen.

The unusual excitation of the levels B_{10} and B_6 in the same tube as the negative bands, but with weaker currents, gives us a very complete reproduction of the nitrogen part of the auroral spectrum. The existence of streamers and curtains in auroral displays, and their rapid motion, are indications of the unsteady nature of the phenomenon, and they may well be due to variations in an electrical current which is responsible for the excitation of the auroral display. That idea would fit in well with the present results.

This hasty account of the present experiments will be extended in the near future. The role of metastable nitrogen molecules will be discussed both for the aurora and for the light of the night sky. As a result of the present work we are tempted to conclude that the auroral display is really an electrical discharge in a nitrogen-oxygen mixture in which metastable molecules abound. There is, however, a better time for such a conclusion, namely, after more experiments have been performed.

Theory of Vibrational Isotope Effects in Polyatomic Molecules

By E. O. SALANT AND JENNY E. ROSENTHAL
New York University

(Received October 28, 1932)

Following Dennison's general, noncentral force treatment of the normal modes of vibration of symmetrical triatomic and tetratomic molecules, we derive expressions for the effects of isotopy on the normal frequencies. The isotope effect of any particular normal frequency depends on and may serve to evaluate the force constants of the molecule, but sums of certain isotope effects are independent of the constants. For triatomic molecules, the isotope effect of the vibration perpendicular to the symmetry axis depends on the value of the apex angle of the molecule. The sum of the isotope effects of the parallel vibrations is calculable from the masses alone. Definite criteria of collinearity of the molecule from isotope effects are given. For tetratomic molecules, the sum of isotope effects of vibrations parallel to the altitude of the molecular pyramid is calculable from the masses alone, the sum of isotope effects perpendicular to the altitude from the masses and from the ratio of the altitude to the length of side of the triangular base. Whereas the molecule YX_3 has four distant normal frequencies of vibration, it is shown that replacement of one of the X atoms of mass m by an atom of mass $m+\Delta m$ removes the degeneracy of the motion, the resulting molecule having six normal frequencies of vibration. Special relations between the various isotope effects serve as criteria for co-planar molecules.

INTRODUCTION

THERE have been few investigations, experimental or theoretical, of isotope effects in band spectra of polyatomic molecules, the most outstanding being the studies of the vibrational effects in the electronic bands of chlorine dioxide, made by Goodeve and Stein[1] and by Urey and Johnston.[2] Besides the interest of the isotope effects themselves, Urey and Johnston showed them to be of value as an aid in the assignment of certain spectral frequencies to particular modes of vibration of the ClO_2 molecule.

This they accomplished by comparing the measured isotope effects with those calculated from their expressions for the effects of isotopy of the Y atoms on the normal vibrations of symmetrical triatomic molecules YX_2; the expressions were derived from equations of Bjerrum[3] for the normal vibrations of symmetrical triatomic molecules, Bjerrum's equations having been based upon the special assumption of valence forces.

It is our purpose here to begin with the more general noncentral force equations of Dennison[4] for the vibrations of polyatomic molecules and to derive therefrom expressions for the isotope effects of the normal frequencies. We shall obtain equations for the effects of isotopy of the Y atoms, and also of the X atoms, in symmetrical triatomic molecules YX_2 and symmetrical

[1] C. F. Goodeve and C. P. Stein, Trans. Faraday Soc. **25**, 736 (1929).
[2] H. C. Urey and H. Johnston, Phys. Rev. **38**, 2131 (1931).
[3] N. Bjerrum, Verh. d. deutsch. phys. Ges. **16**, 737 (1914).
[4] D. M. Dennison, Rev. Mod. Phys. **3**, 280 (1931).

tetratomic molecules YX_3; we have already referred briefly to some of the results of this study.[5] In Dennison's treatment, it may be recalled, knowledge of the quantitative values of the force constants is quite unnecessary to determine the directions of the displacements with respect to the molecular axis of symmetry, the character of the vibrations following from the basic postulate that the potential energy follows the geometrical symmetry of the molecule.

Besides the assumptions of Dennison's theory, we assume also that, as for diatomic molecules, the forces involved are invariant for an isotopic change of mass. We shall denote the mass of the Y atom by M and the mass of an X atom by m and shall call effects due to isotopes of Y atoms "central isotope effects" and effects due to isotopes of X atoms "end isotope effects." We treat the ratios $\Delta m/m$ and $\Delta M/M$ as small, consequently our results do not apply to isotopes of H atoms.

The general method outlined by Dennison for describing the potential energies T and V will be followed, the normal frequencies ω_i being given by the roots λ_i of the determinental equation

$$\left.\begin{aligned} |\lambda T - V| &= 0 \\ 4\pi^2\omega_i^2 &= \lambda_i \end{aligned}\right\}. \qquad \text{and} \qquad \text{(I)}$$

The roots and frequencies of molecules $Y^{(M)}X_2^{(m)}$ and $Y^{(M)}X_3^{(m)}$ will be denoted by λ_i and ω_i, the roots and frequencies of molecules having one or more atoms $Y^{(M+\Delta M)}$ or $X^{(m+\Delta m)}$ will be denoted by λ_i^* and ω_i^*. The isotope shift $\Delta\omega_i$ of the normal frequency of vibration ω_i will then be given by

$$\Delta\omega_i/\omega_i = \tfrac{1}{2}(\lambda_i^*/\lambda_i - 1). \qquad \text{(II)}$$

Since, as has been shown by Dennison,[6] the expressions for the transition probabilities of the normal vibrations involve the masses, an isotopic change of mass will affect the Einstein coefficients as well as the frequencies. We regard such effects as small, however, and certainly inextricable from the tangle of polyatomic band lines.

The relative intensities of bands due to the same vibration in molecules differing only in their isotopes will, of course, be determined principally by the relative abundance of the isotopes. Relative abundance of molecules $Y^{(M)}X_n$ and $Y^{(M+\Delta M)}X_n$ will be the same as the relative abundance of the isotopes of the Y atoms. Relative abundances in the cases of isotopes of X atoms are, if the relative abundance of $X^{(m)}$ to $X^{(m+\Delta m)}$ is b/a

$$YX_2^{(m)}:YX^{(m)}X^{(m+\Delta m)}:YX_2^{(m+\Delta m)} = 1:b/a:b^2/a^2$$

$$YX_3^{(m)}:YX_2^{(m)}X^{(m+\Delta m)}:YX^{(m)}X_2^{(m+\Delta m)}:YX_3^{(m+\Delta m)} = 1:b/a:b^2/a^2:b^3/a^3.$$

I. Triatomic Molecules

We consider a molecule composed of three particles denoted 1, 2, 3, forming at equilibrium the corners of an isosceles triangle of apex angle 2α and

[5] E. O. Salant and J. E. Rosenthal, Phys. Rev. **39**, 161 (1932).

[6] D. M. Dennison, Phil. Mag. **1**, 195 (1926).

base $2a$, with particle 1 at the apex. Let q_1 be the change in relative displacement of the base particles 2 and 3, q_2 and q_3 the changes in relative displacements of the particles 1 and 2 and of the particles 2 and 3, respectively. The potential energy is then written:

$$V = \tfrac{1}{2}[K_1(q_2^2 + q_3^2) + K_2 q_1^2 + K_3 q_1(q_2 + q_3) + K_4 q_2 q_3] \tag{1}$$

where K_1, K_2, K_3, K_4 are constants (which may involve the angle).

We choose moving coordinates x, y with origin at the center of gravity of the molecule, and x-axis parallel to the direction $2\rightarrow 3$, and define new variables q_1, u, v in this system (q_1 unchanged):

$$\left.\begin{aligned} q_1 &= \delta x_3 - \delta x_2 \\ u &= \delta x_1 - \tfrac{1}{2}(\delta x_2 + \delta x_3) = (q_3 - q_2)/2 \sin\alpha \\ v &= \delta y_1 - \tfrac{1}{2}(\delta y_2 + \delta y_3) = (q_2 + q_3 - q_1 \sin\alpha)/2 \cos\alpha \end{aligned}\right\} \tag{2}$$

δx_j and δy_j obviously referring to the displacements of the j-th particle. In these variables, the potential energy becomes

$$\left.\begin{aligned} & V = \tfrac{1}{2}(Aq_1^2 + Bu^2 + Cv^2 + 2Dvq_1), \\ \text{where}\quad & A = (K_1/2)\sin^2\alpha + K_2 + K_3 \sin^2\alpha + (K_4/4)\sin^2\alpha \\ & B = (2K_1 - K_4)\sin^2\alpha \\ & C = (2K_1 + K_4)\cos^2\alpha \quad [7] \\ & D = (K_1 + K_3/\sin\alpha + K_4/2)\sin\alpha\cos\alpha \end{aligned}\right\}. \tag{3}$$

To obtain the expression for the kinetic energy of the vibrating molecule, we first transform to a fixed coordinate system X, Y in the same plane and with the same origin as the moving system,

$$X = x + \theta y; \quad Y = -\theta x + y$$

where θ denotes a small angle in the X, Y plane.

For the molecule $YX^{(m)}X^{(m+\Delta m)}$, let the Y atom be particle 1, $X^{(m+\Delta m)}$ particle 2, $X^{(m)}$ particle 3. Let

$$\mu = \frac{M}{2m + M}, \quad \mu^* = \frac{M}{2(m + \Delta m) + M}, \quad \rho = \frac{M}{2m + \Delta m + M}.$$

Then the transformation from Eq. (2) to the fixed coordinates and the expressions for the conservation of linear momentum lead to the following relations for the displacements δX_j, δY_j in the fixed system:

[7] It is assumed that when $\cos\alpha = 0$; $C \neq 0$; hence $(2K_1 + K_4)$ involves α.

$$\left.\begin{aligned}
\delta X_1 &= \left(\frac{2m+\Delta m}{M}\right)\rho(u + a\theta\cot\alpha) + \frac{\Delta m\rho}{2M}\,q_1; \\
\delta Y_1 &= \left(\frac{2m+\Delta m}{M}\right)\rho v - \frac{\Delta m\rho}{M}\,a\theta \\
\delta X_2 &= -\rho(u + a\theta\cot\alpha) - \frac{q_1}{2}\,\frac{\rho}{\mu}; \quad \delta Y_2 = -\rho v + \alpha\theta\frac{\rho}{\mu} \\
\delta X_3 &= -\rho(u + a\theta\cot\alpha) + \frac{q_1}{2}\,\frac{\rho}{\mu^*}; \quad \delta Y_3 = -\rho v + \frac{a\theta\rho}{\mu^*}
\end{aligned}\right\}. \tag{4}$$

Writing down the expression for the kinetic energy and substituting for $\dot{\theta}$ its value obtained from the condition $\partial T/\partial\dot{\theta}=0$ (conservation of angular momentum), we may then write the kinetic energy letting $\epsilon=\Delta m/(2m+\Delta m)$

$$T = \left(\frac{2m+\Delta m}{4}\right)\left[2\rho(\dot{u}^2+\dot{v}^2) + \dot{q}_1^2 + 2\rho\epsilon\dot{u}\dot{q}_1 - \frac{2\rho^2}{1+\rho\cot^2\alpha}\left(\dot{u}\cot\alpha + \frac{\epsilon\dot{q}_1}{2}\cot\alpha - \epsilon\dot{v}\right)^2\right]. \tag{5}$$

Neglecting all terms in ϵ^2, none of whose coefficients are large, we then have

$$T = \left(\frac{2m+\Delta m}{4}\right)\left[2\rho\left(\frac{\dot{u}^2}{1+\rho\cot^2\alpha} + \dot{v}^2\right) + \frac{\dot{q}_1^2}{2} + \frac{2\rho\dot{u}\epsilon}{1+\rho\cot^2\alpha}(\dot{q}_1 - 2\rho\dot{v}\cot\alpha)\right]. \tag{6}$$

From Eq. (I), (3) and (6), the vibrations λ_1^*, λ_2^*, parallel to the symmetry axis of the molecule, and the vibration λ_3^* perpendicular to the symmetry axis, are given by

$$\left.\begin{aligned}
&\left(\frac{2m+\Delta m}{2}\right)^2\lambda^{*2} - \left(2A + \frac{C}{2\rho}\right)\left(\frac{2m+\Delta m}{2}\right)\lambda^* \\
&\qquad + \frac{1}{\rho}\left(AC - \frac{D^2}{4}\right) = 0 \qquad \text{(a)} \\
&\lambda_3^* = \frac{B(1/\rho + \cot^2\alpha)}{2m+\Delta m} \qquad \text{(b)}
\end{aligned}\right\}. \tag{7}$$

By setting $\Delta m=0$, Eqs. (7) reduce to the known expressions for the normal frequencies of the molecule YX_2[(m)]

$$\left.\begin{aligned}
m^2\lambda^2 - (2A + C/2\mu)m\lambda + (1/\mu)(AC - D^2/4) = 0 \quad \text{(a)} \\
\lambda_3 = B(1/\mu + \cot^2\alpha)/2m \quad \text{(b)}
\end{aligned}\right\}. \tag{8}$$

For a collinear molecule, $D=0$ and $\cot\alpha=0$, Eqs. (7) reducing to

$$\left.\begin{aligned} \lambda_1^* &= \frac{4A}{(2m+\Delta m)}\,;\ \lambda_2^* = \frac{C}{\rho(2m+\Delta m)} && \text{(a)} \\ \lambda_3^* &= B/(2m+\Delta m)\rho && \text{(b)} \end{aligned}\right\}. \tag{7'}$$

(a) Central isotope effects, molecules $Y^{(M)}X_2^{(m)}$ and $Y^{(M+\Delta M)}X_2^{(m)}$

The vibrations of molecules $Y^{(M+\Delta M)}X_2^{(m)}$ will be described by relations obtained by substituting $M+\Delta M$ for M in Eqs. (8). With these equations and with Eqs. (I), (II), and (8), we have the following relations for central isotope effects:

$$\frac{\Delta\omega_1}{\omega_1} = \frac{(8\pi^2 m\mu\omega_2^2 - C)\Delta M}{8\pi^2(\omega_1^2-\omega_2^2)M^2} \tag{9}$$

$$\omega_1\Delta\omega_1 + \omega_2\Delta\omega_2 = -C\Delta M/8\pi^2 M(M+\Delta M) \tag{10}$$

$$\frac{\Delta\omega_1}{\omega_1} + \frac{\Delta\omega_2}{\omega_2} = \frac{-m\Delta M}{(M+\Delta M)(2m+M)} \tag{11}$$

$$\frac{\Delta\omega_3}{\omega_3} = \frac{-m\Delta M}{M(M+\Delta M)(1/\mu+\cot^2\alpha)}\,. \tag{12}$$

Thus, whereas the isotope effect $\Delta\omega_1/\omega_1$ or $\Delta\omega_2/\omega_2$ of either parallel vibration depends on the force constants of the molecule and may have different values in the different electronic states, their sum has a constant value, calculable from the masses alone, for all electronic states. Obviously this relation, Eq. (11), provides a means of assigning bands to particular modes of vibration.

The isotope effect of the perpendicular vibration, $\Delta\omega_3/\omega_3$, may be used to evaluate the molecular angle 2α; before this can be done, however, it must be known that the frequency being so used is actually the perpendicular frequency, information which will have to come from other data, such as intensities.

For a collinear molecule ($2\alpha=180°$, $D=0$), we have

$$\left.\begin{aligned} \Delta\omega_1 &= 0 \\ \frac{\Delta\omega_2}{\omega_2} &= \frac{\Delta\omega_3}{\omega_3} = \frac{-m\Delta M}{(M+\Delta M)(2m+M)} \end{aligned}\right\} \tag{13}$$

a relation that may be used to determine whether or not a given molecule is collinear.

Since change in electronic state may be accompanied by change in the molecular angle, it is of interest to consider how this will affect the isotope effects. Consider $\Delta M>0$. When the molecule is collinear, the inactive frequency ω_1 shows no isotope effect, the isotope effect $\Delta\omega/\omega$ of each active frequency is the same and negative. As the molecule bends away from a straight line, the perpendicular isotope effect takes on smaller absolute values, ap-

proaching zero as the equilibrium positions of the two X atoms approach each other. The absolute value $|\Delta\omega_1/\omega_1|$ increases, but without knowledge of the force constants, it cannot be predicted whether $\Delta\omega_1/\omega_1$ will be positive or negative; the change in $\Delta\omega_1/\omega_1$ will be in the opposite direction to the change in $\Delta\omega_2/\omega_2$, of course, in virtue of (11) and (13).

TABLE I. *Triatomic molecules.* Calculated values of some central isotope effects.

2α	ClO_2	MgI_2	SO_2	H_2S
	$m=16$	127	16	1
	$M=35$	24	32	32
	$\Delta M=2$	1	1	1
	$10^2(\Delta\omega_1/\omega_1+\Delta\omega_2/\omega_2)$ -1.293	-1.82	-0.76	-0.089
180°	$10^2(\Delta\omega_3/\omega_3)$ -1.293	-1.82	-0.76	-0.089
150°	" -1.245	-1.81	-0.73	-0.083
120°	" -1.01	-1.77	-0.65	-0.068
90°	" -0.849	-1.68	-0.51	-0.046
60°	" -0.502	-1.43	-0.30	-0.023

In Table I are some values of $\Delta\omega_3/\omega_3$ as a function of the molecular angle, calculated for several different molecules, and also values of $\Delta\omega_1/\omega_1+\Delta\omega_2/\omega_2$ for the same molecules. For $2\alpha=180°$, Eq. (13) holds.

A relatively heavy end (X) atom renders the perpendicular isotope effect comparatively insensitive to changes in the molecular angle, as may be seen by comparing the values of this effect for MgI_2 and any of the other molecules in the table. Consequently, the isotope effect will not be so reliable in following changes in the angle of molecules with a large m/M.

(b) End isotope effects

The isotope effects for molecules $Y^{(M)}X_2^{(m)}$ and $Y^{(M)}X^{(m)}X^{(m+\Delta m)}$ are easily obtained from Eqs. (I), (II), (7) and (8). Each parallel effect $\Delta\omega_1/\omega_1$ and $\Delta\omega_2/\omega_2$ depends on the force constants, but the sum of the parallel effects is independent of the interatomic forces:

$$\frac{\Delta\omega_1}{\omega_1}+\frac{\Delta\omega_2}{\omega_2}=\frac{-(\mu+1)\Delta m}{2(2m+\Delta m)}. \tag{14}$$

The perpendicular isotope effect depends upon the molecular angle:

$$\frac{\Delta\omega_3}{\omega_3}=\frac{-(1+\cot^2\alpha)\Delta m}{2(1/\mu+\cot^2\alpha)(2m+\Delta m)}. \tag{15}$$

For a collinear molecule

$$\mu\frac{\Delta\omega_1}{\omega_1}=\frac{\Delta\omega_2}{\omega_2}=\frac{\Delta\omega_3}{\omega_3}=\frac{-\mu\Delta m}{2(2m+\Delta m)}. \tag{16}$$

In Table II are calculated values of the perpendicular isotope effect for a few molecules and several angles.

It is seen that, contrary to the behavior of the central isotope effect, the end isotope effect of the perpendicular vibration increases as the angle di-

TABLE II. *Calculated values of perpendicular end isotope effects.*

2α, degrees	$10^3(\Delta\omega_3/\omega_3)$ 180	120	90	60	0
$CS_2^{(32)}$, $CS^{(32)}S^{(33)}$	−0.121	−0.154	−0.210	−0.340	−0.769
$MgCl_2^{(35)}$, $MgCl^{(35)}Cl^{(37)}$	−0.354	−0.436	−0.565	−0.802	−1.40
$HgCl_2^{(35)}$, $HgCl^{(35)}Cl^{(37)}$	−1.01	−1.08	−1.17	−1.27	−1.40

minishes, attaining its maximum value, for $\alpha=0$ of

$$(\Delta\omega_3/\omega_3)_{\max.} = -\Delta m/2(2m+\Delta m).$$

The observation of the perpendicular isotope effect will be favored by a molecule with a small angle and heavy central atom.

By replacing m by $m+\Delta m$ in Eqs. (8), the normal vibrations of molecules $Y^{(M)}X_2^{(m+\Delta m)}$ are obtained. The isotope effects $\Delta\omega_i/\omega_i$ between these molecules and molecules $Y^{(M)}X_2^{(m)}$ are, to the first approximation, twice the value of the corresponding effects between molecules $Y^{(M)}X^{(m)}X^{(m+\Delta m)}$ and $Y^{(M)}X_2^{(m)}$.

II. TETRATOMIC MOLECULES

We consider a molecule composed of four atoms occupying, at equilibrium the corners of a regular pyramid of altitude c and length of side of triangular base a. We consider the Y atom, of mass M, at the apex, and denote its positions by subscript 4; we consider atoms X^*, X, X, with masses $m+\Delta m$, m, m, at the base, denoting their positions by subscripts 1, 2, 3, respectively.

Let p_1, p_2, p_3, q_1, q_2, q_3 be the changes in relative displacements of the respective particles, assumed small quantities of the first order, and write $f=(c^2+a^2/3)^{1/2}$. Then, assuming that the potential energy has the geometrical configuration of the system, we have

$$\begin{aligned} V = \tfrac{1}{2}\{ & K_1(q_1^2+q_2^2+q_3^2) + K_2(q_1q_2+q_1q_3+q_2q_3) + K_3(f^2/a^2)(p_1^2+p_2^2 \\ & + p_3^2) + K_4(f^2/a^2)(p_1p_2+p_1p_3+p_2p_3) + K_5(f/a)(p_1q_1+p_2q_2 \\ & + p_3q_3) + K_6(f/a)[p_1(q_2+q_3)+p_2(q_1+q_3)+p_3(q_1+q_2)]\} \end{aligned} \tag{17}$$

where the K's are undetermined constants.

We now choose a system of axes, x, y, z with origin at the molecular center of mass and moving with the molecule, with x axis parallel to the 2–3 axis and x, y plane parallel to the 1, 2, 3 plane.

Then let

$$\left.\begin{array}{l} \delta x_4 - \tfrac{1}{3}(\delta x_1+\delta x_2+\delta x_3) = x;\ \delta x_1 - \tfrac{1}{2}(\delta x_2+\delta x_3) = u;\ \delta x_3 - \delta x_2 = q_1 \\ \delta y_4 - \tfrac{1}{3}(\delta y_1+\delta y_2+\delta y_3) = y;\ \delta y_1 - \tfrac{1}{2}(\delta y_2+\delta y_3) = v;\ \delta y_3 - \delta y_2 = 0 \\ \delta z_4 - \tfrac{1}{3}(\delta z_1+\delta z_2+\delta z_3) = z;\ \delta z_1 - \tfrac{1}{2}(\delta z_2+\delta z_3) = 0;\ \delta z_3 - \delta z_2 = 0 \end{array}\right\} \tag{18}$$

and at equilibrium, we have

$$\left.\begin{array}{l} x_4^0 - \tfrac{1}{3}(x_3^0+x_2^0+x_1^0) = 0;\ x_1^0 - \tfrac{1}{2}(x_2^0+x_3^0) = 0;\ x_3^0 - x_2^0 = a \\ y_4^0 - \tfrac{1}{3}(y_3^0+y_2^0+y_1^0) = 0;\ y_1^0 - \tfrac{1}{2}(y_2^0+y_3^0) = a(3)^{1/2}/2; \\ y_3^0 - y_2^0 = 0 \\ z_4^0 - \tfrac{1}{3}(z_3^0+z_2^0+z_1^0) = c;\quad z_1^0 - \tfrac{1}{2}(z_2^0+z_3^0) = 0;\quad z_3^0 - z_2^0 = 0 \end{array}\right\} \tag{19}$$

where, of course, the superscript zero refers to the equilibrium positions. Then writing:

$$A = \tfrac{1}{2}(K_3 - K_4/2)$$
$$B = 3(c^2/a^2)(K_3 + K_4)\ ^{8}$$
$$C = \tfrac{1}{4}\left(3K_1 + \frac{3}{2}K_2 + \frac{K_3}{3} + \frac{K_4}{6} + \frac{K_5}{3} + \frac{5K_6}{3}\right)$$
$$D = \tfrac{1}{2}\left(K_1 - \frac{K_2}{2} + \frac{K_3}{9} - \frac{K_4}{18} - \frac{K_5}{3} - \frac{K_6}{3}\right)$$
$$E = \frac{K_3}{6} - \frac{K_4}{12} - \frac{K_5}{4} + \frac{K_6}{4}$$
$$F = (c/a)3^{-1/2}(K_3 + K_4 + (3/2)K_5 + 3K_6)$$

the potential energy in these variables become

$$\begin{aligned} V = \tfrac{1}{2}\{&A(x^2 + y^2) + Bz^2 + (3/2)Cq_1^2 + Du^2 + 2Cv^2 \\ &+ 2[E\{ux + (3^{1/2}/2)yq_1 - yv) \\ &+ Fz((3^{1/2}/2)q_1 + v) + 3^{1/2}(C - D)vq_1]\}. \end{aligned} \tag{20}$$

To obtain the kinetic energy, we first refer to fixed axes X, Y, Z, with same origin as the x, y, z system, and connected by:

$$X = x + \psi y + \theta z; \quad Y = -\psi x + y + \phi z; \quad Z = -\theta x - \phi y + z \tag{21}$$

where ψ, θ, ϕ, are cosines of (X, y), (X, z), and (Y, z), respectively, and the rotation in space is understood to be small.

Neglecting small quantities of the second order, we have

$$\delta X_j = \delta x_j + \psi y_j^0 + \theta z_j^0$$
$$\delta Y_j = -\psi x_j^0 + \delta y_j + \phi z_j^0$$
$$\delta Z_j = -\theta x_j^0 - \phi y_j^0 + \delta z_j.$$

With these relations and Eqs. (18) and (19) and applying the condition for conservation of linear momentum, the kinetic energy becomes

$$\begin{aligned} T = \tfrac{1}{2}\left(m + \frac{\Delta m}{3}\right)\Big\{&3\rho(\dot{x}^2 + \dot{y}^2 + \dot{z}^2) + \tfrac{2}{3}(1 + \epsilon)(\dot{u}^2 + \dot{v}^2) + \tfrac{1}{2}(1 - \epsilon)\dot{q}_1^2 \\ &- 4\rho\epsilon(\dot{u}\dot{x} + \dot{v}\dot{y}) + (\beta - \epsilon)\frac{a^2}{2}\dot{\theta}^2 + \frac{a^2}{2}(\beta + \epsilon)\dot{\phi}^2 + a^2\dot{\psi}^2 \\ &+ 2\dot{\theta}c\rho(3\dot{x} - 2\epsilon\dot{u}) + 2\dot{\phi}c\rho\left(3\dot{y} - 2\epsilon\dot{v} + 3^{1/2}\epsilon\frac{a}{c}\dot{z}\right) \\ &+ 2\dot{\psi}a\left[-\rho\epsilon(3^{1/2})\dot{x} + \left(\frac{1 + \epsilon}{3^{1/2}}\right)\dot{u}\right] - 2\rho(3^{1/2})ac\epsilon\dot{\psi}\dot{\theta}\Big\} \end{aligned} \tag{22}$$

[8] It is assumed that for $c=0$, $B\neq 0$.

where

$$\left.\begin{aligned} \mu &= \frac{M}{3m+M}, \quad \rho = \frac{M}{3m+\Delta m+M}, \quad \epsilon = \frac{\Delta M}{3m+\Delta m} \\ b &= 6\mu(c^2/a^2)+1, \ \beta = 6\rho(c^2/a^2)+1 \end{aligned}\right\}. \tag{23}$$

From the conservation of angular momentum

$$(\partial T/\partial\dot{\phi} = 0, \ \partial T/\partial\dot{\theta} = 0, \ \partial T/\partial\dot{\psi} = 0)$$

and dropping terms in ϵ^2, we have

$$\begin{aligned} T = \tfrac{1}{2}\left(m+\frac{\Delta m}{3}\right)\Bigg\{ & \frac{3\rho}{\beta}\left[1-\epsilon\left(1-\frac{1}{\beta}\right)\right]\dot{x}^2 + \frac{3\rho}{\beta}\left[1+\epsilon\left(1-\frac{1}{\beta}\right)\right]\dot{y}^2 \\ & + 3\rho\dot{z}^2 + \tfrac{1}{2}(1-\epsilon)\dot{q}_1^2 + \tfrac{1}{3}\dot{u}^2 + \tfrac{2}{3}(1+\epsilon)\dot{v}^2 \\ & - 2\rho\frac{\epsilon}{\beta}\left(\dot{u}\dot{x} + 2\dot{y}\dot{v} + 6\rho\frac{c}{a}(3^{1/2})\dot{y}\dot{z}\right)\Bigg\}. \end{aligned} \tag{24}$$

Eqs. (I), (20), and (24) then yield the following equations for the vibrations of the molecule $Y^{(M)}X_2^{(m)}X^{(m+\Delta m)}$:

$$\left(m+\frac{\Delta m}{3}\right)^2\lambda^{*2} - \left(m+\frac{\Delta m}{3}\right)\left(\frac{B}{3\rho}+6C-3D\right)\lambda^* + \frac{2BC-BD-F^2}{\rho} = 0 \tag{25}$$

$$\left(m+\frac{\Delta m}{3}\right)^2\lambda^{*2} - \left(m+\frac{\Delta m}{3}\right)\left\{\frac{\beta A\left[1-\epsilon(1-1/\beta)\right]}{3\rho}+3D-2\epsilon E\right\}\lambda^* + \frac{\beta}{\rho}(AD-E^2)\left[1-\epsilon(1-1/\beta)\right] = 0 \tag{26}$$

$$\left(m+\frac{\Delta m}{3}\right)^2\lambda^{*2} - \left(m+\frac{\Delta m}{3}\right)\left\{\frac{\beta A\left[1+\epsilon(1-1/\beta)\right]}{3\rho}+3D+2\epsilon E\right\}\lambda^* + \frac{\beta}{\rho}(AD-E^2)\left[1+\epsilon(1-1/\beta)\right] = 0. \tag{27}$$

We denote the roots of (25) by λ_1^*, λ_3^*, of (26) by λ_2^*, λ_4^* of (27) by λ_5^*, λ_6^*. Each of the roots is distinct, so that the molecule $Y^{(M)}X_2^{(m)}X^{(m+\Delta m)}$ has six normal frequencies of vibration. By setting $\Delta m = 0$, these equations reduce to those of the molecule $Y^{(M)}X_3^{(m)}$, Eq. (25) becoming

$$m^2\lambda^2 - m(B/3\mu+6C-3D)\lambda + (2BC-BD-F^2)/\mu = 0 \tag{28}$$

and Eqs. (26) and (27) giving

$$\left[m^2\lambda^2 - m(bA/3\mu+3D)\lambda + (b/\mu)(AD-E^2)\right]^2 = 0. \tag{29}$$

Dennison has shown that the vibrations represented by (28) are parallel to the altitude c of the molecular pyramid, that the vibrations represented

by (29) are perpendicular to the altitude and that whereas the perpendicular vibrations are four in number, only two are distinct, or, calling the roots of (29) $\lambda_2, \lambda_5, \lambda_4, \lambda_6$, then

$$\lambda_2 = \lambda_5, \ \lambda_4 = \lambda_6 \tag{30}$$

the molecule $Y^{(M)}X_3^{(m)}$ having four distinct normal frequencies of vibration. Thus the substitution of an atom of mass $(m+\Delta m)$ for one of the base atoms of mass m removes the degeneracy of the parallel mode of vibration, and a gas composed of molecules of $Y^{(M)}X_3^{(m)}$ and $Y^{(M)}X_2^{(m)}X^{(m+\Delta m)}$ will show ten fundamental infrared bands (disregarding, of course, the possibility of one or more being inactive in absorption).

Just as in the triatomic case, any particular isotope shift $\Delta\omega_i/\omega_i$ can be calculated only if the force constants are known, but the sum of the relative isotope effects of the parallel frequencies can be calculated from the masses alone, and the sum of the isotope effects of the perpendicular frequencies from the masses and the ratio of the altitude to the length of side of the base. As it must now be obvious, from the triatomic case, how each individual $\Delta\omega_i/\omega_i$ may be written down, merely by applying Eq. (II), we shall not state these, but shall state only the more interesting and useful expressions for the sums of isotope effects.

(a) Central isotope effects, molecules $Y^{(M)}X_3^{(m)}$ and $Y^{(M+\Delta M)}X_3^{(m)}$

These relationships apply to molecules such as $Cl^{(35)}O_3$ and $Cl^{(37)}O_3$, $B^{(10)}I_3$ and $B^{(11)}I_3$.

The normal vibrations of molecules $Y^{(M+\Delta M)}X_3^{(m)}$ are obtained simply by substituting $M+\Delta M$ for M in Eqs. (28) and (29). Then for the parallel vibrations we have

$$\frac{\Delta\omega_1}{\omega_1} + \frac{\Delta\omega_3}{\omega_3} = \frac{(\mu - 1)\Delta M}{2(M + \Delta M)} \tag{31}$$

and for the perpendicular vibrations:

$$\frac{\Delta\omega_2}{\omega_2} + \frac{\Delta\omega_4}{\omega_4} = \frac{(\mu - 1)\Delta M}{2b(M + \Delta M)}. \tag{32}$$

For a co-planar molecule, that is, for one where $c=0$, $b=1$ and hence

$$\frac{\Delta\omega_1}{\omega_1} + \frac{\Delta\omega_3}{\omega_3} = \frac{\Delta\omega_2}{\omega_2} + \frac{\Delta\omega_4}{\omega_4} = \frac{(\mu - 1)\Delta M}{2(M + \Delta M)}. \tag{33}$$

(b) End isotope effects, molecules $Y^{(M)}X_3^{(m)}$ and $Y^{(M)}X_2^{(m)}X^{(m+\Delta m)}$

These relationships apply to molecules such as $PCl_3^{(35)}$ and $PCl_2^{(35)}Cl^{(37)}$. From Eqs. (II), (25) and (28) we get, for the parallel vibrations

$$\frac{\Delta\omega_1}{\omega_1} + \frac{\Delta\omega_3}{\omega_3} = -\frac{(\mu + 1)\Delta m}{2(3m + \Delta m)} \backsimeq -\frac{(\mu + 1)\Delta m}{6m}. \tag{34}$$

From (II), (26), (27) and (29) the isotope effects of the perpendicular vibrations are related by:

$$\frac{\Delta\omega_2}{\omega_2}+\frac{\Delta\omega_4}{\omega_4}=-\frac{\Delta m}{6m}\left(\frac{\mu-2}{b}+3\right) \tag{35}$$

$$\frac{\Delta\omega_5}{\omega_5}+\frac{\Delta\omega_6}{\omega_6}=-\frac{\Delta m}{6m}\left(\frac{\mu}{b}+1\right) \tag{36}$$

where, it must be recalled, $\omega_2=\omega_5$, $\omega_4=\omega_6$, but

$$\Delta\omega_2\neq\Delta\omega_5 \text{ and } \Delta\omega_4\neq\Delta\omega_6.$$

For co-planar molecules, $b=1$ and hence

$$\frac{\Delta\omega_1}{\omega_1}+\frac{\Delta\omega_3}{\omega_3}=\frac{\Delta\omega_2}{\omega_2}+\frac{\Delta\omega_4}{\omega_4}=\frac{\Delta\omega_5}{\omega_5}+\frac{\Delta\omega_6}{\omega_6}=-\frac{(\mu+1)\Delta m}{6m}. \tag{37}$$

To the first order, the isotope effects of $Y^{(M)}X^{(m)}X_2^{(m+\Delta m)}$ are approximately twice the corresponding effects of $Y^{(M)}X_2^{(m)}X^{(m+\Delta m)}$ and isotope effects of $Y^{(M)}X_3^{(m+\Delta m)}$ approximately three times the corresponding effects of the latter.

It is hoped that the above relations for isotope effects may be of use in the analysis of bands of tetratomic molecules.

It may be superfluous to emphasize that the expressions here refer to the frequencies of small vibration and not *exactly* to the (0, 1) bands, but it is expected that the difference in those values may be neglected and our results applied to the (0, 1) bands themselves.

We take this opportunity of thanking Professor D. M. Dennison of the University of Michigan for his interest and advice in this work. This work was begun while one of us (J.E.R.) was a National Research Fellow.

On Radiation Diffusion and the Rapidity of Escape of Resonance Radiation from a Gas

By CARL KENTY
General Electric Vapor Lamp Company, Hoboken, N. J.

(Received August 25, 1932)

The radiation diffusion process is considered from the standpoint of the free paths of the diffusing resonance quanta as influenced by the Doppler and other line broadening effects. Abnormally long free paths are found to be of such importance as to enable resonance radiation to escape from a body of gas faster than has usually been supposed. It is assumed that a large concentration of diffusing resonance quanta will, on the basis of Doppler broadening only, give rise to a characteristic excitation of atoms, as dependent on their speeds, which can be represented by a distribution function which will lie between two limiting distribution functions, namely (1) Maxwell's distribution function and (2) a distribution function expressing a lower relative excitation of the high speed atoms than that of Maxwell, based on the excitation of all atoms as if by absorption of the core of the line. On the basis of (1) and (2), limiting expressions are derived for: (a) the fraction of emitted quanta traversing at least a given distance before absorption, (b) the diffusion coefficient, (c) the average square free path, (d) the average free path. A fundamental difference between radiation diffusion and molecular diffusion appears in that whereas (a) decreases exponentially with the distance in the latter case it is found to decrease only linearly (roughly) with the distance in the former case. For this reason very long free paths are found to be of relatively great importance in radiation diffusion. It is found that, for a gas container of infinite size, (b), (c), and (d) are all infinite. For a gas container of finite size, estimates of the order of magnitude of the apparent or effective values of (b), (c), and (d) are made on the basis of special assumptions. It is found that (b) $=(\frac{1}{6})\overline{p^2}/\tau$ where $\overline{p^2}$ is the average square free path and τ is the mean life of the excited atom. The same formula is found to hold for the coefficient of molecular diffusion if $\overline{p^2}$ is used to denote the average square molecular free path and τ is used to represent the mean time between collisions. It is pointed out that coupling and other line broadening effects will still further increase the importance of extremely long free paths and hence also the rapidity of escape of resonance radiation from a gas. The results of the Hg resonance radiation imprisonment experiments of Zemansky and of Webb and Messenger are discussed and are shown to be in accord with the conclusions arrived at above that resonance radiation escapes from a gas faster than according to classical theories of radiation diffusion, the effect being the greater the larger the gas volume or density. The rapidity of escape of $\lambda 2537$ at the lower gas densities ($N=10^{15}$ cm^{-3} or less) in these experiments can be largely accounted for by the Doppler effect on the basis of a diffusion coefficient proportional to the effective average square free path as calculated by the methods of the present paper; at the higher gas densities ($N=30\times10^{15}$ cm^{-3}) the escape is more rapid than can be accounted for by these methods and this is attributed to coupling or other pressure broadening.

I. INTRODUCTION

THE THEORY of resonance radiation imprisonment and diffusion was first worked out by K. T. Compton[1] on the basis of analogy with mole-

[1] K. T. Compton, Phys. Rev. **20**, 283 (1922); Phil. Mag. **45**, 752 (1923). See also R. W. Wood, Phil. Mag. **23**, 689 (1912).

cular diffusion. Milne[2] later, using Einstein's theory of radiation, arrived at a very general theory of the passage of resonance radiation through a gas.[3] He developed an equation describing this process which at appreciable gas densities, such as are usually met with in practice, reduces to the standard diffusion equation of Compton (except for a slight difference in the numerical factor appearing in the expression for the diffusion coefficient). At very low gas densities, however, where the radiation has a considerable chance of escaping completely from the gas without absorption (mean free path of the radiation greater than the dimensions of the gas container), and where, therefore, diffusion in the usual sense of the term can no longer be thought of, Milne's equation is still applicable, by virtue of an additional term appearing in it, and expresses the fact that the radiation cannot escape from the body of gas faster than according to the exponential constant $1/\tau$ where τ is the mean life of the excited (resonance) state of the atom.

The expression for the diffusion coefficient appearing in these theories is[4] $1/(3\alpha^2\tau)$ where α is the absorption coefficient of the gas for the resonance radiation. Since because of the Doppler effect or other causes of line broadening a resonance quantum may be absorbed at one frequency by an atom and given out at another,[5] the question arises as to what value of α should be used in this expression. Compton (in effect) and Milne have assumed an average value of α taken over the breadth of the line (the breadth of the line in emission being taken to be the same as that in absorption) and treated the diffusing resonance quanta as if they had at all times a frequency corresponding to this average value of α. Zemansky[5] pointed out that, where the line breadth is greater than given by the Doppler effect, as is found to be the case at appreciable gas densities, the diffusion process is probably more complicated; he was, however, led to believe from his experiments in mercury vapor that the resonance radiation diffused as a whole through the gas with a "mean or equivalent" absorption coefficient the numerical value of which was to be found by experiment. According to his measurements, the atomic absorption coefficient calculated from this mean or equivalent absorption coefficient decreased greatly with increasing vapor density (see below). Essentially similar results were obtained by Webb and Messenger[6] who ascribed the lessening of the apparent atomic absorption coefficient at higher vapor densities to line broadening caused by absorption or other effects.

Later the writer,[7] and Langmuir and Found[8] have carried out experiments which indicate that in Ne at a pressure of the order of 1 mm the mean free paths of the scattered resonance radiations are much greater than those

[2] E. A. Milne, Jour. Lond. Math. Soc. **1**, 40 (1926).

[3] A number of applications of Milne's theory have been made by M. W. Zemansky, Phys. Rev. **36**, 919 (1930) and a number of preceding papers.

[4] In Milne's theory the numerical factor is $\frac{1}{4}$ instead of $\frac{1}{3}$.

[5] M. W. Zemansky, Phys. Rev. **29**, 513 (1927); see p. 521.

[6] H. W. Webb and Helen A. Messenger, Phys. Rev. **33**, 319 (1929). See particularly p. 325.

[7] Carl Kenty, Phys. Rev. **40**, 633L (1932). A more complete account of these experiments will be given in a later paper.

[8] I. Langmuir and Clifton G. Found, unpublished work.

usually thought of for resonance lines[9] at such gas pressures. The cause of these abnormally long mean free paths has been tentatively attributed to Holtsmark coupling broadening[10] of the resonance lines or to broadening caused by the formation of loosely bound molecules.[11] That there is probably some cause of broadening of these lines more important than the Doppler effect, in the case of Ne at pressures of the order of 1 mm, appears from heating experiments to be described in a later paper. But even at low gas densities where the Doppler effect is known to be the main cause of broadening closer scrutiny of the diffusion process* has revealed that very abnormally long free paths will be developed by this process and that under certain circumstances these will be of great importance in aiding the escape of resonance radiation from a gas.[12]

II. An Attempt to Calculate More Accurately the Diffusion Coefficient

Let it be assumed that the only cause of line broadening in the case to be considered is the Doppler effect. Then in Fig. 1 suppose that a quantum of

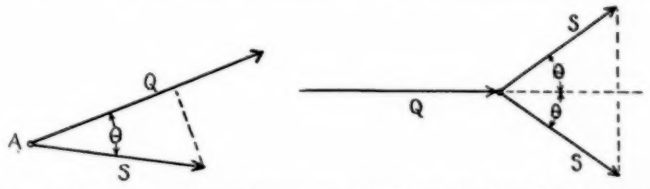

Fig. 1. S: direction of motion of emitting atom. Q: direction of emitted radiation quantum.
Fig. 2. Q: direction of radiation quantum; S: direction of absorbing atoms.

resonance radiation is emitted at A by an atom of speed S in a direction making an angle between θ and $\theta+d\theta$ with the direction of S. The component of S in the direction of the quantum is $S\cos\theta$. We desire to calculate first the absorption coefficient α of the gas for such a quantum (or for such quanta). In order to be capable of absorbing such a quantum, an atom must have a component of velocity in the direction of the quantum which lies between U and $U+\Delta U$ where $U=S\cos\theta$ and ΔU may be regarded as a "limit of tolerance." Now the fraction of all atoms which have components of velocity in a given direction between U and $U+\Delta U$ is by kinetic theory equal to $(m/2\pi kT)^{1/2}[\exp-U^2/w^2]\Delta U$ where m is the mass of an atom, k is Boltzmann's gas constant, T is the absolute temperature and $w=(2kT/m)^{1/2}$ is the most probable speed. Clearly α will be proportional to this fraction so

[9] It has been pointed out to the writer that in the case of the longer wave-length resonance line of Ne ($^1S_0-{}^3P_1$), a relatively long mean free path would be expected in view of the fact that this line is an intercombination line, such lines being usually found relatively weak in absorption in elements of low atomic number.

[10] J. Frenckel, Zeits. f. Physik **59**, 198 (1930). See also the original and later papers by J. Holtsmark and L. Mensing.

[11] W. Weizel, Phys. Rev. **38**, 642 (1931).

* For a recent theory of resonance radiation diffusion which takes into account the Doppler effect see E. W. Samson, Phys. Rev. **40**, 940 (1932) and the following note by M. W. Zemansky.

[12] Carl Kenty, Phys. Rev. **41**, 390A (1932).

that $\alpha = A(m/2\pi kT)^{1/2}[\exp - U^2/w^2]\Delta U$ where A is a constant of proportionality. By substituting $U=0$ in this expression it is evident that the absorption coefficient for the core of the line, α_0, will be obtained. Thus $\alpha_0 = A(m/2\pi kT)^{1/2}\Delta U$.

By division of the two expressions, and replacing U by $S\cos\theta$ it is found that

$$\alpha = \alpha_0 \exp - [S^2 \cos^2\theta/w^2]. \tag{1}$$

The fraction of all such emitted quanta which travel at least a distance r, say, before absorption, will be given by

$$\exp(-r\alpha) = \exp(-r\alpha_0 e^{-(S^2\cos^2\theta/w^2)}).$$

On the consideration that all angles of emission are equally likely, the fraction of all quanta emitted by atoms of speed S, say, in directions making angles between θ and $\theta+d\theta$ with the directions of motion of the emitting atoms is simply the fractional solid angle denoted by $\frac{1}{2}\sin\theta d\theta$. Since, as far as the absorption coefficient is concerned, θ is not distinguished from $\pi-\theta$, it will be convenient to treat θ as varying only from 0 to $\pi/2$ and hence to take twice the above fractional solid angle, namely $\sin\theta d\theta$, as the fraction of all quanta emitted at angles between θ and $\theta+d\theta$. The fraction of all quanta emitted by atoms of speed S, which traverse at least a distance r before absorption is then given by

$$f(S, r) = \int_0^{\pi/2} \exp(-r\alpha_0 e^{-(S^2\cos^2\theta)/w^2}) \sin\theta d\theta = \frac{w}{S}\int_0^{S/w} \exp(-r\alpha_0 e^{-x^2})dx$$

where $x = S(\cos\theta)/w$.

Let it first be considered that all atoms are equally likely to be excited and to emit a resonance quantum regardless of their speed—the condition under which a thin emitting layer of gas would emit a line the intensity distribution of which would be the commonly assumed Gauss error curve. Then the fraction of all emitted quanta which are emitted by atoms having speeds between S and $S+Sd$ is given by Maxwell's distribution law, namely

$$f_1(S)dS = (4S^2/\pi^{1/2}w^3)e^{-S^2/w^2}dS \tag{2}$$

and as we have just seen the fraction of these which go at least a distance r before absorption is given by $f(S, r)$. The total fraction of *all* emitted quanta which go at least a distance r before absorption is then given by

$$f_1(r) = \frac{4}{\pi^{1/2}w^3}\int_0^{\infty} S^2 \exp(-S^2/w^2)dS \cdot \frac{w}{S}\int_0^{S/w} \exp(-r\alpha_0 e^{-x^2})dx. \tag{3}$$

By writing $S/w = y$ and $r\alpha_0 = R$, this may be written

$$f_1(R) = \frac{4}{\pi^{1/2}}\int_0^{\infty}\int_0^{y} y \exp(-y^2) \exp(-Re^{-x^2})dxdy. \tag{4}$$

Here $f_1(R)$ is the fraction of all emitted quanta which traverse at least a distance R times the mean free path, $1/\alpha_0$, of the core of the line. The values of

$f_1(R)$ for several numerical values of R, as calculated from Eq. (4) by graphical integration, are given in Table I.

TABLE I. *$f_1(R)$: fraction of all emitted quantat traversing at least a distance R/α_0 assuming all atoms equally likely to emit. $f_2(R)$: the same assuming "weighted distribution function."*

R	$f_1(R)$	$f_2(R)$	$Rf_1(R)$	$Rf_2(R)$
10^2	2.73×10^{-3}	9.2×10^{-4}	0.273	0.092
10^3	2.10×10^{-4}	6.5×10^{-5}	0.21	0.065
10^4	1.7×10^{-5}	4.7×10^{-6}	0.17	0.047
10^5	1.6×10^{-6}	3.96×10^{-7}	0.16	0.039

The question may be raised as to whether or not the above assumption is correct that the diffusion process results in a concentration of excited atoms in which one atom is as likely to be excited as another regardless of speed. In order to obtain at least a partial answer to this question consider the hypothetical case in which all atoms are excited through the absorption of radiation which has been emitted by atoms of speed S_0 in the direction of their motion. Let the direction of this radiation be denoted by Q in Fig. 2. Then an atom of speed S, in order to be able to absorb such radiation, must be moving in a direction, making an angle between θ and $\theta+d\theta$ with Q such that, within a certain "limit of tolerance," $S\cos\theta = S_0$. Let it be supposed that this limit of tolerance is ϵw, for convenience. Then $d(S\cos\theta) = \epsilon w = -S\sin\theta d\theta$, or $d\theta = \epsilon w/S\sin\theta$, neglecting the minus sign. Now the probability that an atom will be moving in a direction making an angle between θ and $\theta+d\theta$ with Q is $\frac{1}{2}\sin\theta d\theta$. By substituting the value of $d\theta$, above, it is evident that the relative probability that an atom of speed S, $S>S_0$, will be able to absorb the given radiation will be $\epsilon w/2S$. Since the fraction of all atoms having speeds between S and $S+dS$ is given by Maxwell's distribution law, Eq. (2) the chance that a quantum of the given radiation will be absorbed by an atom of speed between S and $S+dS$ is proportional to the product of this fraction and the above probability, namely

$$\frac{2K\epsilon S}{(\pi)^{1/2}w^2}e^{-S^2/w^2}dS = f_2(S)dS, \qquad f_2(S) = 0 \text{ for } S < S_0$$

where K is a constant of proportionality. Since the quantum is certain to be absorbed by one atom or another (assuming a sufficiently large volume of gas)

$$\int_{S_0}^{\infty} f_2(S)dS = 1. \tag{4a}$$

By choosing $S_0 \ll w$, the fraction of atoms whose speeds are so low as to preclude their being able to absorb the radiation can be made negligibly small. For convenience, suppose $S_0 = 0$, corresponding to excitation by the core of the resonance line. Then Eq. (4a) gives the result that $K\epsilon = (\pi)^{1/2}$ so that

$$f_2(S)dS = (2/w^2)Se^{-S^2/w^2}dS. \tag{5}$$

This may be called the "weighted distribution" function, for the purpose of this paper, in order to distinguish it from the normal distribution function

$f_1(S)dS$ of Maxwell.[13] It follows from the above that $f_2(S)dS$ represents the fraction of all excited atoms which have speeds between S and $S+dS$ under the assumptions considered. With this weighted distribution function the fraction of all emitted quanta which traverse at least a distance R times the mean free path, $1/\alpha_0$, of the core of the line is found to be given by

$$f_2(R) = 2\int_0^\infty \int_0^y \exp(-y^2) \exp(-Re^{-x^2})dxdy \qquad (6)$$

as follows by the method of deriving Eq. (4). Values of $f_2(R)$, calculated by graphical integration, for a number of values of R, are given in Table I.

Let us now consider the two functions $f_1(S)dS$ and $f_2(S)dS$ as limiting distribution functions. In view of the appearance of S in the denominator of the expression $\epsilon w/2S$, above, for the relative probability of excitation of an atom of speed S, and the fact that the *bulk* of the diffusing resonance radiation will not have an abnormally large displacement from the core of the line, it is evident that $f_1(S)dS$ expresses a relative excitation of the high speed atoms which is too great to be characteristic of the average excitation by the diffusion process (only if the exciting radiation density were uniform with respect to frequency would $f_1(S)dS$ be attained). On the other hand, since $f_2(S)dS$ was derived on the assumption of excitation by the core of the line ($S_0=0$) this function expresses a relative excitation of the very low speed atoms which is too high (since the actual diffusing radiation has a line breadth which is greater than zero). The true distribution function characteristic of the diffusion process must therefore lie somewhere between these two limiting functions; its actual form would be very difficult to calculate. Further, as will be seen below, it will probably vary from one point to another in a body of gas, depending on geometry and other factors.

The diffusion coefficient of resonance radiation may now be calculated on the basis of Eqs. (3) and (5) as limiting cases.[14] In Fig. 3 let $(N+zdN/dz)$ represent the concentration of excited atoms at any point distant z from the XY plane. Then the number of excited atoms in the element of volume dv, at a distance r from the origin is $(N+r\cos\theta dN/dz)dv$ where θ is the angle between r and the Z axis. If the average life of the excited atoms is τ, then $(N+r\cos\theta dN/dz)dv/\tau$ quanta will be emitted per second from this volume element and of these a fraction $(d\sigma\cos\theta)/4\pi r^2$ will be emitted in directions passing through the surface element $d\sigma$ in the XY plane at the origin. Of all such quanta, a fraction $f_1(r)$ will, by Eq. (3) (to take, first, the case of the normal distribution function), traverse a distance at least as great as r and will hence pass through $d\sigma$. By expressing the volume element in terms of polar coordinates, $dv=r^2\sin\theta dr d\theta d\phi$ and the total number of quanta passing downward through $d\sigma$ per second is

[13] It is to be noted that gaseous collisions during the lifetime of the excited state, as at the higher pressures, will tend to bring about the normal distribution function $f_1(S)dS$.

[14] The method used is somewhat analogous to a well-known method for finding molecular diffusion coefficients. See for example, L. B. Loeb, *Kinetic Theory of Gases*, pp. 224, 225. The method indeed seems to be more naturally applicable to radiation diffusion than to molecular diffusion.

$$\iiint (d\sigma/4\pi\tau)\left(N + r\cos\theta\frac{dN}{dz}\right)\cos\theta\sin\theta d\theta d\phi f_1(r)dr$$

where ϕ must be integrated from 0 to 2π, θ from 0 to $\pi/2$ and r from 0 to ∞. Similarly, the total number of quanta passing per sec. upward through $d\sigma$ is

$$\iiint (d\sigma/4\pi\tau)\left(N - r\cos\theta\frac{dN}{dz}\right)\cos\theta\sin\theta d\theta d\phi f_1(r)dr.$$

The resultant flux of quanta passing through $d\sigma$ is the difference between the above two expressions, namely

$$\frac{\sigma}{2\pi\tau}\frac{dN}{dz}\iiint rf_1(r)\cos^2\theta\sin\theta d\theta d\phi dr$$

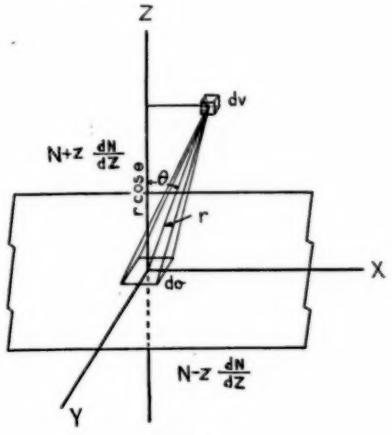

Fig. 3.

and this flux is by definition equal to $Dd\sigma dN/dz$ where D is the diffusion coefficient. By carrying out the integrations for θ and ϕ and writing $r=R/\alpha_0$ as above it follows that

$$D = (1/3\alpha_0^2\tau)\int_0^\infty Rf_1(R)dR. \tag{7}$$

Here it may be noted that on the view that all diffusing resonance quanta have the same absorption coefficient α_0 we may write $f_1(R)=\exp(-R)$, simply, $f_1(R)$ denoting the fraction of all emitted quanta which traverse at least a distance $r=R/\alpha_0$ before absorption and this fraction, on the present assumption, being denoted by $\exp -r\alpha_0=\exp(-R)$, in which case Eq. (7), would give $D=1/(3\alpha_0^2\tau)$ which is the standard expression for the diffusion coefficient already referred to.

In the actual case considered, however, $Rf_1(R)$ has values some examples of which are given in Table I and it is found that graphical integration of Eq. (7) will yield a value of D which is indefinitely large compared with the standard expression.

On the basis of the weighted distribution function, the diffusion coefficient may be similarly found to be given by

$$D = (1/3\alpha_0^2\tau)\int_0^\infty Rf_2(R)dR. \tag{8}$$

Some examples of the values of $Rf_2(R)$ are given in Table I. It will be observed that these values are falling off with increasing R more rapidly than is the case with $Rf_1(R)$; nevertheless it appears that D as given by Eq. (8) will also be indefinitely large compared with the standard expression. Now $f_2(R)$, being based on $f_2(S)dS$, represents a lower limit for the fraction of emitted quanta traversing at least a distance R/α_0 before being absorbed; since the actual fraction must be greater than this, we may safely regard the diffusion coefficient as indefinitely large compared with $1/(3\alpha_0^2\tau)$.

Essentially, the same result may also be obtained in the following manner. A quantum for which the absorption coefficient is α will have a mean free path, $1/\alpha$. Representing individual free paths by p, we may denote by $\bar{p}$ the average free path taking into account all values of α. The effective average speed of the quantum through the gas[1] will then be $\bar{p}/\tau$. By analogy with molecular diffusion,[1] where the diffusion coefficient is given by $D=\frac{1}{3}v_mL$ where v_m is the average molecular speed and L is the mean free path, one might write for the diffusion coefficient of radiation $D=\frac{1}{3}(\bar{p}/\tau)\cdot\bar{p}$. If the analogy with molecular diffusion were complete and the speed p/τ did not depend on p (in the molecular diffusion case v does not depend on L, at least to a first approximation) it would be justifiable to multiply the average speed $\bar{p}/\tau$ by the average free path $\bar{p}$ and so obtain for the diffusion coefficient $\frac{1}{3}(\bar{p})^2/\tau = \frac{1}{3}(\overline{1/\alpha})^2/\tau$. But in the case of radiation diffusion a high value of p is *always accompanied by* a high value of $v=\bar{p}/\tau$ (in contradistinction to the molecular diffusion case) and it is clear that the *average square* free path must be taken, that is[15]

$$D \sim \tfrac{1}{3}\overline{p^2}/\tau \tag{9}$$

where, in view of the method of obtaining the result, no significance is to be placed on the factor $(\frac{1}{3})$ (see below).

The average square free path on the present assumptions may be found as follows. The average free path of the quantum represented by Q in Fig. 1, which is supposed to be emitted from an atom of speed S in a direction making an angle between θ and $\theta+d\theta$ with the director of S is $1/\alpha=(1/\alpha_0)\exp S^2\cos^2\theta/w^2$ and the average square free path of such a quantum is[16] $(2/\alpha_0^2)\exp 2S^2\cos^2\theta/w^2$. Averaging over all values of θ and all values of S, using the one or the other of the two distribution functions $f_1(S)dS$ or $f_2(S)dS$, one obtains for the average square free path, respectively

[15] Although expression (9) may appear like the usual form of the diffusion coefficient, it is really very different because the average of p^2, is an enormously larger quantity than the reciprocal of the square of the average α. The latter quantity has been evaluated on the basis of either $f_1(S)dS$ or $f_2(S)dS$ and found to be only slightly greater than $1/\alpha_0^2$.

[16] This follows on integration of $x^2f(x)dx$ from $x=0$ to $x=\infty$ where $f(x)dx=\alpha(\exp-\alpha x)dx$ is the fraction of all free paths lying between x and $x+dx$.

$$\overline{p_1^2} = \frac{4(2)^{1/2}}{(\pi)^{1/2}\alpha_0^2}\int_0^\infty \int_0^{(2)^{1/2}y} ye^{-y^2}e^{x^2}dxdy \tag{10}$$

$$\overline{p_2^2} = \frac{2(2)^{1/2}}{\alpha_0^2}\int_0^\infty \int_0^{(2)^{1/2}y} e^{-y^2}e^{x^2}dxdy \tag{11}$$

where $y=S/w$ as before and $x=(2)^{1/2}(S\cos\theta)/w$. Graphical integration of Eqs. (10) and (11) indicates that both expressions for the average square free path are infinite and hence by Eq. (9) that the diffusion coefficient must be infinite, in agreement with the result already obtained. Indeed the expressions for D obtained by the two methods are mathematically identical if the numerical factor in Eq. (9) is taken as $\frac{1}{6}$ instead of $\frac{1}{3}$, as may be shown as follows. Assume $f(R)$ is the true function representing the fraction of all free paths which are greater than R times the "core mean free path" $1/\alpha_0$. Then the fraction of all free paths which are of length between R/α_0 and $(R+dR)/\alpha_0$ will be $df(R)$ and the average square free path may be written as

$$\overline{p^2} = \frac{1}{\alpha_0^2}\int_{f(R)=0}^{1} R^2 df(R).$$

But from the standpoint of the area under a curve this is numerically equivalent to

$$\frac{1}{\alpha_0^2}\int_{R^2=0}^{\infty} f(R)d(R^2) = \frac{2}{\alpha_0^2}\int_{R=0}^{\infty} Rf(R)dR$$

so that, referring to Eqs. (7) or (8), we have[17]

$$D = (1/6)\overline{p^2}/\tau. \tag{12}$$

The fact that the coefficient of radiation diffusion is infinite has been seen to depend on the importance of extremely long free paths. The result will evidently not apply to most cases met with in practice where such free paths would be greater than the dimensions of the gas container. Hence for practical purposes, it appears that there is no quantity which can properly be defined as the diffusion coefficient of resonance radiation; as the dimensions of the gas container are made larger, (or the density of the gas larger) the apparent diffusion coefficient will increase beyond the value $\frac{1}{3}/\alpha_0^2\tau$ without limit.

[17] It is a curious fact that in a familiar method of finding the coefficient of molecular diffusion (see reference 14) there appears an expression of the form $\int_0^\infty re^{-r/L}dr$, where L is the mean molecular free path, which is equivalent to $(1/\alpha_0)^2\int_0^\infty Rf(R)dR$, above, and that the ordinary coefficient of molecular diffusion, $(1/3)v_mL$, where v_m is the mean thermal speed, may be written as $(1/6)\overline{p^2}v_m/L$ or as $(1/6)\overline{p^2}/t$ where $t=L/v_m$ is the mean time between collisions. (Compare Eq.(12) above.) This follows at once of course from $D=(1/3)v_mL$ since in the case of molecular free paths $\overline{p^2}=2L^2$ (see reference 16). From the present point of view it would appear to be the average square free path, which is of fundamental importance for the coefficient of molecular diffusion as well as for the coefficient of radiation diffusion, and that formula (12) may be of rather general significance.

In dealing with actual cases, for example in attempting to calculate the rate of decay of the resonance radiation emerging from a resonance cell with plane parallel sides after the exciting radiation is cut off (see § IV), the method that has been adopted is to assume that the diffusing radiation can be treated as if it had an apparent or effective diffusion coefficient limiting expressions for which are given by

$$D_1 = (\tfrac{1}{6})\overline{p_1}^2(y_1)/\tau \tag{13}$$

$$D_2 = (\tfrac{1}{6})\overline{p_2}^2(y_1)/\tau \tag{14}$$

where $\bar{p}_1^2(y_1)$ and $\bar{p}_2^2(y_1)$ are supposed to be the limiting expressions for the effective average square free path as found by the integrating y in Eqs. (10) and (11), respectively, from 0 to y_1 (instead of from 0 to ∞) and y_1 is defined by

$$(1/\alpha_0) \exp y_1^2 = l \tag{15}$$

where l is the thickness of the cell. By choosing y_1 in this way we disregard those excited atoms whose speeds are such that the mean free paths of the quanta emitted by them in their directions of motion would be greater than l.[18] This procedure is an approximate method of taking into account the fact that free paths greater than the dimensions of the cell are meaningless. The method is roughly justified only in cases where $l \gg 1/\alpha_0$; under these circumstances the fraction of free paths which would be much greater than l will be so small that they can approximately be neglected—only when there are no walls to limit them will such free paths make their really important contribution to the average square free path.

With the above assumptions we may write

$$\overline{p_1^2}(y_1) = \frac{4(2)^{1/2}}{(\pi)^{1/2}\alpha_0^2} \int_0^{y_1} \int_0^{(2)^{1/2}y} ye^{-y} e^{z}\, dxdy \tag{16}$$

$$\overline{p_2^2}(y_1) = \frac{2(2)^{1/2}}{\alpha_0^2} \int_0^{y_1} \int_0^{(2)^{1/2}y} e^{-y^2} e^{z^2} dxdy. \tag{17}$$

As pointed out by Dr. Zemansky Eqs. (13) and (14), on substitution from Eqs. (16) and (17), are mathematically identical with Eqs. (7) and (8), respectively, if the complete expressions for $f_1(R)$ and $f_2(R)$ from Eqs. (4) and (6) are substituted in Eqs (7) and (8) and the integrations first performed for R, R varying from 0 to ∞ and the upper limit of integration for y being y_1 in all cases. The integration of R from 0 to ∞ here is approximately justified on account of the limitation placed on y_1.

Considering the very approximate nature of the assumptions involved we could scarcely expect the present method to yield more than an order of magnitude, for example, for the rate of decay of the radiation emerging from a resonance cell. Further, as discussed above, the method will only be ap-

[18] This follows since the absorption coefficient of quanta emitted by atoms of speed S_1 in their direction of motion will be $\alpha_0 \exp -S_1^2/w^2$ (see above) and the mean free path of such quanta will be $(1/\alpha_0)\exp S_1^2/w^2 = (1/\alpha_0)\exp y_1^2$.

plicable to cases where $l \gg 1/\alpha_0$ i.e., to cases where the great majority of quanta undergo a large number of absorptions and reemissions before escape.

Using the one or the other of the two distribution functions $f_1(S)dS$ or $f_2(S)dS$, we obtain, in a manner similar to the manner of obtaining Eqs. (10) and (11) the following expressions, respectively, for the average free path

$$\overline{p_1} = \frac{4}{(\pi)^{1/2}\alpha_0}\int_0^\infty \int_0^y ye^{-y^2}e^{x^2}dxdy = \frac{4}{(\pi)^{1/2}\alpha_0}\int_0^\infty \phi_1(y)dy \tag{18}$$

$$\overline{p_2} = \frac{2}{\alpha_0}\int_0^\infty \int_0^y e^{-y^2}e^{x^2}dxdy = \frac{2}{\alpha_0}\int_0^\infty \phi_2(y)dy \tag{19}$$

for the case of a resonance cell of infinite size, where $y = S/w$ and $x = S(\cos\theta)/w$. The functions $\phi_1(y)$ and $\phi_2(y)$ are plotted in Fig. 4. Graphical integra-

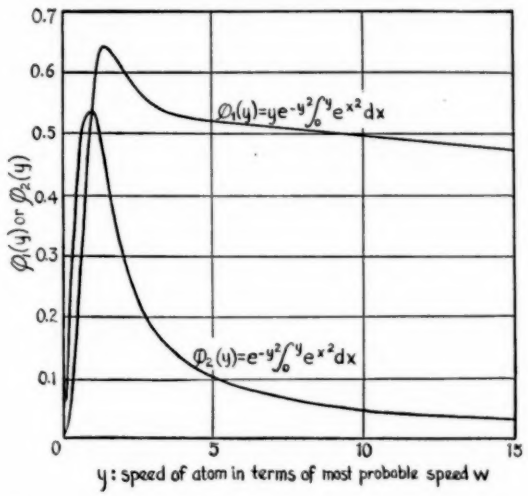

Fig. 4. Plot of functions $\phi_1(y)$ and $\phi_2(y)$ as occurring in Eqs. (18) and (19), respectively.

tion of Eq. (18) from $y=0$ to $y=15$ has yielded the result that $\bar{p}_1 > 16.8/\alpha_0$, 16.8 being the value of $[4/(\pi)^{1/2}]\phi_1(y)dy$ integrated from $y=0$ to $y=15$. In the same way $2\phi_2(y)dy$ integrated from 0 to 15 gave $\bar{p}_2 > 3.6/\alpha_0$. Integration from $y=0$ to $y=\infty$ would evidently yield values of $\bar{p}_1$ and $\bar{p}_2$ indefinitely larger than the above. In the case of a cell of finite size an estimate of the order of magnitude of the effective average free path can be obtained through the integration of Eq. (18) or (19) from $y=0$ to $y=y_1$ where y_1 is to be determined by Eq. (15).

Let us consider the case where resonance quanta are liberated at the center of a large spherical mass of gas of radius r. Suppose that the effective average free path inside this sphere is λ and that λ will increase only very slowly with r (as indeed it is found to do according to the method of defining the effective average free path discussed above, l in Eq. (15) being replaced by r). The number of free paths which a quantum will execute before escaping

from the surface of the sphere will on the average be of the order of n where[19]

$$n \sim (r/\lambda)^2. \tag{20}$$

Let us consider the chance that a free path will be produced which is greater than r (in which case the quantum will escape directly from the gas) and the dependence of this chance on r. Table I shows that the fraction of all free paths greater than $r = R/\alpha_0$ is decreasing roughly in proportion as R (i.e., r) increases. But the chance of such a free path being produced will be proportional to the average number of free paths made by the quantum before escaping and will therefore increase according to r^2. Hence the chance that the quantum may escape by making a free path at least of the order of r would appear to increase approximately in proportion to r. But this will not strictly be the case because, as discussed above, the value of λ which can be used in Eq. (14) will increase slowly with r. Nevertheless it seems justifiable to infer that the larger r becomes, the greater will be the line breadth of the emerging radiation. The problem of calculating the actual line breadth, or structure, in any given such case would appear to be one of great difficulty. The case is different from that of absorption broadening as usually considered because the absorbed radiation cannot be neglected—all the radiation must emerge from the sphere, it being assumed here, as elsewhere, above, that there are no losses of quanta in the gas phase as a result of dissipative collisions or otherwise.

Since, as has been seen above, the apparent values of the diffusion coefficient, average square free path, etc., will all increase with the volume of the gas, it is reasonable to suppose that the distribution function itself will vary from one point to another and depend on the geometry of the boundaries of the gas and the point of entry (or production) of the resonance quanta. For example, in the spherical case above it would be reasonable to infer a relative excitation of the high speed atoms which would be higher near the surface than at the center; for near the surface the outward flux of radiation will be preponderantly of frequencies which can only be absorbed by the high speed atoms.

III. The Effect of Pressure Broadening

It is well known that at appreciable gas densities the breadth of the resonance line, in the case of the alkali metals, Hg, etc., is much greater than that characteristic of the Doppler effect.[20] According to Waibel's[20] measurements the half breadth in absorption of the $1s - 6p(1^2S_{1/2} - 6^2P_{3/2})$ line of Cs, for example, at a vapor pressure of 17.5 mm (403°C) is about 2.2×10^{11} sec.$^{-1}$. This is calculated to be about 150 times the Doppler breadth for Cs at this temperature. Since the broadening was found by Waibel to increase

[19] See the treatment of the analogous problem of electron diffusion by W. Harries and G. Hertz, Zeits. f. Physik **46**, 177 (1927).

[20] W. Schütz, Zeits. f. Physik **35**, 260 (1925); **45**, 30 (1927); R. Minkowski, Zeits. f. Physik **36**, 839 (1926); F. Waibel, Zeits. f. Physik **53**, 459 (1929). See also B. Trumpy, Zeits. f. Physik **34**, 715 (1925) and others. Most studies have been made on the breadth in absorption.

towards lower series members, it is to be inferred that the breadth of the resonance line would be much greater than this. Hopfield[21] found the He resonance line (λ584A) in emission at about 1 mm pressure to be greatly broadened asymmetrically toward the short wave side. Weizel[22] states that the broadening on Hopfield's plates is about 500 cm^{-1}. This is calculated to be about 1000 times the Doppler broadening. Weizel has discussed this broadening in He on the basis of forces of the molecular type between the excited He atom and the normal He atom.

Foreign atoms (as in the case of an added gas) do not have nearly the same broadening effect as atoms of the same kind. These effects are commonly referred to as Lorentz collision broadening and Holtsmark coupling broadening,[23] respectively. As an example of the relative magnitude of the two effects, the result of Waibel[20] may be cited that the broadening in Cs vapor is about 200 times as great as the broadening due to the same pressure (of the order of 10 mm) of foreign gases.

In cases where such broadening exists, the reasoning used in §II can, of course, have no significance since there only Doppler broadening was assumed.[24] Such broadening as is here considered may be inferred to greatly accentuate the effects described above, namely the abnormally rapid escape of resonance radiation from a body of gas and an apparent diffusion coefficient increasing indefinitely, with the size of the vessel and with the gas density, beyond the value usually assumed.

§IV. The Resonance Radiation Imprisonment Experiments of Zemansky

Zemansky,[5] repeating an experiment of Miss Hayner,[25] excited the mercury vapor in a quartz cell by irradiating it with light from a quartz mercury vapor lamp and studied the rate of falling off of the resonance radiation emerging from the far side of the cell after the exciting radiation was cut off. Extending Milne's theory of radiation diffusion[2] to take into account the diffusion of excited atoms and the effect of dissipative collisions, Zemansky arrived at the following expression for the exponential constant of decay, I/T, of this radiation

$$\frac{1}{T} = \frac{\pi^2}{4\tau l^2 \beta^2 N^2} + \frac{\pi c}{3(2)^{1/2} l^2 s^2 N} + (2)^{1/2} \pi b s^2 c N. \tag{21}$$

Where τ is the mean life of the excited state, l is the thickness of the cell, β is the "mean or equivalent" atomic absorption coefficient for the radiation,

[21] J. J. Hopfield, Astrophys. J. **72,** 133 (1930).

[22] W. Weizel, Phys. Rev. **38,** 642 (1931).

[23] L. Mensing, Zeits. f. Physik **34,** 611 (1925); J. Holtsmark, Zeits. f. Physik **34,** 722 (1925); **54,** 761 (1929); J. Frenckel, Zeits. f. Physik **59,** 198 (1930); Lucy Schutz-Mensing, Zeits. f. Physik **61,** 655 (1930).

[24] R. Minkowski, see reference 20, found that the coupling broadening in Na vapor began to be of relative importance at about 0.02 mm and to increase progressively thereafter with increasing pressure.

[25] L. J. Hayner, Phys. Rev. **26,** 364 (1925).

supposed by Zemansky to be characteristic of the radiation diffusion process, N is the number of Hg atoms per cm³, c is the root mean square speed, s is the distance between centers at impact and b is the probability that a collision between a normal Hg atom and an excited Hg atom will be of the second kind (quenching efficiency; such collisions will in this case presumably result in the production of 2^3P_0 atoms). In this expression the first term represents the rate of decay of the radiation due to the radiation diffusion process, the second the rate of decay due to the diffusion of excited atoms to the walls and the third the rate of decay due to quenching collisions. The experimental values of the exponential constant of decay as obtained by Zemansky for a number of different vapor pressures and for two different cells are represented graphically in Fig. 5. By numerical substitution it was

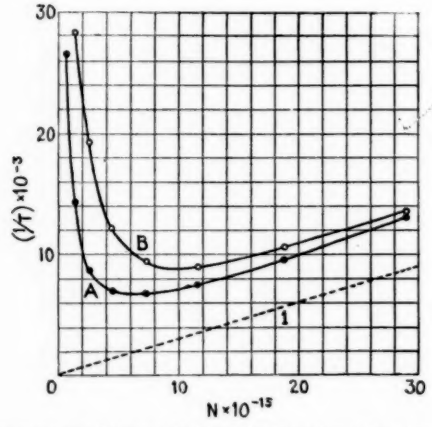

Fig. 5. Exponential constant of decay $(1/T)$ of λ2537 found by Zemansky (see reference 5). A, 1.95 cm cell; B, 1.3 cm cell; N, number of Hg atoms per cm³.

concluded that the second term on the right-hand side of Eq. (21) was negligibly small compared with the others and therefore that the exponential constant should be capable of representation by an equation of the form $1/T=A/N^2+BN$. Since the experimental curves could not be represented by such an equation, it was inferred that β was not a constant, but decreased as N increased. This inference, which is in agreement with conclusions drawn by Webb and Messenger,[6] from essentially similar experiments, is in accord with the views arrived at in §§II and III, and will be discussed further below. The line 1 of Fig. 5 was chosen to represent the last term on the right-hand side of Eq. (21). The slope of this line was 3×10^{-13} from which, by substituting the values of $c=2.2\times10^4$ cm/sec., and $s=6\times10^{-8}$ cm,[26] the quenching efficiency b, was calculated to be about 10^{-3}. In the more recent notation we may call $bs^2=\sigma_1^2$, the effective cross section for quenching, from which it follows that σ_1^2 is about 0.0025 times the normal cross section $(3.6\times10^{-8})^2$. This is in sufficient accord with the known small quenching cross sections of other monatomic gases for Hg resonance radiation (see below).

[26] The kinetic theory radius of the normal mercury atom being about 1.8×10^{-8} cm, it is evident that the radius of the excited atom was taken as 4.2×10^{-8} cm.

Zemansky[27] later interpreted his results in a completely different manner. (The two theories will hereinafter be referred to as the first and second theories.) He assumed that the emerging radiation was produced entirely as a result of the raising of 2^3P_0 atoms to the 2^3P_1 state by collisions of the first kind with normal atoms. He assumed further that the resulting resonance radiation escaped from the gas without a new metastable atom being formed and also that the time of imprisonment of this radiation, was small compared with (or at least shorter than) the mean life of the 2^3P_0 atoms, so that the rate of decay of the emerging radiation should be the same as the rate of decay of the 2^3P_0 atoms. On the basis of these assumptions, it was found that the concentration of 2^3P_0 atoms decayed exponentially with the time, with an exponential constant given by the expression

$$1/T = c'/\sigma_d^2 N + 9.04 \times 10^4 \gamma \sigma_d^2 N \tag{22}$$

where c' is a numerical constant, depending on the geometry of the cell and the thermal speed of the atoms, having the value 3.4×10^3 for the large cell (1.95 cm thick) and 6.8×10^3 for the small cell (1.3 cm thick), σ_d is the distance between the center of the 2^3P_0 atom and center of the normal atom at impact, N is the concentration of normal atoms, and γ is the probability that, on collision with a normal atom, a 2^3P_0 atom will be raised to the 2^3P_1 state. The first term on the right-hand side of this equation represents the exponential constant of decay due to diffusion to the walls; it is the important term at the lower pressures. The second term represents the exponential constant of decay due to collisions of the first kind; it is the important term at the higher pressures.

Zemansky found that the experimental curves of Fig. 5 were well represented by Eq. (22) provided σ_d were taken as 2.3×10^{-8} cm and γ as 0.0096. Subtracting from the above value of σ_d the radius of the normal Hg atom, 1.8×10^{-8} cm, a radius of 0.5×10^{-8} cm for the metastable atom was obtained, or 0.3 times the normal radius (diffusion cross section about 0.4—i.e., $(2.3/3.6)^2$—times the normal cross section). We may write $\gamma\sigma_d^2=(1+\epsilon/kT)(\exp-\epsilon/kT)\sigma_0^2$,[28] where $\epsilon=0.218$ volt is the energy difference between the 2^3P_0 and 2^3P_1 states of Hg, k is Boltzmann's constant, T is the absolute temperature and σ_0^2 is the effective cross section for collisions of the first kind between normal and metastable Hg atoms raising the latter to the 2^3P_1 state. (Here $(1+\epsilon/kT)(\exp-\epsilon/kT)$ is the fraction of all collisions within a distance σ_0 in which the kinetic energy of relative motion is $\geqq\epsilon$. This fraction is of the order of 0.01 at the upper temperatures in Zemansky's experiments.) It follows from Zemansky's results that $\sigma_0^2\sim5\times10^{-16}$ cm^2 which is again of the order of 0.4 the normal cross section $(3.6\times10^{-8})^2$.

In regard to these consequences of the second theory it is unusual to find a diffusion cross section (σ_d^2) for the metastable atom which is so much

[27] M. W. Zemansky, Phys. Rev. **34**, 213 (1929).

[28] See for example E. W. Samson, Phys. Rev. **40**, 940 (1932).

smaller than the normal cross section. Webb and Messenger[29] and Samson[28] have found for 2^3P_0 Hg atom diffusing in N_2 cross sections slightly greater than the normal cross section. However in the case of 2^3P_0 Hg atoms diffusing in Hg *vapor* the possible frequent exchange of the energy of these atoms with normal atoms at collisions (exchange of identity) might, as has been pointed out to the writer, account for an apparent abnormally small σ_d^2. In view of this possibility undue emphasis should probably not be placed on the smallness of σ_d^2 resulting from the second theory.

Of more significance, it is believed, is the value of σ_0^2 of 0.4 times the normal cross section to which the second theory leads. Such a large value of σ_0^2 does not accord with the results of Orthmann and Pringsheim.[30] These authors studied the resonance of λ2537 and the fluorescence of certain Tl lines as a function of Hg vapor pressure when a quartz Hg vapor resonance cell containing Tl at a fixed vapor pressure of 0.02 mm (610°C) was illuminated with light from a water-cooled quartz mercury arc. As the vapor pressure of the Hg was raised from a few millimeters to 760 mm the resonance of λ2537 decreased to almost zero; but the fluorescence of the Tl lines, caused by collisions of the second kind of Tl atoms with metastable Hg atoms, lost practically none of their brilliancy. Since at 760 mm there were roughly 30,000 times as many Hg atoms as Tl atoms present, it follows that a 2^3P_0 Hg atom made roughly this many collisions with normal Hg atoms before colliding with a Tl atom. At the temperature in question, somewhat greater than 610°C, roughly $\frac{1}{4}$ of these collisions, or about 7000, involved relative kinetic energy $\geqq \epsilon$ and hence it seems that a 2^3P_0 Hg atom must have been able to withstand at least many hundreds and possibly thousands[31] of kinetic theory collisions with normal Hg atoms energetically capable of raising it to the 2^3P_1 state. Thus the experiments of Orthmann and Pringsheim indicate σ_0^2 to be at most hundreds of times less than the normal cross section, a result, which is in accord with other evidence now to be discussed.

In all cases known to the writer where there is an appreciable energy exchange (e.g., as great as the 0.218 volts here considered) between the kinetic energy of relative motion of the colliding atoms or molecules and the potential energy of one of them the effective cross sections for these collisions are very small compared with the normal cross sections. As examples there may be mentioned the well-known very small quenching cross sections ($2^3P_1 \rightarrow 2^3P_0$) of monatomic gases for Hg resonance radiation. According to the results of

[29] H. W. Webb and Helen A. Messenger, Phys. Rev. **40**, 466L (1932).

[30] W. Orthmann and P. Pringsheim, Zeits. f. Physik **35**, 626 (1926).

[31] We cannot use the number 7000 here because, when a 2^3P_0 atom is raised to the 2^3P_1 state, this 2^3P_1 atom, or another produced by the absorption of λ2537 emitted from it, may be returned to the 2^3P_0 state by a quenching collision. This process probably did not take place very many times, however, for otherwise λ2537 would not have been completely quenched. This follows since the average free path of the diffusing λ2537 in the resonance cell was probably not less (on account of large coupling or other pressure broadening) than the original average depth of penetration of the exciting light (water-cooled source) and since the cross section for quenching is probably very small.

Zemansky[32] the quenching cross sections in the case of He and A are <0.001 times the normal cross section.[33] Finally may be cited the observed long lives of metastable Ne atoms in Ne at pressures of a few millimeters. From these lives Penning[34] has calculated that the s_5 metastable state is able to withstand some 10^5 kinetic theory collisions with normal Ne atoms at room temperature without being raised to the s_4 state. ϵ being only about 0.05 volt in this case nearly half of these collisions are energetically capable of causing the transfer in question.[35]

It appears therefore that the value of σ_0^2 of 0.4 times the normal cross section which follows from the second theory is higher than any known similar cross sections in cases involving other gases by a factor of at least 100 (and possibly by a factor of 1000 or more).[36]

Insofar as the conclusions resulting from the second theory (especially the conclusion regarding σ_0^2) are unusual they are deserving of special attention. It is believed, however, that they require further confirmation, not only in view of the discussion already given, but because the experimental results can be sufficiently accounted for, as will be shown below, on the basis of the first theory and §§II and III of the present paper.

Undoubtedly all the processes treated in both theories take place; and a more comprehensive treatment, along the lines of the treatment of Samson,[28] would include them all. But it seems highly probable that the collisions of the first kind postulated in the second theory take place only so slowly that this process can, to a first approximation, be disregarded. On this view, the production of $\lambda 2537$ as a result of these collisions was probably so faint as not to have been observed in the experiments, and most of the energy of the 2^3P_0 atoms was probably lost at the walls.

[32] M. W. Zemansky, Phys. Rev. **36,** 919 (1930).

[33] The apparent small quenching effects of He and A observed by Stuart, (Zeits. f. Physik **32,** 262 (1925)), which have been discussed by many writers, are probably largely explicable in terms of pressure line broadening (see the recent work of v. Hámos, Zeits. f. Physik **74,** 631 (1932)) and the effects of traces of impurities.

[34] F. M. Penning, Zeits. f. Physik **46,** 335 (1928) see also some remarks in this connection by Kenty, Phys. Rev. **40,** 633L (1932).

[35] It is to be noted that when the kinetic energy of relative motion is exactly equal to ϵ the cross section for collisions of the first kind is zero because of the infinitely small chance that angular momentum can be conserved in such collisions (see for example Ruark and Urey, *Atoms Molecules and Quanta*, p. 475). When the kinetic energy of relative motion is but very little in excess of ϵ the cross section for such collisions will presumably be small for the same reason. The condition for the conservation of angular momentum should be easier of fulfillment in the case where one of the colliding partners is a molecule for this can take on angular momentum in varying amounts, (see reference 36).

[36] M. L. Pool, Phys. Rev. **38,** 955 (1931) has suggested that collisions of the first kind in the case of 2^3P_0 Hg atoms in N_2 may be associated with resonance transfers of energy between N_2 molecules in the first vibration state and 2^3P_0 Hg atoms. Such an explanation might account for the fact that while Cario and Franck (Zeits. f. Physik **37,** 619 (1926)) found that $\lambda 2537$ of Hg was not quenched by N_2 at 750°C, Oldenburg (Zeits. f. Physik **49,** 609 (1928)) found that this radiation *was* quenched by A at this temperature. Compare also the results of Orthmann and Pringsheim above for Hg at high pressures.

V. Application of the First Theory with the Aid of §§II and III

Whether or not collisions of the first kind as postulated in the second theory were of appreciable importance in the experiments it will be evident that the rate of escape of resonance radiation through the Hg vapor must have been at least as rapid as that following from the first theory. As has been discussed above this rate of escape is considerably greater than can be accounted for on the basis of classical theories of resonance radiation diffusion; let us see if it can be accounted for by means of the developments of the present paper.

Having chosen the line 1 of Fig. 5 to represent the last term on the right-hand side of Eq. (21), Zemansky found that in order to account for the decay curves A and B of Fig. 5, the quantity β, defined by him as the mean or equivalent atomic absorption coefficient, would have to decrease as N increased. The values of β for $N=1.4\times10^{15}$ Hg atoms per cm^3 are found to be 0.131 $\alpha_0{}^1$ and 0.124 $\alpha_0{}^1$ for the small (1.3 cm) and large (1.95 cm) cells, respectively, $\alpha_0{}^1$ being the atomic absorption coefficient for the core of the line, for the appropriate temperature, as calculated from the mean life of the $2{}^3P_1$ Hg atom according to the method used by Zemansky.[37] Similarly for N $=29\times10^{15}$ cm^{-3} the values found for β are 0.0169 $\alpha_0{}^1$ and 0.0116 $\alpha_0{}^1$ for the small and large cells, respectively.

It will be more in line with the reasoning of §II to study the quantity $(1/\beta)$,^{2} appear ing in Eq. (21) rather than β. In the derivation of Eq. (21) the quantity $1/(4\tau N^2\beta^2)$ occurs as the diffusion coefficient of the resonance radiation, which may be equated to D_1 or D_2 in Eqs. (13) and (14), respectively. If this is done, it is found that $3/(2N^2\beta^2)=\overline{p_1{}^2}(y_1)$ or $\overline{p_2{}^2}(y_1)$, respectively, and we may regard the quantity $3/(2N^2\beta^2)=\overline{p_E{}^2}$ as the experimentally determined effective average square free path, as calculated from the experimental results.

Table II shows the comparison, for two values of N, and for the two cells used, of the quantity $\overline{p_E{}^2}$ with the values of $\overline{p_1{}^2}(y_1)$ and $\overline{p_2{}^2}(y_1)$ as calculated by Eqs. (16) and (17), respectively, (with the help of Eq. (15)). All values for

Table II. *$\overline{p_1{}^2}(y_1)$, $\overline{p_2{}^2}(y_1)$: limiting values for the effective average square free path as calculated by Eqs. (16) and (17), respectively. $\overline{p_E{}^2}=3/(2N^2\beta^2)$: effective average square free path as calculated from Zemansky's experimental results. All these quantities are expressed in terms of $p_0{}^2$, the square of the mean free path of the core of the line.*

	1.3 cm cell			1.95 cm cell		
N $\times10^{-15}$	$\overline{p_1{}^2}(y_1)/p_0{}^2$	$\overline{p_2{}^2}(y_1)/p_0{}^2$	$\overline{p_E{}^2}/p_0{}^2$	$\overline{p_1{}^2}(y_1)/p_0{}^2$	$\overline{p_2{}^2}(y_1)/p_0{}^2$	$\overline{p_E{}^2}/p_0$
1.4	66	28	88	94	38	99
29	910	300	5300	1330	490	11200

[37] M. W. Zemansky, Phys. Rev. **36,** 219 (1930). See particularly pp. 228, 229. In making the calculations used in the present paper the value of τ of 1.08 and 10^{-7} sec. as found by P. M. Garrett, Phys. Rev. **40,** 779 (1932) has been used in place of the value 1.0×10^{-7} sec. used by Zemansky. The values found for $\alpha_0{}'$ are 1.21×10^{-13} and 1.11×10^{-13} for $T=70$°C and 130°C, respectively, ($N=1.4\times10^{15}$ and 29×10^{15}, respectively).

average square free paths are expressed in terms of p_0^2 where $p_0 = 1/N\alpha_0^1$ is the mean free path of the core of the line, (α_0^1 being the atomic absorption coefficient for the core of the line as calculated in each case for the temperature in question). From Table II it is seen that the observed effective average square free path increases with the thickness of the cell. The theoretical calculations are in agreement with this in that they also predict an increase in the effect average square free path with the size of the cell. Theoretically and experimentally also the effective average square free path (expressed as a multiple of p_0^2) is seen to increase with the gas density. Regarding the actual magnitude of the observed effective average square free path, the near agreement of the order of magnitude of this quantity and the corresponding calculated limiting values in the case of the lower gas density (especially as regards $\overline{p_1^2}(y_1)$) indicates that this quantity could probably be accounted for, with a more rigorous theory, largely on the basis of Doppler broadening only. At the higher gas density ($N = 29 \times 10^{15}$ cm^{-3}) however, this does not appear to be within the range of possibility in view of the great discrepancies between the observed and calculated values of the average square free path. This is taken to indicate that at the higher gas densities in Zemansky's experiments coupling or other broadening was already of great importance in increasing the rate of escape of the radiation.[7,38]

The reasoning so far has been based on the assumption that the line 1 of Fig. 5, of slope 3×10^{-1}, is the true line representing the effect of quenching collisions (i.e., the last term on the right-hand side of Eq. (21)). However, the experimental results admit of the assumption of any line of slope between 0 and about 4.5×10^{-13}, to represent the term in question, the variation of β with N being supposed to be such as to enable the experimental curves to be accounted for in any case. It appears, however, that a slope as great as 4.1×10^{-13} cannot be assumed because it is found that a line of this slope would require that $(1/N\beta)^2$ be the same for both cells whereas theory requires, as has been seen above, that this quantity be greater for the larger cell. About all that can be said is that the line, 1, chosen by Zemansky seems to represent a reasonable upper limit for the slope and hence, by Eq. (21) for the quenching efficiency, b (or the quenching cross section, see §IV). The effect of choosing a line of smaller slope than this line would be to increase the observed values of the average square free path and hence to increase the discrepancy between the observed and calculated values of this quantity; but the effect of coupling or other broadening can always be supposed (at least until further data are available) to make up for this discrepancy.

The experiments of Webb and Messenger[6] on the imprisonment of λ2537 of Hg are essentially similar to those of Zemansky. They cover, for the most part, a lower range of vapor densities; but, insofar as the density ranges overlap, the results are in sufficient quantitative agreement; and in general they are in agreement in that both sets of results show that resonance radiation

[38] At N 29×10^{15} atoms per cm the pressure is of the order of 1 mm and Minkowski found the coupling broadening in Na vapor to begin to be of relative importance at 0.02 mm. See reference 24.

escapes from a gas progressively faster than can be accounted for on classical theories of radiation diffusion the higher the gas density. The conclusions arrived at in the present paper are thus also in qualitative agreement with these results of Webb and Messenger. It would appear in view of the near agreement of the orders of magnitude of the observed and calculated average square free paths at the lower densities in Zemansky's experiments (see the first row of Table II), that the exponential constants of decay in Webb and Messenger's experiments, except possibly at the highest densities, could be accounted for on the basis of the Doppler effect alone. Webb and Messenger concluded that their experiments had to do mainly with radiation diffusion (rather than with metastable atoms, at least for all but the higher densities), and that existing theories of radiation diffusion would have to be revised to account for their results; the results of the present paper are in accord with these conclusions.

Since the main body of this paper was written, a paper by Samson[28] has appeared in which the effect of Doppler (or other) broadening on the radiation diffusion problem is considered from a different aspect. In the following note, Dr. Zemansky discusses the relationship (particularly as regards the results obtained) of Samson's theory to the present one.

My best thanks are due to Dr. M. W. Zemansky who has read the manuscript and made a number of important suggestions.

Note on the Equivalent Absorption Coefficient for Diffused Resonance Radiation

By M. W. ZEMANSKY
College of the City of New York

(Received August 25, 1932)

It is shown that the ideas expressed in the preceding theoretical paper by Kenty when applied to the diffusion of resonance radiation in a layer of gas of finite thickness provide a method of calculating an equivalent absorption coefficient of the gas for all the frequencies due to the Doppler effect that are present in the diffusing radiation. This average absorption coefficient is calculated and compared with a similar quantity calculated on the basis of a different point of view by Samson. Both average absorption coefficients are discussed in connection with the author's experiments (1927) on the rapidity of escape of resonance radiation emitted from a slab of mercury vapor after the cut-off of the excitation.

IN THE preceding theoretical paper, Kenty gives a treatment of the emission and absorption of quanta by moving atoms, in which it is pointed out that, owing to the Doppler effect, the group of frequencies comprising a Doppler line can pass from one part of a gas to another much more readily than an infinitesimal frequency band at the center of the line when no Doppler effect is present. According to Kenty, his equations are strictly applicable only to a gas of infinite volume, in which case both the diffusion coefficient and the mean free path of the radiation are found to be infinite. An approximate method is given, however, of treating the case of a finite layer of gas. It is not the purpose of this note to scrutinize Kenty's ideas carefully, but instead to examine the consequences of his method of handling the finite case. It will be seen that this method is essentially a device for obtaining an equivalent absorption coefficient of a gas for the group of frequencies generated by the Doppler effect.

According to Kenty, the diffusion coefficient of Doppler radiation in a gas is given by his Eq. (7).

$$D = (1/3\tau k_0^2) \int_0^\infty R f_1(R) dR \qquad (1)$$

where k_0 is the absorption coefficient of the gas for the center of the line, τ the lifetime of the excited state to which the atoms are raised by the radiation, and $f_1(R)$ is a distribution function corresponding to a situation in which the atoms are originally excited by a continuous spectrum (in practise by a line much broader than the Doppler line). Of the two distribution functions, $f_1(R)$ and $f_2(R)$, given by Kenty, $f_1(R)$ has been chosen because it is believed that it approximates more closely the actual conditions of an experiment. $f_1(R)$ is given by his Eq. (4), namely

$$f_1(R) = (4/\pi^{1/2}) \int_0^\infty \int_0^y y e^{-y^2} e^{-Re^{-x^2}} dx dy. \tag{2}$$

Substituting Eq. (2) in Eq. (1) and integrating R from 0 to ∞, we obtain

$$D = [2(2)^{1/2}/3\pi^{1/2}\tau k_0^2] \int_0^\infty y e^{-y^2} dy \int_0^{2^{1/2}y} e^{x^2} dx. \tag{3}$$

The integration over y is an integration over the velocities of the emitting atoms. If all velocities are taken into account D becomes infinite. Kenty's approximate method of handling a practical situation is to integrate y from 0 to an upper limit y_1, where y_1 is given by the formula

$$k_0 e^{-y_1^2} = 1/l, \tag{4}$$

l being the thickness of the layer of gas. Eq. (3) then becomes

$$\begin{aligned} D &= [2(2)^{1/2}/3\pi^{1/2}\tau k_0^2] \int_0^{y_1} y e^{-y^2} dy \int_0^{2^{1/2}y} e^{x^2} dx \\ &= [2^{1/2}/3\pi^{1/2}\tau k_0^2] \int_0^{y_1} 2y e^{y^2} F(2^{1/2}y) dy \end{aligned} \tag{5}$$

where

$$F(t) = e^{-t^2} \int_0^t e^{x^2} dx. \tag{6}$$

The integral in Eq. (5) can be expressed in terms of the F function defined by Eq. (6) as follows: Integrating by parts,

$$\int_0^{y_1} 2y e^{y^2} F(2^{1/2}y) dy = [e^{y^2} F(2^{1/2}y)]_0^{y_1} - \int_0^{y_1} e^{y^2} dF(2^{1/2}y)$$

and, in virtue of the relation $(d/dt)F(t) = 1 - 2tF(t)$,

$$\begin{aligned} \int_0^{y_1} 2y e^{y^2} F(2^{1/2}y) dy &= e^{y_1^2} F(2^{1/2}y_1) - 2^{1/2} \int_0^{y_1} e^{y^2} [1 - 2(2)^{1/2} F(2^{1/2}y)] dy \\ &= e^{y_1^2} F(2^{1/2}y_1) - 2^{1/2} e^{y_1^2} F(y_1) + 2 \int_0^{y_1} 2y e^{y^2} F(2^{1/2}y) dy \end{aligned}$$

whence, finally

$$\int_0^{y_1} 2y e^{y^2} F(2^{1/2}y) dy = e^{y_1^2} [2^{1/2} F(y_1) - F(2^{1/2}y_1)]. \tag{7}$$

From Eqs. (4), (5) and (7) the diffusion coefficient is found to be

$$D = [(2)^{1/2} l/3\pi^{1/2}\tau k_0] [2^{1/2} F(\ln k_0 l)^{1/2} - F(2 \ln k_0 l)^{1/2}]. \tag{8}$$

On the basis of the Einstein theory of radiation, without appeal to the analogy with molecular diffusion, and neglecting Doppler effect, Milne

showed that radiation of infinitesimal spectral width diffused through a gas with a diffusion coefficient equal to

$$D' = 1/4\alpha^2\tau \tag{9}$$

where α stands for the absorption coefficient of the gas for the radiation in question. In the case of the diffusion of a band of frequencies comprising a line we may define an *equivalent absorption coefficient* as a quantity, $\bar{k}$ which, when substituted for α in Eq. (9), will give the correct diffusion coefficient to be used when the diffusing radiation is not of infinitesimal spectral width.

Kenty's expression for the diffusion coefficient, Eq. (8), enables us to compute $\bar{k}$ when the Doppler effect is present. For, by definition of $\bar{k}$,

$$1/4\bar{k}^2\tau = [2^{1/2}l/3\pi^{1/2}\tau k_0][2^{1/2}F(\ln k_0l)^{1/2} - F(2\ln k_0l)^{1/2}]$$

and

$$\bar{k}l = \left[\frac{3}{4}\left(\frac{\pi}{2}\right)^{1/2}\right]^{1/2}\left[\frac{k_0l}{2^{1/2}F(\ln k_0l)^{1/2} - F(2\ln k_0l)^{1/2}}\right]^{1/2}. \tag{10}$$

From the splendid table of values of the F function given by Miller and Gordon,[1] $\bar{k}l$ was evaluated for various values of k_0l and the result is shown in Table I and curve A of Fig. 1. It is seen from the curve that Kenty's method breaks down for small values of k_0l, which is to be expected in view of the approximations made.

TABLE I. *Kenty's equivalent absorption coefficient.*

k_0l	$\bar{k}l$	k_0l	$\bar{k}l$
1.5	3.05	100	21.2
2	2.76	200	31.4
3	2.97	500	54.2
4	3.31	1000	77.8
5	3.70	2000	114
10	5.39	3000	142
15	6.85	4000	166
20	8.10	5000	186
30	10.4	6000	205
40	12.3	7000	223
50	14.1	8000	240

The problem of calculating an equivalent absorption coefficient for Doppler radiation to be used in conjunction with Milne's radiation diffusion equation was attacked in a different way by Samson[2] without considering the motions of individual atoms or the free paths of individual groups of quanta. Samson defined an equivalent absorption coefficient $\bar{k}$ as the absorption coefficient that a gas would have for that infinitesimal frequency band which would show the same percentage transmission that is shown by a Doppler line.

The transmission of an infinitesimal frequency band by a gas whose absorption coefficient is $\bar{k}$ is $e^{-\bar{k}l}$, whereas the transmission of a line of the form

[1] W. L. Miller and A. R. Gordon, Phys. Chem. **35**, 2878 (1931).

[2] E. W. Samson, Phys. Rev. **40**, 940 (1932).

$I_0 e^{-\omega^2}$ by a gas whose absorption coefficient has the form $k_0 e^{-\omega^2}$ is

$$\frac{\int_{-\infty}^{\infty} \exp(-\omega^2) \exp(k_0 l e^{-\omega^2}) d\omega,}{\int_{-\infty}^{\infty} \exp(-\omega^2) d\omega}.$$

whence Samson's $\bar{k}l$ is given by the relation

$$\exp(-\bar{k}l) = \frac{\int_{-\infty}^{\infty} \exp(-\omega^2) \exp(-k_0 l e^{-\omega^2}) d\omega}{\int_{-\infty}^{\infty} \exp(-\omega^2) d\omega}. \tag{11}$$

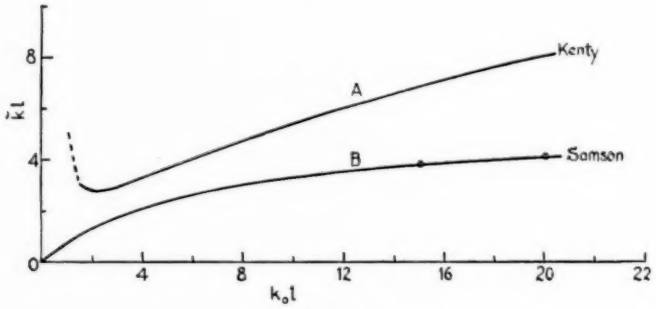

Fig. 1.

Samson's equivalent absorption coefficient is given for a number of values of $k_0 l$ in Table II, and is shown as curve B in Fig. 1. The curve shows that

TABLE II. *Samson's equivalent absorption coefficient.*

$k_0 l$	$\bar{k}l$	$k_0 l$	$\bar{k}l$
0	0	4	2.104
1	0.665	9.7	3.29
2	1.241	14.4	3.76
3	1.715	19.9	4.15

for small values of $k_0 l$, $\bar{k}l$ behaves as it should, becoming zero when $k_0 l$ is zero. For large values of $k_0 l$ however, judging from the very slow rate at which the curve is rising, it appears that $\bar{k}l$ is too small. One might hazard the guess that Samson's method is valid at low opacities (small values of $k_0 l$) and Kenty's method at high opacities.

In Kenty's experimental paper, the author's experiments on the escape of resonance radiation[3] from mercury vapor after the cut-off of the excitation, are interpreted as being due entirely to radiation diffusion rather than to metastable atoms. A complete discussion of the relative merits of these two interpretations is beyond the scope of this note. It should be pointed out,

[3] M. W. Zemansky, Phys. Rev. **29**, 513 (1927).

however, that, since the two theories are not mutually exclusive, it is quite possible that the correct explanation involves both radiation diffusion and metastable atoms, in a manner similar to Samson's treatment of the afterglow of mercury resonance radiation from a mixture of mercury vapor and nitrogen.

With the assumption that radiation diffusion takes place in these experiments it is instructive to calculate the equivalent absorption coefficient by both Kenty's and Samson's method, and with the aid of Milne's equation for the exponential constant of decay of the escaping radiation, calculate the exponential constant to be expected. This is done as follows:
With the equation[4]

$$5\left(\frac{\pi}{4\ln 2}\right)^{1/2} k_0 \Delta\nu_D = \frac{\lambda_0^2}{8\pi\tau}\frac{g_2}{g_1} N, \tag{12}$$

it is possible to compute $k_0 l$ at a given vapor pressure (which determines N), a given temperature (which determines $\Delta\nu_D$), and with the most reliable value of τ[5](1.08×10^{-7} sec.). Knowing $k_0 l$, $\bar{k}l$ is obtained either by Kenty's or by Samson's method. Then making use of Milnes equation for the decay constant neglecting impacts,

$$\beta = (1/\tau)/[1 + (\bar{k}l/\lambda_1)^2] \tag{13}$$

where λ_1 is approximately $\pi/2$, β is calculated and compared with the experimental values of β at low vapor pressures before impacts begin to play an important role.

With Kenty's method of calculating $\bar{k}l$, the results are shown in Table III, where it is seen that there is agreement in order of magnitude. With

TABLE III.

$T°K$	l=1.95 cm		l=1.30 cm	
	Exp. β	β from Eq. (13)	Exp. β	β from Eq. (13)
333	26600	29500		
343	14200	15000	28100	24500
353	8810	7940	19300	12000
363	7070	4380	12100	6750

Samson's equivalent absorption coefficient, the results show a disagreement by a factor of at least 10. This is in line with the statement made previously, namely, that Samson's equivalent absorption coefficient is too small at large values of $k_0 l$.

[4] M. W. Zemansky, Phys. Rev. **36,** 219 (1930).
[5] P. H. Garrett, Phys. Rev. **40,** 779 (1932).

The Effect of Tension on the Electrical Resistance of Single Bismuth Crystals

By MILDRED ALLEN
Research Laboratory of Physics, Harvard University

(Received October 19, 1932)

The compensated potentiometer method of measuring minute variations in small resistances which was developed by P. W. Bridgman has been used in the study of the effect of tension, applied parallel to the direction of current flow, on the resistance of single bismuth crystals. The tension coefficient of resistance at 30°C has been found to depend on the orientations both of the principal (111) and secondary ($11\bar{1}$) cleavage planes with respect to the tension. For the limiting case of the principal cleavage plane perpendicular to the tension, the coefficient is independent of the orientation of the secondary cleavage planes; in that of the principal cleavage plane parallel to the tension, the coefficient varies very little and is very probably independent of the secondary orientation. In the case where the normal to the principal cleavage plane makes an angle of about 60° with the tension, the variation of the coefficient with the orientation of the secondary cleavage plane seems to be a maximum. This variation involves a change in sign as well as in magnitude, so that for certain orientations the coefficient becomes positive instead of remaining negative. The coefficient shows trigonal symmetry, as it must do if it is to be consistent with the known corporeal trigonal symmetry of the bismuth crystal. The paper presents only these empirical results.

THE EFFECT on the resistance of single crystals of various elements produced by hydrostatic pressure[1] has previously been studied, but not the effect of tension.[2] It is to be expected that the effect of tension will be more complicated than that of hydrostatic pressure, since in the case of the latter the symmetry of the crystal is unchanged. As a result the pressure coefficient of resistance is a function only of a single parameter, the orientation of the main cleavage plane with respect to the direction of the electric current, and, as Professor Bridgman has shown, may be expressed in terms of but two constants, one associated with the current flowing perpendicular to the normal to the principal cleavage plane and the other with a current parallel to it. In the case of tension, on the other hand, the applied force must cause a change in the symmetry of the crystal, a change which depends not only on the orientation of the principal cleavage plane with respect to the tension, but also on the orientation of the secondary cleavage planes. The problem is thus a more complicated one, since the effect may very possibly depend on more than the change of symmetry. Experimentally, however, it has been found that the coefficient may be represented within experimental error as a function of only two parameters which may be taken to

[1] P. W. Bridgman, Proc. Amer. Acad. **60**, 305 (1925); **63**, 351 (1929).

[2] Trapeznikowa (K. Akad. Amsterdam **34**, 840 (1931)) finds no effect of tension or of unidirectional pressure on the resistance of bismuth crystals. However, the sensitiveness of his apparatus was such that he could not detect changes of less than 1 percent whereas the changes to be reported in this paper are at most 0.2 percent of the initial resistance.

be the primary and secondary orientations of the crystal with respect to the tension. At the present time, it is only possible to arrange these experimental results of the effect of tension on the resistance of single bismuth crystals in a consistent set of curves without, however, giving any theoretical basis for the curves.

Experimental Arrangement

To measure the small changes in resistance involved, the compensated potentiometer method developed by Professor Bridgman,[3] was used. Fig. 1 gives the electrical connections of this method. The potential difference V_{AB} across the potential leads to the crystal AB is balanced against the potential fall V_{CD} of the supplementary compensating circuit Q, and, when the effect of the tension on the resistance is large enough, this in turn is balanced

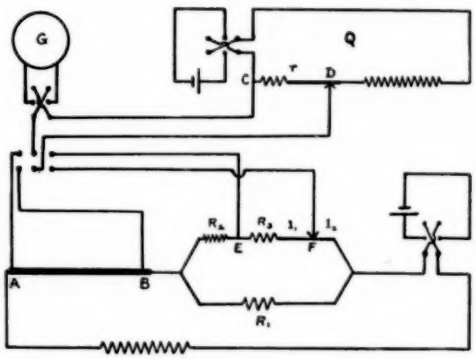

Fig. 1.

against the fall V_{EF}, so that the unknown resistance R_{AB} is calculable in terms of the known resistances R_1, R_2, R_3, l_1 and l_2. The fractional change in resistance is then

$$\Delta R/R = \Delta R_{AB}/R_{AB} = \Delta l/(l_1 + R_3) \qquad (1)$$

where the slide wire lengths are reduced to ohms. As Professor Bridgman has pointed out, the advantage of this method is that the result is independent of the current flowing through the crystal provided that that remains constant during a single reading. This is cared for by using a large and heavy 6-volt storage battery as the source of the current which was usually kept at about 0.45 amp. The largest value of the fraction $\Delta R/R$ actually measured was 22×10^{-4}. Inasmuch as the bismuth resistances themselves were less than 0.01 ohm, the precision of the method is very high. When the effect was too small to be measured by this *null* method, the average change in reading of the galvanometer due to the application of the tension was determined by reading the galvanometer alternately with and without the tension, plotting the observed readings against the time scale and finding the average distance between the two curves. Ideally, both curves should be straight horizontal lines, but the zero drift of the galvanometer, small changes in the voltage

[3] P. W. Bridgman, Proc. Amer. Acad. **56**, 61 (1921).

of the compensating circuit, and slight variations in temperature which produce in addition to small changes in resistance small thermal e.m.f.'s give rise to small drifts, as in Fig. 2, which is representative of the type of curve obtained in this way. The deflections in most cases were much greater than the drifts observed. These changes in galvanometer readings with tension are proportional to the changes in potential difference and thus to the resistance changes of the crystal, the constants of proportionality[4] depending in an easily ascertainable manner on the known e.m.f.'s and resistances of the circuit. This *deflection* method was used in each determination of the tension coefficient to check the linearity of the change of resistance with tension and was checked in the case of the greatest tension against the *null* method for absolute value.

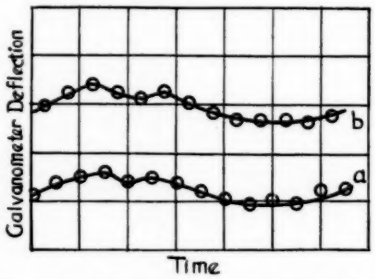

Fig. 2. *a* without tension; *b* with tension.

Since temperature fluctuations produce undesirable changes in the resistance to be measured, the crystal was mounted in a constant temperature bath of kerosene. This was thoroughly stirred and was kept at the constant temperature of approximately 30°C by means of a metal thermostat which, although it drifted slightly, prevented any large sudden change in temperature. In Fig. 3 is sketched the general arrangement of the crystal mounting and constant temperature bath. The heating coil is not shown in the figure, but is wound on a square frame larger than the brass box *mmmm* so that the heat source is not concentrated in one spot. The crystal itself AB is mounted on a brass support inside a heavy copper cylinder *pp* 5/32 inch thick, and this

[4] The voltage sensitivity of the galvanometer, which was made as great as possible by placing the scale about five meters from the galvanometer, varied with each value of the total crystal resistance. The reason for this is obvious. For, applying Kirchhoff's laws to the network, we have, where ΔE is the increase in V_{AB}, Δi_{CD} the change in current in CD produced by the lack of balance, and I_G the current through the galvanometer,

$$\Delta i_{CD} = I_G \tag{a}$$

a relation arising from the condition on current at the junction C, and

$$I_G R_G = (V_{AB})_0 + \Delta E - (V_{CD})_0 - \Delta i_{CD} r \tag{b}$$

arising from the condition on potential falls in the closed circuit $ABCD$. But $(V_{AB})_0$ and $(V_{CD})_0$ are the values of the potential falls for the balanced case and so are equal; hence

$$I_G R_G = \Delta E - I_G r. \tag{c}$$

The voltage sensitivity is consequently

$$\Delta E / I_G = R_G + r. \tag{d}$$

This method will then function with the maximum of ease, if r has approximately the value of the critical damping resistance of the galvanometer.

whole mounting is placed in air inside the brass box. The addition of the brass box seemed advisable, since in its absence it seemed impossible to stir the kerosene sufficiently inside the copper cylinder to insure constancy of temperature. With the addition of the brass box, erratic fluctuations in temperature were no longer observed.

The crystals used which were from $1\frac{1}{2}$ to 3 inches long and had a diameter of approximately $\frac{1}{8}$ inch, had all been made by Professor Bridgman from bismuth furnished by Kahlbaum, and were most generously put by him at the writer's disposal. He had previously used these same crystals in his determination of the specific resistance of bismuth crystals and of their

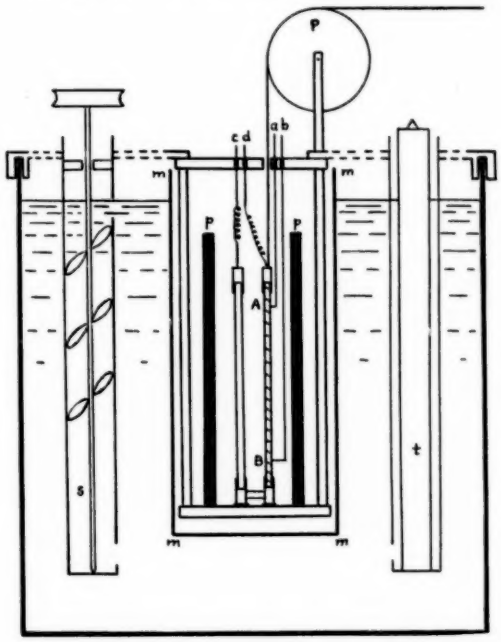

Fig. 3. *AB* crystal; *a*, *b* potential leads; *c*, *d* current leads; *pp*, copper cylinder; *mmmm* brass box; *s* stirrer; *t* metal thermostat (shown without amplifying levers); *P* pulley.

hydrostatic pressure coefficient of resistance.[1] These crystals were soft-soldered into brass holders at either end, one of which holders was fastened firmly to the large brass support which held the Bakelite pulley *P* over which the string carrying the tension passed. Fine copper wires of 0.01 inch diameter were soft-soldered to the crystal a few millimeters from each end for potential leads and a thermocouple was soldered close to one end. The other end of this thermocouple was inserted in the kerosene and so enabled one to know when the crystal temperature had come to that of the kerosene; with the air layer between the brass box and the crystal, coming to equilibrium was a slow process and at least an hour was required before equilibrium was obtained. The string carrying the tension passed over another pulley near the galvanometer telescope; weights were hung on a steel spring attached to this end. The steel spring prevented the sudden application of the whole tension

to the crystal. In view of the low elastic limit (22.1 kg/cm² shearing stress across the principal cleavage plane)[5] of single bismuth crystals, 1200 grams was the greatest force applied with crystals of the given cross section, or about 15–20 kg/cm².

Results

Forty-five single bismuth crystals of different orientations were studied, the adiabatic tension coefficient of resistance β at 30°C being determined in each case. This coefficient is defined as the ratio of the change in resistance produced by a tension of 1 kg/cm² to the total resistance. It is adiabatic in that the time intervals between consecutive applications of the tension were about one minute, so that each reading was taken within half a minute of the establishment of the new state. This short interval would not allow for the establishment of thermal equilibrium. On the basis of an adiabatic process

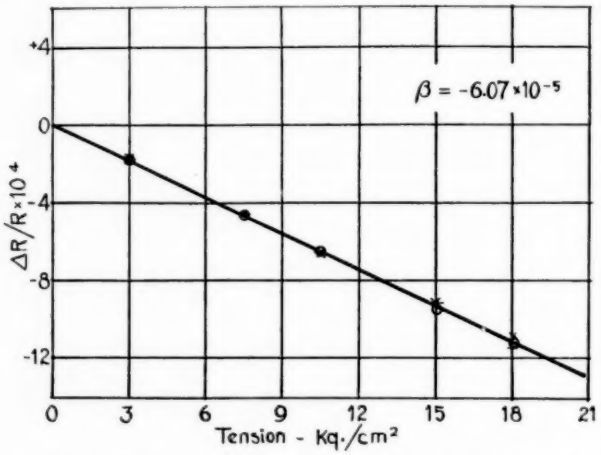

Fig. 4. Circles, plus signs and crosses signify different days' readings.

taking place, the change of temperature arising from the sudden application of the maximum tension comes out by computation to be about —0.006°C. Since the temperature coefficient of resistance of bismuth crystals is 0.00445, this change of temperature produces a relative change in the resistance of -0.27×10^{-4} which corresponds to a change in the computed value of the coefficient β of about -0.18×10^{-5} in each case, the correction to be subtracted in passing from the adiabatic to the isothermal case. Furthermore, no correction was made for the change in resistance arising from the change in dimensions caused by the application of the tension. This varies with the orientation of the crystal, but the correction of the tension coefficient β was always less than -0.4×10^{-5}. Both these corrections were usually negligible with respect to the values of the coefficient actually found and were always of the same order of magnitude as the experimental errors to be expected.

Fig. 4 shows the value of $\Delta R/R$ for a given crystal taken on different days with different tensions and with different distances between the potential

[5] Georgieff and Schmid, Zeits. f. Physik **36,** 759 (1926).

leads. The linearity of the relation between $\Delta R/R$ and the tension applied is clearly in evidence as well as the fact that the experiments under different conditions gave entirely consistent results. It was further checked that the value of the coefficient was independent of the direction and magnitude of the current through the crystal. The specific resistance was determined roughly in every case and with a few exceptions came within 1 percent of Professor Bridgman's value for the given orientation; the dimensions of the crystals, particularly the distance between the potential leads, were not found with sufficient accuracy to warrant any better check.

The tension coefficient of resistance of a given single bismuth crystal was thus shown to be independent of the experimental variables, and so to be a constant characteristic of the given crystal; but in different crystals it varied with the orientation of the cleavage planes of the crystal with respect to the direction of the electric current. In these experiments the crystals were all cylindrical in shape with a diameter much smaller than the linear length; the direction of the electric current coincided with that of the axis of this cylinder and with the direction of the tension. The orientation of the crystal with respect to the axis of the cylinder can be defined in terms of two angles, θ and ϕ. The angle θ determines the orientation of the principal cleavage plane (111) which is perpendicular to the trigonal axis of the crystal and is defined as the angle between the normal to the principal cleavage plane and the longitudinal cylindrical axis of the crystal. The angle ϕ determines the orientation of a secondary cleavage plane with respect to the principal cleavage plane and the cylindrical axis. If the crystal is split along a principal cleavage plane, the section obtained is elliptical in shape. The major axis of this ellipse is the intersection of the plane through the normal to the principal cleavage plane and the cylindrical axis of the crystal with the principal cleavage plane. On the surface of this ellipse are found fine lines making angles of 60° with each other; these are the intersections of secondary cleavage planes with the principal cleavage plane. If the crystal be cleaved along one of these lines, the normal to the new cleavage plane will be found to make either an angle of 71° with that of the principal cleavage plane, or an angle considerably greater than 90°.[6] Those planes making angles of 71° are the ones to be considered. The angle ϕ is then to be defined as the angle between the projection on the principal cleavage plane of the normal to this secondary cleavage plane and the major axis of the elliptical section of the principal cleavage plane. Since bismuth has trigonal symmetry, these secondary planes will recur every 120°; and if the change in resistance depends on the orientation of these secondary planes, it should show a periodicity of 120°. It is to be noted that the angle ϕ as measured at one end of the crystal is, because of the known symmetry of the bismuth crystal, the negative of that measured at the other end, and hence it is impossible to differentiate between ϕ and $-\phi$, or between ϕ and $120-\phi$, since the tension is double-headed and always

[6] The writer is indebted to Professor Charles Palache of the Department of Mineralogy and Petrography of Harvard University for pointing out to her the characteristics of bismuth crystals here described.

involves two forces which are opposite in direction but equal in magnitude and act on the two ends of the crystal. Thus if the values of the tension coefficient are found between 0° and 60°, those between 60° and 120° are immediately known. With these definitions of the angle determining the orientation of the crystal with respect to the direction of the electric current, crystals having approximately the same orientations gave consistent values for β;

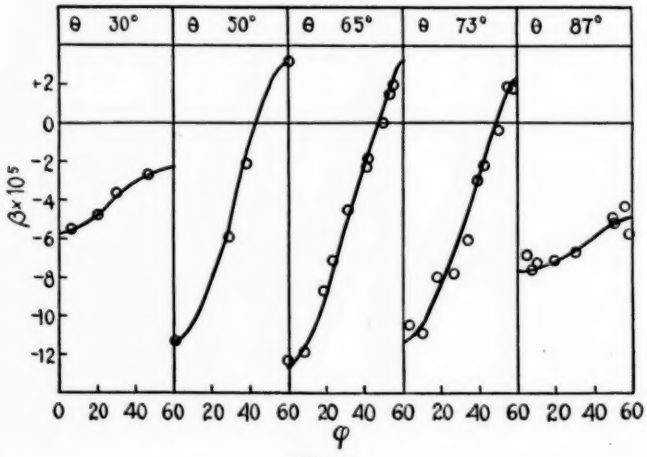

Fig. 5.

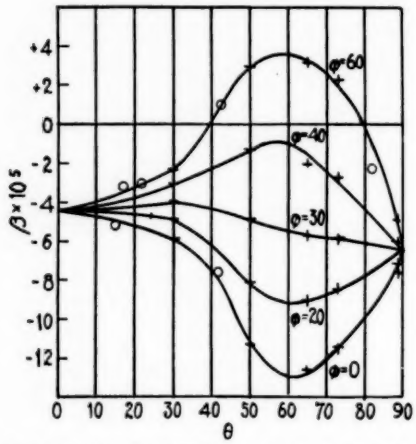

Fig. 6. Plus signs indicate points interpolated from Fig. 5; circles indicate additional points given directly by experiment.

e.g., one crystal defined by $\theta=63°$ and $\phi=9°$ gave β as -11.82×10^{-5} while another with $\theta=69°$ and $\phi=9°$ gave -11.83×10^{-5}. The angle ϕ was not determined to better than 5° and θ was uncertain to half that amount; hence this agreement is satisfactory.

The dependence of the tension coefficient β on θ and ϕ may be plotted in two ways: (1) giving β as a function of ϕ with θ constant, Fig. 5; and (2) giving β as a function of θ with ϕ constant, Fig. 6. In Fig. 5, thirty-eight of the forty-five experimental points were plotted in five groups, each group

containing the points for which θ was approximately that of the group. The 50° group, for instance, was composed of four observations, for $\theta = 50°$, 54°, 50° and 50°. There was an even greater divergence in values for the other groups, which gives one good reason why the points do not lie directly on a smooth curve; the 65° group, for instance, includes orientations of 60° to 69°, although the greater number of observations are nearer the mean value. Seven observations lay too far from any one of the group values to be included in Fig. 5, but six of these, indicated by circles, fell readily into Fig. 6. Except for these points, Fig. 6 was plotted by interpolation from Fig. 5. One point for $\theta = 41°$ and $\phi = 47°$ could not be fitted into either figure, but when its value of $+0.35 \times 10^{-5}$ is considered in the light of Fig. 6 it is seen to be fairly

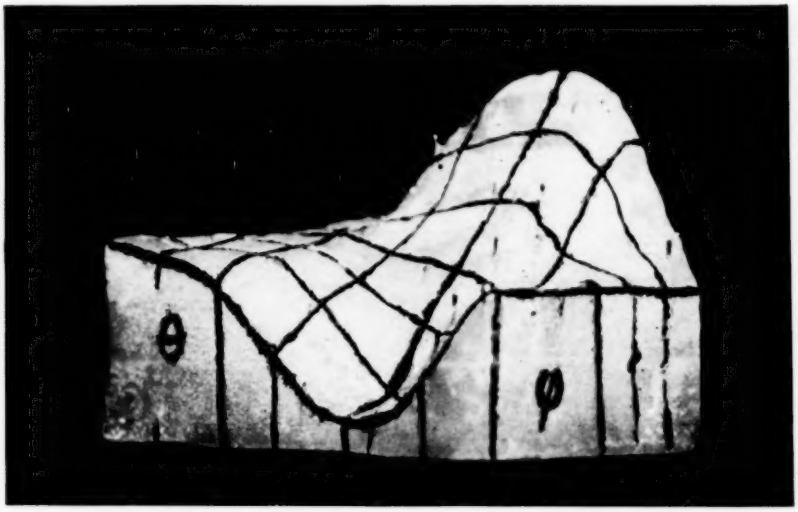

Fig. 7. Three-dimensional model of the variation of β with θ and ϕ. θ increases from left to right from 0° to 90°, intermediate lines being drawn every 15°. ϕ increases from front to back from 0° to 60°, intermediate lines being drawn every 10°. It is to be noted that the intersection of the surface with the plane $\theta = 90°$ gives a very nearly horizontal line and so leads to the conclusion that β (represented by the vertical heights of the model) is independent of ϕ for $\theta = 90°$.

consistent with the curves shown there. Since in plotting the results separately with respect to θ and ϕ, only approximate orientations could be used for each point, it was deemed desirable to plot the coefficient directly as a function of the two variables in the form of a solid model, Fig. 7. This showed nothing very different from the information given by Figs. 5 and 6, although it seemed to point more clearly to the probability that the coefficient is completely independent of the secondary orientation for $\theta = 90°$.

In studying Fig. 5, which gives the dependence on ϕ of the tension coefficient of resistance for crystals with θ constant, it is immediately seen that the coefficient β has trigonal symmetry since, with ϕ and $120 - \phi$ indistinguishable, the curves must be symmetrical about 60° and return to the 0° values at 120°. Furthermore, β depends very markedly on the secondary

orientation ϕ. For instance in the case of $\theta=65°$, it varies from -12.6×10^{-5} at $\phi=0°$ to $+3.5\times10^{-5}$ at $\phi=60°$. This variation is interesting, both as regards magnitude and sign. Bismuth is abnormal in that the tension coefficient for the polycrystalline form is negative, but as shown in Fig. 5 for certain orientations of single crystals it becomes positive. It is further to be noted that when θ is close to 0° or to 90°, β varies less with the orientation of the secondary cleavage plane. At small angles of θ, this is to be expected, for in the limiting case of $\theta=0$, the elliptical cross section becomes circular so that ϕ is entirely indeterminate. Or considering it from a physical point of view, in this case the tension is applied perpendicular to the principal cleavage plane and so does not deform the elementary triangles or hexagons formed on the surface by the intersections of the secondary with the principal cleavage planes; thus the same change of symmetry will occur irrespective of the orientation of the secondary planes. Thus symmetry demands that for $\theta=0°$ β be independent of ϕ. For $\theta=90°$ it is more difficult to understand why the effect should not depend on the angle ϕ, since symmetry does not here demand any such independence of ϕ. In this case the elliptical cross section has become indefinitely elongated and consequently has the well-defined direction of the axis of the cylinder. It would appear that the tension would change the symmetry of the elementary triangles or hexagons differently depending on their position relative to the axis of the cylinder. Experimentally, however, there is found little or no variation of the coefficient with ϕ when the principal cleavage plane is parallel to the axis of the crystal. The evidence, although not conclusive, is in the direction that the coefficient is independent of ϕ at $\theta=90°$. This appears more clearly in Figs. 6 and 7. The points are not sufficiently numerous at either $\theta=0°$ or 90° to determine the limiting values with a high degree of accuracy. However, there seems to be little doubt that at $\theta=0$, β is somewhat less negative than it is at $\theta=90°$. There is some evidence from these curves that the tangent to these curves becomes horizontal at $\theta=60°$; in most cases this means a minimum or maximum, but for $\phi=30°$ it would seem to indicate a point of inflection only. The rapid variation of β with θ near 90° explains the comparatively wide scattering of the points in Fig. 5 for $\theta=87°$.

The fact that the tension coefficient varies so much with the orientation of the crystal may explain the discordance of the various values of β found for polycrystalline bismuth by different observers. Table I gives the various

TABLE I.

Williams[7]	-5.35×10^{-5} per kg/cm²
Zavattiero[8]	−4.25 "
	−3.30 "
Bridgman[9]	−4.66 "
	−2.92 "
Rolnick[10]	−2.81 "

[7] W. Ellis Williams, Phil. Mag. **13,** 635 (1907).
[8] E. Zavattiero, Rend. Accad. Lincei **29,** (1), 48 (1920).
[9] P. W. Bridgman, Proc. Amer. Acad. **57,** 41 (1922).
[10] Harry Rolnick, Phys. Rev. **35,** 506 (1930).

values found. The discrepancies are far greater than can be accounted for by experimental error. It is reasonable to assume that the procedure of each of these observers in producing the specimen of bismuth was such as to emphasize different crystalline orientations in the polycrystalline pieces; such an assumption would be sufficient to explain the differences observed.

The hydrostatic pressure coefficient for bismuth single crystals[1] is for $\theta=0°+2.45\times10^{-5}$ and for $\theta=90°+7.5\times10^{-5}$; these are of the same order of magnitude as the tension coefficients found here. The sign of the pressure coefficient is positive and hence abnormal for pressure, in the same way that a negative coefficient is abnormal for a tension effect.

Conclusion

In this study of the tension coefficient of resistance in single bismuth crystals at 30°C, where the tension has been applied parallel to the axis of the cylinder in which the crystal is cast and along which the current flows, the coefficient has been found to depend both on the orientation of the principal cleavage plane and of the secondary cleavage planes with respect to the axis of this cylinder. For $\theta=0°$ and $\theta=90°$, this coefficient is apparently very little dependent on the orientation of the secondary cleavage planes, whereas for θ close to 60° its dependence on the orientation of the secondary cleavage planes becomes a maximum. This variation involves a change in sign as well as in magnitude, so that for certain orientations the coefficient becomes positive instead of remaining negative. The coefficient shows trigonal symmetry, as it must if it is to be consistent with the corporeal trigonal symmetry of the bismuth crystal.

This paper has been successful, therefore, in finding empirical relations between the tension coefficient of resistance and the orientations of the principal and secondary cleavage planes. To make the solution of the problem complete, a physical theory should be formulated to predict the relations found. However, progress would be made if a formal geometrical theory could be established which would permit the results to be expressed in terms of the parameters θ and ϕ and of three or more unknown but determinable constants. Further experimental work is planned in this field with other crystals of the same type of symmetry, of different types of symmetry, and possibly at radically different temperatures.

It is a pleasure to thank the Director of the laboratory and the authorities of Harvard University for the privilege of working in the Research Laboratory of Physics, and Professor P. W. Bridgman for the suggestion of the problem itself and also of practical details involved in carrying the work to completion.

The Effect of Homogeneous Mechanical Stress on the Electrical Resistance of Crystals

By P. W. BRIDGMAN
Harvard University

(Received October 24, 1932)

It is shown from general considerations of symmetry that the effect of homogeneous mechanical stress on the electrical resistance of a conducting crystal can be expressed in terms of a set of constants, the number of which is equal to the number of elastic moduli, and which connect the resistance with stress by equations very much like the equations connecting strain with stress, except for the difference of a factor 2 in some of the terms. The results are explicitly applied to the case of bismuth, and formulas developed for the change of resistance of a rod cut from the crystal in any direction when subjected to a longitudinal tension. The formulas are checked against the recent experimental results of Miss Allen for bismuth, and agreement found within the limits of error. It is shown that tension measurements alone do not permit an evaluation of all the constants, but if the tension measurements are supplemented by measurements of the effect of hydrostatic pressure in two independent directions, the six constants are then completely determined. Numerical values of the six constants are given for bismuth. Finally the geometrical meaning of the coefficients is briefly discussed and attention called to an effect produced by stress in crystals which is the analogue of the Hall effect produced by a magnetic field in isotropic materials.

IN SPITE of the great amount of work published on the necessary formal geometrical symmetry of all sorts of physical phenomena in crystals, as, for example, most extensively set forth in W. Voigt's *Lehrbuch der Kristallphysik*, the question of the effect of general mechanical stress on the electrical resistance of crystals has not yet been examined. Doubtless the reason for this is that up till now the only such effects which have been studied experimentally are the effects of hydrostatic pressure, and here the symmetry relations are so simple as to be almost intuitively evident. The first experimental attack on the general question has now been made, however, by Miss Allen,[1] who has measured the effect of mechanical tension on the resistance of single crystal rods of bismuth of different orientations. The time is therefore ripe for an examination of the formal symmetry relations, and in particular the number of physical constants necessary to completely characterize the current flow in a conducting crystal subjected to the most general sort of homogeneous mechanical stress. It is obviously not necessary to complicate the problem by considering non-homogeneous stress, for the solution in any such case may be obtained by an integration of the effects in infinitesimal homogeneous elements.

It is natural to attempt to construct a general geometrical theory along the lines suggested in Voigt's book, but a slavish following of pattern is not quite possible because this problem is more complicated than any treated

[1] Mildred Allen, Phys. Rev. **42**, 848 (1932).

by Voigt. Here we are concerned with the cooperation of four factors; within the crystal the three factors, current vector, potential gradient vector (in general not in the same direction as the current vector), and stress tensor must be connected with the fourth factor, the physical constitution of the crystal, which is to be represented by an array of coefficients, in such a way as to be consistent with the symmetry of vectors, tensor, and crystal.

By splitting the problem into two parts, the methods of Voigt may be applied. Consider first the relation between current vector, q, and potential gradient, E. The most general linear relation (we assume of course Ohm's law), expresses E as a linear vector function of q. This involves nine coefficients. Experimentally, however, these nine coefficients are always found to reduce to six, the so-called rotary terms being absent. Since there is no reason to suppose that mechanical stress will so essentially modify the constitution of the crystal as to call into existence rotary terms, six coefficients will be assumed to suffice for this analysis. Further experimental justification of this assumption will be afforded by the agreement with experiment in the case of bismuth. We shall have then:

$$\left.\begin{aligned} E_x &= r_{11}q_x + r_{12}q_y + r_{13}q_z \\ E_y &= r_{12}q_x + r_{22}q_y + r_{23}q_z \\ E_z &= r_{13}q_x + r_{23}q_y + r_{33}q_z\ . \end{aligned}\right\} \qquad \text{(A)}$$

A relation of this form holds in general, whether or not there is a stress acting. Now specialize the coefficients above, defining them as those valid in the absence of stress. If a stress is allowed to act, the effect will be to somewhat change the coefficients, so that when the stress is acting we shall have:

$$\left.\begin{aligned} E_x &= (r_{11} + \delta r_{11})q_x + (r_{12} + \delta r_{12})q_y + (r_{13} + \delta r_{13})q_z \\ E_y &= (r_{12} + \delta r_{12})q_x + \text{etc.} \\ E_z &= (r_{13} + \delta r_{13})q_x + \text{etc.} \end{aligned}\right\} \qquad \text{(B)}$$

The problem is now to determine the most general form allowable for the δr's as a function of the stress (restricting ourselves to the linear terms), which shall be consistent with all the symmetry requirements. It is proved in Voigt that the coefficients above have the geometrical nature of the components of a tensor (understanding by tensor the sort of thing of which an ordinary mechanical stress is the simplest example). It follows that the δr's must also be tensor components. The problem reduces, therefore, to finding the most general tensor a linear function of the applied stress which shall be consistent with the symmetry of the crystal. The strain produced by the stress at once springs to mind. But the actual strain is not quite a tensor, and so does not answer the requirements. It is proved in Voigt, however, that a slightly modified strain is in character a tensor, that is, the aggregate of six quantities obtained by leaving unchanged the three strain components with equal indices, and by dividing by 2 the three shearing components of strain with unlike indices.

The solution, therefore, is now in our hands. Build up from the stress a set of quantities involving coefficients entering in the same way as the coefficients which determine the ordinary elastic strains as a function of stress, except that the constants in the terms analogous to the shearing strains must be divided by 2. This completes the formal solution, since, given the stress, we can now compute the δr's, and then the equations determine E completely as a function of q, so that the particular connections between E and q which may be expressed in terms of resistance may also be computed under any desired conditions. In particular, we have found that the number of constants necessary to completely define resistance is equal to the number of ordinary elastic constants, 21 at a maximum.

As an illustration of this general analysis I now apply it to the case of bismuth, eventually coming out with the numerical values of the coefficients. The starting point is the relation between strain and stress. The necessary information is on page 585 of Voigt's book, 1928 printing, noticing, however, that our scheme calls for the use of the elastic moduli as distinguished from the elastic constants, which Voigt tabulates, and that this change of itself introduces a factor 2 in certain places. Following the instructions above we now obtain:

$$\left.\begin{aligned}
\delta r_{11} &= \rho_{11}X_x + \rho_{12}Y_y + \rho_{13}Z_z + \rho_{14}Y_z \quad 0 \quad 0\\
\delta r_{12} &= \rho_{12}X_x + \rho_{11}Y_y + \rho_{13}Z_z - \rho_{14}Y_z \quad 0 \quad 0\\
\delta r_{33} &= \rho_{13}X_x + \rho_{13}Y_y + \rho_{33}Z_z \quad 0 \quad 0 \quad 0\\
\delta r_{23} &= \tfrac{1}{2}\rho_{14}X_x + \tfrac{1}{2}\rho_{14}Y_y \quad 0 + \tfrac{1}{2}\rho_{44}Y_z \quad 0 \quad 0\\
\delta r_{31} &= 0 \quad 0 \quad 0 \quad 0 \quad \tfrac{1}{2}\rho_{44}Z_x + \rho_{14}X_y\\
\delta r_{12} &= 0 \quad 0 \quad 0 \quad 0 \quad \rho_{14}Z_x + (\rho_{11} - \rho_{12})X_y
\end{aligned}\right\} \qquad \text{(C)}$$

in which 6 stress-resistance coefficients appear, which, of course, have no numerical relation to the elastic coefficients, but only a formal relation. In this scheme the Z axis is the axis of trigonal symmetry, and the X axis is the axis of two-fold rotational symmetry in the basal plane.

Furthermore it is known that with this choice of axes the resistance coefficients of equations (A) reduce to 2 only, r_{11} and r_{33}. The connection between E and q therefore becomes:

$$\left.\begin{aligned}
E_x &= (r_{11} + \delta r_{11})q_x + \delta r_{12}q_y + \delta r_{13}q_z\\
E_y &= \delta r_{12}q_x + (r_{11} + \delta r_{22})q_y + \delta r_{23}q_z\\
E_z &= \delta r_{13}q_x + \delta r_{23}q_y + (r_{33} + \delta r_{33})q_z.
\end{aligned}\right\} \qquad \text{(D)}$$

This solution is now to be applied to the case of a slender cylindrical rod cut from the crystal in any direction, making angles α, β, and γ with the X, Y, Z axes. The cross section of the rod may be of any shape. The current q has access to the rod only through electrodes at the two ends, so that within the rod the current flow is entirely along the rod, with no transverse components. This gives $q_x = q\cos\alpha$ etc., and hence:

$$\left.\begin{aligned} E_x &= q[(r_{11}+\delta r_{11})\cos\alpha + \delta r_{12}\cos\beta + \delta r_{13}\cos\gamma] \\ E_y &= q[\delta r_{12}\cos\alpha \qquad \text{etc.} \qquad] \\ E_z &= q[\delta r_{13}\cos\alpha \qquad \text{etc.} \qquad]. \end{aligned}\right\} \tag{E}$$

In general, E has components transverse to the rod, but it is only the component along the rod which determines the measured resistance. The resistance is obviously $R=(E_x\cos\alpha+E_y\cos\beta+E_y\cos\gamma)/q$, or:

$$R = (r_{11}+\delta r_{11})\cos^2\alpha + (r_{11}+\delta r_{22})\cos^2\beta + (r_{33}+\delta r_{33})\cos^2\gamma + 2\delta r_{23}\cos\beta\cos\gamma + 2\delta r_{31}\cos\gamma\cos\alpha + 2\delta r_{12}\cos\alpha\cos\beta. \tag{F}$$

Next consider the effect of a mechanical tension T applied along the rod. The stress system thereby produced within the rod must satisfy the following conditions:

$$\left.\begin{aligned} X_x\cos\alpha + X_y\cos\beta + X_z\cos\gamma &= T\cos\alpha \\ X_y\cos\alpha + Y_y\cos\beta + Y_z\cos\gamma &= T\cos\beta \\ X_z\cos\alpha + Y_z\cos\beta + Z_z\cos\gamma &= T\cos\gamma \end{aligned}\right\} \tag{G}$$

and

$$\left.\begin{aligned} X_x\cos\alpha' + X_y\cos\beta' + X_z\cos\gamma' &= 0 \\ X_y\cos\alpha' \qquad + \text{etc.} \qquad &= 0 \\ X_z\cos\alpha' \qquad + \text{etc.} \qquad &= 0 \end{aligned}\right\} \tag{H}$$

where α', β', and γ' are any direction angles satisfying the condition

$$\cos\alpha'\cos\alpha + \cos\beta'\cos\beta + \cos\gamma'\cos\gamma = 0. \tag{I}$$

The conditions (G) come from the requirement that the force across any plane perpendicular to the length of the rod must be T, perpendicular to this plane, and the conditions (H) from the requirement that there is no external force acting across any lateral surface of the rod. By reflecting that the stress quadric in this case reduces to a couple of planes, the solution may be found almost by inspection, and is:

$$\begin{aligned} &X_x = T\cos^2\alpha, \qquad Y_y = T\cos^2\beta, \qquad Z_z = T\cos^2\gamma, \\ &Y_z = T\cos\beta\cos\gamma,\ Z_x = T\cos\gamma\cos\alpha,\ X_y = T\cos\alpha\cos\beta. \end{aligned} \tag{J}$$

The δr's now assume the values:

$$\left.\begin{aligned} \delta r_{11} &= T[\rho_{11}\cos^2\alpha + \rho_{12}\cos^2\beta + \rho_{13}\cos^2\gamma + \rho_{14}\cos\beta\cos\gamma] \\ \delta r_{22} &= T[\rho_{12}\cos^2\alpha + \rho_{11}\cos^2\beta + \rho_{13}\cos^2\gamma - \rho_{14}\cos\beta\cos\gamma] \\ \delta r_{33} &= T[\rho_{13}\cos^2\alpha + \rho_{13}\cos^2\beta + \rho_{33}\cos^2\gamma] \\ \delta r_{23} &= T[\tfrac{1}{2}\rho_{14}(\cos^2\alpha - \cos^2\beta) + \tfrac{1}{2}\rho_{44}\cos\beta\cos\gamma] \\ \delta r_{31} &= T[\tfrac{1}{2}\rho_{44}\cos\alpha\cos\gamma + \rho_{14}\cos\alpha\cos\beta] \\ \delta r_{12} &= T[\rho_{14}\cos\alpha\cos\gamma + (\rho_{11}-\rho_{12})\cos\alpha\cos\beta]. \end{aligned}\right\} \tag{K}$$

The material is now at hand for substituting in the expression (F) for R. Comparison with experiment will be simplified by introducing two new

angles. Project the length of the rod on the basal plane and denote the angles between this projection and the X and Y axes by α'' and β'', where $\cos\alpha'' = \cos\alpha/(\cos^2\alpha+\cos^2\beta)^{1/2}$, and $\cos\beta'' = \cos\beta/(\cos^2\alpha+\cos^2\beta)^{1/2}$. Substitution gives, after some simple reductions, for the tension coefficient of resistance:

$$K_T \equiv \frac{1}{T}\frac{\Delta R}{R_0}$$
$$= \frac{\rho_{11}\sin^4\gamma+(\rho_{44}+2\rho_{13})\cos^2\gamma\sin^2\gamma+\rho_{33}\cos^4\gamma-2\rho_{14}\cos\gamma\sin^3\gamma\cos 3\beta''}{r_{11}\sin^2\gamma + r_{33}\cos^2\gamma}. \quad \text{(L)}$$

Notice that the constant ρ_{12} has cancelled, and ρ_{44} and ρ_{13} enter only through the combination $\rho_{44}+2\rho_{13}$. Tension measurements are, therefore, not sufficient to exhaustively determine the coefficients, but at most only four relations between the six coefficients can be fixed by such measurements. Explicitly, by appropriately varying the orientation, the constants ρ_{11}, ρ_{33}, and ρ_{14} may be determined, and the combination $\rho_{44}+2\rho_{13}$. Furthermore, K_T is seen to have three-fold symmetry about the Z axis, as insured by the term in $\cos 3\beta''$. This, of course, is necessary, and constitutes one check on the correctness of the analysis. Another important feature is that K_T has complete rotational symmetry (that is, the term in β'' vanishes) both when the rod is parallel to the trigonal axis and when it is in the basal plane. That this must be the case when the length is along the trigonal axis is evident from most elementary symmetry considerations, but it is not so easily obvious that the coefficient should be independent of orientation in the basal plane. This latter fact was found experimentally by Miss Allen, and was looked on as one of the important results of the paper, although at the time it did not appear whether this was general, or only a fortuitous result for bismuth. The relation now appears necessary for any crystal of the same symmetry as bismuth.

The two remaining relations necessary to completely determine the six constants must be determined by the imposition of other kinds of stress. The simplest is a hydrostatic pressure, and the calculations can be made at once for this case. The stress system is $X_x = Y_y = Z_z = -P$, $Y_z = Z_x = X_y = 0$.

If the rod is cut parallel to the Z axis:

$$\left(\frac{1}{P}\frac{\Delta R}{R_0}\right)_{\parallel} = -\frac{2\rho_{13}+\rho_{33}}{r_{33}}, \quad \text{(M)}$$

and when the rod is perpendicular to the Z axis, parallel to the basal plane:

$$\left(\frac{1}{P}\frac{\Delta R}{R_0}\right)_{\perp} = -\frac{\rho_{11}+\rho_{12}+\rho_{13}}{r_{11}}. \quad \text{(N)}$$

Examination shows at once that these two additional relations permit explicit solution for the remaining coefficients, so that the six coefficients may be completely determined in terms of tension measurements on four orientations and hydrostatic pressure measurements on two orientations.

The detailed data of Miss Allen permit further check of the above expression for K_T. Such a check may be made in various ways. For example, at constant γ the variation of K_T with β'' may be studied. The formula demands that the variable part of K_T be proportional to cos $3\beta''$. Miss Allen's Fig. 5 exhibits the coefficients in this way, and inspection will show that within the limits of experimental error each of the curves of Fig. 5 has the shape of a cosine curve. (Her ϕ and θ are the β'' and γ of this paper respectively.) It may be taken, therefore, that the geometrical theory checks sufficiently well against experiment.

The numerical coefficients may now be computed. The tension coefficients are given in Miss Allen's paper. The pressure coefficients I have found[2] to be 1.05×10^{-5} for $\gamma=90°$, and 2.03×10^{-5} for $\gamma=0°$. The specific resistance I have also found to be $r_{11}=114.0\times10^{-6}$ and $r_{33}=144.2\times10^{-6}$. All these values are at 30°C. The numerical coefficients are now found:

$$\rho_{11} = -7.7\times10^{-9},\ \rho_{33} = -6.6\times10^{-9},\ \rho_{12} = +5.6\times10^{-9}$$
$$\rho_{13} = +1.8\times10^{-9},\ \rho_{14} = +31.3\times10^{-9},\ \rho_{44} = -12.3\times10^{-9}.$$

The stress unit is 1 kg/cm². In this computation the corrections for change of dimensions and of angle with stress are neglected. These corrections are just about on the margin of experimental error.

Finally, it is interesting to go back and examine the geometrical significance of the various coefficients by determining what sort of simple measurement would give the isolated coefficient. ρ_{33} and ρ_{11} have already been dealt with, and are directly determined in terms of the tension coefficient of rods parallel and perpendicular to the trigonal axis. The coefficients ρ_{12} and ρ_{13} determine transverse components of e.m.f. when current flows lengthwise in a rod subjected to tension acting lengthwise. For example, if a rod is cut parallel to the Y (or X) axis, and a current passed lengthwise of the rod, then when a tension is applied along the rod, a transverse component of e.m.f. will appear along the X (or Y) axis which determines ρ_{12}. The other cross coefficient ρ_{13} has similar significance with a proper change of letters. The term ρ_{14} points to a formal analogy in crystals to the Hall effect in isotropic metals, the magnetic field being replaced by a compressional force. If a rod of rectangular section is cut with its length along the Z axis and with the X and Y axes along the sides of the rectangular section, and if a current is passed lengthwise of the rod, then a transverse e.m.f. along the Y axis will appear if a compression along the X axis is applied between the opposite faces of the section. Finally, if a bar of rectangular section is cut along the X axis and a shearing stress Y_z is applied to the sides of the bar distorting the cross section, and if a transverse current is led between opposite faces along the Z axis, an e.m.f. between the other two faces is produced by the shearing stress, the magnitude of the effect being determined solely by ρ_{44}.

[2] P. W. Bridgman, Proc. Amer. Acad. **63**, 351 (1929).

Reflection of Metallic Atoms from Alkali Halide Crystals*

By ROBERT REX HANCOX
Department of Physics, Olivet College, Olivet, Michigan

(Received October 26, 1932)

The scattering of molecular beams of mercury from crystals of lithium fluoride, lithium chloride, sodium fluoride, and potassium iodide has been studied as a function of crystal and beam temperatures. A similar study has been made of the scattering of a molecular beam of cadmium from sodium chloride crystals. In all cases a quasi-specular beam of the type reported by Zahl and Ellett (Phys. Rev. **38**, 977 (1931)) for other alkali halide crystals was observed, with the same characteristic temperature changes. Former failures to detect a directed beam in the case of mercury scattered from potassium iodide were shown to have been due to moisture on the crystal surface. The relative number of atoms in the directed beam has been found to decrease with time at low crystal temperatures.

INTRODUCTION

BEAMS of heavy atoms and molecules whose de Broglie wave-lengths, at ordinary thermal velocities, are small compared to crystal spacings do nevertheless when incident upon certain crystals give rise to an apparently coherent scattering.[1,2,3,4] A beam of cadmium atoms incident upon a rock-salt crystal is not simply absorbed and more or less quickly reevaporated, for this would result in a random distribution of atoms leaving the crystal surface. Only in the case of mercury and certain alkali halide crystals has this scattering been studied in detail. The use of the ionization gauge to determine the spacial distribution of mercury atoms scattered from alkali halide crystals revealed a dependence of the relative probabilities of random and directed scattering and of the direction of maximum intensity in the directed beam upon crystal and beam temperatures. This had not been observed in earlier studies carried out by the condensation method.

The only obstacle to the application of the ionization gauge with other heavy atoms, such as cadmium, is their lower vapor pressure which makes condensation in the gauge more likely. However as it is never necessary to build up a pressure in the ionization gauge greater than say 10^{-5} mm of mercury this obstacle is not a very serious one. The gauge has been used to study the scattering of cadmium from sodium chloride crystals. The phenomena observed in the scattering of mercury from these crystals are observed with cadmium also. The anomalous behavior of potassium iodide re-

* A thesis submitted in partial fulfillment of the requirements for the degree of doctor of philosophy in the department of physics in the graduate college of the State University of Iowa, August, 1932.

[1] A. Ellett and H. Olson, Phys. Rev. **31**, 645 (1928).

[2] A. Ellett, H. Olson and H. Zahl, Phys. Rev. **34**, 493 (1929).

[3] H. A. Zahl, Phys. Rev. **36**, 893 (1930).

[4] H. A. Zahl and A. Ellett, Phys. Rev. **38**, 977 (1931).

ported by Zahl and Ellett has been found to be due to the effect of moisture upon the crystal surface. Crystals of lithium fluoride, sodium fluoride, and lithium chloride, not previously available have been used with an incident beam of mercury atoms. Lithium fluoride is found to indicate especially clearly the existence of both directed and random scattering.

Apparatus

The apparatus, shown in Figs. 1 and 2, is essentially the same as that used by Zahl and Ellett,[4] the only major modification being that the gauge and crystal are mounted on the same rigid metal support. This change was made

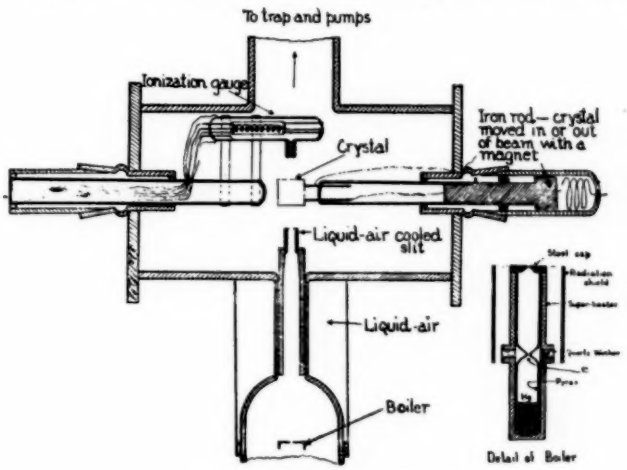

Fig. 1. Diagram of apparatus.

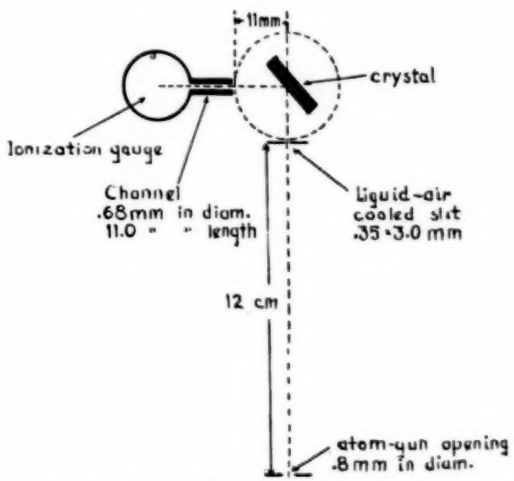

Fig. 2. Essential details of beam system.

to avert the possibility of the gauge and crystal changing their positions after being lined up. The dimensions of the slit defining the incident beam, and the gauge opening were also changed somewhat in order to obtain greater resolving power.

In the use of the apparatus it is necessary that the area on the face of the crystal which is illuminated by the incident beam shall remain stationary as the crystal is rotated, and that the gauge opening shall point directly at this illuminated spot for all positions of the gauge. In order for these conditions to obtain, the axes of rotation of the gauge holder and the crystal holder must be co-linear, and the illuminated area on the crystal face must lie on this common axis of rotation. The proper relative positions of the gauge and crystal were found by placing a closely fitting needle, equal in length to the radius of the circle about which the gauge rotates, into the cylindrical gauge opening and adjusting the relative positions of the gauge and crystal until the point of the needle remained stationary on the crystal face for all positions of the gauge and crystal. Once fixed, this adjustment was permanent since both gauge and crystal were mounted on the same support. The proper positions of the boiler opening and the slit relative to the crystal were found by placing a source of light 1 mm in diameter directly below the slit, the support on which the gauge and crystal were mounted was moved until a beam of light from this source reflected from the crystal face passed into the gauge for all positions of the crystal and the proper relative position of the gauge. Marks were then made on the walls of the glass tube by means of which the boiler opening was mounted at exactly the position of the light source.

In order that the readings of the ionization gauge may represent the actual distribution of atoms scattered by the crystal it is necessary that atoms from all portions of the illuminated area on the crystal face should be able to pass through the gauge opening without collision with the walls. With the incident beam making an angle of 18° with the crystal face the dimensions of the beam system shown in Fig. 2 allow a width of 1.52 mm on the crystal face to be struck by the incident beam. The gauge will admit atoms from a width on the crystal face of 2.04 mm. It is believed that this allows for more error in alignment than was present at any time.

The gauge was of the same type used by Zahl and Ellett,[4] and was of approximately the same dimensions except for the capillary tube forming the opening into the gauge which was 11 mm long and 0.68 mm in diameter. With a galvanometer of sensitivity 4.5×10^{-9} A/mm (ampere per millimeter) and a filament to grid current of 16 m.A. (milliamperes) in the gauge it is estimated that a galvanometer deflection of 1 mm corresponds to a pressure change in the gauge of 2.1×10^{-8} mm of mercury.

For the experiments with an incident beam of cadmium and with mercury at very low boiler pressures, a galvanometer of sensitivity 4.2×10^{-10} A/mm was used. This, coupled with a filament to grid current of 36 m.A. increased the sensitivity of the gauge by a factor of 21.

The calculation of the gauge sensitivity is based upon the fact that at the equilibrium condition as many atoms leave the gauge per second as enter it. The gauge opening offers no impedance to the incident beam provided the divergence of the beam is negligible. However, to atoms leaving the gauge the impedance is that characteristic of a tube of the dimensions of the gauge opening. This means that a pressure will be built up in the gauge by the

incident beam. If we know the number of atoms entering the gauge per second we can calculate the pressure which they produce and by observing the galvanometer deflection can calculate the sensitivity of the gauge.

By using the galvanometer of sensitivity of 4.4×10^{-9} A/mm it is found that a pressure of 0.708 mm in the boiler and a filament to grid current of 1 m.A. give a galvanometer deflection of 10 cm when placed in the main beam. With kinetic theory formula[5] for the mass of a gas striking the walls of a container per unit area per second, and for the number of molecules striking unit area per second,

$$n = 3.53 \times 10^{22} \times P/MT^{1/2}$$

and the dimensions of the beam system given in Fig. 2 we find that the number of atoms entering the gauge per second is 11.8×10^{11}. Since this is also the number of atoms leaving the gauge per second we can now make use of Knudsen's[6] formula for the pressure difference necessary to produce the flow of a quantity of gas, Q measured in cm³ at 1 bar through a cylindrical tube of length L and radius r, per second.

$$Q = \frac{1}{\rho_1} \frac{P_1 - P_2}{W_1 - W_2}$$

where ρ_1 is the density of the gas at 1 bar pressure and the temperature of the apparatus, and W_1 and W_2 the partial impedance of the tube are given by,

$$W_1 = (2\pi)^{1/2}/S$$

$$W_2 = 3L/4(2\pi)^{1/2}r^3.$$

A thermocouple placed in contact with the glass walls of the gauge read 220°C. Since the temperature of the gauge varies somewhat over different parts of the gauge and the point at which the thermocouple junction was placed was in a cooler part of the gauge. 250°C will be used as the mean temperature of the gauge.

Using the ordinary gas laws we find that the density of mercury vapor at 1 bar pressure and 250°C is 4.26×10^{-10} g/cm³. Substituting these in Knudsen's equation we find for the pressure difference,

$$P_1 - P_2 = 4.53 \times 10^{-2} \text{ dynes/cm}^2$$

$$= 3.4 \times 10^{-5} \text{ mm of mercury}.$$

This is the pressure produced in the gauge by the incident beam of mercury atoms. Since this pressure produced a galvanometer deflection of 10 cm with a filament to grid current of 1 m.A. it is easily calculated that with a current of 16 m.A. the sensitivity is 2.1×10^{-8} mm pressure change per mm galvanometer deflection.

If care was taken to maintain the liquid air about the slit at the same level, the drift of the low sensitivity galvanometer could be kept less than 2

[5] Saul Dushman, *High Vacuum*, pp. 234.

[6] M. Knudsen, Ann. d. Physik **28,** 75 and **28,** 999 (1909).

mm per half hour. However, when taking readings of the scattered beam, no attempt was made to keep this level constant. A period of about ten minutes was required to sweep the gauge across the crystal face and during this interval the liquid air level lowered sufficiently to allow a drift of 2 to 4 mm. This is probably due to the liberation of gas from the walls of the apparatus and since it appeared quite uniform could be corrected for.

With the crystal heater at 350°C the residual pressure in the gauge gave a galvanometer deflection of 20 to 30 cm corresponding to a pressure, in mercury vapor, of approximately 5.75×10^{-6} mm. The actual pressure in the gauge was probably greater than this since the gases present would give a lower ionization current than mercury vapor. On the other hand, the pressure in the gauge was probably greater than the pressure in the experimental chamber, due to the continuous liberation of gas from the walls of the gauge. With the crystal heater at 50°C the residual pressure was approximately half the above figure. The residual deflection was balanced out by an opposing potential across the galvanometer.

The system was ordinarily kept evacuated and dry nitrogen admitted for a few minutes while the crystal was being placed in the apparatus. Under these conditions it was only necessary to run the pumps for the period required to outgas the gauge before readings could be taken. The gauge was superheated at a filament current sufficient to give a grid current of 50 m.A. for a period of 4 to 6 hours before readings were taken.

When the high-sensitivity galvanometer was used and the grid current run at 36 m.A., longer outgassing periods were required and an unsteadiness in the residual deflection of the order of a millimeter was usually present. This unsteadiness was approximately one percent of the maximum reading in the scattered beam.

All the crystals used in this work, with the exception of those noted in the table, were grown in this laboratory by R. M. Zabel and the writer. The method used was similar to that used by Strong.[7]

Experimental Results

Data obtained by Zahl and Ellett[4] on the scattering of mercury from several alkali halide crystals indicated the following points: (1) The existence of a directed beam; (2) the deviation of the direction of maximum intensity in this beam from the direction of specular reflection; (3) the decrease of this deviation with higher beam and lower crystal temperatures and with lighter atoms; (4) better definition of the directed beam (narrowing of the beam) at low crystal temperatures, accompanied by an increase in the relative amount of random scattering.

The results of the present investigation agree with all except the third of these points. The shift in the position of the directed beam with a decrease in crystal temperature or an increase in beam temperature is found to be toward lower grazing angles. At sufficiently large angles of incidence the directed beam lies below the specular position and the shift in its position

[7] John Strong, Phys. Rev. **35**, 1663 (1930).

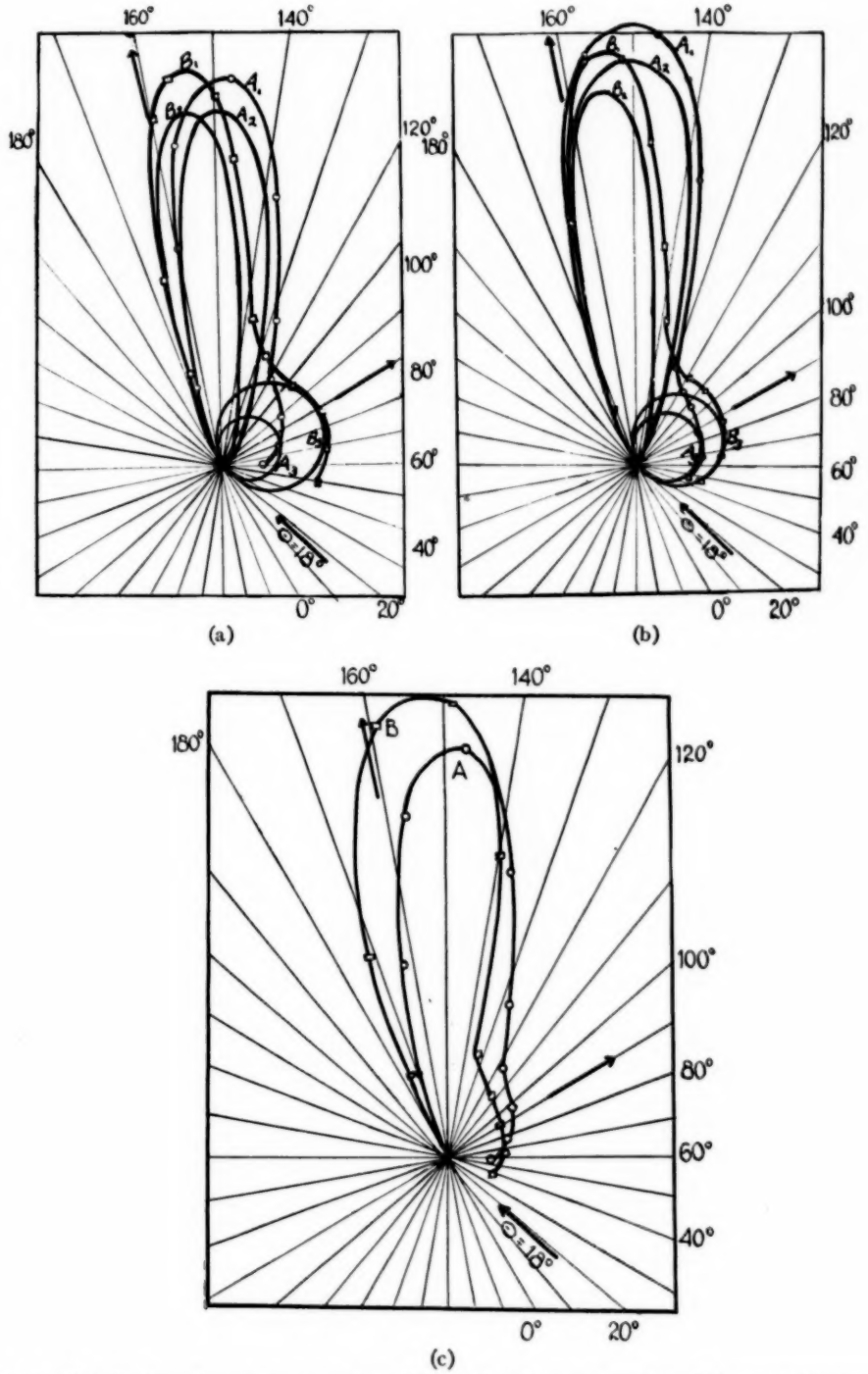

Fig. 3. Distribution of mercury atoms from lithium fluoride as a function of the crystal temperature and the temperature of the incident beam. Table I.[3]

[3] The detailed analysis of all curves is given in the appropriate table.

which accompanies a decrease in crystal temperature is away from the specular. Data were not taken by Zahl and Ellett at sufficiently large angles of incidence to bring out this fact.

The observations made by Zahl and Ellett[4] led them to conclude that the increase in random scattering which accompanied a decrease in crystal temperature was not due to the formation of a gas layer on the crystal surface. The data obtained in this work indicate that the formation of a gas layer on the crystal surface is an important factor when the temperature of the crystal is below that at which occluded gas atoms are driven off the crystal.

I. Reflection of mercury from lithium fluoride

Fig. 3 shows typical sets of curves obtained for mercury beams scattered from a lithium fluoride crystal. Fig. 3a shows the distribution in the scattered beam with a beam temperature of 375°C and an angle of incidence of 18°. Curves A_1 and B_1 are obtained experimentally, A_1 being taken with a crystal temperature of 470°C, and B_1 with the crystal at 50°C. These curves, as Zahl and Ellett pointed out, appear to be the result of superimposing two curves of very simple type, one a circle and the other a symmetrical curve represented approximately by an equation of the form $r = C \cos M\theta$. It appears reasonable to suppose that these curves represent distinct processes one resulting in random scattering, the other giving rise to a directed or coherently scattered beam.

The analysis in this manner of the experimental curves A_1 and B_1 is given in the figure, A_1 being broken up into the circle A_3 and the symmetrical curve A_2, B_1 into B_2 and B_3. A similar notation is used throughout. The directed beams, A_2 and B_2, lie between the specular position and the normal. Comparison of the directed beams shows that the beam from the cold crystal has been shifted away from the normal by 6.3°. The beam from the crystal at 50°C has also been narrowed, and the relative number of atoms scattered at random has been increased as evinced by the larger circle necessary to represent these atoms.

Fig. 3b shows curves taken with a beam temperature of 525°C. Fig. 3c shows the distribution for different beam temperatures, the crystal being at 470°C in both cases. Curve A is taken with the incident beam at 375°C and B with the beam at 525°C. An increase in beam temperature causes the quasi-specular beam to shift in the same direction as a decrease in crystal temperature.

Fig. 4a shows the distribution with an angle of incidence of 57°. The beam in this case has crossed over the specular position and lies closer to the crystal face than a regularly reflected beam. This change in the position of the beam relative to the specular position for varying angles of incidence was consistently observed as an inspection of the table will show. The cosine correction is somewhat uncertain in this case since the larger angle of incidence does not allow the gauge to be rotated over as large an angle. However, the beam is below the specular position whether a cosine correction is made or

not. Also the shift of the quasi-specular beam for a decrease in crystal temperature is definitely away from the specular position. Fig. 9 of the paper by Zahl and Ellett[4] shows evidence of a similar shift.

The above curves were taken with the crystal oriented so that alternate positive and negative ions were parallel and perpendicular to the plane of the

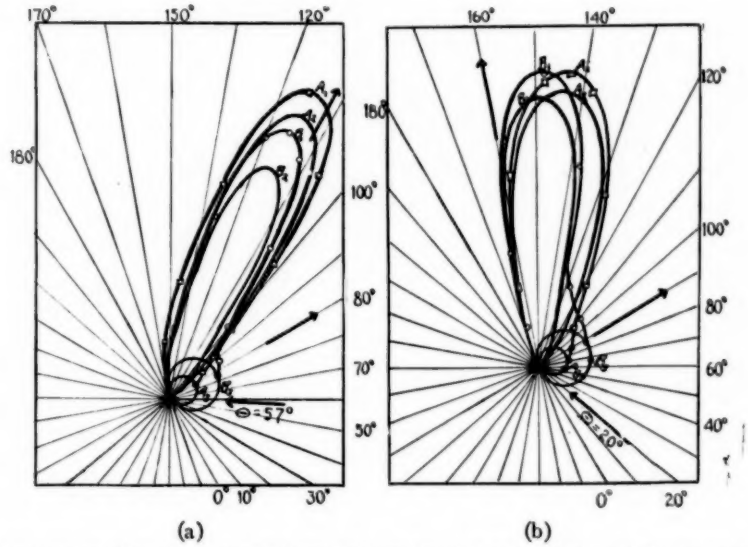

Fig. 4. Distribution of mercury atoms from lithium fluoride as a function of the crystal temperature and the temperature of the incident beam. Table I.

incident beam. Fig. 4b shows a set of curves taken with the crystal rotated 45° about an axis perpendicular to the plane of the incident beam. No change in the scattered beam is observed.

II. Reflection of mercury from sodium fluoride

Fig. 5 (a, b, c) shows the distribution obtained for mercury reflected from sodium fluoride. 5a was taken with a beam temperature of 280°C and crystal temperatures of 550°C and 50°C. 5b was taken with a beam temperature of 475°C and the same crystal temperature as 5a. 5c shows two curves taken at same crystal temperatures but different beam temperatures, A_1 being taken at a beam temperature of 280°C and B_1 at a temperature of 475°C. The curves are somewhat broader than for lithium fluoride but show the same behavior for changes in relative temperature of beam and crystal, and for changes in angle of incidence. The unusually large amount of cosine scattering in 5b is believed to be due to the fact that the crystal had been cold for approximately an hour.

III. Reflection of mercury from lithium chloride

Fig. 6 (a, b) shows curves obtained from lithium chloride. 6a was taken at a beam temperature of 260°C and crystal temperatures of 500°C and 50°C. 6b shows curves taken at a crystal temperature of 500°C, but different beam temperatures, A_1 being taken at a beam temperature of 260°C and B_1 at a

temperature of 500°C. They show the same behavior as the cases discussed above. Crystals of lithium chloride are very deliquescent and it was necessary to adopt some means of getting the crystal in the apparatus without exposure

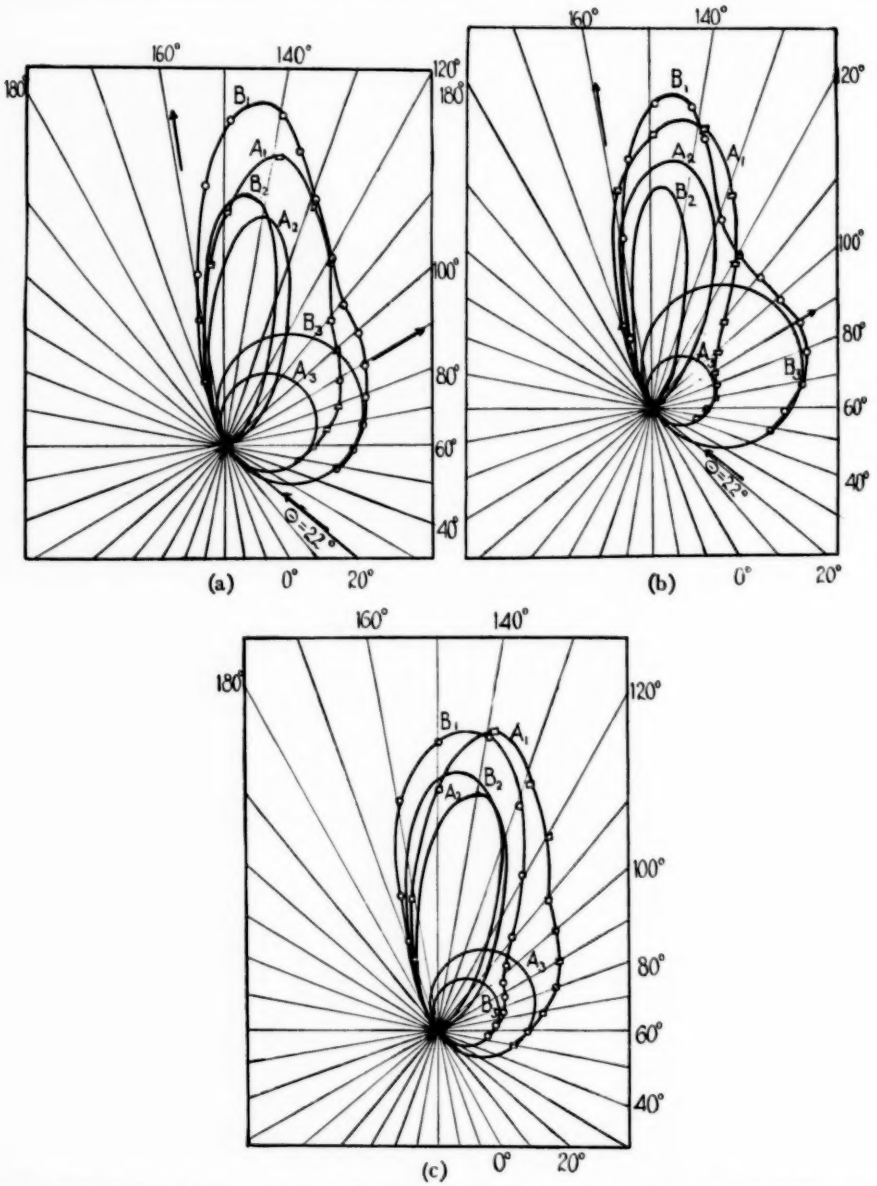

Fig. 5. Distribution of mercury atoms from sodium fluoride crystals as a function of the crystal temperature and the temperature of the incident beam. Table I.

to air. This was done by mounting a tin box with glass windows above the experimental chamber and filling both the box and the entire vacuum system with dry nitrogen at a pressure somewhat above atmospheric, all work on the crystal being done inside this tin box. The connection between the box

and the experimental chamber was made by a short length of tubing made of rubber dam. Long sleeved rubber gloves were attached to the openings in the box through which one worked, so that the crystal could be handled without exposing it to moisture from the hands. The box was thoroughly dried by leaving a dish of phosphorus pentoxide in it for about twelve hours before it was used. The crystal of lithium chloride from which a surface was to be

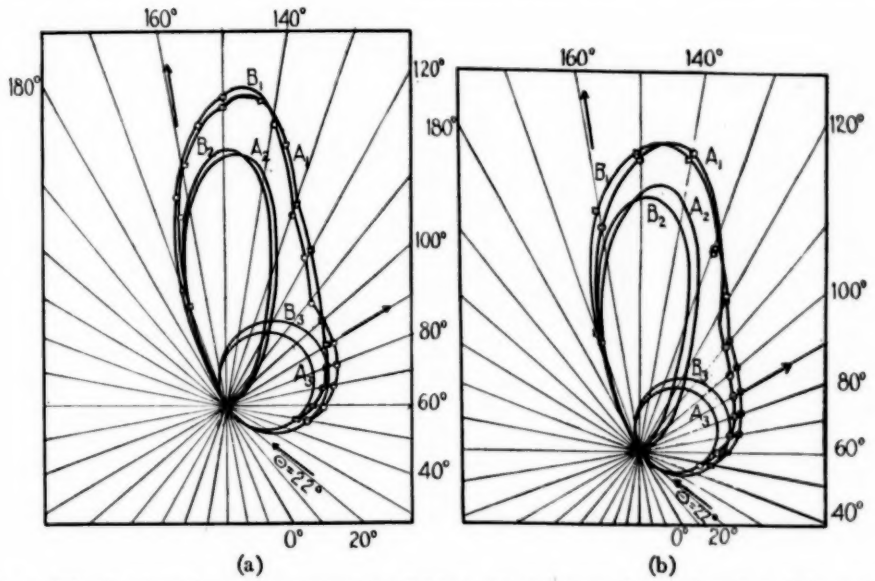

Fig. 6. Distribution of mercury atoms from lithium chloride crystals as a function of the crystal temperature and the temperature of the incident beam. Table I.

split was heated in a vacuum to a temperature of 400°C for four or five hours and then a small glass bomb containing the crystal was sealed off. The glass bomb was broken in the atmosphere of dry nitrogen inside the tin box, the crystal split, mounted on the crystal holder, placed in position and the pumps started immediately. About one minute elapsed from the time the crystal was split until the pumps were started. After taking these precautions in mounting, lithium chloride crystals were found to reflect as well as other non-deliquescent crystals used.

IV. Reflection of mercury from potassium iodide

Other experiments carried out in this laboratory had indicated that in certain cases, exposure to air had an action on the crystal surface which was not reversed by heating in a vacuum. In view of the success attained with lithium chloride it was decided to try the same method of mounting with potassium iodide. It was found that under these conditions a crystal of potassium iodide did give a directed beam. Fig. 7a shows the type of curves obtained. They were taken at a beam temperature of 170°C and crystal temperatures of 400°C and 50°C. In order to determine the effect of air on the reflecting power of the crystal, air was admitted to the system for a period of twenty minutes. This air flowed through a liquid air trap before reaching

the experimental chamber and although the trap was at room temperature within a few minutes after the air was admitted it is doubtful whether much water vapor had diffused into the experimental chamber by the end of the twenty minutes. After outgassing the system and heating the crystal at 400°C for several hours it was found to reflect as well as before. The curves obtained were practically identical with these shown in 7a. The system was then opened again and moist air from the room was driven past the crystal for several minutes by running oil pumps. The pumps were then shut off and the system left open for a period of eighty minutes. Fig. 7b shows the

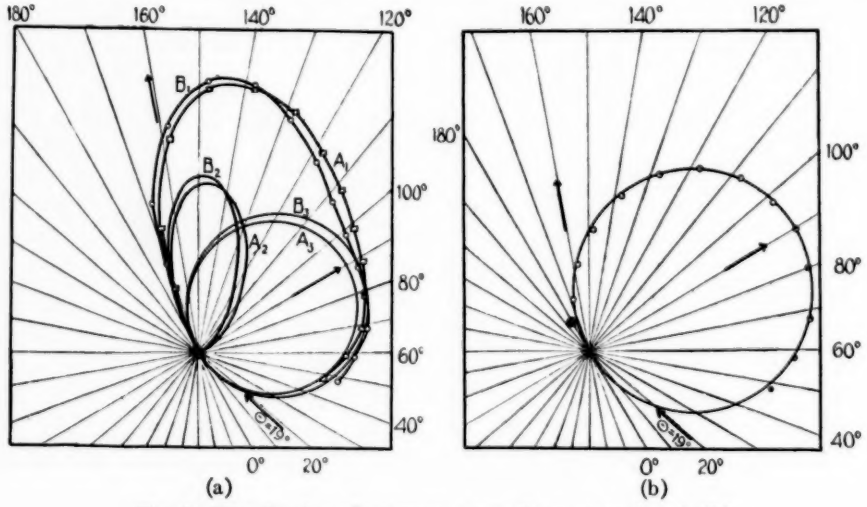

Fig. 7. Distribution of mercury atoms from potassium iodide as a function of the crystal temperature. Table I.

distribution obtained after this exposure. After prolonged heating at a temperature of 450°C the crystal still failed to show any indication of a directed beam. The crystal surface had apparently been completely and permanently ruined as far as its reflecting power was concerned.

V. Reflection of cadmium from NaCl

Since cadmium has a much lower vapor pressure than mercury it appeared that in order to prevent condensation in the gauge, two things were necessary, (1) the sensitivity of the gauge should be increased as much as possible so as to use low vapor pressures, and (2) the gauge should be kept at as high a temperature as possible. Several runs with different galvanometer sensitivities and with different ionization gauges were made before it was found possible to prevent condensation in the gauge. Condensation was always indicated by an unsteady drift of the galvanometer off the scale, and if the condensation became very great, by a marked decrease in the filament to grid current.

By using the gauge at a filament to grid current of 36 m.A. in conjunction with the more sensitive galvanometer, which increased the sensitivity of the gauge by a factor of approximately 21 and allowed the use of much lower vapor pressures, this difficulty was overcome.

Fig. 8 shows a set of curves obtained for cadmium reflected from sodium chloride. They were taken at a beam temperature of 480°C and crystal temperatures of 350°C and 50°C. The deviation from the specular position is not as large as usually observed for mercury incident at the same angle. However, individual crystals of sodium chloride show such a deviation in the angle of the reflected beam that one cannot be certain of this point.

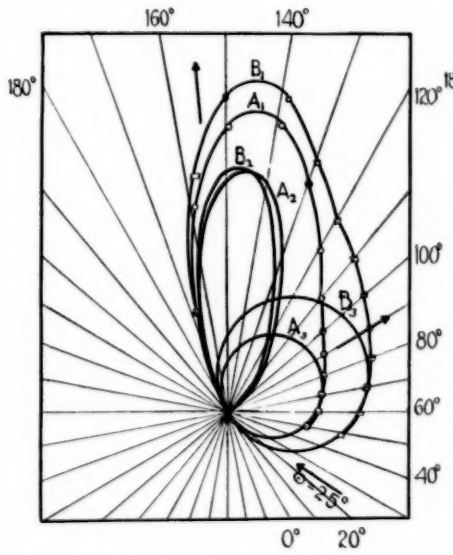

Fig. 8. Distribution of cadmium atoms from sodium chloride as a function of the crystal temperature. Table I.

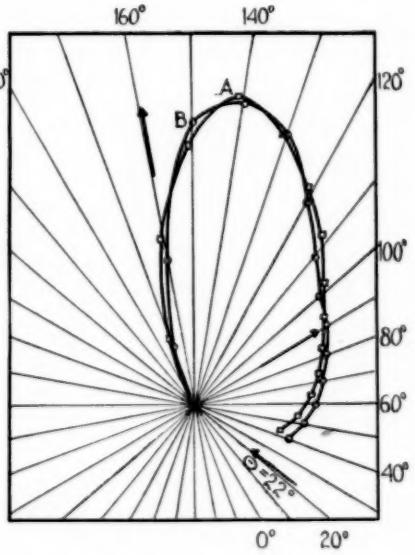

Fig. 9. Distribution of mercury atoms from sodium chloride as a function of the vapor pressure at the gun opening.

VI. Effect of varying pressure in atom-gun on the reflected beam

Fig. 9 shows two curves for mercury reflected from sodium chloride at different boiler pressures. Curve *A* was taken at a pressure of 0.35 mm corresponding to a mean free path of approximately 0.6 mm. Curve *B* was taken at a pressure of 3 mm corresponding to a mean free path of approximately 0.075 mm. The two curves show no appreciable difference. Other curves (not shown) and the data obtained by Zahl and Ellett[4] show very little difference up to a boiler pressure of 10 mm. This indicates that the deviations from a Maxwell distribution which occur in this range of pressure are not significant as far as these experiments are concerned.

VII. Variation in random scattering from a cold crystal with time

Fig. 10a shows the scattering of a beam of mercury atoms from a sodium fluoride crystal at 50°C as a function of time. The crystal was heated at a temperature of 550°C for several hours while outgassing the system. Curve *A* was taken immediately after the crystal had been cooled to 50°C. Curve *B* after remaining at this temperature for 20 minutes and curve *C* after 60 minutes. The curves show an increase in the random scattering with time, the

positions of the quasi-specular beam apparently remaining unchanged. Fig. 10b shows the distribution as the crystal was reheated. The crystal was heated to 275°C and curve *B* taken. The temperature was then increased to 400°C and curve *C* taken.

These curves show the peak shifted toward the normal from its position with the crystal at 50°C but very little change in the amount of random scattering. Curve *D* taken at 600°C shows the peak still farther shifted toward the normal and the amount of cosine scattering very greatly reduced.

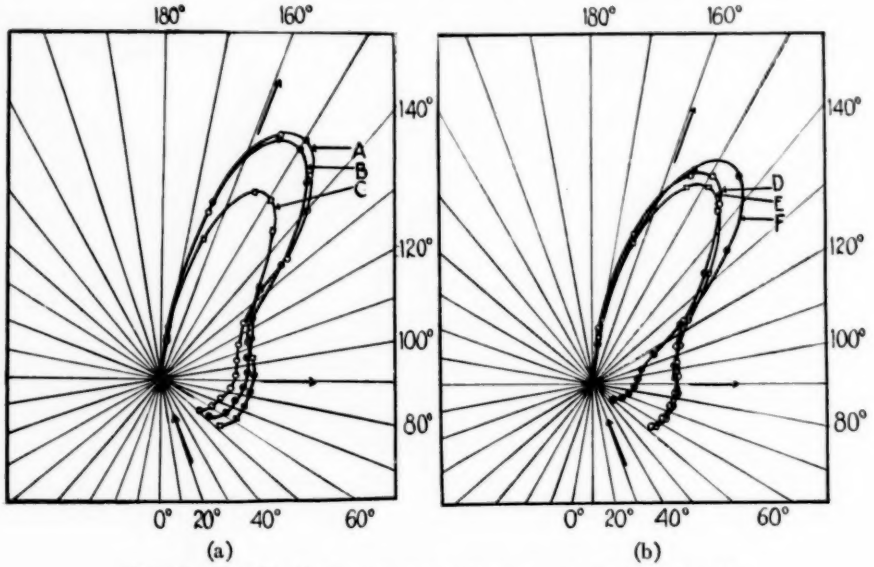

Fig. 10. Distribution of mercury atoms from a sodium fluoride crystal as a function of time and temperature of crystal.

It should be noted that when a crystal of sodium fluoride was exposed to air when placed in the apparatus it was always necessary to heat it at a temperature of at least 550°C for approximately an hour before a directed beam could be obtained.

The tables show the results obtained for the various cases discussed above. The relative number of atoms in the directed beam and in the random scattering were computed by the method described by Zahl and Ellett.[4]

Conclusion

A directed beam has been obtained for all the cases investigated. The former unsuccessful attempts to detect a directed beam from crystals of potassium iodide are shown to have been due to contamination of the crystal surface by overexposure to air, particularly to moist air, when it was placed in the apparatus. (The writer found no evidence of a directed beam in several attempts before the method of mounting in an atmosphere of dry nitrogen was developed.)

When a crystal surface was exposed to air, even for periods as short as two or three minutes, it was necessary to heat the crystal to drive off the

TABLE I. *Reflection of mercury from alkali-halide crystals.*

Crystal	Figure identification number	Angle of incidence	Angle of reflection	Temperature of crystal	Change in angle of reflection due to change in crystal temperature	Temperature of mercury beam	Curve describing directed beam	Intensity of directed beam	Intensity of of cosine scattering	Total intensity	Percent of atoms contributing to directed beam
(1) LiF*		18°	32°	470°C		285°C	$\cos 3.3\Theta$	23.34	75	98.34	23.8
(1) LiF		18	26	50	6	285	$\cos 4.\ \Theta$	16.90	68	84.90	19.9
(1) LiF	3(a), *A*	18	32	470		375	$\cos 3.8\Theta$	31.5	75.3	106.8	25.9
(1) LiF	3a, *B*	18	25.7	50	6.3	375	$\cos 5.5\Theta$	20	81.6	101.6	19.7
(1) LiF	3b, *A*	18	29	470		525	$\cos 3.8\Theta$	25.5	67.8	93.3	33.2
(1) LiF	3b, *B*	18	25	50	4	525	$\cos 5.\ \Theta$	15.8	88.3	104.1	15.4
(1) LiF		36	40.6	470		285	$\cos 3.6\Theta$	26.52	70.8	97.32	27.2
(1) LiF		36	34.7	50	5.9	285	$\cos 4.\ \Theta$	30.36	92.4	122.76	24.4
(1) LiF		35	39	470		375	$\cos 3.8\Theta$	47.1	75.6	122.7	38.3
(1) LiF		35	33	50	6	375	$\cos 4.8\Theta$	27.9	94.0	121.9	23
(1) LiF		34	35	470		525	$\cos 4.4\Theta$	25.87	75.3	101.17	25.6
(1) LiF		34	31		4	525	$\cos 4.6\Theta$	25.05	77.85	103.9	24.3
(1) LiF		56	52	470		285	$\cos 3.6\Theta$	26.1	42.4	68.5	38.1
(1) LiF		56	48	50	4	285	$\cos 4.8\Theta$	24.01	70.2	94.21	23
(1) LiF		56	55	470		375	$\cos 4.4\Theta$	28.4	64.4	92.8	30.7
(1) LiF		56	53	50	2	375	$\cos 4.6\Theta$	26.9	72	98.9	27.8
(1) LiF	4a, *A*	57	55	470		525	$\cos 4.7\Theta$	30.51	56.62	87.13	34.6
(1) LiF	4a, *B*	57	53	50	2	525	$\cos 5.5\Theta$	18.8	89.6	108.4	17.7
(2) LiF		39	48	700		500	$\cos 4.\ \Theta$	12	17.3	29.3	41
(2) LiF		39	43	50	5	500	$\cos 5.7\Theta$	8.77	25.1	33.87	26
(2) LiF		39	45	50	3	360	$\cos 5.2\Theta$	7.97	22	29.97	26.6

TABLE I. (*Continued*).

Crystal	Figure identification number	Angle of incidence	Angle of reflection	Temperature of crystal	Change in angle of reflection due to change in crystal temperature	Temperature of mercury beam	Curve describing directed beam	Intensity of directed beam	Intensity of cosine scattering	Total intensity	Percent of atoms contributing to directed beam
	5c, *A*										
(3) NaF	5b, *A*	22	37	550		475	$\cos 2.8\Theta$	39.75	46.9	86.65	45.7
(3) NaF	5b, *B*	22	33	50	4	475	$\cos 4.4\Theta$	6.14	77	83.14	7.4
(3) NaF		37	42.5	550		475	$\cos 3.2\Theta$	15.4	42.6	58	22.7
(3) NaF		37	38	50	4.5	475	$\cos 3.6\Theta$	12.6	53.5	66.1	19.2
(3) NaF		52	49	550		475	$\cos 2.8\Theta$	43.5	42.5	86	50.6
(3) NaF		52	47	50	2	475	$\cos 3.6\Theta$	14	54.5	66.5	25.7
	5c, *A*										
(3) NaF	5a, *A*	22	40.5	550		280	$\cos 3.2\Theta$	12.2	49	61.2	19.8
(3) NaF	5a, *B*	22	35.5	50	4.7	280	$\cos 3.6\Theta$	10.6	72	82.6	12.9
(3) NaF		37	45.5	550		280	$\cos 3.2\Theta$	17.4	62.8	80.2	21.7
(3) NaF		37	43	50	2.5	280	$\cos 3.6\Theta$	11	76	87	12.3
(3) NaF		52	53	550		280	$\cos 3.2\Theta$	19.7	45.7	65.4	30
(3) NaF		52	51	50	2	280	$\cos 4\ \Theta$	9.8	52	61.8	15.8
(4) NaF		21	32.5	700		500	$\cos 2.8\Theta$	15	18.9	33.9	43.3
(4) NaF		46	45	700		500	$\cos 3\ \Theta$	11.2	18.9	30.1	37.5
	6b, *B*										
(5) LiCl	6a, *A*	22	33	500		500	$\cos 3.2\Theta$	8.82	29.8	38.62	22.9
(5) LiCl	6a, *B*	22	31	50	2	500	$\cos 3.4\Theta$	7.4	32.6	40	18.5
(5) LiCl	6b, *A*	22	35	500		260	$\cos 3.2\Theta$	8.48	25.2	33.68	25.1
(5) LiCl		50	54**	500		500					
(5) LiCl		50	52**	50	2	500					
(5) LiCl		50	55**	500		260					

TABLE I. (*Continued*)

Crystal	Figure identification number	Angle of incidence	Angle of reflection	Temperature of crystal	Change in angle of reflection due to change in crystal temperature	Temperature of mercury beam	Curve describing directed beam	Intensity of directed beam	Intensity of cosine scattering	Total intensity	Percent of atoms contributing to directed beam
(6) KI	7a, *A*	19	34	400		170	$\cos 2.6\Theta$	7.8	47.8	55.6	14.8
(6) KI	7a, *B*	19	31	50	3	170	$\cos 2.8\Theta$	6.9	50.5	57.4	12
(6) KI		27	35	400		170	$\cos 2.2\Theta$	11.6	53.7	65.3	17.8
(6) KI***		27	35	400		170	$\cos 2.4\Theta$	13.2	55.6	68.8	19.1
(6) KI***		27	35	50	2	170	$\cos 2.6\Theta$	9.9	55	64.9	15.2
(6) KI		41	50	400		170					
(6) KI		41	46	50	4	170					
(7) NaCl****	8*A*	25	36	350		480	$\cos 3.2\Theta$	8.2	31.6	39.8	21
(7) NaCl	8*B*	25	34	70	2	480	$\cos 3.4\Theta$	4.2	25.1	29.3	14.4
(7) NaCl		34	40	350		480	$\cos 2.6\Theta$	10.2	17.1	27.3	37.3
(7) NaCl		34	37	70	3	480	$\cos 3.2\Theta$	6.1	19.5	25.6	23.8

* The numbers in column one denote different individual crystals. All data for which the number in this column is the same, were taken in a single run.
** These angles represent the peak of the uncorrected beam.
*** After crystal had been exposed to air for 20 minutes.
**** The remainder of the data in this table is for cadmium reflected from natural crystals of sodium chloride.

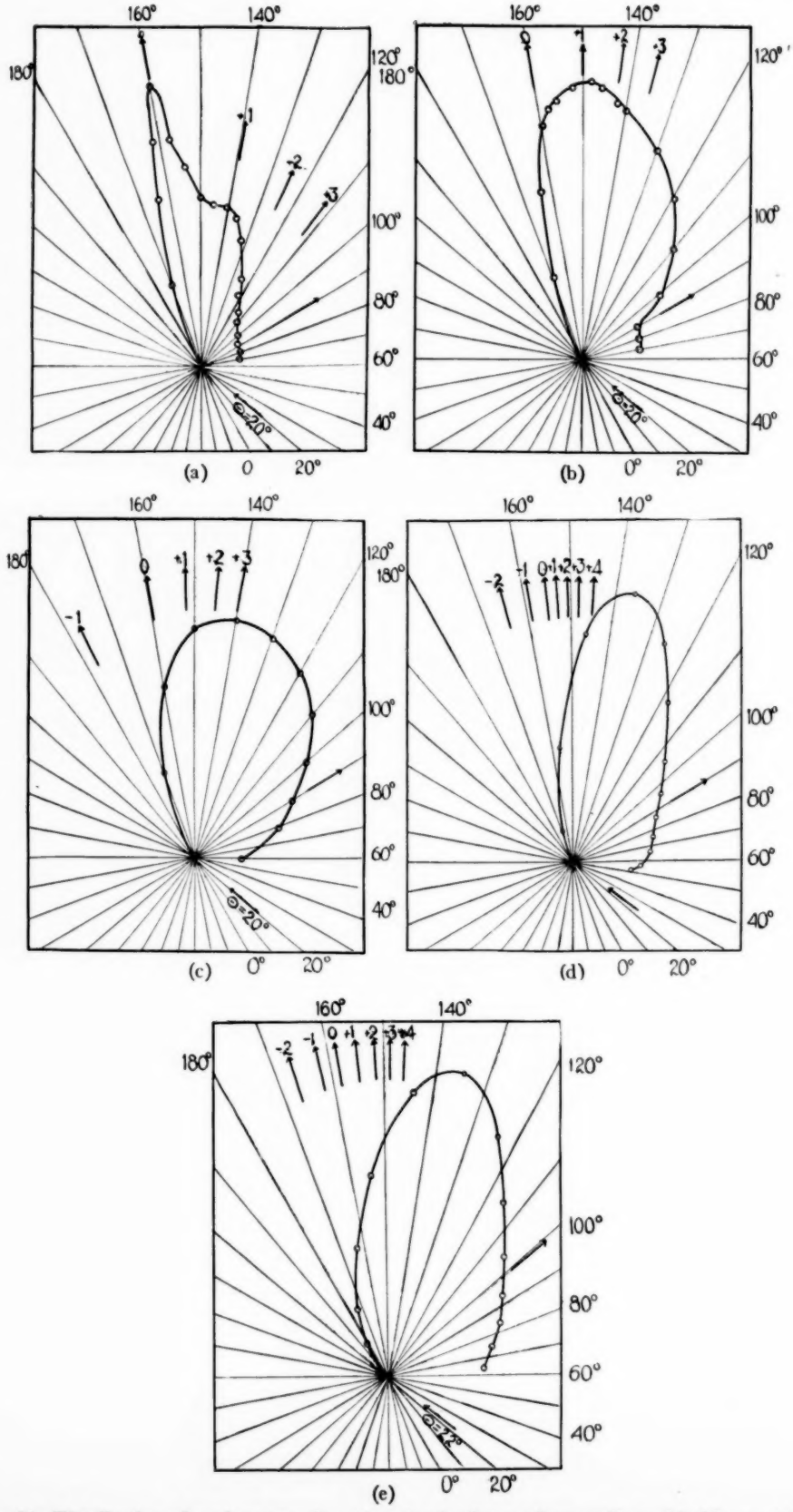

Fig. 11. Distribution of various atomic and molecular beams from sodium chloride crystals; (a) helium, (b) neon, (c) argon, (d) cadmium, and (e) mercury.

adsorbed gas before a directed beam could be obtained. The temperature necessary to accomplish this varied with different crystals, 350°C being sufficient in the case of sodium chloride, for lithium fluoride a temperature of 450°C was necessary and for sodium fluoride a temperature of 550°C was required.

It seems reasonable, as suggested by Zahl and Ellett,[4] that the better definition of the reflected beam at low crystal temperature is due to the decrease in thermal agitation of the crystal and the consequent increased resolving power. The increase in random scattering at low crystal temperatures is evidently largely due to the formation of a gas layer on the crystal surface.

Fig. 11 shows the distribution in the plane of incidence of helium, neon, argon, cadmium, and mercury[9] scattered from sodium chloride. That the asymmetry in the helium curve is due to the presence of a surface grating spectrum incompletely resolved is scarcely to be doubted. It is tempting to infer that the other curves are to be accounted for in the same manner. The maxima of the plus or minus first, the plus or minus second, and the plus third and fourth order spectra of the several beams incident upon sodium chloride would lie at the positions indicated by the arrows. If we take this point of view we will then attempt to account for the temperature shift in the direction of maximum scattering by supposing that it is due to a change in the force field at the surface of the crystal of such a character as to make spectra of positive orders relatively more intense at higher crystal temperatures. Thus the observed phenomena may be interpreted qualitatively at least in terms of surface grating diffraction. However, it is difficult to see, if this interpretation is correct, why rotation of the crystal in its own plane produces so little change in the scattering of mercury. With helium quite radical changes occur while no data are available on neon and argon.

In conclusion the writer wishes to express his appreciation to Professor A. Ellett under whose direction the work was done.

[9] The curves of helium, neon and argon were very kindly loaned to the writer by R. M. Zabel.

The Theory of the Ferromagnetic Anisotropy of Single Crystals

By RICHARD M. BOZORTH
Bell Telephone Laboratories

(Received October 27, 1932)

It is well known that in single crystals of iron and nickel the direction of magnetization is not generally parallel to the direction of the magnetic field, although these crystals belong to the cubic system. When the magnetization in a crystal has a certain value as measured in the direction of the field, there will be also, in general, a component of magnetization measured in the direction at right angles. This paper describes the calculation according to the domain theory, of the normal component of magnetization, using certain assumptions which are almost identical with those used by Heisenberg in his calculation of the magnetostriction of iron crystals. Theoretical curves are shown for a variety of crystallographic directions. Each of these curves shows all of the possible positions and magnitudes of the vector representing the magnetization in iron crystals as the magnetic field parallel to any given direction in the crystal increases in strength from zero to a high value. The theoretical curves are compared with the experimental curves of Honda and Kaya, and show good agreement with them.

INTRODUCTION

RECENTLY Heisenberg[1] has calculated the magneto-striction of a single crystal of iron as dependent upon magnetization, for the three principal directions in the crystal. Restated in my own words, the assumptions used by Heisenberg are as follows:

1. The crystal is composed of a large number of domains, considered for convenience to be equal in size.

2. When the crystal as a whole is in the unmagnetized state, each domain is magnetized to saturation in the direction of a cubic axis, <100>, the directions of the magnetizations of the domains being equally distributed among the six possible directions.

3. When magnetization of the crystal as a whole has a value chosen between zero and a certain limit, the directions of magnetizations in the domains are distributed by chance among the six possible <100> directions, and that distribution will occur which is the most probable one, subject to the condition that the vector sum of the magnetizations of the domains shall be equal to the previously specified magnetization of the crystal. The precise meaning of the term probability of a distribution is stated in Eq. (2) below.

4. After magnetization of the crystal has increased so that the directions of magnetizations of the domains have become parallel to that cubic axis (or axes) most nearly aligned with the direction of the magnetic field, as-

[1] W. Heisenberg, Zeits. f. Physik **69**, 287–297 (1931). Similar assumptions were previously stated by W. L. Webster, Proc. Phys. Soc. London **42**, 431–440 (1930), but no quantitative treatment was given nor were calculations made. For a discussion of the domain theory, see E. C. Stover, *Magnetism*, E. P. Dutton and Co., 65–66 (1929), and R. M. Bozorth and J. F. Dillinger, Phys. Rev. **41**, 345 (1932).

sumption (3) no longer applies and they leave the cubic axes and approach the field direction continuously until saturation is attained.

5. Associated with each domain is a measurable "magnetostriction," i.e., a deformation of the domain which increases its length in the direction of its magnetization. The magnetostriction of the crystal is the sum of the separate magnetostrictions of the domains, added according to the method of Akulov.[2]

The magnetostriction curves so calculated for progressive magnetization along the crystallographic directions <100>, <110> and <111> have been compared by Heisenberg with the data of Webster[3] and show good agreement with them.

Heisenberg limited himself to the calculation of the *magnetostriction*. On the other hand, by using similar but somewhat different assumptions, and extending his general mathematical procedure, it is possible to predict the *direction of magnetization* in a single crystal subjected to a magnetic field having any chosen direction and magnetized to any fraction of saturation.

It is known experimentally that when the crystal is more than about half saturated the direction of magnetization is different from the direction of the field unless the field lies in one of the three principal crystallographic directions (cube edge, face diagonal, and body diagonal) considered by Heisenberg. As the field increases in strength, remaining always constant in direction, the magnetization changes in direction as well as in magnitude.

We now have a satisfactory theory which predicts correctly in all cases the direction of deviation of magnetization from field, and predicts also within the experimental error the magnitude of the deviation observed by Honda and Kaya, whose experimental data are as yet the most complete.

Specifically, the quantities which are calculated for the first time in this paper are the magnitude and direction of the magnetization in a single crystal corresponding to selected values of the component of magnetization in the field direction. These may be calculated for any direction of the field with respect to the crystal axes.

The assumptions made are assumptions (1) to (4) above, with a slight change in assumption (3): the distribution of the directions of magnetization in the domains is now subject to the condition that the vector sum of these magnetizations shall have a component in the direction of the magnetic field equal to the observed value of the magnetization along that direction.

The simplest way to express the results of the calculations seems to be to plot I_H, the component of magnetization parallel to the field, along one axis; and I_n, the component normal to the field, along an axis at right angles. The line joining the origin to any point on the curve so plotted is then a vector representing the total magnetization of the crystal, and the curve is the locus of the end of the vector as the strength of the field directed along the I_H axis increases from a very small to a very large value. Typical curves are shown in Figs. 4 to 6, where the several directions of the field are shown by the arrows.

[2] N. S. Akulov, Zeits. f. Physik **59**, 254–264 (1930).

[3] W. L. Webster, Proc. Roy. Soc. London **109A**, 570–584 (1925).

It should be understood that the theory gives no information regarding the *strength* of the magnetic field which is associated with a given magnetization of the crystal, but does define completely all of the magnetic states of the crystal which must occur as the field, acting in any direction, increases indefinitely from zero.

Calculations

Following Heisenberg's procedure, let N denote the number of domains per unit volume of the crystal. We employ a right-handed set of rectangular coordinate axes which coincide with the crystallographic axes. We consider "distributions" of the elementary domains, each distribution being defined by the numbers, N_1, N_3, N_5, of elementary regions per unit volume having their magnetic moments in the directions of the positive x, y and z axes, respectively, and by the numbers N_2, N_4, N_6, of regions having their magnetic moments in the directions of the negative x, y and z axes, respectively. Thus a distribution is represented by a set of positive numbers $(N_1, N_2, \cdots, N_6)$ with $N_1+N_2+\cdots+N_6=N$. The components of the magnetization along the x, y and z axes are then given by

$$\begin{aligned} I_x/I_\infty &= (N_1 - N_2)/N, \\ I_y/I_\infty &= (N_3 - N_4)/N, \\ I_z/I_\infty &= (N_5 - N_6)/N, \end{aligned} \tag{1}$$

respectively, where I_∞ is the saturation value of magnetization. With Heisenberg we write the probability of the distribution $(N_1, N_2, \cdots, N_6)$

$$P(N_1, N_2, \cdots, N_6) = \frac{N!}{(N_1!)(N_2!)\cdots(N_6!)}\left(\frac{1}{6}\right)^N. \tag{2}$$

Imposing the condition that the component of magnetization in the direction defined by direction cosines (λ, μ, ν) has a given value I_H, let us seek the most probable distribution consistent with this condition .We have

$$\lambda(N_1 - N_2) + \mu(N_3 - N_4) + \nu(N_5 - N_6) = NI_H/I_\infty. \tag{3}$$

We also have

$$N_1 + N_2 + \cdots N_6 = N. \tag{4}$$

Introducing Lagrangian multipliers, α' and β, we construct the function

$$\begin{aligned} F = \log P &+ \alpha'[N_1 + N_2 + \cdots N_6 - N] \\ &+ \beta[\lambda(N_1 - N_2) + \mu(N_3 - N_4) + \nu(N_5 - N_6) - NI_H/I_\infty]. \end{aligned} \tag{5}$$

For the most probable distribution we must have

$$\partial F/\partial N_i = 0,\ i = 1, 2, \cdots, 6. \tag{6}$$

Making use of the approximation

$$\log n! = (n + \tfrac{1}{2})\log n - n + \tfrac{1}{2}\log(2\pi),$$

we obtain from (6) the set of approximate equations

$$\begin{aligned}
\log N_1 &= \alpha' + \log (N/6) + \beta\lambda, \\
\log N_2 &= \alpha' + \log (N/6) - \beta\lambda, \\
\log N_3 &= \alpha' + \log (N/6) + \beta\mu, \\
\log N_4 &= \alpha' + \log (N/6) - \beta\mu, \\
\log N_5 &= \alpha' + \log (N/6) + \beta\nu, \\
\log N_6 &= \alpha' + \log (N/6) - \beta\nu.
\end{aligned}$$

Write $\alpha' + \log (N/6) = \alpha$. Then we have

$$\left.\begin{aligned}
N_1 &= e^{\alpha+\beta\lambda},\ N_3 = e^{\alpha+\beta\mu},\ N_5 = e^{\alpha+\beta\nu}, \\
N_2 &= e^{\alpha-\beta\lambda},\ N_4 = e^{\alpha-\beta\mu},\ N_6 = e^{\alpha-\beta\nu}.
\end{aligned}\right\} \tag{7}$$

On substituting from (7) in (3) and (4), we obtain the following equations for the determination of α and β:

$$\frac{\lambda sh(\lambda\beta) + \mu sh(\mu\beta) + \nu sh(\nu\beta)}{ch(\lambda\beta) + ch(\mu\beta) + ch(\nu\beta)} = \frac{I_H}{I_\infty}, \tag{8}$$

$$2e^{\alpha}[ch(\lambda\beta) + ch(\mu\beta) + ch(\nu\beta)] = N. \tag{9}$$

Eq. (8) gives β in terms of λ, μ, ν, I_H; then (9) gives α in terms of λ, μ, ν, I_H, N. Eqs. (7) then give the most probable distribution $(N_1, N_2, \cdots, N_6)$ from which the figures have been plotted.

In Figs. 1 and 2 there are shown the most probable distributions as functions of I_H/I_∞ for two directions (λ, μ, ν). It is to be understood that the preceding theory cannot apply if the value of I_H/I_∞ is greater than that for which one of the N_i's vanishes. In extending the results into the range of these higher values of I_H we make use of assumption (4) of the introduction.

For purposes of comparison with certain experiments it is necessary to discuss cases in which the magnetization I lies always in a given plane. Accordingly, let us impose the conditions that: (1) the component of magnetization in a given direction (λ', μ', ν') be zero, (2) the component in another direction (λ, μ, ν) have a given value I_H; and let us seek the most probable distribution consistent with these conditions.

We have Eqs. (3) and (4) and the additional equation

$$\lambda'(N_1 - N_2) + \mu'(N_3 - N_4) + \nu'(N_5 - N_6) = 0. \tag{10}$$

Proceeding as before, we find the values

$$\left.\begin{aligned}
N_1 &= e^{\alpha+\lambda\beta+\lambda'\gamma},\ N_3 = e^{\alpha+\mu\beta+\mu'\gamma},\ N_5 = e^{\alpha+\nu\beta+\nu'\gamma}, \\
N_2 &= e^{\alpha-\lambda\beta-\lambda'\gamma},\ N_4 = e^{\alpha-\mu\beta-\mu'\gamma},\ N_6 = e^{\alpha-\nu\beta-\nu'\gamma},
\end{aligned}\right\} \tag{11}$$

where the Lagrangian multipliers α, β, γ, are determined by the equations

$$\lambda' sh(\lambda\beta + \lambda'\gamma) + \mu' sh(\mu\beta + \mu'\gamma) + \nu' sh(\nu\beta + \nu'\gamma) = 0, \tag{12}$$

$$\frac{\lambda sh(\lambda\beta + \lambda'\gamma) + \mu sh(\mu\beta + \mu'\gamma) + \nu sh(\nu\beta + \nu'\gamma)}{ch(\lambda\beta + \lambda'\gamma) + ch(\mu\beta + \mu'\gamma) + ch(\nu\beta + \nu'\gamma)} = \frac{I_H}{I_\infty}, \tag{13}$$

$$2e^{\alpha}[ch(\lambda\beta + \lambda'\gamma) + ch(\mu\beta + \mu'\gamma) + ch(\nu\beta + \nu'\gamma)] = N. \tag{14}$$

Eq. (12) determines γ in terms of β and the direction cosines; then (13) determines β, and so also γ, in terms of the direction cosines and I_H, then (14) gives α in terms of the direction cosines, I_H, and N. Finally the Eqs. (11) give the required most probable distribution.

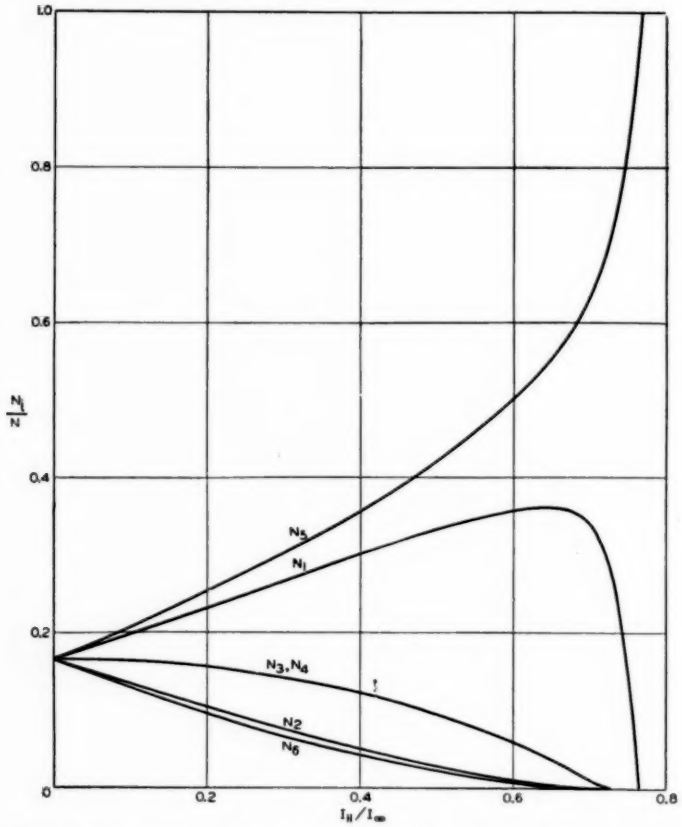

Fig. 1. Curves showing the distribution of directions of magnetizations of the domains among the six <001> directions. For these curves the direction of the field is defined by the direction cosines $\lambda = 0.643$, $\mu = 0$, $\nu = 0.766$, and is therefore inclined at 40° to a <001> direction in a {001} plane.

The curves in Figs. 2 and 3 show the most probable distributions as functions of I_H/I_∞ for one set of values of λ, μ and ν; in the case of Fig. 2 the magnetization is not restricted to a plane, in Fig. 3 it is confined to the $(11\bar{1})$ plane $(\lambda' = \mu' = -\nu' = 1/3^{1/2})$.

The results may also be expressed in a different way. From the most probable distributions may be determined I_n, the component of magnetization perpendicular to the direction defined by λ, μ and ν; and therefore knowing

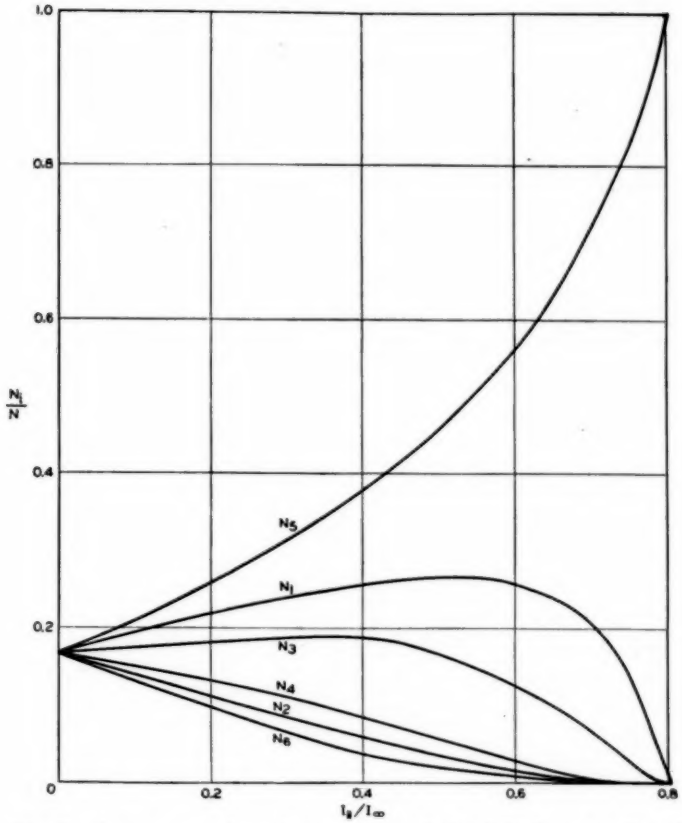

Fig. 2. Distribution curves when the direction of the field has the direction cosines $\lambda = 0.525$, $\mu = 0.279$, $\nu = 0.804$, and therefore lies in the $(11\bar{1})$ plane 10° from the [112] direction. The magnetization is not constrained to lie in the $(11\bar{1})$ plane.

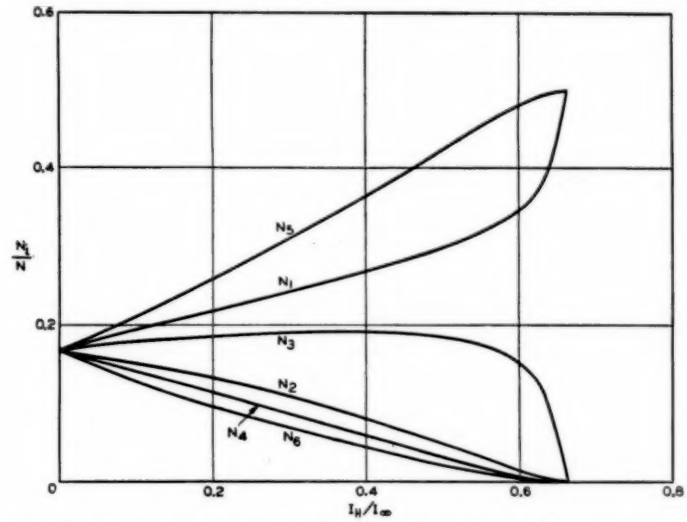

Fig. 3. Distribution curves when the direction of the field is the same as for Fig. 2. The magnetization for this case, however, is confined to the $(11\bar{1})$ plane by the additional condition $N_1 - N_2 + N_3 - N_4 - N_5 + N_6 = 0$.

I_H which lies in the latter direction, I may be determined in magnitude and direction. In the polar diagram of Fig. 4, referring to the (001) plane, each curve marked "CALC." is the locus of the end of the vector representing I,

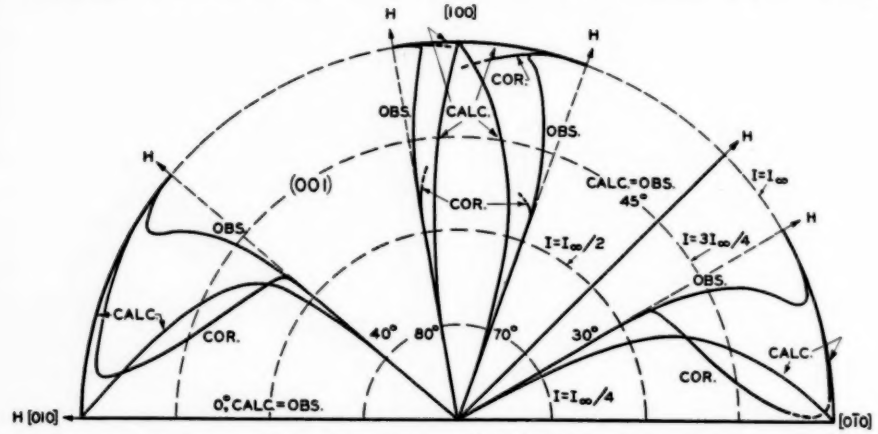

Fig. 4. Polar diagram of magnetization in a $\{001\}$ plane of iron. Each curve is the path traced from the center of the semi-circle by the end of the vector representing I as I increases in magnitude from zero to I_∞ (the limit of the figure). The direction of the field is that indicated by the arrow, and is the same as the direction of the curve at the origin.

as it passes from the center of the circle to its circumference, while I increases in magnitude from 0 to I_∞. When I_H becomes so large that one of the N_i's

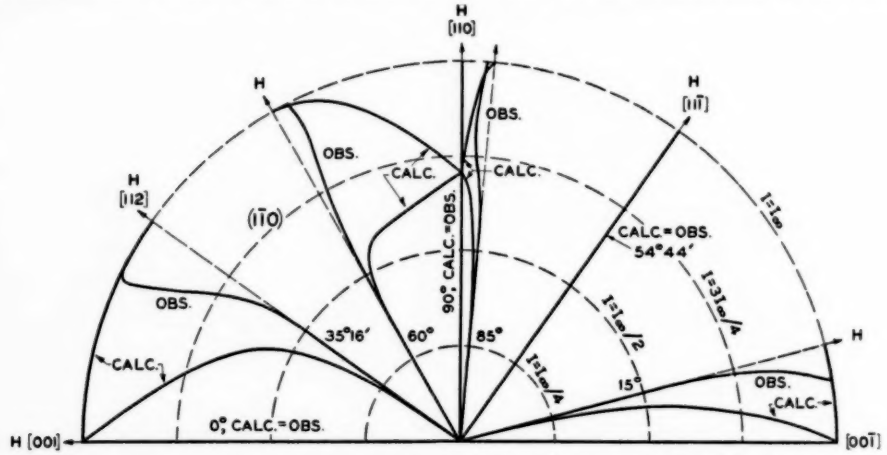

Fig. 5. Polar diagram of magnetization in a $\{110\}$ plane. The observed curves have not been corrected for the demagnetizing effect of the normal component of magnetization.

vanishes (generally when $I = I_\infty$) it is assumed that I turns in a plane into the direction defined by λ, μ and ν).[4]

The calculated curves shown in Figs. 5 and 6 are similarly determined but

[4] In the special cases where the direction defined by λ, μ and ν makes the same angle with two (or three) of the axes, this last stage begins when $I = I_\infty/2^{1/2}$, (or $I = I_\infty/3^{1/2}$) and it is assumed that each of the two (or three) vectors then directed along the axes turns in a plane into the direction of the field.

are complicated by the fact that I may not equal I_∞ when the redistribution process is complete. In Fig. 6 I does not always lie in the plane of the figure, $(11\bar{1})$. In the latter figure the curve marked "CALC. (1)" is obtained without confining I to the plane, while for curves "CALC. (2)" I is so confined. In Figs. 4 and 5, I is automatically confined to the plane by symmetry.

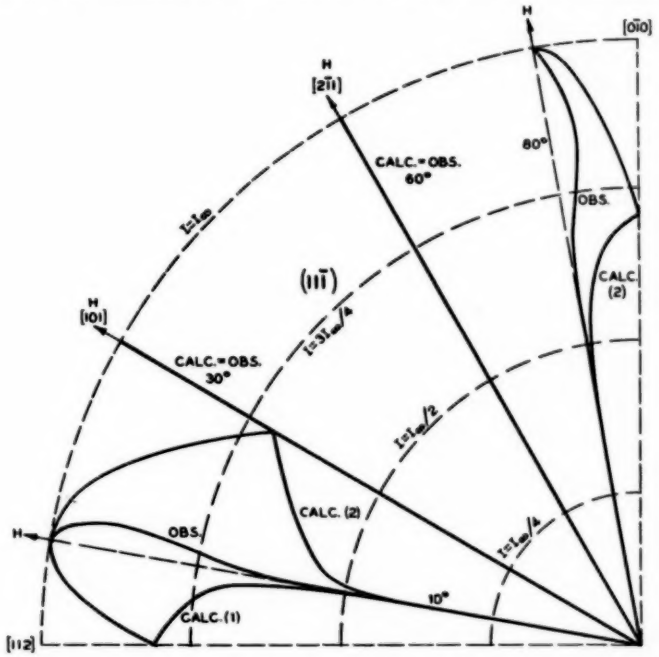

Fig. 6. Polar diagram of magnetization in a $\{111\}$ plane. Curves marked (2) are derived with the magnetization confined to the plane of the figure, corresponding to the experimental data. The observed curves are uncorrected for the demagnetizing effect of the normal component of magnetization.

Comparison with Experiment

The most complete data with which to compare the theoretical results are those of Honda and Kaya,[5] who measured the magnetization parallel and perpendicular to the applied field in an oblate ellipsoid having axes 0.4 mm, 20 mm and 20 mm. From the applied field, they subtract the demagnetizing field acting anti-parallel to the applied field. Considering the resultant field, acting in the same direction as the applied field, to be the effective field, the data are plotted in Figs. 4 to 6 as curves marked "OBS."

These effective fields, however, are not the true magnetic fields acting on the crystal, because no account has yet been taken of the demagnetizing field due to the perpendicular component of the induced magnetization. Proper consideration of this additional field changes considerably the direction of the field which is effective, as shown in Fig. 7. Here the solid arrows are vectors measured from the common point; H' represents the applied field; $H_{H'}$ the field parallel to H' corrected for the demagnetizing field due to the parallel

[5] K. Honda and S. Kaya, Sci. Rep. Tohoku Imp. Univ. (1) **15**, 721 (1926).

component of magnetization $I_{H'}$ shown on a different scale by the dotted line; H_n represents the field due to I_n and equal to I_n multiplied by the demagnetizing factor 0.189, and H represents the (true) field equal to the vector sum of $H_{H'}$ and H_n. This correction has been made to all of the data referring to the (001) plane, and the corresponding curves marked "COR." are shown in Fig. 4. These curves lie much nearer to the calculated curves than the "OBS." curves do, and it is obvious that this correction accounts for most of the original difference between the calculated and experimental results.

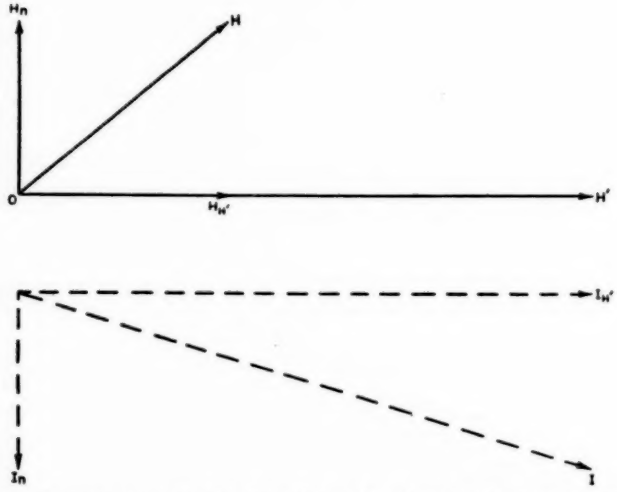

Fig. 7. Vector diagram showing the direction of the (true) field, H, as determined from the applied field, H', and the demagnetizing fields due to the components of magnetization parallel ($I_{H'}$) and perpendicular (I_n) to the applied field.

The corrected curves were derived from the data in the following way. For a given direction of the applied field H', and a certain value of the magnetization $I_{H'}$ parallel to the applied field as taken from the tables of Honda and Kaya, the direction of the field H was determined as indicated in Fig. 7 and the component of I parallel to H, I_H was calculated. This was done for all of the data relating to one direction of the applied field and curves plotted relating both θ_I (the angle between I and a particular $<100>$ axis) and θ_H (the angle between H and the same $<100>$ axis) with I_H. Similar curves were plotted for each of the four directions of the applied field in the (001) plane for which data exist. Selecting a definite value of I_H, these curves were used to obtain values of θ_H and θ_I by interpolation, one pair of values of the latter being obtained for each of the four directions of the applied field for which measurements were made. With the four points so obtained, a curve was plotted relating θ_H and θ_I, with I_H constant. Other curves were similarly plotted with I_H as parameter, and values of θ_I were read from these as a function of I_H for definite values of θ_H and the results plotted as in Fig. 4. This process naturally was subject to inaccuracies due to interpolation, and the final curves are not to be considered as representing the data exactly. Extrapolations of the curves were avoided, and sometimes no values of θ_I could be

assigned for certain values of θ_H and I_H, the curves in this case being dotted or omitted entirely.

Because these calculations were rather laborious, they were made only for the (001) plane, but since they show that the curves so corrected lie very much closer to the calculated curves it follows that a similar effect would be noted in the other planes. The correction is always in the right direction.

There is still another limitation in comparing the calculations with experiment. The perpendicular component of magnetization was determined by rotation of the single crystal specimen, so that rotational hysteresis is present. These two factors, hysteresis and the inaccuracy in the determination of the direction of the field on account of the large demagnetizing factor, are sufficient to account for the discrepancies between the corrected and calculated curves. The limitations of the data can easily be noticed when the corrected curve is plotted for $\theta_H = 45°$. Although this curve is not reproduced here it swings to within 20° of the cubic axis when I is about 0.8 of saturation. This deviation of I from the direction of H is known to be in error since the "OBS." curve is a straight line, i.e., there is no perpendicular component when the applied field is in this direction.

The results for the $(11\bar{1})$ plane are particularly interesting, for if H lies in this plane I will generally not do so. When H is inclined 10° to the [211] direction, curve marked "CALC. (1)" in Fig. 6 indicates that the theory predicts an effect in the direction opposite to that observed. In the extremely oblate ellipsoid used in the experiments, however, the magnetization is constrained to lie almost completely in the plane. When this condition is added to the others in the mathematical expression of the theory as described in the preceding section (Eqs. (10) et seq.), the direction of the perpendicular component is the same as that observed, as shown in curve "CALC. (2)."

The agreement between theory and experiment seems to be within the experimental error.

DISCUSSION

In making the calculations and plotting the results in the figures, nothing has been said explicitly about the magnitude of the magnetic field H which in the actual experiment induces the magnetization. The energy associated with each of the six directions of easy magnetization is supposed to be the same irrespective of the magnitude or direction of the field. The field is influential only in producing a magnetization having a component of given magnitude parallel to the field, the component at right angles being determined by probability considerations. There is little question but that this supposition is justified when the magnetization is small, perhaps even when it is as large as one-half of its saturation value, for then the corresponding field-strength is known to be small compared to the internal or molecular fields and cannot change the distribution function appreciably. On the other hand, when I becomes equal to I_∞ the probability considerations no longer apply and the vector representing I_∞ is assumed to turn slowly into the direction of the field, remaining always in the same plane.[6]

[6] R. Gans, following a proposal of Heisenberg's, has recently indicated how to calculate the position of this vector as dependent upon the field strength. Phys. Zeits. **33**, 15 (1932).

The transition between these two situations is undoubtedly not perfectly sharp, and it may be expected that a more complete calculation, taking account of the magnitude of the field, would show the curves to be rounded at the point of contact with a <100> axis instead of sharp as shown in the figures.

Akulov[2] has made an extended theoretical study of the ferromagnetic properties of crystals, and has based many of his conclusions on the assumption that the magnetization in a domain may have any direction with respect to the crystal axes—that the domain is magnetically isotropic—as long as the magnetization is less than half of the saturation value. This assumption was made because experiments have shown the magnetization perpendicular to the field to be small or zero when the total magnetization of the crystal is less than half of saturation. Our theory accounts for this experimental fact but is based on the contrary assumption that the domains are saturated in a <100> direction even for the smallest values of the crystal magnetization. Thus it is unnecessary to accept Akulov's rather artificial picture of isotropic domains suddenly becoming anisotropic when the magnetization of the crystal exceeds a critical value. The curves of Figs. 4 to 6 show how slight is the difference between the directions of H and I when $I<I_\infty/2$. The difference between the calculated and observed curves in this region may well be due to the inaccuracy of the data, for it is in this region of small field strengths that the demagnetizing action of the perpendicular component, discussed at length above, is a maximum. Rotational hysteresis also would tend to make the observed perpendicular component too small.

Powell[7] has proposed a theory of the magnetic anisotropy of crystals which expresses the direction of the magnetization as a function of the magnitude and direction of the field. When the field is applied in a {111} plane of iron or nickel, however, and the magnetization is constrained also to lie in that plane, his theory requires that I should be parallel to H. The data show that the degree of anisotropy is smaller than in the other planes, but still it appears quite definite, especially for iron. On the other hand, my theory indicates that in this plane and under this condition there should be a deviation of I from H in the observed direction and approximately of the observed amount. This casts considerable doubt on the validity of Powell's theory. Mahajani's[8] theory is also open to the same objection. It may be mentioned that in comparing his theory with experiment, Powell considered the field H to coincide in direction with the applied field, whereas in general their directions are different as remarked above.

The theory may obviously be applied to nickel, in which the directions of easy magnetization are <111> instead of <100> as in iron.

I take pleasure in expressing my indebtedness to L. A. MacColl for the mathematical work of the second section.

[7] F. C. Powell, Proc. Roy. Soc. London **130A**, 167–181 (1930).
[8] G. S. Mahajani, Phil. Trans. Roy. Soc. London **228**, 63–114 (1929).

An Empirical Equation of State

By HENRY S. FRANK AND FOO-SONG LEI
Department of Chemistry, Lingnan University, Canton, China

(Received August 22, 1932)

The law of Ramsay and Young, $P=\psi T-\Phi$, is shown to hold for diethyl ether both as a gas and as a highly compressed liquid. A single expression for ψ, $\psi=(R/V)e^{a/Vb}$ is shown to reproduce the experimental data for both conditions, with the same values of the constants a and b. Similar relations exist for carbon dioxide. Hildebrand's expression for Φ for ether is shown to require alteration in order to fit the accurate values for Φ here obtained. His value of about 79 cc for V_0, the molal volume at the absolute zero of temperature and zero external pressure is verified with a more precise calculation of 79.46 cc. It is suggested that the close fit of Φ to a simple formula at high pressures and the deviations at lower pressures may be due to the existence of a more pronouncedly microcrystalline structure (Andrade Stewart) in the liquid at the higher pressures. The combination of expression for Ψ and Φ is shown to produce an equation of state which is accurate for the dilute gas and the highly compressed liquid, but which fails for intermediate pressures.

A NUMBER of important advances have been made recently in the discussion of the equation-of-state problem. On the theoretical side it has been shown[1] how the quantum mechanics can be applied to the calculation of constants for gases of simple molecular structure, thus for the first time enabling a purely theoretical calculation to be made for a real gas, yielding values for the pressure in substantial agreement with experiment. Of more immediate practical importance is the equation of Beattie and Bridgeman[2] which represents with great precision the PVT relationships for real gases over wide ranges of temperature and pressure, and has been successful in reproducing pressure and temperature changes of Joule-Thomson coefficients[3] and of the ammonia equilibrium.[4]

Neither of the treatments referred to touches on the problem of the continuity of states, nor the possibility of a single equation representing accurately both gaseous and liquid phases. A contribution in this direction has been made by Hildebrand,[5] who gives an equation for the "internal pressure" $(\partial E/\partial V)_T$ of diethyl ether in both gaseous and liquid states. Whether it is logical to expect a single equation to fit both phases has become questionable, however, in view of recent theories based on x-ray diffraction[6] and the inter-

[1] (a) J. C. Kirkwood and F. G. Keyes, Phys. Rev. **37**, 832 (1931); (b) J. C. Slater, ibid **38**, 237 (1931); (c) H. Margenau, ibid **38**, 1785 (1931); (d) J. G. Kirkwood, Phys. Zeits. **33**, 39 (1932).

[2] J. A. Beattie and O. C. Bridgeman, Proc. Am. Acad. Arts and Sci. **63**, 229 (1928).

[3] J. A. Beattie, Phys. Rev. **35**, 643 (1930).

[4] L. J. Gillespie and J. A. Beattie, Phys. Rev. **36**, 743 (1930); **36**, 1008 (1930); also J. Am. Chem. Soc. **52**, 4239 (1930).

[5] J. H. Hildebrand, Phys. Rev. **34**, 984 (1929). Cf. also R. K. Schofield, Phil. Mag. **5**, 1171 (1928).

[6] G. W. Stewart, Phys. Rev. **35**, 726 (1930) and later papers.

pretation of viscosity in liquids.[7] If liquids are actually microcrystalline in structure, as these theories postulate, then they are less similar to gases than has been supposed, and the "continuity of states" expressed in the equations of van der Waals and Dieterici may require a new interpretation.

In view of the complexity of the subject not only of the structure of liquids but even of collision processes in only moderately compressed gases, we feel that it is still profitable to discuss empirical relationships connecting P, V and T, particularly where these touch liquids. At worst such relationships, if substantiated, will serve as numerical checks upon theoretical equations which may later be worked out.

The equation of Ramsay and Young, $P=\Psi T-\Phi$ where Ψ and Φ are volume functions, has been verified for dilute gases by a number of workers. The van der Waals equation is simply a more explicit form of it, as is also the Keyes equation, $P=RT/V-\delta-a/(V+b)^2$ where $\delta=\alpha V^3$. The Beattie-Bridgeman equation is a further development of the Keyes equation correcting for deviations from the Ramsay-Young law on the assumption that these are due to association.

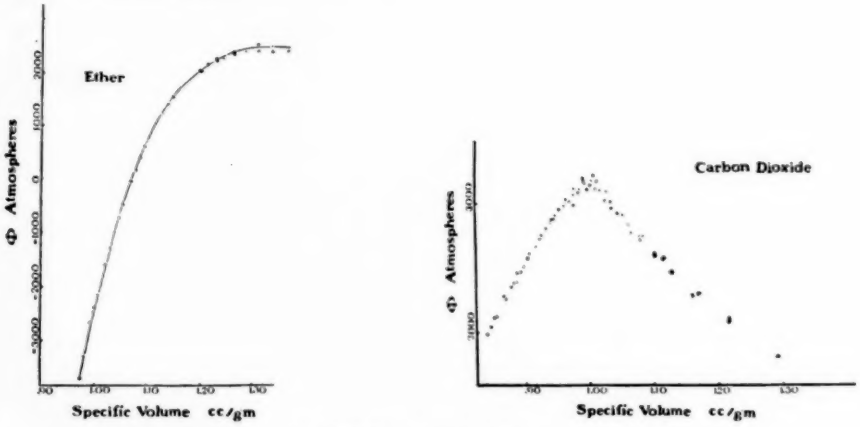

Fig. 1. Measurements at 20°C represented by squares; 40° by crosses; 60° by circles; 80° by triangles.
Fig. 2. Measurements at 0°C represented by squares; 10° by crosses; 20° by circles; 30° by triangles.

We have found empirically that for diethyl ether and carbon dioxide the function Ψ of Ramsay and Young is well represented by $(R/V)e^{a/Vb}$ for specific volumes which are not too small. What interests us particularly is the fact that the same expression with the same numerical constants seems to fit the data for the compressed liquids with great accuracy. The test of this is to assume $P=(RT/V)e^{a/Vb}-\Phi$ and calculate Φ from experimental data. If data for different values of T give calculated Φ's which fall on the same curve when plotted against volume, it is clear that not only $(\partial P/\partial T)_V$ but also its volume coefficient $\partial^2 P/\partial V\partial T$ is correctly represented. Such curves for ether and CO_2 are reproduced in Fig. 1 and Fig. 2. The data are those of

[7] E. N. DaC. Andrade, Nature **125**, 580 (1930); S. E. Sheppard and R. C. Houck, J. Rheology **1**, 349–71 (1930).

Bridgeman and Amagat, and are shown in Tables I and II together with the calculated Φ values. The constants a and b were obtained from the accurate values for Ψ given by Beattie[8] for gaseous ether and by Bridgeman[9] for gaseous CO_2. Log log $(\Psi V/R)$ was plotted against log V, and the slope and intercept determined for the straight line obtained. The slope is b and the intercept a.

TABLE I. *$V-\Phi$ curve for ether. $P=(RT/V)e^{a/Vb}-\Phi$, where $a=3.153$, $b=0.844$ and $R=1.1078$*

Volume (cc/g)	Pressure (atm.)	ψT (atm.)	Φ (atm.)	Temperature (°C)
0.9748	12,000	8287	−3713	20
0.9812	12,000	8707	−3293	40
0.9949	12,000	9330	−2670	80
1.0018	11,000	8612	−2388	60
1.0021	10,000	7525	−2475	20
1.0092	10,000	7853	−2147	40
1.0232	10,000	8422	−1578	80
1.0314	9000	7710	−1290	60
1.0416	8000	7006	−994	40
1.0491	8000	7263	−737	60
1.0564	8000	7515	−485	80
1.0705	6000	5951	−49	20
1.0801	6000	6164	+164	40
1.0887	6000	6390	+390	60
1.0960	6000	6607	+607	80
1.1311	4000	5257	1257	40
1.1417	4000	5416	1416	60
1.1517	4000	5547	1547	80
1.2018	2000	4029	2029	20
1.2032	2500	4529	2029	60
1.2157	2000	4136	2136	40
1.2316	1500	3709	2209	20
1.2316	2000	4214	2214	60
1.2479	2000	4286	2286	80
1.2680	1000	3381	2381	20
1.2680	1500	4842	2342	60

TABLE II. *$V-\Phi$ curve for CO_2. $P=(RT/V)e^{a/Va}-\Phi$, where $a=18749$, $b=0.9210$ and $R=1.8652$.*

Volume (cc/g)	Pressure (atm.)	ψT (atm.)	Φ (atm.)	Temperature (°C)
0.8377	1000	2990	+1990	0
0.8430	950	3001	+2051	0
0.8483	900	3026	2126	0
0.8525	1000	3127	2127	10
0.8645	750	3039	2289	0
0.8682	1000	3268	2268	20
0.8771	800	3173	2373	10
0.8817	900	3295	2395	20
0.8843	1000	3398	2398	30
0.8850	600	3075	2475	0
0.8915	950	3427	2477	30
0.8961	800	3324	2524	20
0.9036	750	3339	2589	20
0.9048	600	3227	2627	10
0.9154	800	3480	2680	30
0.9208	400	3145	2745	0
0.9238	500	3267	2767	10

[8] J. A. Beattie, J. A. C. S. **46,** 350 (1924).
[9] O. C. Bridgeman, J. A. C. S. **49,** 1130 (1927).

TABLE II. (*Continued*).

Volume (cc/g)	Pressure (atm.)	ψT (atm.)	Φ (atm.)	Temperature (°C)
0.9316	700	3516	2816	30
0.9382	550	3415	2865	20
0.9401	650	3536	2886	30
0.9435	300	3193	2893	0
0.9454	400	3314	2914	10
0.9507	600	3561	2961	30
0.9598	350	3346	2996	10
0.9613	450	3468	3018	20
0.9626	550	3590	3040	30
0.9680	225	3246	3021	0
0.9739	200	3198	2993	0
0.9739	300	3376	3076	10
0.9744	500	3620	3120	30
0.9752	400	3501	3101	20
0.9824	275	3399	3124	10
0.9844	175	3283	3108	0
0.9893	450	3657	3207	30
0.9902	350	3539	3189	20
0.9916	250	3422	3172	10
0.9950	150	3275	3125	0
1.0020	225	3426	3201	10
1.0050	400	3631	3231	30
1.0080	125	3252	3127	0
1.0090	300	3476	3176	20
1.0140	200	3312	3112	10
1.0220	100	3131	3031	0
1.0250	350	3450	3100	30
1.0320	75	3050	2975	0
1.0320	250	3274	3024	20
1.0420	150	3080	2930	10
1.0500	300	3222	2922	30
1.0600	200	3050	2850	20
1.0620	50	2824	2774	0
1.0770	175	2925	2750	20
1.0780	100	2820	2720	10
1.0800	250	3005	2755	30
1.1000	75	2676	2606	10
1.1000	150	2771	2621	20
1.1130	200	2783	2583	30
1.1270	125	2606	2481	20
1.1590	50	2343	2293	10
1.1680	150	2456	2306	30
1.2140	75	2159	2084	29
1.2140	125	2233	2108	30
1.2900	100	1927	1827	30
1.4770	75	1250	1175	30

In the regions where Ramsay and Young's law holds, $\Phi = (\partial E/\partial V)_T$ the so-called "internal pressure" of the substance. Hildebrand has represented this for ether by the equation

$$\Phi = \frac{3180 \times 10^4}{V^2}\left[1 - \left(\frac{79}{V}\right)^8\right]^{10},$$

verifying his equation against Bridgeman's data. He obtained the form of Φ by analogy with the Born-Landé theory of compressibility of crystal lattices,

[10] Φ is in atmospheres and V in cc per mol. Changing V to cc per gram so as to compare with our figures, Hildebrand's equation becomes

$$\Phi = 5794/V^2 - 9692/V^{10}.$$

and considers its agreement with experiment to speak for the existence of rather simple relations in the structure of liquids. Hildebrand's method of calculating Φ from Bridgeman's data does not give results of high accuracy, and the points do not fit his curve very perfectly. Using our calculated Φ's for liquid ether, and the accurate values of Beattie[8] for Φ for gaseous ether, we have modified the constants in Hildebrand's equation, and obtained the following:[11]

$$\Phi = 3834/V^{1.892} - 6295/V^{7.94}.$$

Taking this equation for Φ, and our Ψ, we obtain for an equation of state for ether:

$$P = (RT/V)e^{a/V^b} - K/V^n + C/V^d,$$

where P is in atmospheres, V is in cc/g. $R=1.1078$, $a=3.153$, $b=0.844$, $k=3834$, $n=1.892$, $c=6295$, and $d=7.94$. Values for P calculated from this equation are compared with experimental ones in Table III.

TABLE III. *Ether. A comparison of pressures observed by others and those calculated from our equation of state. Pressure in atmospheres; temperature in °C; $T=t+273.13$.*

V(cc/g)	P (calc.)	P (obs.)	t (°C)	Observer
0.9812	12,044	12,000	40	Bridgeman
1.0092	9942	10,000	50	"
1.0416	8012	8000	40	"
1.0801	6266	6000	40	"
1.1311	4587	4000	40	"
0.9949	12,016	12,000	80	"
1.0232	9997	10,000	80	"
1.0564	8073	8000	80	"
1.0960	6425	6000	80	"
20	16.89	16.88	150	Beattie
25	14.40	14.48	150	"
35	11.08	11.19	150	"
100	4.37	4.32	150	Ramsay & Young
15	25.32	25.04	200	Beattie
20	20.25	20.47	200	"
25	17.13	17.23	200	"
35	12.93	13.05	200	"
15	38.06	37.71	325	"
20	29.34	29.39	325	"
25	23.96	24.05	325	"
35	17.56	17.66	325	"
100	4.90	4.88	195	Ramsay & Young
200	2.52	2.50	195	"
250	1.98	2.01	195	"
300	1.71	1.80	195	"

[11] Born and Mayer have recently (M. Born and J. E. Mayer, Zeits. f. Physik **75,** 1 (1932); J. E. Mayer and L. Helmholtz, ibid. **75,** 19 (932); J. E. Mayer and M. C. Maltbie, ibid. **75,** 748 (1932)) shown that an exponential law is better able to express the repulsive potential in a crystal lattice than is a simple inverse power. We find that their form, $be^{-r/\rho}$, for repulsive potential, or $C_1V^{-2/3}e^{-C_2V^{1/3}}$ for the repulsive part of Φ does not fit our data as well as the form, C/V^a, which we have used.

It will be observed that the representation of Φ as the algebraic sum of an attractive and a repulsive term each varying as an inverse power of the volume holds with good accuracy in the dilute gas and the highly compressed liquid, but fails for the liquid at lower pressures, and for the compressed gas. It is not clear that the agreement for the highly compressed liquid would persist at still higher pressures, but there seems to be no reason to doubt this. It may be mentioned that the critical constants calculated from this equation by writing $(\partial P/\partial V)_T=0$ and $(\partial^2 P/\partial V^2)_T=0$ do not agree with the experimental ones, that is, the critical region lies in the middle range for which the equation does not hold.

The range of pressures covered by the data for CO_2 is not extended enough for this method to furnish any interesting information concerning the form of Φ. As an indication of the limits of accuracy of our values of Ψ, however, we have used our Ψ and Bridgeman's Φ to obtain the results shown in Table IV.

TABLE IV.[10] *CO_2 A comparison of pressures observed by Amagat and those calculated from our equation of state. Pressure in atmospheres; temperatures in °C; $T=t+273.13$.*

V cc/g		0	10	20	30	40	50
40	obs.	11.16	12.15	12.67	13.17	13.69	14.19
	calc.	11.70	12.20	12.69	13.19	13.69	14.18
	Δ	0.54	0.05	0.02	0.02	0.00	−0.01
30	obs.	15.08	15.76	16.47	17.15	17.86	18.54
	calc.	15.15	15.82	16.50	17.17	17.85	18.52
	Δ	0.07	0.06	0.03	0.02	−0.01	−0.02
25	obs.	17.66	18.48	19.35	20.19	21.06	21.90
	calc.	17.76	18.58	19.40	20.22	21.05	21.87
	Δ	0.10	0.10	0.05	0.03	−0.01	−0.03

It is not required of an empirical equation that it conform to preconceived ideas of functional form, nor that it lend itself to simple interpretation. If an interpretation is to be given, however, we are inclined to correlate the good agreement of Hildebrand's form of Φ at higher pressures, as well as the poorer agreement at lower pressures, with the cybotactic, or microcrystalline theories of the liquid state already referred to. It seems likely that the orderly arrangement of molecules in the liquid would become more marked at higher pressures, and one might predict that in the pressure region where our equation fits Bridgeman's data the x-ray diffraction rings of ether would be found to be sharper than has yet been observed, and that the fluidity of the liquid would be found to be greatly diminished. Another possibility is that the simpler relations at high pressures correspond to a pressure-inhibition of molecular rotation in the liquid somewhat along the lines suggested for temperature effects in Meyer's[12] interpretation of the transitions observed by Wolfke and Mazur.[13]

In the matter of functional form, it has been customary to express the attractive and repulsive terms in crystals by inverse integral powers of the volume. On the other hand, until the quantum mechanical theory is further

[12] L. Meyer, Zeits. f. Physik **75**, 421 (1932).

[13] M. Wolfke and J. Mazur, Zeits. f. Physik **74**, 110 (1932).

developed than at present it will not be certain whether the powers for liquids and compressed gases have to be integral. We have therefore taken the powers empirically as slopes of logarithmic plots. The failure of the equation for liquid ether at lower pressures can be corrected by adding other terms to Φ, but this only serves up to a specific volume of 1.15 cc/g. Beyond this point ΨT fails to represent the effect of temperature, either because Ψ is no longer of the right form, or, more probably, because Ramsay and Young's law no longer holds. The $\Phi - V$ plots for both ether and CO_2 make it seem likely that in the intermediate region the dependence of P upon T becomes more complicated, as is demonstrated for gases under high pressures by the success of the Beattie-Bridgeman equation.

As to the form of Ψ, in searching the literature available to us we have failed to find the form $(R/V)e^{a/V^b}$ used by any previous author, though other forms involving exponentials are not rare. So far as we can tell none of the other forms that have been proposed has the property of representing the liquid phase of ether or of CO_2. In our form, since the liquids give volumes near 1 cc/g, and b is not far from unity, the fit for the liquid is not very sensitive to changes in b, though such changes are important in the gas phase. There is thus possibly something fortuitous in the fit for the liquid so far as concerns the constant b. This is hardly the case with the constant a, however, and it would be very desirable to learn whether this form of equation applies also to other substances. Unfortunately, the number of substances for which data over considerable temperature and pressure ranges are available for both liquid and gas is small. Even in the case of CO_2, as has been mentioned, the range of measured pressures is not so great as is desirable.

Hildebrand has assumed that at the absolute zero of temperature and under no external pressure the volume V_0 of any substance is that at which $\Phi = 0$. His value of V_0 for ether, about 79 cc/mol., is verified by our calculation, which gives 1.0727 cc/g, or 79.46 cc/mol.

PROCEEDINGS
of the
AMERICAN PHYSICAL SOCIETY

MINUTES OF THE CHICAGO MEETING, NOVEMBER 25–26, 1932

The 180th regular meeting of the American Physical Society was held in Chicago, Illinois at the Ryerson Physical Laboratory and Eckhart Hall of the University of Chicago on Friday and Saturday, November 25 and 26, 1932. The presiding officers were W. F. G. Swann, President of the Society, Paul D. Foote, Vice-President, Arthur H. Compton, A. J. Dempster and H. A. Erikson.

Judson Court, one of the University dormitories, was the Society headquarters and the Society dinner was held there on Friday evening. About ninety guests were present. President Swann presided and the after dinner speakers were Arthur H. Compton, who related some of his experiences in his cosmic-ray expedition, Editor John T. Tate, who reviewed the returns on the publication questionnaire and pointed out the probable savings to be secured by the new program under the American Institute of Physics, and Karl K. Darrow who recalled numerous interesting features of past meetings of the Society.

The new College Physics Museum in Belfield Hall was kept open both days for inspection by the members of the Society.

Meeting of the Council. At its meeting on Friday, November 25th, the Council approved the transfer of four members to the grade of fellowship. Thirty-nine candidates were elected to membership. *Transferred from membership to fellowship:* Richard M. Badger, Kenneth T. Bainbridge, Weldon G. Brown and G. B. Kistiakowsky. *Elected to membership:* Hollis S. Baird, Victor W. Cohen, William T. Cooke, Edward M. Cratty, W. P. Cunningham, Robert W. Ditchburn, John Dropkin, P. O. Ewald, Guy Forman, G. Norris Glasoe, G. G. Harvey, Clarence D. Hause, Laurence B. Heilprin, Banesh Hoffman, Joseph Joffe, Joseph S. Knapper, Homer C. Knauss, Walter H. Mais, H. E. Malstrom, J. Carlisle Mouzon, Elton M. Palmer, Anna W. Pearsall, John M. Pearson, Fred G. Person, H. S. Polin, Seymour Rosin, Angus S. Roy, Harold L. Saxton, George K. Schoepfle, Sidney L. Siegel, Selby M. Skinner, Frank M. Sparks, Alexander W. Stern, Herbert M. Strong, B. J. Thompson, Clinton E. Trimble, Louis R. Weber, George W. Wheelwright, and Henry L. Yeagley.

The regular scientific session consisted of fifty-five papers, six of which, numbers 10, 11, 20, 40, 41 and 44, were read by title. A complete list of authors and abstracts will be found in the following pages.

W. L. SEVERINGHAUS, *Secretary*

ABSTRACTS

1. The magnetic susceptibilities of some common gases. G. G. HAVENS, *University of Wisconsin.*—In view of the large differences among the results of various observers for the magnetic susceptibilities of common gases, it seemed desirable to apply to some of these gases the method described in a previous article. (Phys. Rev. **41,** 339 (1932)). Being a comparison method, the values obtained are relative to a provisional value of $X_{O_2}=3335\times10^{-6}$ for the molecular susceptibility of oxygen at 20°C. If the value for oxygen should later prove to be different, the values for these gases will be changed proportionally. The results obtained are: $X_{H_2}=-4.014\times10^{-6}$, $X_{He}=-1.925\times10^{-6}$, $X_{N_2}=-11.94\times10^{-6}$, $X_{CO_2}=-20.81\times10^{-6}$. The results for H_2, He and N_2 are in good agreement with those obtained by Wills and Hector. (Phys. Rev. **23,** 209 (1924).) The value of the temperature presented the largest uncertainty in the measurement of susceptibilities at liquid air temperatures; however it was found that the molecular susceptibilities of H_2 and He at liquid air temperatures vary less than 4 percent from those obtained at room temperatures. This result disagrees with that of Bitter (Phy. Rev. **36,** 1648 (1930)) which indicates a decrease of more than 40 percent in the molecular susceptibility of H_2 in going from room to liquid air temperatures. Preliminary observations indicate that the susceptibilities of ortho- and para-hydrogen are the same within 1 percent.

2. The paramagnetic susceptibility of Cu^{++}. O. M. JORDAHL, *University of Wisconsin.*—Calculations have been made for the susceptibility of the Cu^{++} ion subject to a crystal potential field of predominantly cubic symmetry with a small rhombic field superposed. The Hamiltonian is

$$Ax^2+By^2-(A+B)z^2+E(x^4+y^4+z^4)+\lambda(\boldsymbol{L}\cdot\boldsymbol{S})+\beta\boldsymbol{H}(\boldsymbol{L}+2\boldsymbol{S})$$

By proper choice of the parameters, the resulting expressions for the principal susceptibilities are capable of agreement with the known experimental data. To a good approximation, the expression for the mean (i.e. powder) susceptibility X_m is independent of both the magnitude and the asymmetry of the rhombic field, and gives a linear dependence on temperature for the quantity $(X_m kT/N\beta^2)$. This agrees with the Leiden data of de Haas and Gorter on $CuSO_4\cdot5H_2O$ from 14°K to 290°K. In order to fit the data of Bartlett on the principal susceptibilities of $Cu(NH_4)_2(SO_4)_2\cdot6H_2O$ and $CuK_2(SO_4)_2\cdot6H_2O$ (Phys. Rev. **41,** 818 (1932)) it is necessary to choose the parameters so that the cubic field produces a splitting of approximately 20,000 cm^{-1} and the splitting of the lower cubic level by the rhombic field is about 300 cm^{-1}. These values agree approximately with those found for Co, Ni and Cr by R. Schlapp and W. G. Penney. (Phys. Rev., in press.)

3. A compact high potential electrostatic generator. HENRY A. BARTON, *American Institute of Physics,* D. W. MUELLER, *Princeton University and* L. C. VAN ATTA, *Massachusetts Institute of Technology.*—An inexpensive and compact continuous high-potential source was desired for nuclear research. A Van de Graaff, belt-type, electrostatic generator has been built. To overcome the corona limitation due to high potentials and small dimensions, the entire apparatus is mounted in a cylindrical steel drum and the insulating air raised to a pressure of several atmospheres. A cylindrical electrode is supported in the center of the drum by two textolite cylindrical tubes of the same diameter. In one of these runs a silk charging belt similar to that in the original Van de Graaff generator. The other supporting tube can be evacuated and it will be used in applying high potentials to the acceleration of charged particles. At a pressure of seven atmospheres, a potential of about one million volts was generated. High pressures also permit greater charge to be carried on the belt. In a separate test, also at seven atmospheres pressure, the belt transported charge at the rate of 0.1 m.a. It will be possible to operate at twice the pressure so far used. The belt can be driven twice as fast as now and a parallel belt added. It is hoped to generate a kilowatt at about two million volts.

4. The production of high-velocity protons by repeated accelerations. A. J. DEMPSTER, *University of Chicago.*—The principle of a simple method for repeated acceleration of canal rays has been tested. The positive rays from a high potential hydrogen discharge tube pass into hydrogen at higher pressure where some of the atoms become neutral and the equilibrium

ratio between positive and neutral particles is approached. The neutral rays then cross a high retarding field into a positively charged metallic chamber 32 mm long connected to the anode. During their passage through this chamber, at a pressure of 0.2 mm Hg, a number of the neutral atoms revert to the positively charged state. On leaving the positively charged metallic chamber, these positively charged atoms are accelerated and attain twice their original energy. The process may be repeated indefinitely with a loss of intensity at each passage through an accelerating chamber. An experiment was carried out with one acclerator in which the energy of the rays was deduced from the deflection, by a short transverse electric field, of the spot produced by the rays on a fluorescent screen. With the accelerator grounded a maximum energy of 22,500 volts was observed, and with the accelerator joined to the anode of the discharge tube a new spot appeared with half the deflection, corresponding to an energy of 45,000 volts.

5. Polarization of collecting electrodes in high vacua. A. E. SHAW, *University of Chicago*—In an experiment to determine e/m by electron deflection in superimposed electrostatic and magnetic fields, it was found possible to determine accurately the value of the surface charges that form on the plates to which the electric potential is applied and which must be corrected for. These surface layers have been found to vary with the material of the plates, the gas pressure and the intensity of the electron beam. They are independent of the intensity of the electrostatic field. With bronze at pressures of 5×10^{-7} mm Hg and an electron current of 3×10^{-12} ampere, the surface potential was 0.263 volt. With a current of 10^{-9} ampere the pressure remaining the same, the potential increased to 0.998 volt. With gold the surface potential was less than 0.005 volt, at pressures of 5×10^{-7} mm Hg and an electron current of 3×10^{-12} ampere.

6. Ionization of He by electron impact. W. W. WETZEL, *University of Minnesota*.—The Born collision theory (neglecting exchange effects) is applied to the ionization of He by electron impact. The distributions in angle and energy of the scattered electrons have been calculated for initial electron energies of 50, 100, 200, and 500 volts. The curves are in qualitative agreement with the experiments of Van Atta in He for the distribution in energy and with those of Tate and Palmer in Hg for the angular distribution. The most probable mode of ionization is for scattering in the forward direction with a loss of about one volt energy, the probability dropping rapidly to zero just at the ionization potential. The theoretical curves show, however, a continually increasing total probability of ionization due to excessive scattering in the forward direction. To obviate this difficulty the distortion of the wave forms of the incident and scattered electrons is being studied. Preliminary considerations indicate also a reasonably good probability for ionization and simultaneous excitation in He.

7. Ionization by electron impact in water vapor and sulphur dioxide. H. D. SMYTH AND D. W. MUELLER, *Princeton University*.—Ionization in water vapor and sulphur dioxide has been studied with the mass-spectrograph previously used by Smyth and Stueckelberg. In water vapor the results of previous investigators have been confirmed and extended. Two I.P.'s for H_2O^+ were found, 12.7 ± 0.3 and 16.0 ± 0.6 volts. Other positive ions in much smaller numbers appeared as follows: H^+ at 18.9, OH^+ at 18.9, H_3O^+ with H_2O^+, O^+ at 18.5, H_2^+ at 33.5 and O_2^+ (very weak). In sulphur dioxide which has apparently never before been studied, SO_2^+ ions appeared at 13.1 ± 0.3 volts. SO^+ ions at 16.5 ± 0.5 and ions of mass 32, either S^+ or O_2^+, at 16.0 ± 0.7, increasing sharply at 22.3 ± 1.0. No O^+ ions were observed. The existence of a strong second I.P. for H_2O^+ had been suggested by Smyth and Stuckelberg on experimental grounds and by Mulliken for theoretical reasons. Consideration of the probable ionization processes corresponding to the other results shows one point of special interest. Evidently the processes $H_2O\rightarrow H_2+O^+$ and $SO_2\rightarrow S^++O_2$ both occur and at very nearly the minimum energy calculated. This means that in the process of ionization not only are the chemical bonds between the O (or S) and H (or O) atoms broken but new bonds are established between the H (or O) atoms themselves which did not exist in the normal state.

8. Radiation excited by canal ray impact. F. L. VERWIEBE, *University of Chicago*.—Hydrogen canal rays accelerated in a field up to 50 kv were allowed to impinge on a metal

target, and the beam of particles and radiation emitted from the target was investigated. Pinhole images of the focal spot were obtained on Schumann plates and plates coated with molybdenum tri-oxide. The tri-oxide indicates the presence of atomic hydrogen. By means of a deflecting magnetic field it was found that the beam coming from the target consisted mainly of neutral particles or of radiation, and also of a fainter beam of protons which had a velocity practically equal to that of the protons in the incident canal rays. The presence of uncharged hydrogen atoms in the neutral beam was shown by the image of characteristic light blue color formed on a molybdenum tri-oxide plate. A grating was used to determine whether the undeflected beam also contained electromagnetic radiation. A diffraction pattern was obtained and the value of the wave-length was found to agree within the limits of the accuracy of the measurements with that of the first Lyman line, 1216A'. No wave-lengths shorter than this of observable intensity were found.

9. Radiation from positive ions in argon, neon, helium. A. I. McPherson, *University of Chicago* (*Introduced by A. J. Dempster*).—Light excitation was produced by a stream of high speed—20,000 volt—positive ions of argon, neon, helium in passage through rarefied argon, neon, helium respectively. The spectra observed in the direction of motion show groups of doublets, whose separation varies with the velocity of the positive ions, a sharply marked Doppler displacement. In argon and neon, the first spark lines are strongly excited in both the gas at rest and in the moving particles, the intensity of the displaced line in each doublet being only slightly less than that of the undisplaced line. The arc lines appear relatively weak, an in the very few cases where an arc line has an accompanying Doppler line, it is very faint indeed. In helium many of the lines of both arc and spark spectra show the effect clearly but the intensity of the displaced line is usually much less than that of the rest line, and the relative intensity varies greatly from line to line.

10. The actinium branching ratio. Forrest Western and Arthur Ruark, *University of Pittsburgh*.—The actinium branching ratio is $\lambda_{Ac}N_{Ac}/E$; $\lambda_{Ac}N_{Ac}$ is the activity of the actinium in equilibrium with a sample of uranium of activity $2E$. Assuming one or two actino-uranium isotopes, the ratio $B=\lambda_{Ac}N_{Ac}/\lambda_1N_1$ is more useful. (Subscripts 1, 2, 3, 4 refer to isotopes 238, 234, 239, 235.) B is determined from the saturation currents i_U and i_{Pa}, from a sample of uranium and its associated protoactinium, and the alpha particle ion numbers k_{Pa}, $k_1, \cdots k_4$. Ziegert's determinations of ion numbers and the above actinouranium hypothesis, necessitate revision of branching ratios given by Widdowson-Russell and Hahn-Meitner. Assuming two actinouranium isotopes of masses 235 and 239, we find that

$$B=[(k_1+k_2)i_{Pa}]/[k_{Pa}i_U-(k_3+k_4)i_{Pa}].$$

If U_3 does not exist, put $k_3=0$. k_1, k_2 and k_{Pa} are known. It seems probable from work of Ziegert and of Wilkins-Ra· ton that $k_3 \leqq k_4 \leqq k_2$. If so, data of Widdowson-Russell and Hahn-Meitner yield $B=0.0281$ or 0.0320 if U_3 is non-existent; and $B=0.0285$ or 0.0325, if U_3 exists. Data of Wildish are not appreciably affected; von Grosse, details unpublished, obtained 0.04.

11. The atomic weights of radioactive substances. Forrest Western and Arthur Ruark, *University of Pittsburgh*.—Given the isotopic weights of Ra *G*, Ac *D*, and Th *D*, that of any other radioactive substance can be obtained by adding the masses of the particles emitted and the mass equivalent of the energy lost, in the intervening disintegrations. Such computations were made by St. Meyer but we do not agree with all his conclusions. Using Aston's analyses of leads, chemically-determined atomic weights, and the packing fraction curve, one finds in three ways that the weight of Pb^{216} is 205.984 ± 0.03 on the chemical scale. The weights of Pb^{207} and Pb^{208} are assumed to differ from this by integers, by analogy with the behaviors of Hg and Kr. We then obtain the following isotopic weights.

	Calculated	Accepted chemical value
Radium	226.027	$225.96_7 \pm 0.012$
Protoactinium	231.039	
U^{234}	234.040	
U^{235}	235.045	
U^{238}	238.046	$238.13_7 \pm 0.013$ (U mixture)
U^{239}	239.051	
Thorium	232.035	232.120 ± 0.014

Any reasonable assumption as to half-lives of possible actinouranium isotopes yields an atomic weight for U unreconcilable with that obtained chemically. The calculated atomic weights of Ra, Th, and U should be used in preference to currently accepted values.

12. Argon in the ionization method of measuring cosmic rays and γ-rays. JOHN J. HOPFIELD, *Basic Science Division, A Century of Progress, Chicago.* (*Introduced by H. G. Gale.*)—Ionization current-voltage curves of argon at 31 atm. and 71 atm. and at four γ-ray intensities of ratios 1, 10, 100 and 1000 were not convertible into one another by constant factors. The superiority of argon over air for ionization chambers, and the slower recombination of its ions is shown in the following:

Pressure in atm.	10	20	30	40	50	60	70	80	90	100
I, ions/cc/sec. per atm, (argon)	3.75×10^2	3.45	3.09	2.80	2.57	2.36	2.19	2.03	1.89	1.77
I, ions/cc/sec. per atm, (air)	1.80×10^2	1.44	1.18	1.02	0.90	0.80	0.71	0.65	0.59	0.55
$I_{argon.}/I_{air.}$	2.08	2.40	2.61	2.73	2.84	2.95	3.05	3.12	3.18	3.23

It is seen from these data that the argon ionization-pressure curve is more nearly linear than that of air; furthermore the argon curve is rising rapidly even at the end pressure. Preliminary results indicate that the ratio of intensity of cosmic rays to γ-rays is a function of the argon pressure. At 36 atm. it was 0.117, and at 74 atm., 0.139. This change could be accounted for by insufficient voltage for saturation. A smaller ratio of cosmic rays to γ-rays was measured in argon (0.117) than in air (0.149), at the same pressure. This seems to be the first direct comparison of the action of cosmic rays on monatomic and diatomic gases. This smaller ratio accords with the suggestion that the primary attack of cosmic rays is on atomic nuclei, since argon has half as many as air. Other explanations are tenable. These experiments were carried out through the courtesy of the University of Chicago.

13. Sea level intensity of cosmic rays in certain localities from 46° south to 68° north latitude. ARTHUR H. COMPTON, *University of Chicago.*—Measurements have been made, with the help of many cooperating physicists, of the cosmic rays at typical stations in Hawaii, New Zealand, Australia, east and west equatorial Pacific ocean, Panama, Peru, Mexico, United States, Canada and Switzerland. When reduced to normal barometric pressure, or sea level, these data show nearly uniform intensity for latitudes north of 34° in United States and south of 34° in Australasia. Between these latitudes the intensity drops sharply to a value about 87 percent as great as that in the temperate zones. As compared with northern North America, northern Europe has sensibly the same intensity of cosmic rays, while the data indicate that in temperate Australasia the intensity is 2 or 3 percent greater. These data are probably in error by about 1 percent. A comparison of the data taken in Peru and Mexico shows a much closer correlation of the intensity of the cosmic rays with the dip of the magnetic needle than with the geographic latitude. The differences in intensity thus seem to be due to the earth's magnetic field, which would seem to imply that the cosmic rays are electrical in character.

14. Diffraction of low-speed electrons by a tungsten single crystal. WAYNE T. SPROULL, *University of Wisconsin.*—The (1–1–2) and (1–0–0) planes of a tungsten crystal were bombarded at normal incidence with primary electrons and the intensity of the full-velocity secondary beams measured as a function of azimuth, co-latitude (θ), and primary voltage. A new magnetic deflection method of analyzing the secondaries permitted observations at co-latitudes down to zero. The crystal was outgassed 1550 hours at temperatures up to 1600°C at pressures of 10^{-7} mm of Hg or less. Beams fitting the usual theory were found for the (1–1–2) plane in the azimuth parallel to the diagonals of the lattice cubes, but in the azimuth (A) perpendicular at the cube diagonals strong sharp beams were found at every primary voltage tried, their positions accurately obeying the volume law $n\lambda = d/\sqrt{6} + 2d/\sqrt{6}\sin(30° - \theta)$ after making the usual allowance for the work function W_a. Beams found in the (1–0–0) plane obeyed the usual theory, except that during growth and decay they also obeyed the volume law and not the surface law. Consistent values were obtained for W_a, the average being 4.82 volts. The effect of variation of angle of incidence was briefly studied. A possible explanation of the peculiar behavior of the beams in the A azimuth of the (1–1–2) plane is outlined.

15. Intensity distribution in electron diffraction patterns of ZnO. H. J. YEARIAN AND K. LARK-HOROVITZ, *Purdue University.*—A well-defined electron beam from a hot filament has been used in the range between 3.3 and 25 kv for the production of diffraction patterns of ZnO powder. Purest ZnO has been prepared directly on the slit using a zinc arc, or has been deposited chemically. The geometry of the diffraction pattern is identical with the corresponding x-ray pattern, giving C^4_{6v}, $a=3.22$ A°, $c/a=1.61$; there appear however also forbidden lines (fractional orders). The intensity distribution shows marked deviations from the intensity distribution of the x-ray patterns. It has been shown that these deviations are not due to pre-

hkl	$10\bar{1}0$	0002	1011	$10\bar{1}2$	$1120\cdots$	$11\bar{2}4$	$12\bar{3}2$
Elec. int.	St.	V.V.St.	V.St.	V.St.	St.	F	V.St.
X-ray int.	St.	Med.	St.	Med.	St.	F	F

ferred orientation, differences in structure due to methods of preparation, or coincidences with another form of ZnO. The theoretical explanation of the F curves thus obtained is discussed on the basis of additional surface reflection, dynamic reflection, and finally under the assumption that nuclear parameter is slightly greater than the electronic parameter. A partial explanation of the intensity distribution on this basis is possible.

16. Deflection of a beam of HCl molecules by a non-homogeneous electric field. EDWIN MCMILLAN, *Princeton University.*—It was found possible to use a film of ammonia frozen on to a polished metal surface by liquid air as a quantitative detector for a beam of HCl; this was done by putting a number of exposures on the target during each run to serve as intensity marks, and photographing and photometering the resulting deposits of NH_4Cl. The intensity distribution in a beam broadened by passage through a nonhomogeneous electric field was measured by this means, and found to agree with the theory. An attempt was made to resolve the deflected beam into components by the use of a mechanical velocity filter. This failed because of lack of intensity of the beam after filtration.

17. A determination of e/m by means of photoelectrons excited by x-rays. G. G. KRETSCHMAR, *University of Chicago.*—A value of e/m has been obtained by a magnetic deflection method making use of x-ray photoelectrons and the magnetic spectrograph. Electrons were ejected from thin evaporated or sputtered films of gold, silver, copper and platinum by the x-radiation from a molybdenum target metal tube placed close to the film and working at an input of 1.5 kilowatts. The velocity of ejection of the photoelectrons was computed from the difference between the energies associated with Mo K radiation and the various absorption limits of the sputtered films. Relativity corrections were made since these velocities correspond to 8000 to 15,000 equivalent volts. The α_1 and α_2 components of the molybdenum $K\alpha$ line were clearly resolved since the magnetic field was kept very constant by the use of a potentiometer and continuous hand control. The weighted mean value of e/m_0 obtained from five plates is $1.7555 \pm 0.0026 \times 10^7$ e.m.u. per gram. It is to be noted however, that the absolute accuracy of this result is dependent upon the values of x-ray wave-lengths from crystal measurements.

18. Theory of the energy distribution of photoelectrons. LEE A. DUBRIDGE, *Washington University, St. Louis, Mo.*—The success of Fowler's theory in predicting the form of photoelectric spectral distribution curves at various temperatures leads one to expect that similar methods would yield expressions for the energy distribution and voltage-current curves. Considering first only the energies normal to the surface (plane parallel electrodes) and using the Fermi statistics, an expression has been derived for the voltage-current curve which is identical with Fowler's equation for the total emission, except that the surface potential jump W_a is replaced by $(W_a + Ve)$ where V is the retarding potential. The theoretical curve is in good agreement with preliminary experimental results, and yields a method of determining the maximum emission energy at 0°K. At all higher temperatures the voltage-current curves should approach the axis symptotically. This has an important bearing on the photoelectric determination of h. When the total energies of the emitted electrons are considered a more complex expression results, which can, however, be put in a form for comparison with experiment. The predicted curve is widely different from those usually observed experimentally, and experiments are under way to determine the cause of the discrepancy.

19. Energy distribution of secondary electrons from molybdenum. L. J. HAWORTH, *University of Wisconsin.*—A careful study has been made of the distribution in energy of secondary electrons emitted by a thoroughly outgassed Mo target when bombarded with a narrow, homogeneous beam of primary electrons. As observed by Farnsworth, Soller, and others, two groups of secondary electrons predominate; the usual large group of "full velocity" secondaries of energy equal to that of the primaries, and an equally large group of very slow secondaries of energy from zero to 15 volts. In addition to the general distribution several small groups of secondaries may be distinguished. These may be divided into two classes: (1) groups similar to those reported by Rudberg (P.R.S. **127,** 111 (1930)) consisting of electrons of energies certain fixed amounts less than that of the primary electrons; (2) groups of electrons of fixed energy relative to the absolute scale, independent of the energy of the primary electrons. A study was also made of the number of "full velocity" secondaries as a function of primary energy. An attempt has been made to explain the results obtained on the basis of theory developed by Kronig, Penney, and others, relative to allowed energy levels for electrons in a metallic lattice.

20. Scattering of slow electrons by caesium ions. C. BOECKNER AND F. L. MOHLER. *Bureau of Standards, Washington, D.C.*—Measurements were made of the gradient and the temperature and concentration of the electrons in the positive column of a caesium vapor discharge. From such measurements the electron mobility and the effective cross section of the caesium atoms for electron scattering can be deduced. (T. J. Killian, Phys. Rev. **35,** 1238 (1930).) It is found that the scattering cross section increases linearly with electron concentration, the increase being very rapid for low pressures. The variation at all caesium pressures can be explained by the assumption that scattering is due to the sum of the effects of the ions and neutral caesium atoms. The cross section of ions for the interception of slow electrons (0.3 volts) obtained by means of this assumption is very large, 80×10^{-14} cm². The cross section of the neutral atoms is 3.8×10^{-14}, a value in fair agreement with that obtained from more direct measurements. The large cross section of the ions can be explained by the ordinary electrostatic attraction between particles of opposite charge. A 0.3 volt electron, for example, whose original direction of motion passes 40A from an ion is deflected through 60° by the action of the electrostatic forces.

21. The scattering of lithium ions from a nickel surface. ANDREW LONGACRE, *Princeton University.*—The velocity and intensity of lithium ions scattered from a metal surface have been measured by allowing the ions scattered to pass through openings into a Faraday collector. The source (heated spodumene) and collimating apertures could be rotated around the target so that the latter could be bombarded from any arbitrary angle. The Faraday collector was supported rigidly in order to obtain satisfactory insulation and the angle of scattering varied by rotating the source and target together. With a homogeneous initial beam the ions are scattered in the general direction corresponding to the specular reflection of light. There is no evidence of a general scattering obeying a cosine law. In the immediate neighborhood of maximum intensity the scattering obeys a form of cosine law. By means of retarding potentials the energies of the scattered ions was measured and the scattered beam was found to have a more homogeneous distribution the greater the angle of scattering. The most probable energy, E, of the scattered ions varies with the angle of scattering, θ, and may be expressed by the following relation, $E=a\theta+b$, where a is a constant depending only upon the angle of incidence and b is a constant depending upon the incident energy as well as upon the angle of incidence.

22. The behavior of crystalline test bodies in streaming solutions. T. W. MOORE, *Purdue University,* (*Introduced by K. Lark-Horovitz*).—The change in shape of test bodies of rock salt in NaCl solutions of various concentrations and flowing with different velocities has been studied. In dilute solutions the influence of the solubility of the salt is prevalent. In more concentrated solutions the test body assumes the shape determined by the hydrodynamic forces exerted on the material by the streaming liquid. In saturated solutions the test body assumes a shape which is practically determined by the hydrodynamic forces only: hydrodynamic profile. The results are applied to the observations on the erosion of natural rock and technically used material.

23. The electrical properties of surface layers. K. LARK-HOROVITZ AND J. E. FERGUSON, *Purdue University.*—With a polonium electrode as a sounding device, the potential at the interface air-liquid has been investigated for pure water, electrolyte solutions and monomolecular layers of stearic and oleic acid spread on the surface of electrolytic solutions. It has been found that the surface of electrolyte solutions in pure water is not consisting of a pure water layer, but that ions are diffusing into the surface layers (behavior in HCl, NaOH, NaCl solutions). The monomolecular layers of stearic and oleic acid act like solid electrolytes, behaving for a change from acid to alkali similar to a hydrogen electrode on the acid side and similar to a sodium electrode on the alkaline side. The surface of pure water which has not been cleaned as for surface tension experiments appears to be covered with a film of organic substance acting like the fatty acid mentioned above. The phenomena observed with these layers present a striking analogy to the phenomena observed with glass, quartz, and paraffin films.

24. The cybotactic condition of ethyl ether in the region of the critical point. ROSS D. SPANGLER, *The State University of Iowa.*—X-ray diffraction curves of ethyl ether are taken at various temperatures, pressures, and specific volumes with special emphasis in the region of the critical point. With constant pressure and increasing temperature and specific volume, the diffraction curve changes from that typical of a liquid, with a pronounced peak, signifying cybotactic molecular grouping, to that typical of a polyatomic gas with no peak signifying randomly arranged molecules. The peak disappears approximately at the critical volume but not at the critical temperature. At intermediate temperatures and specific volumes, the curve is a composite of a gas and a liquid curve indicating that some of the molecules are in groups and others are randomly arranged. Within the present range of pressures, the type of curve obtained does not change with temperature if the specific volume is held constant. For example, no difference is found between curves taken at ten degrees above and below the critical temperature of 194.6°C. Beyond a certain specific volume, approximately the critical one, no indications of groups are found and the type of curve obtained is independent of temperature pressure, and specific volume within the ranges used.

25. On the process of liquefaction. G. W. STEWART, *University of Iowa.*—The paper at this meeting by Spangler calls attention to a necessary revision in current ideas concerning liquefaction. It has long been thought that liquefaction is dependent upon some type of aggregation of molecules. It is now seen that while well-defined aggregates are essential to liquefaction, yet they exist also under other conditions, for example at a higher temperature and less specific volume than the critical values. The process of liquefaction does not require an increase in the number of molecules per cm^3 in the cybotactic groups. It may occur with the number of aggregated molecules either constant or decreasing and pressure and temperature decreasing. The extent of the groups depends most importantly upon the specific volume. Liquefaction depends by definition on the possible existence of a second fluid phase in equilibrium and not as directly upon aggregation as formerly supposed.

26. Diffuse scattering of x-rays from a complicated crystal. G. E. M. JAUNCEY AND PAUL EHRENFEST II, *Washington University, St. Louis.*—Jauncey has recently obtained a formula for the diffuse scattering of x-rays from a crystal consisting of different kinds of atoms and possessing a lattice of any kind. In order to test this formula we have measured the diffuse scattering of x-rays from calcite at various angles. We find that the S curve for calcite falls between the S curve for sodium fluoride and that for sylvine and close to the S curve for rocksalt. This is as it should be according to the theory. Another interesting point is that the intensity of the diffuse scattering from a crystal does not depend upon the perfection of the crystal as is the case for Bragg reflection—calcite being a nearly perfect crystal and rocksalt a very imperfect (or mosaic) crystal.

27. Diffuse scattering of x-rays from an NaF crystal at low temperatures. P. S. WILLIAMS AND G. E. M. JAUNCEY, *Washington University, St. Louis.*—Using the photographic method described by Jauncey and Harvey, we have obtained for each of several scattering angles the ratio of the intensity of x-rays diffusely scattered from a crystal of sodium fluoride at the temperature of dry ice in butyl alcohol (about −70°C in the apparatus used) to that of the rays

scattered from the same crystal at room temperature (+22°C). The value of (sin $\frac{1}{2}\phi$)/λ was found for each angle of scattering. The ratios are as follows, the first of each pair of numbers being the value of (sin $\frac{1}{2}\phi$)/λ: 0.14, 0.932; 0.27, 0.917; 0.41, 0.919; 0.54, 0.931; 0.67, 0.947; 0.80, 0.973; 0.93, 0.980. The experiment is being continued with the crystal cooled to the temperature of liquid air.

28. The relative intensities of the $L\alpha_1$ and $L\beta_2$ lines in the fluorescent x-ray spectrum of uranium. REGINALD J. STEPHENSON, *University of Chicago.* (*Introduced by S. K. Allison.*)—Radiation from a metal x-ray tube with a molybdenum target fell on a secondary radiator of uranium and excited its fluorescent spectrum. The Mo K lines lie between the L_{II} and L_{III} absorption limits of uranium, hence the lines from the L_{III} limit will be excited strongly while those from L_I and L_{II} are excited comparatively weakly by the general radiation of the primary x-rays. A source of constant high voltage was used and the tube run at constant voltage and current. A single crystal ionization spectrometer served to analyze the radiation emitted by the uranium. In order to compare the fluorescent intensities with those observed in primary x-rays, it was necessary to measure the absorption coefficients of uranium for its L-series lines. The following results were obtained:

Line	Wave-length	Atomic absorption coef.
$L\gamma_1$	0.6163Å	2.8×10^{-20}
$L\beta_3$	0.7088	4.3 "
$L\beta_2$	0.7531	2.2 "
$L\alpha_1$	0.9087	2.8 "

After making all necessary corrections it was found that the relative intensity of the lines $L\alpha_1$ and $L\beta_2$ from the L_{III} level was the same in the fluorescent spectrum as in the primary spectrum observed by Allison (Phys. Rev. **32,** 1 (1928)).

29. The dynamic reflection of x-rays from ZnS. I. G. GEIB AND K. LARK-HOROVITZ, *Purdue University.*—It has been suggested by Ewald (Zeits. f. Krist. **65,** 251 (1927)) that for absorbing atoms the intensity distribution of an x-ray pattern depends on the direction of the x-ray beam relative to the crystal. ZnS crystals cut normally to the trigonal axis give plane parallel plates, one of which exhibits the 111, the other the −111 plane as has been shown directly by Lark-Horovitz in adsorption experiments with radioactive vapors (Proc. Vienna Acad. 1925). Using two such plates a Seeman slit spectrograph has been constructed with the +111 (Zn) and −111 (S) faces adjusted accurately in one plane to reflect gold, tungsten and tungsten-tantalum L radiation. These radiations contain lines on both sides of the Zn absorption limit and should therefore exhibit the effect predicted by theory. The photographic plate shows the L spectrum reflected simultaneously but with different intensity distributions from the Zn and S surfaces, due to absorption in the Zn atoms. The ratios (averages) of reflecting powers are:

Wave-length	1298.8	1285.0	1279.2	1273.8	1259.9	1242.0 x.u.
R_S (first order)						
Ratio						
R_{Zn}	1.00	1.00	1.42	1.38	1.22	1.12
R_{Zn} (third order)						
Ratio						
R_S	1.00	1.00	2.13	1.68		1.36

(in good agreement with the results of Coster (Zeits. f. Physik **63,** 345 (1930)).

30. A direct comparison of photographic and ionization methods of measuring x-ray intensities. ELMER DERSHEM, *University of Chicago.*—This investigation was undertaken to determine the relative precision which might practically be obtained by the photographic and ionization methods. The Mo $K\alpha_1$ line was isolated by crystal reflection and the ratio by which the intensity was reduced by passage through aluminum filters was measured by both methods. The photographic density determinations were made with the use of the photoelectric photometer previously described (R.S.I. **3,** 43 (1932)) and the ionization intensity measurements were made with an argon filled ionization chamber and Lindemann electrometer. The results show an average probable error for a single observation of 0.52 percent in the case of ionization measure-

ments and of 2.1 percent when the photographic method is used. However, the ionization method is more subject to errors which may not be reduced by repeated measurements. The results show that the errors introduced by assuming the exact validity of the reciprocity law of blackening of a photographic plate by x-rays is not greater than one percent for intensity ratios up to twenty to one, if one assumes the ionization measurements to be correct.

31. Absorption coefficients in optically excited mercury vapor. M. L. POOL AND S. J. SIMMONS, *Ohio State University.*—Mercury vapor at room temperature with various pressures of admixed purified nitrogen was optically excited by the resonance radiation from three quartz mercury arcs. From a fourth arc, magnetically deflected and water cooled, the radiation 4047, 2967 and 2752, all terminating on the 2^3P_0 state, was passed through the resonance tube of excited mercury vapor, and the absorption for each wave-length for various lengths of absorbing vapor was measured photometrically. It was found that the intensity of 2752 decreased nearly exponentially giving a linear absorption coefficient that varied slightly with the nitrogen pressure. However, for the lines 4047 and 2967 it was found that the simple exponential absorption law was not obeyed but that the fractional decrease in intensity per unit length of path decreased rapidly as the total length of the absorbing vapor increased. This peculiar decrease in intensity was further dependent upon the pressure of the admixed nitrogen. No other lines showed measurable absorption. The behavior of the 4047 and 2967 absorption for any given pressure may be adequately described by the sum of two exponentials with two quite different linear absorption coefficients.

32. The Zeeman effect of the spectra of Sb II and Sb III. J. B. GREEN AND R. A. LORING, *Ohio State University.*—The spectra of SbII and SbIII have been investigated at field strengths of about 40000 gausses. Zeeman patterns of the lines of SbII show general agreement with Lang's (in print) classifications in the spectra, and quite general disagreement with D'Lavale's classifications (Proc. Roy. Soc. June, 1931). The spectrum of SbIII shows that the two principle valence electrons have practically $j-j$ coupling, so that, except for a few cases, the assignment of l-values to the levels is not possible. Lang's classification of the s^2p^2 configuration is in good agreement with Goudsmit's theory. The Zeeman patterns of SbIII are also in good agreement with Lang's classification (Phys. Rev. **45,** 435 (1930)) of this spectrum. Several of the lines of this spectrum, as well as of SbII show broadening and extra components due to the hyperfine structure. The levels of the s^2ps configuration of Sb II and the $s^2 \cdot s$, s^2p and sp^2 of Sb III show this effect most strongly, as is to be expected from the theory.

33. The two vector problem in Pb V and Bi VI. A. T. GOBLE AND J. E. MACK, *University of Wisconsin.*—The configurations $5d^{10}$, $5d^96s$, and $5d^96p$ of Pb V and Bi VI have been identified (except d^9p, $J=0$) from Arvidsson's wave-length list (Ann. d. Physik **12,** 787 (1932)). The coupling exhibited is the most nearly pure jj of any known in optical spectra. The d^9p levels lie in four separate groups, and the visually estimated intensities agree roughly with the expectations. The d^9s intervals, like similar intervals in the spectra of other very heavy elements, show some departure from the exact theoretical formulas (Houston, Laporte, Inglis) which can hardly be attributed to neighboring configurations. The exact formulas of Johnson (Phys. Rev. **38,** 1628 (1931)) have been applied to d^9p after transformation of the energy matrix to the jj system of representation to give the two coupling coefficients and five electrostatic parameters. These parameters, reapplied in the formulas, give roots in fair agreement with the observed terms, but in view of the inexactness of the d^9s check the approximate success in expressing the ten available intervals in terms of the seven parameters may be considered a significant check upon the theory. The line $d^9{}_{3/2}s)_2 - d^9{}_{3/2}p_{1/2})_1$ of Bi VI shows partially resolved hyperfine structure.

34. Dispersion of the Kerr effect in the near infrared. L. R. INGERSOLL AND W. R. WINCH, *University of Wisconsin.*—Measurements of the Kerr electro-optic effect have been made on carbon bisulphide, nitrobenzene, halowax, and a number of other liquids over a spectral region extending from the sodium lines to about 2μ, or some four times the wave-length range investigated by other observers. The method is a spectro-bolometric one, involving effectively the measurement of the minor axis of the ellipse into which the plane polarized light is converted by the electrostatic stress in the Kerr cell. The high potential of 2000 to 40,000

volts, or more, is furnished by a kenotron and condenser equipment. The Havelock formula $B=C(n^2-1)^2/\lambda n$ for the dispersion of the Kerr double refraction fits the measured dispersion fairly well for a short region beyond the visible spectrum—to $\lambda=0.9\mu$ in some cases—but the discrepancy increases for longer wave-lengths.

35. The theory of refraction shooting. MORRIS MUSKAT, *Gulf Research Laboratory, Pittsburgh, Pa.*—Considerations of geometrical optics indicate that the limiting refracted rays travelling along the interface between two homogeneous elastic media should carry inappreciable amounts of energy. Nevertheless, the "first arrival" waves in refraction shooting processes which give linear time distance curves, can only be interpreted geometrically on assuming that they are due to such limiting rays travelling along the interface with the speed of the high velocity medium. A wave theory analysis of the problem resolves the difficulty. By an extension of Jeffrey's treatment for the case of fluid media to that of general elastic media it was found that *four* kinds of "refracted" waves of the above type will be produced upon the incidence at a plane interface of either a longitudinal or transverse spherical wave pulse. Two of the waves will be recorded as longitudinal waves and the other two as transverse. One of each pair effectively travels along the interface with the longitudinal velocity of the refracting medium and the other two travel with the transverse velocity. Their amplitudes vary inversely as the square of the distance from the source and correspond to vertical displacements of the same order as those due to the directly reflected waves.

36. Light intensities at different depths in water as determined by means of a quartz spectrograph. HENRY A. ERIKSON, *University of Minnesota.*—A quartz prism dispersing system in a specially designed housing was used for evaluating the intensities of different wave-lengths in the visible spectrum at different depths in water on Gunflint Lake on the northern border of Minnesota. The spectrum was photographed at different points down to 70 ft. and from these the intensities of the different wave-lengths were evaluated from characteristic curves obtained from standard exposures using wire screens. It was found that the variation of the intensity with depth was exponential in the case of some wave-lengths but not in the case of all. From the results obtained absorption constants were obtained for the different wave-lengths.

37. A twenty-one foot grazing incidence vacuum spectrograph. P. GERALD KRUGER AND F. S. COOPER, *University of Illinois.*—A grazing incidence vacuum spectrograph, for a twenty one foot focal length grating, ruled 30,000 lines per inch, has been set up and adjusted. The angle of incidence is 79 degrees. This gives the following dispersions at various wave-lengths between 0 and 500A.

λ	Dispersion
100A	0.332Å per mm
150	0.360
200	0.387
300	0.435
400	0.477
500	0.516

Copper electrodes were used in a "hot spark" for the light source during adjustment. The power was supplied at 100,000 volts d.c., by a four kenotron bridge set. The lines obtained were very sharp so that it was possible to measure their wave-lengths more accurately than has been done previously in this region.

38. A high-pressure spectrometer. FRANKLIN E. POINDEXTER AND LOUIS E. JAMES, *St. Louis University.*—A spectrometer has been constructed for the study of the change in the refractive index of liquids with pressure. The pressure on the liquid prism is measured directly by means of a plunger and lever. The index of refraction of water for each of the Hg lines 4359A, 5461A, and 5790A has been obtained at a series of pressures from 1 to 1440 atmospheres. We find that the Lorentz-Lorentz relation, $(n^2-1)/(n^2+2)\cdot 1/\rho=K$, where n=index of refraction, ρ=density, and K=constant does not hold; i.e., the K's at the lowest and highest pressures are:

	K 1 atmosphere	*K* 1440 atmospheres
4359A	0.2106	0.2092
5461A	0.2074	0.2070
5790A	0.2067	0.2062

39. The influence of pressure on the formation of the latent photographic image, particularly its effect on reversal in the region of solarization. KARL A. MARING, S.J., *St. Louis University.* (*Introduced by F. E. Poindexter.*)—Photographic materials were exposed, so that a central region was under pressure and a rim area without pressure. The pressure area showed a reduction in density over the rim area depending, in amount, on the exposure and the pressure. This reduction in density fell off with increasing exposure, gained with increasing pressure. However, this reduction of the density is not a linear factor of either exposure or pressure. In the region of solarization, a marked acceleration of reversal is noted in the pressure region. This pressure effect seems to call attention again to the photomechanical disintegration theory of the latent image formation.

40. Direct measurement of the gravitational effect of the moon. KENNETH HARTLEY, *Hartley Gravity Balance Corporation, Houston, Tex.*—The sensitivity of the gravity balance described in the March number of Physics is such that a correction must be made for the effect of the attraction of the moon. This lunar effect has been measured by hourly readings over one complete cycle and agrees, within the observational error, with the effect calculated for the vertical component of the pull of the moon without any compensation for the centrifugal effect of the earth's motion around the center of gravity of the system. The effect has a period of 24.8 hours and not 12.4 hours as the tides, there is no trace of the twelve-hour period. Values of gravity plotted against time follow accurately a sine curve which shows a small time lag as compared with the theoretical curve. This does not seem to be accidental but has not been explained.

41. Thermal expansion of antimony. PETER HIDNERT AND H. S. KRIDER, *Bureau of Standards, Washington, D. C.*—Measurements were made on the linear thermal expansion of three samples of cast antimony between room temperature and 560°C and the data were correlated with available results obtained by previous investigators to 300°C. The minimum and maximum values for the coefficients of expansion of the three samples are given in the following table.

Temperature range	Average coefficients of expansion per degree centigrade
20 to 60°C	8.5 to 10.8×10^{-6}
20 to 100	8.4 to 11.0
20 to 200	8.7 to 11.3
20 to 300	9.2 to 11.4
20 to 400	9.2 to 11.5
20 to 500	9.5 to 11.6
20 to 550	9.7 to 11.6

A manuscript giving additional details and indicating the cause of the differences obtained in the expansion of different samples of antimony, is being prepared for publication in the Bureau of Standards Journal of Research.

42. Refractory materials for melting pure metals. H. B. WAHLIN, O. D. FRITSCHE AND J. F. OESTERLE, *University of Wisconsin.*—A study of various refractories has shown that porcelain as well as magnesia crucibles volatilize and reduce sufficiently, when heated in a vacuum, to contaminate pure metals contained in them. Crucibles of pure, fused thorium oxide are the most satisfactory and will withstand heating in a vacuum for long periods of time. Special shapes of crucibles may be readily prepared by using moulds made of a fusible alloy which is melted off before firing. The crucibles should be fired to a temperature of 1800°C, care being taken to prevent the formation of thorium carbide which, due to interaction with the moisture of the air, will cause the crucibles to break up.

43. The Joule-Thomson effect in helium. J. R. ROEBUCK AND HAROLD OSTERBERG, *University of Wisconsin.*—Isenthalpic curves have been measured from −190° to +300°C. They are straight lines over the 200 atm. range except at the lowest temperature. Their slope, μ is negative over the whole range. At −190°C μ is increasing sharply with falling temperature moving toward the known-positive value at liquid hydrogen temperatures. From −50 to 150° μ decreases slowly and linearly. It goes through a minimum at about 200° and increases slowly thereafter. The free expansion coefficient, η calculated from these data, is negative and decreasing with rising temperature, between −50 and 200°C. This trend of η makes very improbable any prediction that helium will become a perfect gas at any temperature. With falling temperature η apparently becomes positive. These facts are difficult to reconcile with the older conception of the van der Waals forces but they may be explained qualitatively, at least, by restricting the attractive and repulsive forces to a very small fraction of the mean free path. The data are being used to calculate the Kelvin temperature of the ice point from the helium thermometer work.

44. Oscillations produced by beads of corona discharges. J. TYKOCINSKI TYKOCINER, *University of Illinois.*—The investigation of oscillations due to single bead discharges (Phys. Rev. **39,** 189 (1932) Abs. 52) has been extended to cases when a number N of beads act simultaneously. If the discharge consists of beads equal in size and brightness and distributed at regular distances along the negatively charged wire, the frequency is N times smaller than that obtained for a single bead, provided that the pressure, P, and the total corona current, I, remain constant. For the frequency f the relation was found $f = CIM/N$ where M is the number indicating the harmonic and c is a constant. For beads differing in size and distributed irregularily along the wire, oscillations of a complex character are obtained which contain as many fundamental frequencies as there are beads on the wire. The linear relation between f and I ceases when the current through a single bead reaches a definite value I_p. With further increase of current the rate of frequency increase diminishes and, from a critical value I_c on, the frequency decreases until, at a current $2I_c$, oscillations stop altogether. These relations were investigated for pressures within 5–60 mm Hg. The appearance of the bead gradually changes with the current, but at the characteristic point when oscillations stop sudden changes in the appearance can be observed.

45. Some experiments on electrets. O. J. JOHNSON AND P. H. CARR, *Iowa State College, Ames, Iowa.*—Electrets have been made after the manner of Eguchi from a mixture of Carnauba wax and rosin in electric fields as small as a few hundred volts per centimeter. A series of experiments was made in which the electric field was applied to the wax mixture at different temperatures and allowed to remain until the wax cooled to room temperature. Another series was made in which the electric field was applied when the wax was molten but was removed from each successive sample when it had cooled to a temperature lower than that at which the field was removed from the preceding sample. The strength of the electret resulting from each sample was measured. Results indicate that the molecules of the wax mixture become fixed in their polarized positions, so that random reorientation is negligible, at a temperature definitely lower than the temperature at which solidification takes place. Electrets have also been made from molten sulphur, but their properties have not been studied.

46. The measurement of the piezoelectric deformations of quartz and tourmaline plates by means of a modified optical lever. GEORGE A. FINK, *Iowa State College.* (*Introduced by G. W. Fox.*)—The observation of the piezoelectric deformation of quartz or tourmaline plates used for radio frequency oscillators requires a more sensitive measuring scheme than that afforded by direct optical interference or the ordinary type of optical lever. With a potential difference of 500 volts between the crystal electrodes, a deformation of only 10A is to be expected. To amplify such small movements, a lever has been built having an amplification ratio of 1866, such that, by interferential observation of a mirror on the long end, a movement of the short end of only 0.15A can be detected. Values of the piezoelectric constants for quartz and tourmaline as determined from the inverse effect are in fair agreement with those found by previous

observers from the direct effect. The structure of the quartz crystals was found to be very non-uniform; various crystals and different parts of the same crystal plate giving results differing by more than the experimental error.

47. Modes of vibration of piezoelectric crystals. N. H. WILLIAMS, *University of Michigan.*—(a) A crystal is made to oscillate by subjecting it to the action of an air wave produced at a considerable distance from the crystal by a jet of air escaping from a small tube. The piezo-electric charge developed on the surface of the crystal as a result of the oscillation is mapped out by means of a tuned amplifier, and the vibration is analyzed into a fundamental and many overtones. The crystals are long in one dimension and the vibrations are along the length. Under these conditions the overtones are approximate harmonics. (b) Exciting the crystal electrically by means of two tubes and especially designed electrodes, any harmonic up to the tenth can be produced. The crystal usually has only one mode of vibration for each pair of electrodes.

48. A nonthermionic amplifier tube. HERBERT J. REICH, *University of Illinois.*—Grid control of a glow discharge is obtained in this tube by so designing and placing the grid that it is out of the direct path of the discharge between anode and cathode. Variation of the grid potential modifies the electric field in such a manner as to control the number of electrons which move through a distance sufficient to produce ionization. By maintaining the static grid potential at such a value that the number of positive ions which strike the grid is equal to or slightly in excess of the number of electrons, the grid current may be limited to less than ten microamperes. The discharge is at all times under control of the grid and may be completely extinguished by it. The gas pressure is found to be very important in obtaining satisfactory operation. The relation of structural parameters to tube constants is being studied, but little attempt has yet been made to improve the amplification characteristics. A conservative average for tubes made during the preliminary investigation gives values of 3 for amplification factor and 100 micromhos for mutual conductance. With proper design and choice of gas pressure, little or no ballast resistance is required.

49. The use of vacuum tube electrometers for measuring the potentials of high-resistance cells. ROBERT E. BURROUGHS AND J. E. FERGUSON, *Purdue University.*—By using the relation between the grid potential and the plate current of a thermionic vacuum tube one is able to construct an electrometer of high sensitivity. Such electrometers have been used in the measurements of electromotive forces of cells whose internal resistances are very high. In these measurements the vacuum tube is operated with its grid at floating potential so the current drawn from the cell will be very small. The cell potential is then measured by applying a compensating potential in series with the cell in the grid circuit of the electrometer. Using a null method, when this compensating potential is adjusted so as to give zero indication on the electrometer it is a measure of the electromotive force of the cell. This method gives satisfactory results for cells whose resistances are below 10^{11} ohms. For resistances higher than this a difficulty is encountered. The current to the grid of the vacuum tube is so small that the time required to change the grid potential, sufficiently to secure a balance with precision, is of such length that lack of circuit stability renders the method useless.

50. Improved burner for singing flames. Overtones in vibrating strings. JOHN J. HOPFIELD, *Basic Science Division, A Century of Progress, Chicago.* (*Introduced by H. G. Gale.*)—By using a suitable double burner with the flames at different heights instead of a single flame, the flames vibrate to the resonance tones of a pipe even when the larger flame was several inches long. It was found that the smaller flame starts the singing and the larger one responds. (Demonstration.)

By using a modified 120 cycle tuning fork operated on 60 cycle current, one can produce not only the 120 cycle fundamental in a Melde string but also the note of frequency 60 and many integral multiples of these tones. These are made evident in the point symmetrical form of the standing waves in the string, and also they can be separately sounded in a tube fitted with a sliding plunger and held near a disc attached to the side of the string. (Demonstration.)

51. Atomic wave functions. F. W. BROWN, *University of Illinois.* (*Introduced by J. H. Bartlett, Jr.*) The writer has found a Hartree field for normal F. The use of this field in conjunction with the one already obtained by Hartree for F^- enables one to test the wave equation of the "hole," given by Heisenberg and Dirac (Heisenberg, Ann. d. Physik **10,** 888 (1931); Dirac, Ann. de L'Inst. H. Poincare, Vol. 1 Pt. 4, 357). The equation was found to give the wrong sign for the electron affinity of F, the reason being that in its derivation no account is taken of the difference between the electron functions of F and those of F^-. As a check on the accuracy of the work, a self-consistent field for Ne^+ is being obtained. It is also intended to represent these wave functions of the Hartree field by the analytic functions devised by Slater (Phys. Rev. **42,** 33 (1932)).

52. On Compton's latitude effect of cosmic radiation. G. LEMAITRE AND M. S. VALLARTA, *University of Louvain and Massachusetts Institute of Technology.* By considering the influence of the earth's magnetic field on the motion of charged particles (electrons, protons, etc.) coming to the earth from all directions in space it is shown that the experimental variation of cosmic-ray intensity with magnetic latitude, as found by Compton and his collaborators, is fully accounted for. The cosmic radiation must contain charged particles of energy between 0.5×10^{10} and 3×10^{10} electron-volts for electrons or protons; 0.7 to 5.5×10^{10} electron-volts for alpha-particles. The experimental curve may be represented by a suitable mixture of rays of these energies, but it is not at all excluded that a part of the radiation may consist of photons or neutrons. For predominantly negative particles there must be in the region of rapidly varying intensity a predominant eastward direction, and conversely for positive rays. Because of the fact that in regions near the magnetic equator there is a predominance of rays coming nearly horizontally, the absorption by the atmosphere may be increased. Finally the fact that Compton's result definitely shows that the cosmic rays contain charged particles gives some support to the theory of super-radioactive origin of these rays advanced by one of the present authors.

53. Methods of acquirement of cosmic-ray energies. W. F. G. SWANN, *Bartol Research Foundation of the Franklin Institute.* Consider the growth of a sunspot of diameter ten times that of the earth. The line integral of the electric field around a circuit encircling the magnetic field of this spot is $[\pi H(6.5\times10^9)]^2/(T\times10^8)$ where H is the magnetic field of the spot, and T the time in which it is created. This line integral amounts to 10^{10} volts if the field of the spot is 2000 gauss and is created in about three days. The details of the electronic motion on the field are complicated; but, it appears that acquirement of high energy by such means should be possible, particularly in the case of larger spots which may exist in stars other than our sun. It is probable that the mean free path is sufficiently long in the regions concerned to ensure that the rate of acquirement of energy would be less than the rate of loss by collision. In connection with the foregoing view, attention is called to the increase of auroral activity during sun spot activity. Another suggestion arises from possible electrostatic fields of the stars. A charge on the sun such as would give a field of no more than one volt per centimeter at the surface would correspond to a potential of 5×10^{10} volts. In the case of a galaxy of stars, the potential at the surface of the galaxy would be of the order $Na^2\,X/R$, where N is the number of stars in the galaxy, a the radius of a star, R the radius of the galaxy, and X the surface field of a star. The value of X necessary to result in any assigned value of the potential at the surface of the galaxy decreases with increase of R since N increases more rapidly than R.

54. The neutron, the element neuton, and a nuclear exclusion principle. WILLIAM D. HARKINS, *University of Chicago.* The neutron, discovered in the radiations from beryllium, by M. and Mme. Joliot and particularly by Chadwick, represents an element of atomic number zero, which may be called *neuton.* The composition of the beryllium nucleus was indicated by the writer in 1915 to be two alpha-particles united by a condensed nuclear hydrogen atom, or neutron. The general existence of neutrons and their properties were predicted in 1920 by Harkins (April 12) and by Rutherford (June 3). It was also shown by the writer that a second or *isotopic* number (I) is as necessary as the atomic number (Z) to specify an atomic species. The formula of any nucleus is $(p_2e)_Z(pe)_I$, in which (pe) represents a neutron (n) (Physical Review **19,** 139 and 142 (1922)), and (p_2e) is the nucleus of hydrogen 2, which is the half-alpha-particle. This

formula may be written either as $(n\phi)_Z n_I$ or $(a/2)_Z n_I$ or its equivalent $a_{s/2}n_{a(I/2)}$ which indicates that the neutrons in the half-alpha-particles are almost always paired, and the extra neutrons (n) are usually paired. Now $Z+I=N$ is the total number of neutrons in the nucleus, and Z the number of extra protons, that is those not in neutrons. The following relations hold: (1) Not more than one proton can combine with a neutron. (2) About 125 of every 126 atoms in the earths crust contain an even number of neutrons, so the neutrons seem to be paired. (3) The general stability of atomic nuclei is determined by Z and by either N/P or N/Z, in which $P=N+Z$. (4) The hydrogen 2 or half- alpha-particles are paired in about 95 percent of all atoms, and thus exist as alpha-particles. (5) Less than one atom in ten thousand contains an odd half-alpha-particle with no extra neutrons. (6) If both an odd half-alpha-particle and extra neutrons are present, the total number of extra neutrons is always odd, and no atoms exist (except unstable radioactive species whose half lives are smaller than 8 days) in which this number is even. Thus the total number of neutrons in such an atom must be even, so the neutrons are paired. However, a few of these may not have paired spins.

55. A demountable metal x-ray tube. K. LARK-HOROVITZ AND E. M. MILLER, *Purdue University*. With Pyrex and sillimanite tubes of a special form as insulators and chromium plated brass for anode and cathode parts, an x-ray tube has been constructed, free from any wax joints or seals, which will stand 70 m.a. at 75 kv continuous operation. With these tubes, by using a line focus, it was possible to resolve in a photograph taken in 120th of a second the $K\alpha$ doublet of copper reflected from a calcite crystal with a Seeman wedge (distance plate-crystal 55 cm). The exposures have been timed by using a falling slit between spectrograph and plate (d.c.). Imprints have been made on a falling plate which show that the spectra have been registered in less than 1/200 of a second (a.c.). The $K\alpha$ doublet of copper has been photographed at a distance of three meters between spectrograph and plate in 60 seconds. Diffraction patterns from powders can be obtained in a few seconds.

AUTHOR INDEX TO ABSTRACTS OF CHICAGO MEETING

Barton, Henry A., D. W. Mueller and L. C. Van Atta—No. 3
Boeckner, C. and F. L. Mohler—No. 20
Brown, F. W.—No. 51
Burroughs, Robert E. and J. E. Ferguson—No. 49

Carr, P. H.—See Johnson
Compton, Arthur H.—No. 13
Cooper, F. S.—see Kruger

Dempster, A. J.—No. 4
Dershem, Elmer—No. 30
DuBridge, Lee A.—No. 18

Ehrenfest II, Paul—see Jauncey
Erikson, Henry A.—No. 36

Ferguson, J. E.—see Burroughs
——— see Lark-Horovitz
Fink, George A.—No. 46
Fritsche, O. D.—see Wahlin

Geib, I. G. and K. Lark-Horovitz—No. 29
Goble, A. T. and J. E. Mack—No. 33
Green, J. B. and R. A. Loring—No. 32

Harkins, William D.—No. 54
Hartley, Kenneth—No. 40
Havens, G. G.—No. 1
Haworth, L. J.—No. 19
Hidnert, Peter and H. S. Krider—No. 41
Hopfield, John J.—Nos. 12, 50

Ingersoll, L. R. and W. R. Winch—No. 34

James, Louis E.—see Poindexter
Jauncey, G. E. M.—see Williams, P. S.
——— **and Paul Ehrenfest II**—No. 26
Johnson, O. J. and P. H. Carr—No. 45
Jordahl, O. M.—No. 2

Kretschmar, G. G.—No. 17
Krider, H. S.—see Hidnert
Kruger, P. Gerald and F. S. Cooper—No. 37

Lark-Horovitz, K.—see Geib
——— see Yearian
——— **and J. E. Ferguson**—No. 23
——— **and E. M. Miller**—No. 55
Lemaitre, G. and M. S. Vallarta—No. 52
Longacre, Andrew—No. 21
Loring, R. A.—see Green

McMillan, Edwin—No. 16
McPherson, A. I.—No. 9
Mack, J. E.—see Goble
Maring, Karl A.—No. 39
Miller, E. M.—see Lark-Horovitz
Mohler, F. L.—see Boeckner
Moore, T. W.—No. 22
Mueller, D. W.—see Barton
——— see Smyth
Muskat, Morris—No. 35

Oesterle, J. F.—see Wahlin
Osterberg, Harold—see Roebuck

Poindexter, Franklin E. and Louis E. James—No. 38
Pool, M. L. and S. J. Simmons—No. 31

Reich, Herbert J.—No. 48
Roebuck, J. R. and Harold Osterberg—No. 43

Shaw, A. E.—No. 5
Simmons, S. J.—see Pool
Smyth, H. D. and D. W. Mueller—No. 7
Spangler, Ross D.—No. 24
Sproull, Wayne T.—No. 14
Stephenson, Reginald J.—No. 28
Stewart, G. W.—No. 25
Swann, W. F. G.—No. 53

Tykociner, J. Tykocinski—No. 44

Vallarta, M. S.—see Lemaitre
Van Atta, L. C.—see Barton
Verwiebe, F. L.—No. 8

Wahlin, H. B., O. D. Fritsche and J. F. Oesterle—No. 42
Western, Forrest and Arthur Ruark—Nos. 10, 11
Wetzel, W. W.—No. 6
Williams, N. H.—No. 47
Williams, P. S. and G. E. M. Jauncey—No. 27
Winch, W. R.—see Ingersoll

Yearian, H. J. and K. Lark-Horovitz—No. 15

AUTHOR INDEX TO VOLUME 42

References with (A) are to abstracts of papers presented at meetings of the Physical Society and references with (L) are to Letters to the Editor.

Albertson, Walter. Note on the term system of Ir I —443(L)

Allen, Mildred. Effect of tension on the electrical resistance of single bismuth crystals—848

Allen, P. K. (see Bennett, R. D.)—446(L)

Allis, W. P. (see Morse, Phillip M.)—588(A)

Almy, G. M. and C. D. Hause. Spectrum of potassium hydride—242

Andrew, Victor J. Relative intensities of the $L\alpha_1$, β_1, β_2 and γ_1 lines in tantalum, tungsten, iridium, and platinum—591

Ashley, Muriel F. and F. A. Jenkins. Possibility of the existence of the chlorine isotope Cl^{39}—438(L)

Bainbridge, Kenneth T. Isotopic weight of H^2—1

Barker, E. F. (see Choi, Kyu Nam)—777

——— (see Hardy, J. D.)—279

Barnes, LeRoy L. Emission of positive ions from heated metals—487

——— Temperature variation of the positive ion emission from molybdenum—492

Barnett, S. J. Gyromagnetic ratios for nickel and cobalt—147(L)

Bartlett, J. H., Jr. Structure of atomic nuclei. II—145(L)

——— Errata: Structure of atomic nuclei—737

Barton, Henry A., D. W. Mueller and L. C. Van Atta. Compact high potential electrostatic generator—901(A)

Batho, Harold F. Neutralization and ionization of high-velocity ions of neon, argon and krypton by collision with similar atoms—753

Bear, Richard S. (see Spedding, Frank H.)—58, 76

Beck, Fred J., Jr. and L. W. McKeehan. Monocrystal Barkhausen effects in rotating fields—714

Benade, J. M. Self-recording cosmic-ray electrometer and depth-ionization curve—290

Bennett, Ralph D. (see Stearns, J. C.)—317(L)

——— **J. L. Dunham, E. H. Bramhall, and P. K. Allen.** Intensity of cosmic-ray ionization in Western North America—446(L)

Bhagavantam, S. Raman effect in gases: CO and NO —437(L)

Birge, Raymond T. Value of e/m—736(L)

Bitter, Francis. Some properties of homogeneously distorted cubic ferromagnetic lattices—697

——— Tropism of crystals—731(L)

Boeckner, C. and F. L. Mohler. Scattering of slow electrons by caesium ions—906(A)

Boeker, G. F. (see Wills, A. P.)—687

Bourgin, D. G. Velocity of sound in an absorptive gas—721

Bozorth, Richard M. Theory of the ferromagnetic anisotropy of single crystals—882

Bramhall, E. H. (see Bennett, R. D.)—446(L)

Brasefield, Charles J. Ionization of helium, neon and argon under impact of their own atoms and positive ions—11

Breazeale, William M. (see Slack, Francis G.)—305

Breit, G. Isotope displacement in hyperfine structure—348

Brewer, A. Keith and R. R. Miller. Positive ion current at the cathode in the glow discharge—786

Bridgman, P. W. Effect of homogeneous mechanical stress on the electrical resistance of crystals—858

——— Effect of pressure on the electrical resistance of fifteen metals down to liquid oxygen temperatures—587(A)

Brown, F. W. Atomic wave functions—914(A)

Brown, Weldon G. Absorption spectrum of iodine bromide—355

Broxon, James W. Cosmic-ray ionization as a function of pressure, temperature, and dimensions of the ionization chamber—321

Burroughs, Robert E. and J. E. Ferguson. Use of vacuum tube electrometers for measuring the potentials of high-resistance cells—913(A)

Calbick, C. J. (see Davisson, C. J.)—580(L)

Caldwell, S. Differential analyzer solution for the wave functions of the K-shell—589(A)

Carr, P. H. (see Johnson, O. J.)—912(A)

Child, C. D. Luminosity of sodium flames—146(L)

Choi, Kyu Nam and E. F. Barker. Infrared absorption spectrum of hydrogen cyanide—777

Chylinski, S. Magnetic spectra of secondary electrons from silver—393

——— On the scattering of hard x-rays by solids—153

Colby, M. Y. and Sidon Harris. X-ray reflection from a quartz piezoelectric oscillator in a Bragg spectrograph—733(L)

Collins, George (see Wood, R. W.)—386

Compton, Arthur H. Sea level intensity of cosmic rays in certain localities from 46° south to 68° north latitude—904(A)
Compton, K. T. and E. S. Lamar. Momentum transfer to cathode surfaces by impacting positive ions in a helium arc—588(A)
Coolidge, Albert Sprague. Quantum mechanics treatment of the water molecule—189
Cooper, F. S. (see Kruger, P. Gerald)—910(A)
Cork, J. M. Laue patterns from thick crystals at rest and oscillating piezoelectrically—749
——— (see Witmer, R. B.)—743

Davisson, C. J. and C. J. Calbick. Electron lenses—580(L)
Dempster, A. J. Production of high-velocity protons by repeated accelerations—901(A)
Dennison, D. M. (see Hardy, J. D.)—279
Dershem, Elmer. Direct comparison of photographic and ionization methods of measuring x-ray intensities—908(A)
Ditchburn, R. W. Emission probability for a colliding atom—314(L)
DuBridge, Lee A. Theory of the energy distribution of photoelectrons—905(A)
——— **and W. W. Roehr.** Thermionic and photoelectric work functions of molybdenum—52
Dunham, J. L. (see Bennett, R. D.)—446(L)
Dunnington, Frank G. Determination of e/m for an electron by a new deflection method—734(L)
Duveneck, F. B. (see Webster, D. L.)—141(L)

Ehrenfest, Paul II (see Jauncey, G. E. M.)—907(A)
Erikson, Henry A. Light intensities at different depths in water as determined by means of a quartz spectrograph—910(A)

Farnsworth, H. E. Electron diffraction by a silver film on a gold crystal—588(A)
Feenberg, Eugene. Scattering of slow electrons. Part II—17
Ferguson, J. E. (see Burroughs, Robert E.)—913(A)
——— (see Lark-Horovitz, K.)—907(A)
Fink, George A. Measurement of the piezoelectric deformations of quartz and tourmaline plates by means of a modified optical lever—912(A)
Focken, C. M. Velocities of ions and electrons in pure gases—577(L)
Frank, Henry S. and Foo-Song Lei. Empirical equation of state—893
Fritsche, O. D. (see Wahlin, H. B.)—911(A)

Geib, I. G. and K. Lark-Horovitz. Dynamic reflection of x-rays from ZnS—908(A)
Gerhard, Sherman L. Infrared absorption spectrum and the molecular structure of ozone—622
Goble, A. T. and J. E. Mack. Two vector problem in Pb V and Bi VI—909(A)
Gorter, C. J. Note on the electric field in paramagnetic crystals—437(L)
Granath, L. P. Nuclear spin and magnetic moment of Li^7—44
Green, J. B. and R. A. Loring. Zeeman effect of the spectra of Sb II and Sb III—909(A)
Greene, Ernest W. and John Warren Williams. Variation of dielectric constant with temperature. II. Electric moments of the ethylene halides—119
Gross, E. and J. Khvostikov. Variation of the structure of scattered lines with the frequency of the primary light—579(L)
Grosse, A. v. On the origin of the actinium series of radioactive elements—565
Gruner, J. W. Book review—451
Guillemin, V., Jr. On the possibility of deriving work from statistical fluctuations—589(A)

Hamada, H. (see Okubo, J.)—795
Hancox, Robert Rex. Reflection of metallic atoms from alkali halide crystals—864
Hansen, W. W. (see Webster, D. L.)—141(L)
Hardy, J. D., E. F. Barker and D. M. Dennison. Infrared spectrum of H^2Cl—279
Harkins, William D. Neutron, the element neuton, and a nuclear exclusion principle—914(A)
Harris, Sidon (see Colby, M. Y.)—733(L)
Hartley, Kenneth. Direct measurement of the gravitational effect of the moon—911(A)
Hause, C. D. (see Almy, G. M.)—242
Havens, G. G. Magnetic susceptibilities of some common gases—901(A)
Haworth, L. J. Energy distribution of secondary electrons from molybdenum—906(A)
Heaps, C. W. Effect of strain on magnetostriction and magnetization in nickel—108
Herzfeld, Karl F. Book review—319
Hidnert, Peter and H. S. Krider. Thermal expansion of antimony—911(A)
Hill, E. L. Book review—741
Hoag, J. Barton and Haydn Jones. Permeability of iron at ultra-radio frequencies—571
Hollaender, Alexander (see Williams, John Warren)—379
Hopfield, John J. Argon in the ionization method of measuring cosmic rays and γ-rays—904(A)
——— Improved burner for singing flames. Overtones in vibrating strings—913(A)
Howell, L. G. (see Mott-Smith, L. M.)—314(L)
Hughes, A. L. Angular distribution of electrons scattered in mercury vapor—147(L)
Hukumoto, Y. On the continuous absorption spectrum of alkyl iodides—313(L)

Ingersoll, L. R. and W. R. Winch. Dispersion of the Kerr effect in the near infrared—909(A)
Inglis, D. R. Heisenberg theory of ferromagnetism —442(L)

James, Louis E. (see Poindexter, Franklin E.)—910 (A)
Jauncey, G. E. M. Remarks on the scattering of x-rays by gases and crystals—453
——— (see Williams, P. S.)—907(A)
——— **and Paul Ehrenfest II.** Diffuse scattering of x-rays from a complicated crystal—907(A)
Jen, C. K. Continuous electron affinity spectrum of hydrogen—588(A)
Jenkins, F. A. (see Ashley, Muriel F.)—438(L)
——— **and Andrew McKellar.** Mass ratio of the boron isotopes from the spectrum of BO—464
Johnson, O. J. and P. H. Carr. Some experiments on electrets—912(A)
Johnson, Thomas H. (see Street, J. C.)—142(L)
Jones, Haydn (see Hoag, J. Barton)—571
Jordahl, O. M. Paramagnetic susceptibility of Cu^{++} —901(A)

Kaplan, Joseph. Auroral spectrum—807
——— Luminescence of solid nitrogen—86
——— Products of dissociation in nitrogen—97
Kennedy, Roy J. and Edward M. Thorndike. Experimental establishment of the relativity of time—400
Kenty, Carl. On radiation diffusion and the rapidity of escape of resonance radiation from a gas—823
Khvostikov, J. (see Gross, E.)—579
Kolthoff, I. M. Book reviews—451, 741
Kretschmar, G. G. Determination of e/m by means of photoelectrons excited by x-rays—905(A)
Krider, H. S. (see Hidnert, Peter)—911(A)
Kruger, P. Gerald and F. S. Cooper. Twenty-one foot grazing incidence vacuum spectrograph—910(A)
Kuhn, H. and O. Oldenberg. Errata: Evidence of space quantization of atoms upon impact—312

Lamar, E. S. (see Compton, K. T.)—588(A)
Lang, R. J. and E. H. Vestine. First spark spectrum of antimony—233
Langer, R. M. Book review—738
Laporte, Otto. Approximation of geometric optics as applied to a Dirac electron moving in a magnetic field—340
Lark-Horovitz, K. (see Geib, I. G.)—908(A)
——— (see Yearian, H. J.)—905(A)
——— **and J. E. Ferguson.** Electrical properties of surface layers—907(A)
——— **and E. M. Miller.** Demountable metal x-ray tube—915(A)
Lawrence, Ernest O. Book review —451
———, **M. Stanley Livingston and Milton G. White.** Disintegration of lithium by swiftly-moving protons—150(L)
Lei, Foo-Song (see Frank, Henry S.)—893
Lemaitre, G. and M. S. Vallarta. On Compton's latitude effect of cosmic radiation—914(A)
Libby, W. F. Simple amplifier for Geiger-Müller counters—440(L)
Lippert, T. W. (see Pugh, E. M.)—709
Livingston, M. Stanley. High-speed hydrogen ions—441(L)
——— (see Lawrence, Ernest O.)—150(L)
Locher, Gordon L. Photoelectric quantum counters for visible and ultraviolet light. Part I.—525
Longacre, Andrew. Scattering of lithium ions from a nickel surface—906(A)
Loring, R. A. (see Green, J. B.)—909(A)

Mack, J. E. (see Goble, A. T.)—909(A)
Mahanti, P. C. Band spectra of MgO, CaO and SrO —609
Maring, Karl A. Influence of pressure on the formation of the latent photographic image, particularly its effect on reversal in the region of solarization—911(A)
Matuyama, E. On the lifetime of the metastable $^3P_2$ neon atom—373
Maxwell, Louis R. On the radiation originating from a beam of electrons in mercury vapor and the mean life of the 2^3S_1 state—148(L)
McKeehan, L. W. (see Beck, Fred J., Jr.)—714
McKellar, Andrew (see Jenkins, F. A.)—464
McMillan, Edwin. Deflection of a beam of HCl molecules by a non-homogeneous electric field—905(A)
McPherson, A. I. Radiation from positive ions in argon, neon, helium—903(A)
Miller, E. M. (see Lark-Horovitz, K.)—915(A)
Miller, R. R. (see Brewer, A. Keith)—786
Mohler, F. L. (see Boeckner, C.)—906(A)
Moore, T. W. Behavior of crystalline test bodies in streaming solutions—906(A)
Morse, Philip M. (see Rosen, N.)—210
——— **and W. P. Allis.** Effect of exchange on elastic cross sections—588(A)
Mott-Smith, L. M. and L. G. Howell. Airplane cosmic-ray intensity measurements—314(L)
Mueller, D. W. (see Barton, Henry A.)—901(A)
——— (see Smyth, H. D.)—902(A)
Mulliken, Robert S. On the interpretation of the rotational structure of the CO_2 emission bands—364
Murphy, George M. and Harold C. Urey. Errata: On the relative abundances of the nitrogen and oxygen isotopes—312
Muskat, Morris. Theory of refraction shooting—910(A)

Nedelsky, Leo. Radiation from slow electrons—641
Noll, F. H. Waldemar. X-ray diffraction in ethyl ether near the critical point—336

Oesterle, J. F. (see Wahlin, H. B.)—911(A)
Okubo, J. and H. Hamada. On the nature of active nitrogen—795
Oldenberg, O. (see Kuhn, H.)—312
Olthoff, J. and R. A. Sawyer. Extension of the first spark spectrum of caesium (Cs II)—766
Osterberg, Harold (see Roebuck, J. R.)—912(A)
Overbeck, Wilcox P. (see Stearns, J. C.)—317(L)

Page, Leigh. Momentum relations in crossed fields—101
Patten, C. G. (see Uber, Fred M.)—229
Penney, W. G. Law of force between two He atoms—585(L)
——— (see Schlapp, Robert)—666
Pfund, A. H. Filter for the study of the Raman effect—581(L)
Piekara, A. Dielectric constant and electric polarization of mixtures in the neighborhood of the critical point—448(L)
——— Electric moment of the molecule of nitrobenzene—449(L)
Pielemeier, W. H. Erratum: Supersonic dispersion and absorption in CO_2—436
Pierce, G. W. Some applications of high-frequency sound effects—589(A)
Poindexter, Franklin E. and Louis E. James. High-pressure spectrometer—910(A)
Pool, M. L. and S. J. Simmons. Absorption coefficients in optically excited mercury vapor—909(A)
Pugh, E. M. and T. W. Lippert. Hall e.m.f. and intensity of magnetization—709

Rank, David H. Isotope of hydrogen in the atomic spectrum—446(L)
Reich, Herbert J. Nonthermionic amplifier tube—913(A)
Reichrudel, E. (see Spiwak, G.)—580(L)
Reyerson, L. H. Book review—740
Rieke, Foster F. Anomalous rotational temperature of mercury hydride—587(A)
Roebuck, J. R. and Harold Osterberg. Joule-Thomson effect in helium—912(A)
Roehr, W. W. (see DuBridge, Lee A.)—52
Rosen, N. and Philip M. Morse. On the vibrations of polyatomic molecules—210
Rosenthal, Jenny E. (see Salant, E. O.)—812
Ruark, Arthur (see Western, Forrest)—903(A); 903(A)

Salant, E. O. and Jenny E. Rosenthal. Theory of vibrational isotope effects in polyatomic molecules—812
Saper, Paul G. Rotational analysis of ultraviolet bands of silicon monoxide—498
Sawyer, R. A. (see Olthoff, J.)—766
Schlapp, Robert and William G. Penney. Influence of crystalline fields on the susceptibilities of salts of paramagnetic ions. II. The iron group, especially Ni, Cr and CO—666
Schmid, R. F. Rotational analysis of the first-negative bands of the CO^+ molecule—182
Shaw, A. E. Polarization of collecting electrodes in high vacua—902(A)
Shortley, G. H. (see Ufford, C. W.)—167
Simmons, S. J. (see Pool, M. L.)—909(A)
Sixtus, K. J. and L. Tonks. Propagation of large Barkhausen discontinuities. II—419
Slack, Francis G. and William M. Breazeale. Magneto-optic rotation by condenser discharge—305
Slater, J. C. Analytic atomic wave functions—33
——— Recent developments in the theory of magnetism—589(A)
Smith, Lloyd P. Calculation of the quantum defect for highly excited S states of para- and ortho-helium—176
Smyth, H. D. and D. W. Mueller. Ionization by electron impact in water vapor and sulphur dioxide—902(A)
Spangler, Rose D. Cybotactic condition of ethyl ether in the region of the critical point—907(A)
Spedding, Frank H. and Richard S. Bear. Absorption spectra of the samarium ion in solids. I. Absorption by large single crystals of $SmCl_3 \cdot 6H_2O$—58
——— Absorption spectra of the samarium ion in solids. II. Conglomerate absorption of $SmCl_3 \cdot 6H_2O$ and a partial energy level diagram of the Sm^{+++} ion as it exists in crystalline $SmCl_3 \cdot 6H_2O$—76
Spiwak, G. and E. Reichrudel. On the secondary emission from collectors in neon discharge—580(L)
Sproull, Wayne T. Diffraction of low speed electrons by a tungsten single crystal—904(A)
Stearns, J. C., Wilcox P. Overbeck and Ralph D. Bennett. Solar component of cosmic rays—317(L)
Stehn, J. R. Note on perturbation theory of molecules formed from two $2p$ atoms—582(L)
Stephenson, Reginald J. Relative intensities of the $L\alpha_1$ and $L\beta_2$ lines in the fluorescent x-ray spectrum of uranium—908(A)
Sterne, Theodore E. Vapor pressure constant of methane—556
Stewart, G. W. On the process of liquefaction—907(A)

Street, J. C. and Thomas H. Johnson. Concerning the production of groups of secondaries by the cosmic radiation—142(L)
Strong, John and S. C. Woo. Far infrared spectra of gases—267
Stueckelberg, E. C. G. Theory of continuous absorption of oxygen at 1450A—518
Swann, W. F. G. Methods of acquirement of cosmic-ray energies—914(A)

Thorndike, Edward M. (see Kennedy, Roy J.)—400
Tonks, L. (see Sixtus, K. J.)—419
Tykociner, J. Tykocinski. Oscillations produced by beads of corona discharges—912(A)

Uber, Fred M. and C. G. Patten. Magnitudes of the *L* absorption discontinuities of gold—229
Ufford, C. W. and G. H. Shortley. Atomic eigenfunctions and energies—167
Uhlenbeck, G. E. Book review—738
Urey, Harold C. (see Murphy, George M.)—312

Valasek, Joseph. Book reviews—152
Vallarta, M. S. (see Lemaitre, G.)—914(A)
Van Atta, L. C. (see Barton, Henry A.)—901(A)
Van Dyke, K. S. Temperature variation of viscosity and of the piezoelectric constant of quartz—587 (A)
Varney, Robert N. Non-existence of ion mobility spectrum in air—547
Verwiebe, F. L. Radiation excited by canal ray impact—902(A)
Vestine, E. H. (see Lang, R. J.)—233
Vinti, J. P. Dispersion and absorption of helium—632
Vollrath, Richard E. High-voltage direct-current generator—298

Wahlin, H. B., O. D. Fritsche, and J. F. Oesterle. Refractory materials for melting pure metals—911(A)
Watson, William W. Zeeman effect of perturbed terms in the CO angstrom bands—509
Webster, D. L., W. W. Hansen, F. B. Duveneck. Probabilities of *K*-electron ionization of silver by cathode rays—141(L)
Wensel, H. T. Book review—319
Western, Forrest and Arthur Ruark. Actinium branching ratio—903(A)
——— Atomic weights of radioactive substances—903(A)
Wetzel, W. W. Ionization of He by electron impact—902(A)
White, Milton G. (see Lawrence, Ernest O.)—150(L)
Williams, John Warren (see Greene, Ernest W.)—119
——— **and Alexander Hollaender.** Molecular scattering of light from ammonia solutions. The fine structure of a vibrational Raman band—379
Williams, N. H. Modes of vibration of piezoelectric crystals—913(A)
Williams, P. S. and G. E. M. Jauncey. Diffuse scattering of x-rays from an NaF crystal at low temperatures—907(A)
Williams, S. R. Mechanical hardness as measured by magnetostrictive effects—589(A)
Wills, A. P. and G. F. Boeker. Diamagnetism of water at different temperatures—687
Winans, J. Gibson. Origin of the mercury bands at 2480A—800
Winch, W. R. (see Ingersoll, L. R.)—909(A)
Witmer, Enos E. Unitary theory, pure number ratios and the masses of atomic nuclei—316(L)
——— **and J. M. Cork.** Measurement of x-ray emission wave-lengths by means of the ruled grating—743
Woo, S. C. (see Strong, John)—267
Wood, R. W. and George Collins. Raman spectra of a series of normal alcohols and other compounds—386

Yearian, H. J. and K. Lark-Horovitz. Intensity distribution in electron diffraction patterns of ZnO—905(A)

Zabel, R. M. Reflection of atomic beams from sodium chloride crystals—218
Zemansky, M. W. Note on the equivalent absorption coefficient for diffused resonance radiation—843

ANALYTIC SUBJECT INDEX TO VOLUME 42

References marked (A) are to abstracts of papers presented at meetings of the Physical Society, those marked with (L) are to Letters to the Editor.

Absorption of light (see also Spectra, absorption)
Absorption coefficient for diffused radiation, M. W. Zemansky—843
In optically excited Hg, M. L. Pool, S. J. Simmons—909(A)
Intensities at different depths in water, H. A. Erikson—910(A)

Accommodation coefficient
For He positive ions, K. T. Compton, E. S. Lamar —588(A)

Acoustics
Burner for singing flames, overtones in strings, J. J. Hopfield—913(A)
Erratum: Supersonic dispersion and absorption in CO_2, W. H. Pielemeier—436
Velocity of sound in an absorptive gas, D. G. Bourgin—721

Activated gases
Nature of active N, J. Okubo, H. Hamada—795

Affinity
Continuous electron affinity spectrum of H, C. K. Jen—588(A)

Afterglow
Auroral spectrum, J. Kaplan—807
Nature of active N, J. Okubo, H. Hamada—795

Arcs (see Discharge of electricity in gases)

Astrophysics
Gunn's theory of double stars, L. Page—101

Atomic and molecular beams
Deflection of HCl molecules by a non-homogeneous electric field, E. McMillan—905(A)
Radiation excited by canal ray impact, F. L. Verwiebe—902(A)
Reflection from alkali halide crystals, R. R. Hancox—864
Reflection from NaCl crystals, R. M. Zabel—218
Scattering of Li ions from Ni, A. Longacre—906 (A)

Atomic form factors
Function of temperature, G. E. M. Jauncey—453

Aurora
Auroral spectrum, J. Kaplan—807
Luminescence of solid N., J. Kaplan—86

Barkhausen effect (see Magnetic properties)

Book reviews
Allen, H. Stanley. Electrons and Waves—451
Chase, C. T. A History of Experimental Physics—152
Debye, P. Molekulstruktur—743
Dirac, P. A. M. Les Principes de la Mécanique Quantique—746
Faraday Society. The Adsorption of Gases by Solids—745
Fleury, Pierre. Étalon Photométriques—319
Gmelin's Hankbuch der anorganischen Chemie, 8 auflage, Heransgegeben von der Deutschen chemischen gesellschaft. Teil A. Lieferung 4—746
Gmelin's Handbuch der anorganischen Chemie, 8 auflage, Heransgegeben von der Deutschen chemischen gesellschaft. Teil B. Lieferung 5—451
Houston, R. A. Vision and Colour Vision—152
Knaggs, I. E. and B. Karlik. Tables of Cubic Crystal Structure of Elements and Compounds —451
Kohlrausch, Friedrich. Kleiner Leitfaden der Praktischen Physik—319
Van Vleck, J. H. The Theory of Electric and Magnetic Susceptibilities—743

Constants, physical
Unitary theory and pure number ratios, E. Witmer—316(L)

Cosmic radiation
Acquirement of energies, W. F. G. Swann—914(A)
Airplane intensity measurements, L. M. Mott-Smith, L. G. Howell—314(L)
A in the ionization method of measuring, J. J. Hopfield—904(A)
Compton's latitude effect, G. Lemaitre, M. S. Vallarta—914(A)
Intensity variation with latitude, A. H. Compton —904(A). R. D. Bennett, J. L. Dunham, E. H. Bramhall, P. K. Allen—446(L)
Ionization as a function of pressure and temperature, J. W. Broxon—321
Production of groups of secondaries, J. C. Street, T. H. Johnson—142(L)
Self-recording electrometer; depth-ionization curve, J. M. Benade—290

Cosmic radiation (continued)
Solar component, J. C. Stearns, W. P. Overbeck, R. D. Bennett—317(L)

Crystals and crystal structure
Crystalline fields and the susceptibilities of salts of Ni, Cr, and Co, R. Schlapp, W. G. Penney—666
Electric field in paramagnetic crystals, C. J. Gorter—437(L)
Ferromagnetic anisotropy of single crystals; theory, R. M. Bozorth—882
Homogeneous mechanical stress and electrical resistance, P. W. Bridgman—858
Reflection of metallic atoms from alkali halide crystals, R. R. Hancox—864
Laue patterns from crystals oscillating piezoelectrically, M. Y. Colby, S. Harris—733(L) J. M. Cork—749
Mono-crystal Barkhausen effects, F. J. Beck, Jr., L. W. McKeehan—714
Piezoelectric deformations of quartz and tourmaline plates, G. A. Fink—912(A)
Tension and electrical resistance of single Bi crystals, M. Allen—848
Tropism of crystals, F. Bitter—731(L)
Vibration of piezoelectric crystals, N. H. Williams—913(A)

Cybotactic state
In ethyl ether, F. H. W. Noll—336
Of ethyl ether in the region of the critical point, R. D. Spangler—907(A)
Process of liquefaction, G. W. Stewart—907(A)

Dielectric constants
Moment of nitrobenzene, A. Piekara—449(L)
Of organic liquid mixtures, A. Piekara—448(L)
Temperature variation of moments of ethylene halides, E. W. Greene, J. W. Williams—119

Diffraction of atoms (see Atomic and molecular beams)

Diffraction of electrons (see Electron diffraction)

Diffusion
Of resonance radiation in gas, C. Kenty—823

Discharge of electricity in gases
Currents carried by electrons, K. T. Compton, E. S. Lamar—588(A)
Diffusion of resonance radiation in a gas, C. Kenty—823
Neutralization and ionization of high-velocity ions by collision, H. F. Batho—753
Positive ion current at cathode, A. K. Brewer, R. R. Miller—786
Secondary emission from collectors in Ne discharge, G. Spiwak, E. Reichrudel—580(L)

Disintegration of nucleus
Of Li by protons, E. O. Lawrence, M. S. Livingston, M. G. White—150(L)

Dissociation
In N, J. Kaplan—97

Efficiency of ionization
K-electron ionization of Ag, D. L. Webster, W. W. Hansen, F. B Duveneck—141(L)

Elasticity
And magnetic properties, F. Bitter—697
Theory of "refraction shooting," M. Muskat—910(A)

Electrets
In wax mixtures and S, O. J. Johnson, P. H. Carr—912(A)

Electrical conductivity and resistance
Of fifteen metals down to liquid O temperatures; effect of pressure, P. W. Bridgman—587(A)
Homogeneous mechanical stress and electrical resistance of crystals, P. W. Bridgman—858
Tension and electrical resistance of single Bi crystals, M. Allen—848

Electrical oscillations and waves
By beads of corona discharges, J. Tykocinski Tykociner—912(A)

Electric moment (see Dielectric constant)

Electromagnetic theory
Momentum relations in crossed fields, L. Page—101

Electron diffraction
Intensity distribution, H. J. Yearian, K. Lark-Horovitz—905(A)
By an Ag film on an Au crystal, H. E. Farnsworth—588(A)
By a w-single crystal, W. T. Sproull—904(A)

Electron lenses
A correction, C. J. Davisson, C. J. Calbick—580(L)

Electrons
Dirac electron moving in a magnetic field, O. Laporte—340

Electrons, scattering of
Slow electrons by Cs ions, C. Boeckner, F. L. Mohler—906(A)
Theoretical calculations, W. W. Wetzel—902(A)

Electrons, secondary
From collectors in Ne discharge, G. Spiwak, E. Reichrudel—580(L)
Energy distribution of electrons from Mo, L. J. Haworth—906(A)
Magnetic spectra from Ag, S. Chylinski—393

Electro-optical effects (see also Photoelectric effect)
Kerr effect in infrared, L. R. Ingersoll, W. R. Winch—909(A)

e/m
Determination for an electron by a new deflection method, F. G. Dunnington—734(L)
Determination by means of photoelectrons excited by x-rays, G. G. Kretschmar—905(A)
Value of, for electron, R. T. Birge—736(L)

Energy states of atoms (see also Spectra, atomic)
Atomic eigenfunctions and energies, C. W. Ufford, G. H. Shortley—167

Energy states of molecules (see Molecular structure and constants; Spectra, molecular)

Errata
Abundances of N and O isotopes, G. M. Murphy, H. C. Urey—312
Electron lenses, C. J. Davisson, C. J. Calbick—580(L)
Probable values of e, h, e/m and α, R. T. Birge—736(L)
Space quantization of atoms upon impact, H. Kuhn, O. Oldenberg—312
Structure of atomic nuclei, J. W. Bartlett, Jr.—737
Supersonic dispersion and absorption in CO_2, W. H. Pielemeier—436

Ferromagnetism (see Magnetic properties)

Flames
Luminosity of sodium flames, C. D. Child—146(L)

Gases (see Kinetic theory of gases)

Geophysics
Erosion of rock, T. W. Moore—906(A)
Measurement of the gravitational effect of the moon, K. Hartley—911(A)
"Refraction shooting," M. Muskat—910(A)

Gyromagnetization (see Magnetic properties)

Hall effect
And intensity of magnetization, E. M. Pugh, T. W. Lippert—709

Heat of dissociation (see Dissociation)

High voltage tubes and machines
Compact high potential electrostatic generator, H. A. Barton, D. W. Mueller, L. C. Van Atta—901(A)
For producing H ions, M. S. Livingston—441(L)

Hyperfine structure
And isotope displacements, G. Breit—348

Instruments (see Methods and instruments)

Ionization by positive ions (see Ionization potentials)

Ionization potentials
Electron impact in water vapor and sulphur dioxide, H. D. Smyth, D. W. Mueller—902(A)
By impact of atoms and positive ions, C. J. Brasefield—11

Ions, high-speed
H ions, M. S. Livingston—441(L)
Neutralization and ionization of high-velocity ions, by collision, H. F. Batho—753
By repeated accelerations, A. J. Dempster—901(A)

Ions in gases
Ions in crossed fields, L. Page—101
Neutralization and ionization of high-velocity ions by collision, H. F. Batho—753
Radiation from positive ions in A, Ne, He, A. I. McPherson—903(A)

Ions, mobility (see also Ions in gases)
Mobility spectrum in air, R. N. Varney—547
In pure gases, C. M. Focken—577(L)

Isotopes
Abundance of H^2 from spectrum, J. D. Hardy, E. F. Barker, D. M. Dennison—279
Atomic weights, of radioactive substances, F. Western, A. Ruark—903(A)
Detection of $H^2\gamma$ line, D. H. Rank—446(L)
Erratum: Relative abundance of N and O isotopes, G. M. Murphy, H. C. Urey—312
Existence of Cl^{39}, M. F. Ashley, F. A. Jenkins—438(L)
And hyperfine structure, G. Breit—348
Ratio of masses in B, F. A. Jenkins, A. McKellar—464
Vibrational isotope effects in polyatomic molecules, E. O. Salant, J. E. Rosenthal—812
Weight of H^2, K. T. Bainbridge—1

Joule-Thomson effect
In He, J. R. Roebuck, H. Osterberg—912(A)

Kinetic theory of gases
Law of force between two He atoms, W. G. Penney—585(L)

Liquids
Crystalline test bodies in streaming solutions, T. W. Moore—906(A)
Electrical properties of surface layers, K. Lark-Horovitz, J. E. Ferguson—907(A)
Ethyl ether in the region of the critical point, R. D. Spangler—907(A)
Process of liquefaction, G. W. Stewart—907(A)

Luminescence
Of solid nitrogen, J. Kaplan—86

Magnetic properties
Barkhausen effects in rotating fields, F. J. Beck, Jr., L. W. McKeehan—714
Diamagnetism of water at different temperatures, A. P. Wills, G. F. Boeker—687
Of distorted cubic ferromagnetic lattices, F. Bitter—697
Effect of strain in Ni, C. W. Heaps—108
Electric field in paramagnetic crystals, C. J. Gorter—437(L)
Ferromagnetic anisotropy of single crystals; theory, R. M. Bozorth—882
Gyromagnetic ratios for Ni and Co, S. J. Barnett—147(L)
And Hall e.m.f., E. M. Pugh, T. W. Lippert—709
Heisenberg theory of ferromagnetism, D. R. Inglis—442(L)
Magnetic moment of Li^7, L. P. Granath—44
Paramagnetic susceptibility of Cu^{++}, O. M. Jordahl—901(A)
Permeability of Fe at high frequencies, J. B. Hoag, H. Jones—571
Propagation of Barkhausen discontinuities, K. J. Sixtus, L. Tonks—419
Susceptibilities of common gases, G. G. Havens—901(A)
Susceptibilities of salts of Ni, Cr and Co, R. Schlapp, W. G. Penney—666

Magneto-optical effects
Rotation by condenser discharge, F. G. Slack, W. M. Breazeale—305

Magnetostriction
Effect of strain in Ni, C. W. Heaps—108

Mass-spectrograph (see also methods and instruments)
Ionization by electron impact in water vapor and sulphur dioxide, H. D. Smyth, D. W. Mueller—902(A)

Mean life
Of $^3P_2$ Ne atom, E. Matuyama—373
Of 2^3S_1 state of Hg, L. R. Maxwell—148

Measurements (see Methods and instruments)

Mechanics, quantum—atomic structure and spectra
Analytic wave functions, J. C. Slater—33
Atomic eigenfunctions and energies, C. W. Ufford, G. H. Shortley—167
Atomic wave functions, F. W. Brown—914(A)
Quantum defect for highly excited S states of para- and orthohelium, L. P. Smith—176

Mechanics, quantum—general
Continuous electron affinity spectrum of H, C. K. Jen—588(A)
Differential analyzer solution for wave functions, S. Caldwell—589(A)
Dirac electron moving in a magnetic field, O. Laporte—340
Dispersion and absorption of He, J. P. Vinti—632
Effect of exchange on elastic cross sections, P. M. Morse, W. P. Allis—588(A)
Ionization of He by electron impact, W. W. Wetzel—902(A)
Possibility of deriving work from statistical fluctuations, V. Guillemin, Jr.—589(A)
Radiation from slow electrons, L. Nedelsky—641
Scattering of slow electrons, E. Feenberg—17
Susceptibilities of salts of paramagnetic ions, R. Schlapp, W. G. Penney—666
Vapor pressure constant, T. E. Sterne—556

Mechanics, quantum—molecular structure and spectra
Calculation on the water molecule, A. S. Coolidge—189
Continuous absorption of O_2; theory, E. C. G. Stueckelberg—518
Molecules formed from two $2p$ atoms, J. R. Stehn—582(L)
Vibrations of polyatomic molecules; NH_3, N. Rosen, P. M. Morse—210

Metastable atoms and molecules
Lifetime $^3P_2$ Ne atom, E. Matuyama—373

Methods and instruments
Amplifier for Geiger-Müller counters, W. F. Libby—440(L)
Burner for singing flames, J. J. Hopfield—913(A)
Compact high-potential electrostatic generator, H. A. Barton, D. W. Mueller, L. C. Van Atta—901(A)
Comparison of photographic and ionization methods of measuring x-ray intensities, E. Dershem 908(A)
Determination of dielectric constant of a vapor, E. W. Greene, J. W. Williams—119
Differential analyzer solution for the wave function of the K-shell, S. Caldwell—589(A)
Filter for Raman effect, A. H. Pfund—581(L)

Methods and instruments (continued)
High-pressure spectrometer, F. E. Poindexter, L. E. James—910(A)
High-velocity protons by repeated accelerations, A. J. Dempster—901(A)
High-voltage direct-current generator, R. E. Vollrath—298
Magneto-optic rotation, F. G. Slack, W. M. Breazeale—305
Measurement of the gravitational effect of the moon, K. Hartley—911(A)
Modified optical lever, G. A. Fink—912(A)
Non-thermionic amplifier, H. J. Reich—913(A)
Photoelectric quantum counters, G. L. Locher—525
Polarization of electrodes in vacua, A. E. Shaw—902(A)
Refractory materials for melting pure metals, H. B. Wahlin, O. D. Fritsche, J. F. Oesterle—911(A)
Self-recording cosmic-ray electrometer, J. M. Benade—290
Vacuum spectrograph, P. G. Kruger, F. S. Cooper—910(A)
Vacuum tube electrometers, R. E. Burroughs, J. E. Ferguson—913(A)
Vibration of piezoelectric crystals, N. H. Williams—913(A)

Mobility of ions (see Ions, mobility)

Molecular structure and constants (see also Spectra, molecular and Raman spectra)
Energy level diagram of the Sm^{+++} ion in solids, F. H. Spedding, R. S. Bear—76
Of HCN, K. N. Choi, E. F. Barker—777
Molecules formed from two $2p$ atoms, perturbation theory, J. R. Stehn—582(L)
Of NH_3, J. W. Williams, A. Hollaender—379
Of ozone, S. L. Gerhard—622
Vibrations of polyatomic molecules; NH_3, N. Rosen, P. M. Morse—210
Of water molecule, A. S. Coolidge—189

Nuclear spin (see also Hyperfine structure)
Of Li^7, L. P. Granath—44

Nucleus
Disintegration of Li by protons, E. O. Lawrence, M. S. Livingston, M. G. White—150
Masses of atomic nuclei, E. E. Witmer—316(L)
Nuclear exclusion principle, W. D. Harkins—914(A)
Structure of, J. H. Bartlett, Jr.—145(L)

Neutrons
And nuclear structure, W. D. Harkins—914(A)

Optical constants and properties
Change of n with pressure, F. E. Poindexter, L. E. James—910(A)
Dispersion and absorption of He, J. P. Vinti—632

Packing fraction
Of H^2, K. T. Bainbridge—1

Permeability (see Magnetic properties)

Photoelectric effect and properties
e/m of photoelectrons, G. G. Kretschmar—905(A)
Energy distribution of photoelectrons, L. A. DuBridge—905(A)
Quantum counters for visible and ultraviolet light, G. L. Locher—525

Photography
Influence of pressure on latent photographic image, K. A. Maring—911(A)

Photometry
Quantum counters for visible and ultraviolet light, G. L. Locher—525

Piezoelectric effect
Temperature variation of constant of quartz, K. S. Van Dyke—587(A)
Work functions of Mo, L. A. DuBridge, W. W. Roehr—52
X-ray reflection from oscillating crystals, M. Y. Colby, S. Harris—733(L); J. M. Cork—749

Polarization, electrical (see Dielectric constants)

Positive ray analysis (see also Mass-spectrograph)
Ions from heated metals, L. L. Barnes—487

Probability of ionization (see Efficiency of ionization)

Quantum defect
For highly excited S states of para- and ortho-helium, L. P. Smith—176

Radioactivity
Ac branching ratio, F. Western, A. Ruark—903(A)
Atomic weights, Forrest Western, A. Ruark—903(A)
Origin of the Ac series, A. v. Grosse—565

Raman spectra
In CO and NO, S. Bhagavantam—437(L)
Filter for Raman effect, A. H. Pfund—581(L)
Fine structure of a Raman band, J. W. Williams, A. Hollaender—379
Of normal alcohols and organic compounds, R. W. Wood, G. Collins—386
Variation of structure of scattered lines with the frequency, E. Gross, J. Khvostikov—579(L)

Relativity
Experimental establishment of the relativity of time, R. J. Kennedy, E. M. Thorndike—400

Resistance, electrical (see Electrical conductivity and resistance)

Resonance radiation
Absorption coefficient for diffused radiation, M. W. Zemansky—843
Diffusion and escape from a gas, C. Kenty—823

Scattering of electrons (see also Electron diffraction)
Angular distribution in Hg vapor, A. L. Hughes—147(L)
Equations for scattering, E. Feenberg—17

Scattering of light (see also Raman spectra)
From NH_3 solutions, J. W. Williams, A. Hollaender—379

Secondary electrons (see Electrons, secondary)

Solutions
Crystalline test bodies in streaming solutions, T. W. Moore—906(A)

Sound (see Acoustics)

Spectra, absorption (see also Absorption of light)
Coefficients in optically excited mercury, M. L. Pool, S. J. Simmons—909(A)
Conglomerate of $SmCl_3 \cdot 6H_2O$, F. H. Spedding, R. S. Bear—76
Continuous absorption of O_2, theory, E. C. G. Stueckelberg—518
Continuous spectrum of alkyl iodides, Y. Hukumoto—313(L)
Of HCN, infrared, K. N. Choi, E. F. Barker—777
Of IBr, W. G. Brown—355
Infrared of ozone, S. L. Gerhard—622
Intensities at different depths in water, H. A. Erikson—910(A)
Of single crystals of $SmCl_3 \cdot 6H_2O$, F. H. Spedding, R. S. Bear—58

Spectra, atomic
Detection of $H^2\gamma$-line, D. H. Rank—446(L)
Emission probability for a colliding atom, R. W. Ditchburn—314(L)
Extension of spectrum of Cs II, J. Olthoff, R. A. Sawyer—766
Of high speed positive ions in A, Ne and He, A. I. McPherson—903(A)
Of Sb II, R. J. Lang, E. H. Vestine—233
Term system of Ir I, W. Albertson—433(L)
Two vector problem in Pb V and Bi VI, A. T. Goble, J. E. Mack—909(A)

Spectra, general
Auroral spectrum, J. Kaplan—807
B isotopes from band spectra, F. A. Jenkins, A. McKellar—464
Lines from Hg vapor in beam of electrons, L. R. Maxwell—148
Radiation excited by canal ray impact, F. L. Verwiebe—902(A)

Spectra, molecular (see also molecular structure and constants)
Anomalous rotational temperature of HgH, F. F. Rieke—587(A)
Far infrared of HCl and NH^3, J. Strong, S. C. Woo—267
First negative bands of the CO^+, R. F. Schmid—182
Hg bands at 2480A, J. G. Winans—800
Infrared of H^2Cl, J. D. Hardy, E. F. Barker, D. M. Dennison—279
Interpretation of the CO_2 emission bands, R. S. Mulliken—364
Of KH, G. M. Almy, C. D. Hause—242
Of MgO, CaO and SrO, P. C. Mahanti—609
Rotational analysis of ultraviolet bands of SiO, P. G. Saper—498
Vibrational isotope effects in polyatomic molecules, E. O. Salant, J. E. Rosenthal—812

Spectroscopy, technique
Grazing incidence vacuum spectrograph, P. G. Kruger, F. S. Cooper—910(A)

Surface phenomena
Electrical properties of surface layers, K. Lark-Horovitz, J. E. Ferguson—907(A)

Susceptibility, magnetic (see Magnetic properties)

Thermal expansion
Of Sb, P. Hidnert, H. S. Krider—911(A)

Thermionic emission of electrons, emitting surfaces
Work function of Mo, L. A. DuBridge, W. W. Roehr—52

Thermionic emission of positive ions
Of metals from metals, L. L. Barnes—487
Temperature variation of emission from Mo, L. L. Barnes—492

Thermodynamics
Possibility of deriving work from statistical fluctuations, V. Guillemin, Jr.—589(A)
Vapor pressure constant, T. E. Sterne—556

Vacuum tubes
Non-thermionic amplifier, H. J. Reich—913(A)
Vacuum tube electrometer, R. E. Burroughs, J. E. Ferguson—913(A)

Vapor pressure
Vapor pressure constant from quantum mechanics, T. E. Sterne—556

Virial coefficient
Force between two He atoms, W. G. Penney—585(L)

Viscosity
Temperature variation in quartz, K. S. Van Dyke—587(A)

Wave Mechanics (see Mechanics, quantum, etc.)

X-rays, diffraction scattering, reflection and refraction
Diffraction in ethyl ether, F. H. W. Noll—336
Diffuse scattering from a complicated crystal, G. E. M. Jauncey, P. Ehrenfest II—907(A)
Dynamic reflection from ZnS, I. G. Geib, K. Lark-Horovitz—908(A)
Laue patterns from crystals oscillating piezoelectrically, M. Y. Colby, S. Harris—733(L), J. M. Cork—749
L discontinuities of Au, Fred M. Uber, C. G. Patten—229
Scattering of from an NaF crystal at low temperatures, P. S. Williams, G. E. M. Jauncey—907(A)
Scattering by gases and crystals, G. E. M. Jauncey—453
Scattering of hard x-rays by solids, S. Chylinski—153

X-rays, emission
Relative intensities of the $L\alpha_1$ and $L\beta_2$ lines in the fluorescent spectrum of U, R. J. Stephenson—908(A)
Relative intensities of the $L\alpha_1$, β_1, β_2, and γ_1 in Ta, W, Ir and Pt, V. J. Andrew—591

X-rays, spectra and spectroscopy, wave-length measurements
Comparison of photographic and ionization methods of measuring x-ray intensities, E. Dershem—908(A)
Wave-lengths by means of the ruled grating, R. B. Witmer, J. M. Cork—743

X-rays, tubes, apparatus
Demountable metal tube, K. Lark-Horovitz, E. M. Miller—915(A)

Zeeman effect
Perturbed terms in the CO angstrom bands, W. W. Watson—509
Of Sb II and Sb III, J. B. Green, R. A. Loring—909(A)

CURRENT LITERATURE OF PHYSICS

Extracts from the Tables of Contents of Some of our Contemporaries

PROCEEDINGS OF THE ROYAL SOCIETY

SERIES A, VOL. 138, No. 835 — NOVEMBER 1, 1932

Adsorption. A Study of Availability and Accessibility. By **Sir William B. Hardy and M. Nottage** 259
On Plasticity and Creep in Solids. By **H. Jeffreys** 283
Explosive Oxidation of Carbon Monoxide at Lower Pressures. By **G. Hadman, H. W. Thompson and C. N. Hinshelwood** 297
Lower Pressure Limit in the Chain Reaction between Hydrogen and Oxygen. By **C. N. Hinshelwood and E. A. Moelwyn-Hughes** 311
γ-Rays of Thorium *B* and of Thorium *C* Bodies. By **C. D. Ellis** 318
Theory of Wave Resistance. By **T. H. Havelock** 339
Resistivity of Polycrystalline Wires in Relation to Plastic Deformation, and the Mechanism of Plastic Flow. By **E. N. da C. Andrade and B. Chalmers** 348
Photochemistry of Phosphine. By **H. W. Melville** 374
Bands due to the Hydrogen Molecule: The $2p^3\pi$ Bands of Hydrogen. By **I. Sandeman** 395
Structure of Surface Films. Part XVI.—Surface Potential Measurements on Fatty Acids on Dilute Hydrochloric Acid. By **N. K. Adam and J. B. Harding** 411
On the Surface Potentials of Unimolecular Films. Part IV.—The Effect of the Underlying Solution and Transition Phenomena in the Film. By **J. H. Schulman and A. H. Hughes** 430

NATURE

VOL. 130, No. 3290 — NOVEMBER 19, 1932

Letters to the Editor:

Limiting Mobilities of Some Monovalent Ions and the Dissociation Constant of Acetic Acid at 25°. By **Duncan A. MacInnes, Theodore Shedlovsky and Lewis G. Longsworth** 774
Emission of Positive Ions from Cold Surfaces under the Influence of Strong Electric Fields. By **W. R. Harper** 775
Origin of Zero-Point Entropy. By **K. Clusius** 775
Eddington's Theory and Physical Constants. By **G. Siva Rama Krishnan** 776
Helium Content of Beryllium. By **Wm. D. Urry** 777

NATURE

VOL. 130, No. 3291 — NOVEMBER 26, 1932

Letters to the Editor:

Continuous Spectrum of Pure Argon. By **S. P. McCallum, L. Klatzow and J. E. Keyston** 810
Continuous Spectrum of Sodium. By **H. Hamada** 810
Angle of Elevation of Short Wave Rays. By **T. Walmsley** 814

ZEITSCHRIFT FÜR PHYSIK

VOL. 78, NOS. 11 and 12 — OCTOBER 28, 1932

Rule of Mixtures for the Electromagnetic Rotation of the Plane of Polarization. By **Otto Shönrock** 707
Diffraction of Fast Protons by Gold Foils. By **E. Rupp** 722
Optical Transparency of Cu_2O in Relation to its Electric Conductivity. By **G. Mönch** 728
Optical Investigation of the Accommodation Coefficient of Molecular Translation and its Distribution Function in a Rarefied Gas. By **L. S. Ornstein and W. R. v. Wyk** 734

Theory of Super-conductivity. By **R. de L. Kronig** 744
Quantum Mechanical Calculation of the Intensities of Infrared Bands. By **Kurt Scholz** ... 751
Investigation of the Hydrocarbon Band at λ3143. By **Tage Heimer** 771
Experimental Determination of the First Piezo-Modulus of Quartz. By **Berta Nussbaumer** 781
Calculation of Specific Heat of Diatomic Gases by Quantum Statistics. By **C. Gregory** 791
Magneto-Mechanical Effect. By **N. Akulov and E. Kondorsky** 801
Influence of Elastic Stretching on the Form of Magnetization Curve. By **N. Akulov, A. Helfenbein and N. Byczkov** 808
Electrical Conductivity of Oxygen Occluded on Palladium. By **Donald P. Smith** 815
Hypothesis of the Transport of Electricity in Metals by Oxygen. By **Alfred Coehn** 824
Collision Phenomena in Optical Excitation of the Different Mercury Isotopes. By **S. Mrozowski** 826
Remarks on the Mean Life of the Mercury Resonance Line 2537A. By **S. Mrozowski** 844
Theory of Electrical Breakdown. By **L. Landau and L. Rosenkewitsch** 847
Space Charge and Its Relation to the Chemical Components of the Atmosphere. By **R. Stoppel** 849
Appendix to the Paper: Investigations of Hardening of Zinc Aluminum Alloys Having the Composition Al_2Zn_3. By **Herbert Meyer** 854

ZEITSCHRIFT FÜR PHYSIK

VOL. 79, NOS. 1 and 2 NOVEMBER 4, 1932

Hyperfine Structure of the Arc Lines and the Nuclear Moment of Copper. By **Rudolf Ritschl** 1
Sauter's Method of Solution of the Dirac Equation without Specialization of the Operators. By **K. Bechert** 26
Infrared and Raman Bands of Carbon Dioxide, Carbon Oxysulphide and Carbon Disulphide Molecules. By **A. B. D. Cassie and C. R. Bailey** 35
Investigation on the Dispersion of Gases and Vapors and their Representation by the Dispersion Theory. III. Dispersion of Oxygen between 6000 and 1920A. By **R. Ladenburg and G. Wolfsohn** 42
Significance of Ultraviolet Absorption Bands of Alkali Halides. By **M. Born** 62
Absorption Spectra of Highly Compressed Oxygen and Existence of the O_4 Molecule. I. The Ultraviolet Bands between 2900 and 2300A. By **W. Finkelnburg and W. Steiner** . 69
Quenching of Iodine Fluorescence by Magnetic Fields and by Foreign Gases. By **Wolfgang Berg** 89
Procedure for the Separation of Gaseous Isotope Mixtures and Its Application to the Isotopes of Neon. By **G. Hertz** 108
Photometric Investigation of the Strongest Emission Bands of Fluorine. By **Jonaton Aars** 122
Does a Fluid Stick to a Surface which it Does Not Wet? By **Markus Reiner** 139
Reply to the Above Paper of M. Reiner. By **S. Erk** 141

ZEITSCHRIFT FÜR PHYSIK

VOL. 79, NOS. 3 AND 4 NOVEMBER 14, 1932

Semi-classical Theory of Chemical Binding. By **W. Heitler** 143
Occurrence of the Selective Photoelectric Effect on Thin Alkali Metal Films. By **R. Suhrmann and A. Schallamach** 153
N X-Ray Series of the Elements 73Ta-81Tl. I. By **Torsten Magnusson** 161
Molecular Absorption of Mixed Halogen Molecules in Ultraviolet. II. By **H. Cordes and H. Sponer** 170
Temperature Dependence of the Total Ion Formation in Air. By **A. Becker and Ilsemarie Schaper** 186
Change of the Reflecting Power of Bismuth by Magnetization. By **E. Englert and K. Schuster** 194
Heat of Relaxation of the Lead Crystal Grating. By **G. v. Hevesy, W. Seith and A. Keil** .. 197

Magnetic Spectrum of Cosmic Rays. By **Paul Kunze** 203
Hyperfine Structures in the Antimony Spark Spectrum and the Nuclear Moment of the Antimony Isotopes. By **J. S. Badami** 206
Hyperfine Structures in the Antimony Arc Spectrum. By **J. S. Badami** 224
Remark on the Space-Charge Field of Gas-Concentrated Electron Beams. By **K. Engel** ... 231
Singular Vibration Condition of a Flat Spring. By **Johannes Jaumann** 235
Calculation of the Long Wave Limit of the Photoelectric Effect from the Atomic Volumes of the Elements. By **G. Schweikert** 248
Measurement of Small Capacities. By **Hermann Lampe** 254
Ionization by Gamma- and Cosmic Rays in Oxygen and Xenon. Preliminary Communication. By **V. Masuch** 264
Electrical Breakdown as Static Ionization. By **Hanns Eisler** 266

DIE NATURWISSENSCHAFTEN

VOL. 20, No. 46 NOVEMBER 11, 1932

(No articles of interest to physicists)

DIE NATURWISSENSCHAFTEN

VOL. 20, No. 47 NOVEMBER 18, 1932

Astigmatism in Grammatical and Technical Aspect. By **M. v. Rohr** 847

Short Original Communications:

Case of Sensitized Phosphorescence. By **Siegfried Rothschild** 850
Significance of Different X-Ray Spectra of Native Starches. By **J. R. Katz and J. C. Derksen** 851

PHYSIKALISCHE ZEITSCHRIFT

VOL. 33, No. 22 NOVEMBER 15, 1932

Original Communications:

Scattering of Light by Sound Waves. By **P. Debye** 849
Velocity Distribution of Electrons in the Positive Column. By **M. J. Druyvesteyn** 856

Papers and Discussions at the VII German Convocation of Physicists in Bad Nauheim, September 20–24, 1932:

Theory of the Diamagnetism of Conduction Electrons. By **R. Peierls** 864
Dia- and Paramagnetism of Metals. By **E. Vogt** 864
Critical Investigation of the Determination of Paramagnetic Ion Moments in Solids. By **H. Auer** 869
Magnetic Properties of the System Mn-Cu-Al. By **S. Valentiner and G. Becker** 872
Experiment on the Selective Photoeffect and the Optical Absorption on Composite Photoelectric Cathodes. By **W. Kluge** 873
Spectra of Chromium in Crystals. By **O. Deutschbein** 874
Regularities of the Line Spectra of Solids. By **R. Tomaschek** 878
Excitation by Impact of Electrons, Ions and Atoms. By **W. Hanle and K. Larché** 884
Hittorf's Dark Space and the First Cathode Layer of a Glow Discharge. By **W. Weizel** ... 887
Excitation and Emission of Light in a Hydrogen Spark at High Pressure. By **W. Finkelnburg** 888
Investigations of Discharges in Mercury Vapor. By **E. Lübcke** 890
ϵ/μ Measurements with Thread-like Rays. By **K. Siebertz** 895
A New Cathode Examination with the Electrical Electron Microscope. By **E. Brüche and H. Johannson** 898
New Method of Mass-Spectrometry. By **J. Mattauch** 899

ANNALEN DER PHYSIK

VOL. 15, SERIES 5, No. 2 1932

Electrical and Optical Behavior of Semi-Conductors. VII. Photoelectric Properties of Semi-Conducting Contact Layers. By **W. Lee** 129
Cinematographical Electron Microscopy of Oxide Cathodes. By **E. Brüche and H. Johannson** 145

On Magnetization by Rotation. By **H. Brion** 167
Viscosity, Heat Conductivity and Diffusion in Gas Mixtures. XXI. Absolute Molecular Cross-Section from Viscosity Measurements, Molecular-Theory Significance of the Critical Temperature and Calculation of the Critical Pressure from η. By **Max Trautz** 198
Electrical Properties of Thin Mixed Crystal Alloys. III. Resistance of Copper and Gold Alloys. Regularities in Mixed Crystal Resistances. By **J. O. Linde** 219

PHYSICA

VOL. 12, No. 8 1932

Rôle of Casper Calthoff in the Development of Modern Steam Engines. By **J. A. Vollgraff** 257
Measurement of Specific Gravity of Granular Material. By **W. F. de Jong and H. J. Stek** . 269
Secondary Electrons in X-Ray Tubes. By **A. Bouwers and J. H. van der Tuuk** 274

COMPTES RENDUS

VOL. 195, No. 16 OCTOBER 17, 1932

Calibration of a Blower of Low Velocity. By **Ch. Sadron** 647
Study of the Brownian Movement in a Field of Force. By **Jacques Métadier** 649
Raman Effect in Copper Salt Solutions. By **A. Da Silveira** 652
Mach Effect. By **F. Wolfers** 653
Weakening of the Nuclear Radiation of Beryllium in Screen Materials. By **J. Thibaud and F. Dupré La Tour** 655

COMPTES RENDUS

VOL. 195, No. 17 OCTOBER 24, 1932

New Formulas for the Calculation of Special Perturbations. By **Henri Roure** 694
Longitudinal Equilibrium of a Wing. By **Gustave André Mokrzycki** 697
Cosmic Rays. By **Émile Sevin** 698
Certain Potentials of a Simple Layer, Generators of Real and Complex Harmonic Functions. By **R. Wavre** 701
Novel Isotopic Effect. By **L. Goldstein** 703
Apparatus for Making Glass Instruments for Micro-Manipulations. By **P. de Fonbrune** . . 706
Effect of Molybdates on the Rotatory Power of Xylose. By **E. Darmois and M. Murgier** . . 707

COMPTES RENDUS

VOL. 195, No. 18 NOVEMBER 2, 1932

Measure of the Aerodynamic Characteristics of a Wing Sustained in a Plane Current. By **Henry Girerd** 731
Fundamental Problem Concerning a Wing of Finite Extent. By **M. L. Malavard** 733

REVUE D'OPTIQUE

No. 10 OCTOBER, 1932

Researches on Photoelectric Photometry and Spectra Photometry. By **Pierre Fleury** 385
Electrodeless Discharge and a Source of Monochromatic Light. By **Felix Esclangon** 399
Total Reflection from Half-Silvered Glass. By **Armand de Gramont** 405

NATIONAL ACADEMY OF SCIENCES

VOL. 18, No. 11 NOVEMBER, 1932

(No articles of interest to physicists.)

JOURNAL OF THE OPTICAL SOCIETY OF AMERICA

VOL. 22, No. 12 DECEMBER, 1932

Analytical Treatment of the Longitudinal Horopter; Its Measurement and Application to Related Phenomena, Especially to the Relative Size and Shape of the Ocular Images. By **Kenneth N. Ogle** 665
Accommodation, Pupillary Width and Stimulus Distance. By **Ellis Freeman** 729
Modified Broca Pupillometer. By **Frank K. Moss** 735
Absorption and Dispersion of Celluloid between 300A and 1000A. By **H. M. O'Bryan** . . . 739

THE REVIEW OF SCIENTIFIC INSTRUMENTS

NEW SERIES. VOL. 3, NO. 12 DECEMBER, 1932

Measurement of X-Ray Intensities as Functions of Voltage, up to 180 kv. By **D. L. Webster, W. W. Hansen and F. B. Duveneck** 729
Filter for an X-Ray Power Supply. By **J. Barton Hoag and Victor J. Andrew** 750
Mechanical Aid to the Analysis of Complex Spectra. By **George R. Harrison** 753
Note on Rating of Photoelectric Tubes. By **Lewis R. Koller** 760
Mercury Sealed Gas Valve. By **Sanford F. Essig** 762
Variable Orifice Flow Meter. By **Graham W. Marks** 764
Improved Vibrograph and Some of Its Uses. By **T. Tirunarayanachar** 766
Novel Optical Screen for Classroom Demonstrations. By **Joseph H. Howey** 777
Automatic Toëpler Pump. By **Arthur Tandy Williamson** 782
Method for Preparing Crystals for Rotation Photographs. By **H. Kersten and W. Lange** .. 790
Laboratory Apparatus for the Determination of the Time of Free Fall of a Body. By **R. M. Bowie** 792
Photoelectric Emission from Different Metals. By **H. C. Rentschler, D. E. Henry and K. O. Smith** 794
Simple Method of Producing and Projecting Mercury Ripples. By **A. R. Harmon and J. B. Brinsmade** 803
Apparatus for Spectroscopic Studies in the Intermediate Infrared Region 20 to 40μ. By **John Strong** 810